United States Nuclear Regulatory Commission

*Protecting People and the Environment*

NUREG/CR-7027

# Degradation of LWR Core Internal Materials due to Neutron Irradiation

Office of Nuclear Regulatory Research

United States Nuclear Regulatory Commission

*Protecting People and the Environment*

NUREG/CR-7027

# Degradation of LWR Core Internal Materials due to Neutron Irradiation

Manuscript Completed: January 2010
Date Published: December 2010

Prepared by
O.K. Chopra

Argonne National Laboratory
9700 South Cass Avenue
Argonne, IL 60439

A.S. Rao, NRC Project Manager

NRC Job Code N6818

Office of Nuclear Regulatory Research

**NUREG/CR-7027**
**ANL-10/11**

# Degradation of LWR Core Internal Materials due to Neutron Irradiation

Manuscript Completed: January 2010
Date Published: December 2010

Prepared by
O. K. Chopra
Environmental Science Division
Argonne National Laboratory
Argonne, IL 60439

Appajosula S. Rao, NRC Project Manager

**Prepared for**
**Division of Engineering**
**Office of Nuclear Regulatory Research**
**U.S. Nuclear Regulatory Commission**
**Washington, DC 20555**
**NRC Job Code N6818**

This page is intentionally left blank.

## Abstract

Austenitic stainless steels are used extensively as structural alloys in the internal components of light water reactor (LWR) pressure vessels because of their relatively high strength, ductility, and fracture toughness. However, exposure to neutron irradiation for extended periods changes the microstructure and microchemistry of these steels and degrades their fracture properties. This report presents a critical assessment of the susceptibility of LWR core internal materials to irradiation effects such as irradiation-assisted stress corrosion cracking (IASCC), neutron embrittlement, void swelling, and irradiation-induced stress relaxation. The existing data, in the open literature as well as from research carried out by the U.S. Nuclear Regulatory Commission (NRC) and industry, have been evaluated to establish the effects of material parameters (such as composition, thermo-mechanical treatment, microstructure, microchemistry, yield strength, and stacking fault energy) and environmental parameters (such as water chemistry, irradiation temperature, dose, and dose rate) on these processes. Differences in radiation-induced degradation in material properties between light water reactors and fast-reactor irradiations are also discussed. The results are used to (a) define a threshold fluence above which irradiation effects on materials properties are significant, (b) develop disposition curves for cyclic and IASCC growth rates for reactor core internal materials, and (c) assess the significance of void swelling and irradiation creep relaxation on the structural and functional integrity of reactor internal components. The report also identifies potential deficiencies or knowledge gaps in the existing experimental data on degradation of LWR core internal materials due to neutron irradiation.

### Paperwork Reduction Act Statement

This NUREG does not contain information collection requirements and, therefore, is not subject to the requirements of the Paperwork Reduction Act of 1995 (44 U.S.C. 3501 et seq.).

### Public Protection Notification

The NRC may not conduct or sponsor, and a person is not required to respond to, a request for information or an information collection requirement unless the requesting document displays a current valid OMB control number.

This page is intentionally left blank.

## Foreword

The internal components of light water reactor (LWR) pressure vessels are fabricated primarily with austenitic stainless steels because of their relatively high strength, ductility, and fracture toughness. During normal reactor operational conditions, the internal components are exposed to high-energy neutron irradiation and high-temperature reactor coolant. However, prolonged exposure to neutron irradiation changes both the microstructure and the microchemistry of these stainless steels such that strength typically increases while ductility and fracture toughness decrease. Irradiation and the environment also may decrease the resistance of core internal materials to both fatigue crack propagation and stress corrosion cracking. These mechanical property changes are caused by a complex interaction among irradiation, stress, and corrosion. As nuclear power plants age and neutron irradiation dose increases, the degradation of the core internal components becomes more likely. This represents an important safety issue associated with long-term operation of nuclear power plants. The U.S. NRC has been sponsoring research on reactor core internals to (a) define threshold fluence levels above which irradiation begins to affect material properties, (b) develop disposition curves for cyclic fatigue and irradiation assisted stress corrosion cracking (IASCC) growth rates, and (c) assess the significance of void swelling and irradiation stress relaxation/creep on the structural and functional integrity of these components.

The objective of this report is to summarize the current knowledge associated with the effect of the reactor environment and neutron irradiation on the mechanical properties of the reactor core internals and to identify gaps in this knowledge that could affect the long-term performance of these components. Significant gaps should be addressed in future industry- or NRC-sponsored research. This report briefly reviews the results of the existing open literature data (on IASCC, neutron embrittlement, void swelling, and irradiation-induced stress relaxation/creep) that have been published by the NRC, industry, academia, and other research agencies. The report also identifies potential deficiencies or knowledge gaps in the existing experimental data with respect to defining the threshold fluence levels above which irradiation begins to affect material properties; the disposition curves for cyclic fatigue and IASCC growth rates; and the significance of void swelling and irradiation stress relaxation/creep on the structural and functional integrity of these components.

The results of this final report may be used to (i) support evaluation of the acceptability of reactor internal aging management programs in license renewal applications, (ii) support revision of the Generic Aging Lessons Learned (GALL) report, (iii) determine appropriate inspection and flaw disposition procedures for reactor internals for use in developing ASME code and for determining needed conditions within Title 10, Section 50.55a, "Codes and Standards," of the Code of Federal Regulations (10CFR 5055a), and (iv) identify issues related to long-term operation (i.e., greater than 60 years) in nuclear power plants. This report will also be used by the NRC to evaluate the acceptability of planned industry- and NRC-sponsored research to address gaps identified in this report.

Michael Case
Director Division of Engineering
Office of Nuclear Regulatory Research
U.S. Nuclear Regulatory Commission

This page is intentionally left blank.

# Contents

Abstract ..... iii

Foreword ..... v

Contents ..... vii

Figures ..... ix

Tables ..... xiii

Executive Summary ..... xv

Acknowledgments ..... xxiii

Acronyms and Abbreviations ..... xxv

Symbols ..... xxvii

1 Introduction ..... 1

2 Irradiation Assisted Stress Corrosion Cracking ..... 3

2.1 IASSCC Susceptibility ..... 3

2.1.1 Microstructure ..... 6

2.1.2 Microchemistry ..... 9

2.1.3 Radiation Hardening ..... 12

2.1.4 Tensile Properties ..... 14

2.1.5 Yield Strength ..... 22

2.1.6 Corrosion Potential ..... 24

2.1.7 Silicon Segregation ..... 26

2.1.8 Sulfur Content ..... 28

2.1.9 Stacking Fault Energy ..... 29

2.1.10 LWR vs. Fast Reactor Irradiations ..... 31

2.2 Crack Growth Rates ..... 31

2.2.1 Quality of Crack Growth Rate Data ..... 33

2.2.2 Stress Corrosion Cracking Growth Rates ..... 40

2.2.3 Fatigue Crack Growth Rates ..... 53

2.3 Initiation of Irradiation-Assisted Stress Corrosion Cracking ..... 57

3 Neutron Embrittlement ..... 63

3.1 Fracture Toughness of Irradiated Austenitic Stainless Steels ..... 64

3.1.1 Fracture Toughness $J_{Ic}$ ..... 65

3.1.2 Fracture Toughness J-R Curve ..... 67

3.2 Fracture Toughness Trend Curve ..... 72

3.3 Synergistic Effect of Thermal and Neutron Irradiation ..... 76

4. Void Swelling ..... 81

4.1 Background Information ..... 81

4.2 Assessment of Void Swelling in PWR Core Internal Components ..... 84

4.3 Embrittlement due to Void Swelling ..... 87

5. Stress Relaxation and Creep ..... 89

6. Summary ..... 93

6.1 Susceptibility to IASCC ..... 93

6.2 IASCC Growth Rates ..... 96

6.3 Fatigue Crack Growth Rates ..... 98

6.4 IASCC Initiation ..... 99

6.5 Neutron Embrittlement ..... 100

6.6 Synergistic Effects of Thermal and Neutron Embrittlement ..... 102

6.7 Void Swelling ..... 102

6.8 Irradiation Creep Relaxation ..... 103

7. Gaps in Available Data ..... 105

References ..... 109

## Figures

1. The effect of fast neutron fluence and average water conductivity on susceptibility of austenitic stainless steels to IASCC shown in field correlations of the core component cracking. ..... 3

2. Dependence of IASCC susceptibility of austenitic stainless steels on fast neutron fluence and corrosion potential as measured from SSRT tests in 288°C water. ..... 4

3. Susceptibility of irradiated austenitic SSs to IGSCC as a function of fluence in high-dissolved-oxygen water. ..... 4

4. Schematic illustrating mechanistic issues that influence IASCC in austenitic stainless steels... 5

5. The change in density and size of interstitial loops as a function of irradiation dose during LWR irradiation at 275-290°C. ..... 7

6. Results from the BOR-60 irradiation experiment with the data for austenitic stainless steels irradiated in a BWR. ..... 8

7. Radiation-induced grain boundary Cr and Si concentration in 300-series stainless steels irradiated in LWRs at 275-290°C. ..... 10

8. Dependence of grain boundary Cr concentration for several 300-series austenitic stainless steels irradiated at about 300°C on neutron dose. ..... 10

9. Comparison of radiation-induced segregation of Cr, Ni, andSi in LWR and BOR-60 fast reactor irradiated stainless steels. ..... 11

10. Engineering stress-strain curves at 289°C for Type 304 SS and Type 316 SS steel irradiated up to 3 dpa in the Halden reactor at 289°C. ..... 12

11. The effects of neutron dose on measured tensile yield strength of 300-series stainless steels, irradiated and tested at about 300°C. ..... 13

12. Effect of irradiation temperature on the yield strength and uniform elongation of CW Type 316 stainless steel irradiated in fast reactors at temperatures between 290-500°C and tested at the irradiation temperature. ..... 13

13. Change in yield strength, ultimate tensile strength, uniform elongation, and total elongation as a function of neutron dose for solution annealed Type 304, 304L, and 347 stainless steels at elevated temperature. ..... 15

14. Change in yield strength, ultimate tensile strength, uniform elongation, and total elongation as a function of neutron dose for CW Type 316 stainless steel at elevated temperature..... 17

15. Change in yield strength, ultimate tensile strength, uniform elongation, and total elongation as a function of neutron dose for Type 308 and 309 weld metal, Type 304 HAZ, and CF-8 cast stainless steel at elevated temperature..... 19

16. Effect of yield strength and martensite content on the SCC growth rate of stainless steels and Alloy 600 at 288°C in high-purity water containing 2000 ppb $O_2$ and 95 or 1580 ppb $H_2$..... 22

17. Crack growth rates of nonirradiated, cold worked, 300-series austenitic SSs in NWC BWR environment as a function of yield strength. ..... 23

18. Change in SCC growth rates of nonirradiated, sensitized and nonsensitized, stainless steels as a function of yield strength in NWC BWR environment at 289°C and PWR environment at 340°C. ..... 23

19. Change in SCC growth rates at 289°C of LWR-irradiated austenitic stainless steels as a function of yield strength in NWC and HWC BWR environments..... 23

20. Effect of yield strength on percent IGSCC in SSRT tests on irradiated 300-series stainless steels in high-DO water. ..... 24

21. Experimental CGR under constant load in NWC and HWC BWR environments at 288°C for austenitic stainless steels irradiated to 1.0-2.5 dpa, 3.0-4.0 dpa, and 13 dpa, plotted as a function of the steel ECP versus a standard hydrogen electrode. ..... 25

22. Crack growth rates versus Si concentration in custom heats of Type 304L stainless steel simulating expected grain boundary microchemistries for high and low corrosion potentials and at various stress intensity factors..... 27

23. Effect of bulk S content on IASCC susceptibility of commercial heats of Type 304, 304L, 316, and 316L tested in high DO water at 289°C. ..... 29

24. Range of bulk S and C contents, in which Type 304 or 316 stainless steels are resistant or susceptible to IASCC, in BWR-like oxidizing water. ..... 29

25. Range of bulk S and C contents, in which Type 304, 316, 321, or 348 stainless steels are resistant or susceptible to IASCC, in PWR water..... 30

26. IASCC susceptibility as measured by percent IG cracking as a function of stacking fault energy..... 30

27. Comparison of the measured yield strength and uniform elongation for several heats of Type 304 and 304L stainless steels irradiated in the Halden reactor at 290°C to 3 dpa and in BOR-60 fast breeder reactor at 320°C to 4.8 dpa. ..... 32

28. Plot of CGR in water vs. CGR in air showing environmental enhancement of growth rates in high-purity water at 289°C. ..... 34

29. Plot of crack length vs. time for irradiated Type 304 stainless steel in high-purity water at 289°C. ..... 35

30. Engineering stress vs. strain curve for Type 304 stainless steel irradiated to 3.0 dpa and tested in air at 289 and 325°C. ..... 37

31. Strain distribution of a moving crack in a strain-softening and a strain-hardening material. ..... 37

32. Crack growth rates for irradiated stainless steels in BWR environments under loading conditions that meet or exceed the proposed K/size criterion. ..... 38

33. Crack length and K vs. time for Type 304L SS in high-purity water at 289°C. ..... 38

34. Side view of the first slice cut from Type 304L SS Specimen C3-C. ..... 39

35. Experimental SCC growth rates in NWC BWR environment of austenitic stainless steels irradiated to 0.75-3.0 dpa, 0.7-4.25 dpa and 5.5-37.5 dpa. ..... 41

36. SCC growth rates in HWC BWR environment of austenitic stainless steels irradiated to 0.75-3.0 dpa, 0.7-4.25 dpa, and 5.5-37.5 dpa. ..... 43

37. CGR under constant load for thermally aged and irradiated CF-8M cast stainless steel specimens in BWR environment at 289°C. ..... 45

38. Crack growth rates of irradiated austenitic stainless steels in NWC and HWC BWR environments at 288°C and K of 20 MPa $m^{1/2}$ plotted as a function of neutron dose. ..... 47

39. Crack growth rates of irradiated austenitic stainless steels in NWC and HWC BWR environments at 288°C and K of 20 MPa $m^{1/2}$ plotted as a function of yield stress. ..... 48

40. SCC growth rates of austenitic stainless steels irradiated to 3.0-37.8 dpa in PWR environment. ..... 49

41. Temperature dependence of SCC growth rates in irradiated CW Type 316+Ti stainless steel in PWR environment. ..... 50

42. Normalized SCC growth rates in PWR environment for austenitic stainless steels irradiated to 3 dpa, 11-25 dpa, and 6-38 dpa. ..... 50

43. Normalized SCC growth rates of austenitic stainless steels irradiated to 0.7-4.25 dpa in HWC BWR and PWR environments at 288°C. ..... 52

44. Crack growth rates for irradiated austenitic stainless steels in HWC BWR water at 288°C or PWR environment at 320°C plotted as a function of neutron dose. ..... 52

45. CGR data under cyclic loading for irradiated SS weld HAZ materials in air at 289°C. ..... 54

46. CGR for irradiated specimens of austenitic SSs under continuous cycling at 289°C in high-purity water with ≈300 ppb and <30 ppb dissolved oxygen. ..... 55

47. CGR data under cyclic loading for nonirradiated SS weld HAZ materials in high-purity water at 289°C. ..... 56

48. CGR for irradiated specimens of Type 304L SA weld HAZ from the Grand Gulf core shroud and laboratory-prepared Type 304 SS SMA weld HAZ under continuous cycling in high-purity water at 289°C. ..... 56

49. CGR data under cyclic loading for two irradiated specimens of CF-8M cast austenitic SS in high-purity water at 289°C. ..... 57

50. Stress as percent of irradiated yield stress vs. time data for IASCC flaw initiation in austenitic stainless steels in a PWR environment. ..... 58

51. Stress as percent of irradiated yield stress vs. neutron dose for IASCC flaw initiation in austenitic stainless steels in a PWR environment. ..... 59

52. Percent of irradiated yield stress vs. time for IASCC flaw initiation in a PWR environment, in an austenitic stainless steel irradiated to 71-76 dpa. ..... 59

53. Time for initiation of IASCC in irradiated austenitic stainless steels as a function of stress. ..... 60

54. Change in fracture toughness $J_{Ic}$ as a function of neutron exposure for austenitic SSs irradiated in fast reactors. ..... 66

55. Change in fracture toughness $J_{Ic}$ as a function of neutron exposure for irradiated austenitic SSs. ..... 67

56. Change in fracture toughness $J_{Ic}$ as a function of neutron exposure for SSs. ..... 68

57. Fracture toughness J-R curves for sensitized Type 304 SS, weld HAZ materials of Type 304 and 304L SS, and CF-8M cast SS in high-purity water at 289°C. ..... 69

58. Fracture toughness J-R curves for irradiated specimens of Type 304 SS SMA weld HAZ and Type 304L SA weld HAZ in air and NWC BWR environment. ..... 70

59. Fracture toughness J-R curves for sensitized Type 304 SS in air and NWC BWR water at 289°C. ..... 70

60. Fracture toughness J-R curves and load vs. loadline displacement curves for thermally aged and irradiated CF-8M cast SS. ..... 71

61. Fracture toughness $J_{Ic}$ of irradiated austenitic stainless steels and welds as a function of test temperature. ..... 71

62. The change in initiation toughness $J_{Ic}$ of wrought austenitic SSs and cast austenitic SSs and weld metals as a function of neutron exposure. ..... 72

63. Change in coefficient C of the power-law J-R curve for wrought austenitic SSs and cast austenitic SSs and weld metals as a function of neutron exposure. ..... 75

64. Experimental values of J-integral at a crack extension of 2.5 mm for wrought austenitic SSs and cast austenitic SSs and weld metals plotted as a function of neutron exposure. ..... 78

65. Void swelling of PWR materials plotted as a function of neutron dose. ..... 84

66. Irradiation temperature and neutron dose for the void swelling data shown in Fig. 65. ..... 84

67. Void swelling of PWR materials plotted as a function of effective full power years. ..... 86

68. Thermal creep and irradiation-enhanced creep of a 20% CW Type 316 stainless steel irradiated in EBR-II. ..... 90

69. Trend line for screening irradiation-induced stress relaxation based on available test data. ..... 91

## Tables

1. Material property equations for irradiated CW Type 316 stainless steel. ..... 14

2. Material property equations for irradiated solution-annealed Type 304 stainless steel. ..... 14

3. Material property equations for solution-annealed and nonirradiated Type 304 stainless steel. 21

4. Screening criteria for thermal-aging susceptibility of cast austenitic stainless steels. ..... 77

5. Fatigue CGR correlations for wrought and cast austenitic stainless steels in BWR environments at 289°C. ..... 99

6. Data gaps in the current understanding of irradiation effects on LWR core internal materials. . 108

This page is intentionally left blank.

# Executive Summary

### Background

Austenitic stainless steels (SSs) are used extensively as structural alloys in the internal components of light water reactor (LWR) pressure vessels because of their relatively high strength, ductility, and fracture toughness. However, exposure to neutron irradiation for extended periods changes the microstructure (radiation hardening) and microchemistry (radiation-induced segregation or RIS) of these steels and degrades their fracture properties. This report addresses the concerns arising from irradiation-induced materials issues such as irradiation-assisted stress corrosion cracking (IASCC), neutron embrittlement, void swelling, and irradiation-induced stress relaxation. The existing data have been reviewed to identify the key material and environmental parameters that influence these processes and to determine their effects. The results are used to (a) define a threshold fluence above which irradiation effects on materials properties are significant, (b) develop disposition curves for cyclic and IASCC growth rates for reactor core internal materials, and (c) assess the significance of void swelling and irradiation creep relaxation on the structural and functional integrity of reactor internal components. This report also identifies potential deficiencies or knowledge gaps in the existing experimental data on degradation of LWR core internal materials due to neutron irradiation.

### Susceptibility to IASCC

Neutron irradiation of austenitic SSs can produce damage by displacing atoms from their lattice position, which creates point defects such as vacancies and interstitials. Most of these defects are annihilated by recombination. The surviving defects rearrange into more stable configurations such as dislocation loops, network dislocations, precipitates, and cavities (or voids). Changes in the microstructure of austenitic SSs due to neutron irradiation vary with the material composition, irradiation temperature, and neutron fluence, flux, and energy spectrum. At temperatures below 300°C, the material microstructure primarily consists of "black spot" defect clusters and faulted dislocation loops, whereas large faulted loops, network dislocations, cavities/voids (clusters of vacancies and/or gas bubbles), and precipitates are observed above 300°C. At LWR operating temperatures, the loop density saturates at about 1 dpa, and the average loop diameter saturates at 5 dpa. The loop size increases and loop density decreases with irradiation temperature. Cavities and voids form at high doses and high temperatures. High irradiation temperatures (above 350°C) also lead to the formation of second phase particles. Metal carbides are the primary stable precipitates in 300-series SSs under LWR conditions, although RIS of Ni and Si to sinks may lead to the formation of γ' phase ($Ni_3Si$) and G phase ($M_6Ni_{16}Si_7$).

The microchemistry of the material is also changed due to RIS. Elements such as Si, P, and Ni are enriched at regions such as grain boundaries that act as sinks for point defects, while Cr, Mo, and Fe are depleted. The extent of RIS depends on the rate of generation and recombination of point defects (i.e., irradiation temperature and dose rate). At LWR temperatures, significant segregation is observed at an irradiation dose of 0.1 dpa, and the effect either saturates or changes very slowly beyond 5 dpa.

The point defect clusters and precipitates act, to varying extent, as obstacles to a dislocation motion that leads to matrix strengthening, resulting in an increase in tensile strength and a reduction in ductility and fracture toughness of the material. The yield strength of irradiated SSs can increase up to five times that of the nonirradiated material after a neutron dose of about 5 dpa. In general, cavities (or voids) are strong barriers, large faulted Frank loops are intermediate barriers, and small loops and bubbles are weak barriers to dislocation motion. For austenitic SSs, the greatest increase in yield strength for a given

irradiation level occurs at irradiation temperatures near 300°C (572°F), which is in the temperature range of LWR operation. The change in yield strength correlates well with the microstructural changes. The yield strength also either saturates or increases very slowly above 5 dpa. Nearly all SSs exhibit strain softening (also termed "dislocation channeling") and little or no uniform elongation at irradiation dose above 5 dpa. The enhanced planar slip leads to a pronounced degradation in the fracture toughness of austenitic SSs.

The significance of material yield strength on IASCC susceptibility, particularly in the LWR environments, is discussed. Data on stress corrosion cracking (SCC) susceptibility indicate that nonsensitized SSs with high tensile strength are susceptible to SCC in ultra-high purity water. The increases in yield strength can originate from surface or bulk cold work, weld shrinkage strain, and precipitation or irradiation hardening; all of these increase SCC susceptibility. At a given yield strength below 800 MPa, a similar cracking behavior is observed for different grades of SSs, although the crack growth rates (CGRs) in low-potential water [less than 50 ppb dissolved oxygen (DO)] are up to an order of magnitude lower. However, at yield strengths of 800 MPa or higher, the CGRs in low- and high-potential environments are also comparable. The significance of Si segregation at grain boundaries, S content in the steel, or stacking fault energy of the material is also discussed.

Correlations, developed by the Materials Reliability Program (MRP), are presented for estimating tensile yield and ultimate strengths and uniform and total elongation of austenitic SSs as a function of neutron dose. The tensile properties reach saturation at 5-20 dpa and do not seem to change significantly at higher dose levels. However, the majority of the data have been obtained on materials irradiated in fast neutron reactors (e.g., EBR-II in the U.S. or BOR-60 in Russia), which use fast neutrons to burn more uranium-238 than conventional LWRs. Data on LWR-irradiated materials are more limited, in particular above 10 dpa. The available data indicate that the yield and ultimate strengths of the LWR-irradiated materials are typically higher, and uniform and total elongations are lower, than those of materials irradiated in fast reactors.

**IASCC Initiation**

The existing IASCC initiation data have been reviewed to evaluate the adequacy of the database for developing screening criteria for IASCC susceptibility of core internal components in pressurized water reactors (PWRs). The screening criteria are defined for a given neutron fluence above a threshold value (i.e., 3 dpa), an apparent stress threshold below which IASCC will not occur in a PWR environment. The fluence threshold of 3 dpa that has been established by the nuclear industry is based on incidents of IASCC failures in operating PWRs and on results from slow strain rate tensile tests in the PWR environment. The stress thresholds are defined from IASCC initiation data. However, the database used for defining neutron dose/applied stress thresholds for austenitic SSs is inadequate to evaluate variability among different grades of SSs, or the differences among solution-annealed or cold-worked materials, or the effect of irradiation temperature. Most of the data are on cold-worked Type 316 SS irradiated at temperatures below 310°C. Also, although the fluence threshold for IASCC is defined as 3 dpa, there are no IASCC initiation data on materials irradiated below 10 dpa. Furthermore, in reactor core internal components, IASCC is likely to occur under creviced conditions (i.e., under off-normal water chemistry).

**IASCC Growth Rates**

Irradiation-assisted stress corrosion cracking is a complex phenomenon that is dependent on several parameters, which interact with each other such that their effect on growth rates is not always the same. As a result of these complexities and uncertainties in experimental measurements, the SCC growth rate data in LWR environments show significant variability, and specific effects of these parameters on

growth rates cannot be accurately assessed under all conditions of interest. Crack growth rate data on irradiated wrought and cast austenitic SSs as well as SS weld metal and weld heat-affected zone (HAZ) materials in LWR environments have been compiled and evaluated to define the threshold fluence for IASCC and to develop disposition curves for cyclic and IASCC growth rates for reactor core internal materials. The importance of test procedures that closely reproduce the loading and environment conditions for reactor core internal components and provide accurate measurements and reproducible results is discussed.

The results indicate that, in the normal water chemistry (NWC) of boiling water reactors (BWRs) environment, neutron irradiation up to 0.45 dpa ($3 \times 10^{20}$ n/cm$^2$) has no effect on CGRs. Additionally, the rates are below the NUREG-0313 disposition curve for nonirradiated materials in high-purity water containing 8 ppm DO. The CGRs for materials irradiated to higher neutron dose levels can be up to a factor of 40 higher. The CGRs for some SSs irradiated to 5-8 dpa (corresponding to a 60-year end-of-life neutron dose for BWRs) are a factor of 20 higher than the NUREG-0313 curve and 2-3 higher than the Electric Power Research Institute (EPRI) disposition curve for BWR core internal components. The CGR data for highly irradiated materials show anomalous behavior. The SCC growth rates, in an NWC BWR environment, for SSs irradiated to 19 or 38 dpa are below the NUREG-0313 disposition curve for nonirradiated SSs. The reason for the low CGRs observed for these highly irradiated materials in the high-potential BWR environment is currently unknown. However, both materials came from the same reactor - a decommissioned PWR. It is possible that this behavior is unique to the materials from this reactor, but their microstructural and microchemistry characterization is not available in the open literature.

The SCC growth rates in the hydrogen water chemistry (HWC) BWR environment show a significant decrease relative to those in the NWC BWR environment for SSs irradiated to less than 3 dpa; little or no reduction for some SSs irradiated to dose levels as low as 3-4 dpa, at least at stress intensity factor (K) values above 18 MPa m$^{1/2}$; and no decrease for all SSs irradiated to 12-14.5 dpa. The CGRs for some materials irradiated to 3-4 dpa are above the CGR disposition curve proposed by EPRI for the HWC BWR environment. However, these results are often screened out because they marginally exceeded the proposed K/size criterion for irradiated materials, in which the irradiation-induced increase in yield stress is discounted by a factor of 2 or 3. However, several investigations on the validity of the proposed K/size criterion do not support a criterion based on an effective yield stress rather than the measured yield stress. Additional CGR data on SSs irradiated to 3-8 dpa are needed to accurately establish the threshold for IASCC susceptibility in low-potential environments.

The SCC growth rates in PWR environment show significant variability. The CGRs for the same material and irradiation condition increase with increasing temperature. The temperature dependence of growth rates may be represented by an activation energy of 100 kJ/mol. In PWR water at 320°C, most of the CGR data for SSs irradiated to 3 dpa are up to a factor of 5 above the NUREG-0313 curve for nonirradiated materials, and those for SSs irradiated to 11 dpa (and SSs irradiated in the BOR-60 reactor to 25 dpa) are up to two orders of magnitude above the same curve. Also, as observed earlier for HWC BWR water, the CGRs in the PWR environment of SSs irradiated to 19 or 38 dpa exhibit anomalous behavior as the rates are below the NUREG-0313 curve for nonirradiated SSs. As discussed above, while the reason for these low rates is unknown, both materials came from the same reactor. Additional data on PWR materials irradiated at different temperatures (e.g., between 300 and 350°C) are needed to better understand the IASCC susceptibility of austenitic SSs in PWR environments.

**Fatigue Crack Growth Rates**

Limited fatigue CGR data in air on austenitic SSs irradiated to 2 dpa under LWR irradiation conditions indicate little or no effect of neutron irradiation on growth rates. Additional results on SSs irradiated in fast reactors at 427°C show only slightly higher CGRs (up to a factor of two higher) at low $\Delta K$ values (less than 44 MPa $m^{1/2}$). Also, tests on Type 304 and 316 SS irradiated in a thermal reactor at 288°C to 2.7 dpa and tested at 427°C showed superior resistance to crack growth; crack growth rates were 25 to 50% lower than those for nonirradiated materials.

In the NWC BWR environment, the cyclic CGRs of SSs irradiated to 0.45 dpa ($3 \times 10^{20}$ n/cm$^2$) are the same as those for nonirradiated materials, whereas the CGRs of SSs irradiated to 0.75-3.0 dpa are higher. The cyclic CGRs at low frequencies (i.e., rise times ≥10 s) are lower by more than an order of magnitude when the DO level is decreased by changing from NWC to HWC. A superposition model has been used to represent the cyclic CGRs of austenitic SSs. The CGR in reactor coolant environment is expressed as the superposition of the rate in air (mechanical fatigue) and the rates due to corrosion fatigue and SCC. Studies at Argonne National Laboratory (NUREG/CR-6960) indicate that the superposition model generally provides the best estimate, or slightly conservative estimates, of fatigue CGRs in NWC and HWC BWR environments. The results indicate that for irradiated materials, the higher fatigue CGRs at long rise times (i.e., low frequencies) are primarily due to the SCC component of crack growth.

Fatigue CGR data are not available for austenitic SSs irradiated to higher neutron dose levels in the BWR environments or on irradiated austenitic SSs in the PWR environment. Additional fatigue crack growth data under these material and environmental conditions are needed to develop fatigue CGR correlations for BWR and PWR core internal components.

**Neutron Embrittlement**

The fracture toughness of austenitic SSs has been divided into three broad categories. The fracture toughness ($J_{Ic}$) is above 150 kJ/cm$^2$ for Category III materials, and 30-150 kJ/cm$^2$ for Category II materials. These materials fracture after stable crack extension at stresses well above or close to the yield stress. Category I materials fracture at stress levels well below the yield stress by unstable crack extension, and their fracture toughness, as characterized with the critical stress intensity factor ($K_{Ic}$), is less than 75 MPa $m^{1/2}$. Nonirradiated wrought and cast austenitic SSs and their welds typically fall in Category III. However, neutron irradiation degrades the fracture toughness of austenitic SSs to the level of Category II or even I at high dose levels.

Fracture toughness data on irradiated wrought and cast austenitic SSs and their welds have been compiled and evaluated to define the threshold neutron dose above which fracture toughness of these materials is reduced significantly. The validity of the fracture toughness J-R curve data and the different methods for determining $J_{Ic}$ are discussed. Comparison of fracture toughness data obtained on different size specimens showed that small specimens yield valid J-R curve data, at least for materials with $J_{Ic}$ below 300 kJ/$m^{1/2}$.

The existing fracture toughness data on austenitic SSs irradiated in LWRs indicate little or no loss of fracture toughness below an exposure of about 0.5 dpa and a substantial and rapid decrease at exposures of 1-5 dpa. Also, fracture toughness appears to saturate at approximately 10 dpa. A similar trend was observed earlier for austenitic SSs irradiated in high-flux fast reactors at 350-427°C and tested at 300-427°C. However, for the LWR-irradiated materials, the saturation fracture toughness ($K_{Ic}$ or $K_{Jc}$) values are in the range of 36.8-40.3 MPa $m^{1/2}$ (33.5-36.6 ksi $in^{1/2}$), and samples at this toughness

typically fail without stable ductile crack extension. These values are lower than the $K_{Jc}$ of 75 MPa $m^{1/2}$ (68.2 ksi $in.^{1/2}$) observed for fast-reactor-irradiated materials.

Most of the fracture toughness data on LWR-irradiated austenitic SSs have been obtained on Type 304 and 304L SSs. Similar data on SS welds, cast SSs, or weld HAZ materials are limited. The available data indicate that for the same irradiation conditions, the fracture toughness of thermally aged cast SS and weld metal is lower than that of HAZ material, which, in turn, is lower than that of solution-annealed materials. Available data indicate a strong orientation effect on fracture toughness; fracture toughness in the T-L orientation* is significantly lower than that in the L-T orientation. Also, several fracture toughness J-R curve tests on Type 304 SS control-rod blade material irradiated to 4.5-5.5 dpa showed no ductile crack extension. Potential effects of the coolant environment and crack morphology on fracture toughness of irradiated SSs are discussed. The available data are inadequate to establish accurately the effects of the irradiation temperature on the fracture toughness of austenitic SSs.

The existing fracture toughness data have been evaluated to develop a fracture toughness trend curve that includes (a) a threshold neutron exposure for radiation embrittlement of austenitic SSs and a minimum fracture toughness for these materials irradiated to less than the threshold value, (b) a saturation neutron exposure and a saturation fracture toughness for materials irradiated to greater than this value, and (c) a description of the change in fracture toughness between the threshold and saturation neutron exposures. However, a review of the existing data indicated very limited data on (a) materials irradiated in LWRs to neutron dose levels of 0.1-1.0 dpa or above 10 dpa and (b) LWR-irradiated cast austenitic SSs and welds. The contribution of additional precipitate phases, voids, and cavities on the fracture toughness of these materials is not accurately known.

**Synergistic Effects of Thermal and Neutron Embrittlement**

Cast and welded austenitic SSs have a duplex structure consisting of austenite and ferrite phases, and are susceptible to thermal embrittlement during service at LWR operating temperatures. Formation of the Cr-rich $\alpha'$ phase in the ferrite is the primary mechanism for thermal embrittlement of these materials; thermal aging has no effect on the austenite phase. Embrittlement of the austenite phase from neutron irradiation under LWR operating conditions occurs at dose levels above 0.5 dpa, and that of the ferrite phase occurs at lower dose levels (above 0.07 dpa). However, for reactor core internal components, concurrent exposure to neutron irradiation can result in a synergistic effect wherein the service-degraded fracture toughness can be less than that predicted for either thermal embrittlement or neutron irradiation embrittlement independently. The available fracture toughness data are inadequate to evaluate the synergistic effects of thermal and neutron embrittlement on the threshold dose for embrittlement. Additional data are needed to better establish the potential for synergistic loss of toughness in these materials in the transition dose range from 0.05 to 2 dpa.

**Void Swelling**

Void swelling refers to the volume change of materials under neutron irradiation. Volume changes can produce dimensional distortions and misfits in reactor internal components, particularly when coupled with irradiation creep, which can compromise the functional integrity of the components. Microscopic voids, developed from vacancy coalescence, give rise to this geometry instability, with important consequences on the strength and resistance to failure of these materials. The void swelling process is

*The first letter represents the direction perpendicular to the plane of the crack and the second letter represents the direction of crack advance. L = longitudinal or rolling direction and T = transverse direction.

divided into two regimes: a transient regime followed by a steady-state swelling rate. As demonstrated by Garner and coworkers, austenitic SSs irradiated in fast reactors at temperatures above 427°C eventually reach a steady-state swelling rate of ~1%/dpa. Additionally, available fast reactor data indicate that the steady-state swelling rate could eventually be attained in PWR internal materials during extended operation. The time to reach the steady-state rate (i.e., the transient regime) depends on the material composition and thermo-mechanical condition, stress state, neutron flux and spectrum, or irradiation temperature (above 300°C).

The existing data have been reviewed and analyzed to assess void swelling in PWR core internal components and to evaluate the effects of key material and environmental parameters. The results indicate that material composition can influence void swelling. In the 300-series SSs, void swelling decreases with increasing Ni, P, or Si contents. However, radiation-induced precipitation of second phase particles can remove Ni, P, and Si from the alloy matrix and thereby increase void swelling. In addition, cold work prolongs the transient regime for void swelling in austenitic SSs. Void swelling in austenitic SSs is typically observed at irradiation temperatures above 340°C (644°F), and shows a strong dependence on temperature. The low temperatures, typical of LWRs, extend the transient regime to much longer times. Nonetheless, depending on the irradiation temperature, dose, and dose rate, voids can form under PWR operating conditions within the reactor lifetime. Available data obtained in fast reactors at 373-444°C and displacement rates of 0.3-10.0 x $10^{-7}$ dpa/s suggest that under comparable irradiation temperatures and neutron dose levels, the lower displacement rates typical of PWRs would result in higher swelling. The effects of applied or swelling-induced stress on void swelling, including the interaction of swelling and irradiation creep relaxation, are discussed.

This section also describes the stress-free swelling rate equations, including the incremental stress-enhanced swelling, developed by the MRP for solution-annealed Type 304 and cold-worked Type 316 SSs. The stress-free swelling rate in PWR core internal components is expressed in terms of the irradiation temperature, neutron dose, and dose rate. The incremental stress-enhanced swelling is expressed in terms of the stress-free rate and the Von Mises effective stress. The results indicate that void swelling for an annealed Type 304 SS former plate at an average temperature of 355°C could be above 5% after 50 effective full power years.

Embrittlement of the material due to voids is also discussed. Typically, austenitic SSs with ≥10% void swelling suffer from severe embrittlement, particularly at room temperature. This behavior has been attributed to a second order process, which involves stress concentration between voids, Ni segregation at void surfaces, and a resultant tendency toward martensite formation when the steel is deformed at room temperature. However, there are few quantitative data correlating void swelling with fracture toughness of the material. The embrittlement of austenitic SSs due to void swelling under PWR irradiation conditions should be further investigated.

**Irradiation-Induced Creep Relaxation**

Loss of preload for bolting and springs due to stress relaxation is another aging degradation effect that needs to be addressed to assure the functional integrity of the reactor core internal components. Stress relaxation represents plastic deformation that occurs under constant strain below the yield point of the material. It is caused by either primary creep (thermal stress relaxation) or a flux of high-energy neutrons (irradiation creep). Thermal stress relaxation data have been obtained from short-term tests (less than 1000 h). As discussed in Materials Reliability Program report MRP-175, the percentage of stress relaxation increases with increasing initial stress and saturates at about 207 MPa (30 ksi). At PWR operating temperatures, thermal stress relaxation saturates within 100 h with a maximum decrease of 10-

20% of the initial preload stress depending on the thermal-mechanical treatment of the material. For PWRs, plastic strains resulting from thermal stress relaxation were considered to be insignificant and not a concern for the dimensional change of core internal components. However, neutron-irradiation-enhanced creep at PWR temperatures can greatly increase the plastic strain by increasing both the transient creep and steady-state creep rates. Empirical models have been developed for irradiation creep based on data obtained from fast reactors. The results have been used to develop expression for estimating stress relaxation as a function of initial stress and neutron dose.

This page is intentionally left blank.

## Acknowledgments

The author thanks Torill Karlsen, OECD Halden Reactor Project, Halden, Norway; Anders Jenssen, Studsvik Nuclear AB, Sweden; and Raj Pathania, Electric Power Research Institute, for providing the experimental data and for their helpful comments. The author is grateful to Bill Shack, Rob Tregoning, and Sri Rao for their invaluable input and guidance in preparing this report. This work is sponsored by the Office of Nuclear Regulatory Research, U.S. Nuclear Regulatory Commission, under Job Code N6818; Program Manager: Appajosula S. Rao.

This page is intentionally left blank.

## Acronyms and Abbreviations

| | |
|---|---|
| ANL | Argonne National Laboratory |
| ASTM | American Society for Testing and Materials |
| ATEM | Analytical Transmission Electron Microscopy |
| ATR | Advanced Test Reactor |
| BWR | Boiling Water Reactor |
| BWRVIP | Boiling Water Reactor Vessels and Internals Project |
| CGR | Crack Growth Rate |
| CIR | Cooperative IASCC Research |
| CNSR | Chevron Notch Short Rod |
| CT | Compact Tension |
| CTOD | Crack Tip Opening Displacement |
| CW | Cold Worked |
| DC | Direct Current |
| DO | Dissolved Oxygen |
| dpa | Displacements per Atom |
| ECP | Electrochemical Potential |
| EFPY | Effective Full Power Year |
| EPFM | Elastic-Plastic Fracture Mechanics |
| EPRI | Electric Power Research Institute |
| FFTF | Fast Flux Test Facility |
| GE | General Electric |
| GG | Grand Gulf |
| GTA | Gas Tungsten Arc |
| HAZ | Heat-Affected Zone |
| HWC | Hydrogen Water Chemistry |
| IASCC | Irradiation-Assisted Stress Corrosion Cracking |
| IG | Intergranular |
| IGSCC | Intergranular Stress Corrosion Cracking |
| JAPEIC | Japan Power Electric Engineering and Inspection Corp. |
| J-R | J Integral Resistance |
| LEFM | Linear-Elastic Fracture Mechanics |
| LWR | Light Water Reactor |
| MRP | Materials Reliability Program |
| NDT | Nil-Ductility Transition |
| NRC | Nuclear Regulatory Commission |
| NWC | Normal Water Chemistry |
| PWR | Pressurized Water Reactor |

| | |
|---|---|
| RIS | Radiation-Induced Segregation |
| SA | Submerged Arc |
| SCC | Stress Corrosion Cracking |
| SE(B) | Single Edge Bend |
| SFE | Stacking Fault Energy |
| SFT | Stacking Fault Tetrahedra |
| SHE | Standard Hydrogen Electrode |
| SIA | Self-Interstitial Atom |
| SMA | Shielded Metal Arc |
| SR | Swelling Rate |
| SS | Stainless Steel |
| SSRT | Slow Strain Rate Tensile |
| TG | Transgranular |
| UE | Uniform Elongation |
| UHP | Ultra High Purity |
| YS | Yield Strength |

## Symbols

| | |
|---|---|
| $a$ | Crack length |
| $B$ | Specimen thickness |
| $B_{eff}$ | Effective specimen thickness |
| $C$ | Power-law constant |
| $D$ | Neutron dose |
| $da$ | Increment in crack length |
| $E$ | Elastic modulus |
| $F$ | Neutron fluence |
| $J$ | J integral, a mathematical expression used to characterize the local stress-strain field at the crack tip region (parameter J represents the driving force for crack propagation) |
| $J_{Ic}$ | Value of J near the onset of crack extension |
| $K$ | Stress intensity factor |
| $K_{Ic}$ | Critical stress intensity factor |
| $K_{Jc}$ | Equivalent critical stress intensity factor |
| $K_{max}$ | Maximum stress intensity factor |
| $K_{min}$ | Minimum stress intensity factor |
| $M$ | Constraint factor |
| $R$ | load ratio |
| $S$ | Stress |
| $t$ | Test duration |
| $T$ | Tearing modulus or temperature |
| $t_{eff}$ | Effective time of loading |
| $t_r$ | Rise time |
| $W$ | Specimen width |
| $\phi$ | Neutron dose |
| $\dot{\phi}$ | Dose rate |
| $\bar{\sigma}$ | Von Mises effective stress |
| $\sigma_f$ | Flow stress, defined as the average of yield and ultimate stress |
| $\sigma_u$ | Ultimate stress |
| $\sigma_y$ | Yield stress |
| $\upsilon$ | Poisson ratio |

This page is intentionally left blank.

# 1 Introduction

In light water reactors (LWRs), austenitic stainless steels (SSs) are used extensively as structural alloys in the internal components of reactor pressure vessels because of their relatively high strength, ductility, and fracture toughness. Fracture of these steels occurs by stable tearing at stresses well above the yield stress, and tearing instabilities require extensive plastic deformation. However, exposure to neutron irradiation for extended periods changes the microstructure (radiation hardening) and microchemistry (radiation-induced segregation or RIS) of these steels and degrades their fracture properties.[1-11] Also, neutron irradiation changes the water chemistry (radiolysis). In boiling water reactors (BWRs), neutron irradiation results in an increase in corrosion potential, whereas it has no effect in pressurized water reactors (PWRs) because hydrogen scavenges the radiolysis products and the corrosion potential remains low.[2]

Loss of fracture toughness due to radiation embrittlement was not considered in the design of LWR core internal components constructed of austenitic SSs, but it has been considered in addressing nuclear plant aging and license renewal issues. In addition, irradiation-assisted stress corrosion cracking (IASCC),[1-3,9-16] change in dimensions due to void swelling,[17-20] and stress relaxation due to radiation creep,[21-25] are other aging degradation process that affect LWR core internal components exposed to fast neutron radiation, and need to be considered in addressing plant aging issues.

The objective of this report is to address the concerns arising from irradiation-induced materials issues. The ultimate goal is to help assure the structural and functional integrity of reactor core internals. The report presents a critical assessment of the susceptibility of austenitic SSs to irradiation effects such as IASCC, neutron embrittlement, void swelling, and stress relaxation in PWR environments. The existing data, in the open literature as well as NRC and industry reports, have been evaluated to establish the effects of material parameters (such as composition, thermo-mechanical treatment, microstructure, microchemistry, yield strength, and stacking fault energy) and environmental parameters (such as water chemistry, irradiation temperature, dose, and dose rate) on these processes. Differences in the radiation-induced degradation of material properties between LWR and fast-reactor irradiations are also discussed. The results are used to:

(a) Identify the key material and environmental parameters that influence irradiation-induced degradation of reactor core internal materials.
(b) Provide a better understanding of the threshold fluence above which irradiation effects on IASCC susceptibility and tensile and fracture properties are significant.
(c) Develop disposition curves that describe the cyclic and stress corrosion cracking (SCC) growth rates as a function of stress intensity factor for austenitic SSs and Ni alloys used for reactor core internal components.
(d) Evaluate the potential of radiation embrittlement under BWR and PWR operating conditions, including the synergistic effects of thermal and neutron embrittlement of cast austenitic SSs.
(e) Assess the effects of void swelling, including its effect on fracture toughness.
(f) Investigate the significance of irradiation creep relaxation on the functional integrity of reactor internal components.

This report also identifies potential deficiencies or knowledge gaps in the existing information or technical bases. A research plan is proposed to address the issues related to these knowledge gaps and help the NRC to develop guidelines for the license renewal for plant life up to and beyond 60 years.

This page is intentionally left blank.

# 2 Irradiation Assisted Stress Corrosion Cracking (IASCC)

## 2.1 IASSCC Susceptibility

A major concern regarding the structural and functional integrity of core internal components is the IASCC of austenitic SSs. Several incidents of IASCC have occurred since the mid 1970s in BWR control blade handles and instrumentation tubes, and since the 1990s in BWR core shroud and PWR baffle bolts. As the name implies, IASCC is literally irradiation-assisted enhancement of SCC susceptibility of austenitic SSs. Neutron irradiation increases the susceptibility of austenitic SSs to IASCC by changing the material microstructure due to radiation hardening and also the material microchemistry due to RIS. The IASCC susceptibility of austenitic SSs has been investigated by conducting slow-strain-rate-tensile (SSRT) tests, crack growth rate (CGR) tests, and crack initiation tests on irradiated material in simulated LWR environments. The effects of fast neutron fluence on the IASCC of SSs have been investigated for BWR control blade sheaths[26-28] and in laboratory tests on BWR-irradiated material.[14,29-34] The results indicate that the extent of intergranular stress corrosion cracking (IGSCC) increases with fluence. The factors that influence the IASCC susceptibility of materials include neutron irradiation conditions (e.g., neutron fluence, flux, and energy spectrum), cold work, material composition, corrosion potential, water purity, temperature, and loading conditions. Both plant[26,27] and laboratory data[15] show increased IASCC susceptibility with neutron fluence, corrosion potential, and water conductivity. In BWRs, instrument dry tubes and control blade handles and sheaths, which are typically subject to very low stress, but under creviced conditions, have shown IASCC (Fig. 1a). Also, the frequency of IASCC increases with increasing conductivity of the reactor water (Fig. 1b).

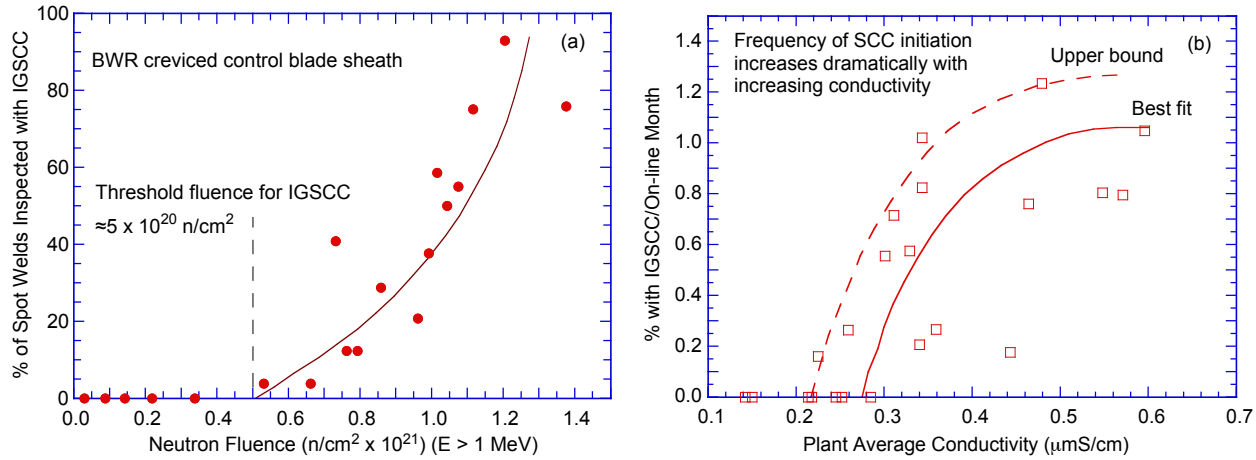


Figure 1. The effect of (a) fast neutron fluence and (b) average water conductivity on susceptibility of austenitic stainless steels to IASCC shown in field correlations of the core component cracking (Refs. 27,26).

Furthermore, radiolysis of water leads to its dissociation into various molecular, ionic, and radical reaction products that interact to form $H_2O_2$, $H_2$, and $O_2$. In BWRs, these species increase the corrosion potential, which is known to increase the susceptibility of SSs to IASCC. The dependence of IASCC susceptibility of austenitic SSs on neutron fluence and corrosion potential is shown in Fig. 2. However, the addition of $H_2$ to the reactor water greatly reduces the effect of radiolysis by scavenging the radiolysis products. For example, the presence of about 500 ppb $H_2$ (5.6 cc/kg) in water can suppress the effect of radiolysis on the corrosion potential in BWRs.[15] Because PWR coolants typically contain 2 ppm $H_2$ (30 cc/kg), radiolysis has no effect on the corrosion potential in PWRs.

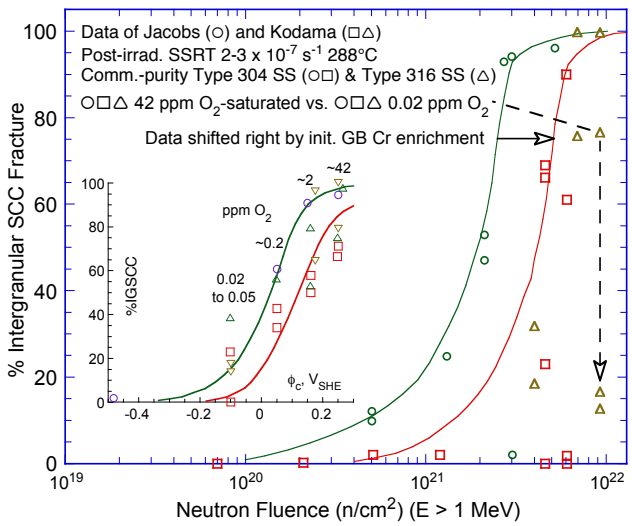


Figure 2.
Dependence of IASCC susceptibility of austenitic stainless steels on fast neutron fluence and corrosion potential as measured from SSRT tests in 288°C water. The inset shows the effect of corrosion potential on %IGSCC (Ref. 15).

Laboratory SSRT data on irradiated austenitic SSs have been used to identify a threshold fluence above which IASCC is significant in austenitic SSs in normal water chemistry (NWC) BWR environments.[14,35] Tests on Types 304 and 347 SS from manual shielded arc weld materials with a heat-affected zone (HAZ) irradiated to 2 x $10^{20}$ n/cm$^2$ (E >1 MeV)* (0.3 dpa) at 290°C show no IGSCC.[36] Also, data on commercial and high-purity austenitic SSs and Alloy 800 irradiated in a BWR between 3 x $10^{20}$ and 9 x $10^{21}$ n/cm$^2$ (0.45-13.5 dpa) show no IASCC below 5 x $10^{20}$ n/cm$^2$ (0.75 dpa) and a rapid increase in IASCC susceptibility above 1 x $10^{21}$ n/cm$^2$ (1.5 dpa).[37] Figure 3 shows a plot of the percent IGSCC measured in irradiated SS specimens as a function of fast neutron fluence. Although a threshold fluence level of 5 x $10^{20}$ n/cm$^2$ (0.75 dpa) has been proposed for austenitic SSs in NWC BWR environments, the results in Fig. 3 suggest a lower threshold for some materials (right triangles). The SSRT data indicate an increase in intergranular (IG) cracking susceptibility in some commercial-purity SSs at fluence levels of about 2 x $10^{20}$ n/cm$^2$ (0.3 dpa) and in high-purity heats of SSs at even lower fluence levels.

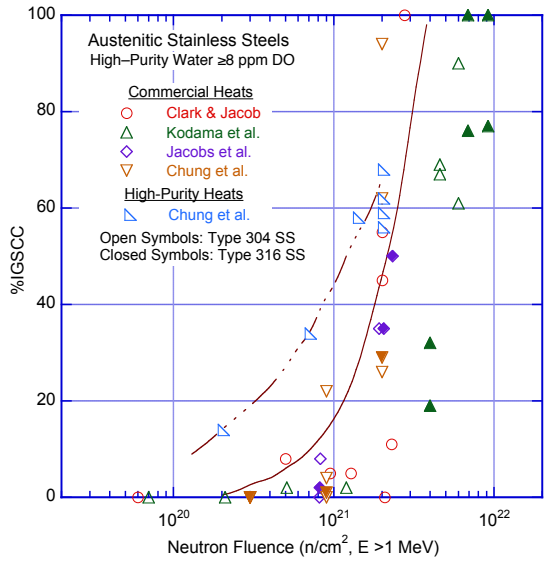


Figure 3.
Susceptibility of irradiated austenitic SSs to IGSCC as a function of fluence in high-dissolved-oxygen water. From slow-strain-rate tensile tests (Refs. 29,31-33).

*All references to fluence levels are calculated for E ≥1 MeV.

The SSRT test data on Type 304 and 316 SS irradiated in commercial BWRs up to 4.0 x $10^{21}$ n/cm$^2$ (6.0 dpa) indicate a beneficial effect of reducing the corrosion potential of the environment.[16,37] A low corrosion potential does not provide immunity to IASCC if the fluence is high enough. For example, IGSCC has been observed in cold-worked (CW), irradiated SS baffle bolts in PWRs. However, threshold fluences for IASCC are higher under low-potential conditions such as BWR hydrogen water chemistry (HWC) or PWR primary water chemistry. The threshold fluences for low-potential environments are not well defined; they could be different for HWC and PWR environments. The SSRT data indicate that threshold fluences also vary with material composition and thermo-mechanical treatment. In general, Type 316 SS is less susceptible than Type 304 SS (i.e., the threshold fluence for IASCC is likely to be lower for Type 304 SS than for Type 316 SS).[37]

It is well known that SCC of materials in high-temperature, high-pressure water depends on three factors: a susceptible material, relatively high stress, and aggressive environment. In the film rupture/slip oxidation model, the fundamental elements of SCC have been described in terms of the processes that occur at the crack tip[14,38-40] and are considered to include: dynamic strain at the crack tip that disrupts the passive film and exposes fresh metal surface, followed by rapid metal oxidation and subsequent surface repassivation. This process can be quantitatively linked to crack advance.[35] The kinetics of repassivation are primarily a function of the local chemistry and material composition, as well as the mass transport processes that establish the local crack tip chemistry.[40] The effect of water chemistry is particularly important because it can change the corrosion reactions at the crack tip. Metallurgical and microstructural parameters are also important because sensitization of the material by thermal treatment or irradiation hardening due to radiation damage can alter the localized deformation and creep processes at the crack tip, thereby changing the film rupture frequency. A schematic illustration of the significant metallurgical, mechanical, and environmental aspects of IASCC is presented in Fig. 4. It shows radiation-induced changes in reactor water chemistry, material microstructure, and grain boundary composition, and the localized deformation processes that impact the crack tip micromechanics that influence IASCC.

A review of the existing data on IASCC susceptibility has identified the following key material and environmental parameters that influence the susceptibility of LWR core internals materials to IASCC.

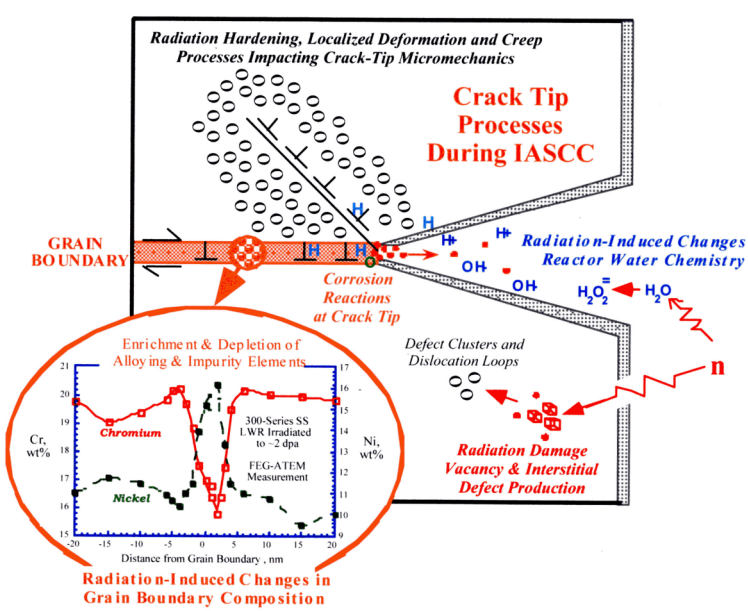


Figure 4.
Schematic illustrating mechanistic issues that influence IASCC in austenitic stainless steels (Ref. 4).

### 2.1.1 Microstructure

Neutron irradiation of austenitic SSs can produce damage by displacing atoms from their lattice position. Irradiation damage is characterized by either the neutron fluence [e.g., neutrons per square centimeter (n/cm$^2$)] or the average number of displacements experienced by each atom, i.e., displacements per atom (dpa).* Each displaced atom creates a vacancy and self-interstitial atom (SIA) pair, known as a Frenkel pair. These defects are unstable, and most of them are annihilated by recombination. The surviving defects rearrange into more stable configurations such as dislocation loops, network dislocations, precipitates, and cavities (or voids), or migrate to sinks such as grain boundaries or surfaces of second phase particles. The production, annihilation, and migration of the point defects lead to changes in the microstructure and microchemistry of the material. Changes in the microstructure of austenitic SSs due to neutron irradiation vary with the material composition and thermo-mechanical treatment and irradiation temperature and dose rate. The effects of material and irradiation conditions on microstructural evolution vary with irradiation temperature.[4] Also, because it affects the recombination rates, increasing temperature reduces embrittlement per dpa and increases swelling per dpa.

Under LWR conditions, the material microstructure produced by irradiation seems to change significantly for irradiation temperatures above 300°C. At LWR operating temperatures (i.e., 275-300°C), the defect structure primarily consists of small "black spot" defect clusters and large dislocation loops. The small defect clusters are less than 4 nm in diameter and consist mostly of interstitial loops and vacancy clusters, which are created from the collapse of damage cascade during irradiation. At higher temperatures (> 300°C) the microstructure contains large faulted loops, network dislocations, and cavities/voids (clusters of vacancies and/or gas bubbles). The large dislocation loops are 4-20 nm in diameter and are primarily faulted interstitial Frank loops that are created from the clustering of self-interstitial atoms.[4] The size of the interstitial loops increases with increasing irradiation dose as more interstitials are absorbed than vacancies. These loops stop growing when vacancies and interstitials are absorbed at the same rate. The saturation size of the interstitial loops depends on the irradiation conditions and material characteristics. The data also indicate that alloying elements can affect the material microstructure during low-temperature irradiations (e.g., P, Ti, and Nb increase the loop density and decrease loop size).[4] Also, precipitates form at higher temperatures and high doses (>20 dpa).[4,41-47]

The change in the density and size of the interstitial loops in austenitic SSs with irradiation dose under LWR conditions at 275-290°C is shown in Fig. 5. Under LWR conditions, the loop density saturates at a relatively low dose (about 1 dpa), and the average loop diameter saturates at about 5 dpa. Cavities or voids have not been reported for SS irradiated under LWR conditions at temperatures below 300°C. The loop size increases and loop density decreases with irradiation temperature. At temperatures of 300-350°C, the microstructure primarily consists of large Frank loops and a network of tangled dislocations that evolve as the larger faults in the Frank loops disappear.[4] Also, cavities and voids form at dose levels above about 20 dpa; they become more important at higher temperatures and higher doses. Typically cavities are associated with precipitates, dislocations, and grain boundaries.

The data on the microstructural evolution in reactor core internal materials irradiated to doses above 10 dpa and at temperatures of 300-350°C are rather limited. The available data indicate that under LWR irradiation conditions at 275-300°C the Frank loop microstructures in Type 304 and 316 SS are similar, and both the Frank loop density and loop size reach a saturation value at 5 dpa. Also, the initial state of the material (i.e., solution annealed or cold worked) does not seem to be important. The initial dislocation

---

*Unless otherwise noted, when neutron dose in dpa was not available, the values of neutron fluence (n/cm$^2$) were converted to dpa as follows: for LWRs, E>1 MeV and $10^{22}$ n/cm$^2$ ≈15 dpa; and for fast reactors, E>0.1 MeV and $10^{22}$ n/cm$^2$ ≈5 dpa.

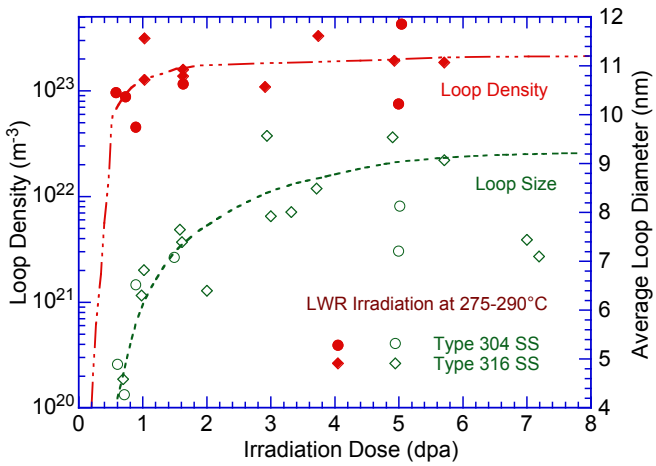


Figure 5.
The change in density and size of interstitial loops as a function of irradiation dose (dpa) during LWR irradiation at 275-290°C (Ref. 4).

structure produced by the cold work is removed by the time a steady-state loop density is achieved and the irradiated microstructure of the CW SSs is similar to that of the solution-annealed SSs.[48] However, although the dislocation microstructure does not change significantly at higher dose levels, cavities, voids, and precipitates are observed in materials irradiated to higher neutron doses.

The Frank loop densities and loop sizes in CW Type 316 SS thimble tube materials irradiated to 33 dpa at 290°C and to 70 dpa at 315°C in a PWR were comparable to the saturation values in Fig. 5.[48] However, a high density of nanocavities (average size less than 3 nm) was observed in both materials, but the density of cavities was slightly higher and their size larger in the higher dose material. There was also some evidence of precipitates in the material irradiated to 70 dpa. The cavities were believed to be He bubbles that form as He accumulates during irradiation from transmutation reactions. Helium can be produced by the $^{10}B$ reaction to form $^{4}He$ and $^{7}Li$, and also from the production of $^{59}Ni$ from $^{58}Ni$ by thermal neutrons. A fine dispersion of He bubbles has also been observed in SSs irradiated at 300°C in reactors with high thermal neutron fluxes.

As noted, some differences in irradiated microstructures are observed in materials irradiated at temperatures above 320°C. The microstructure of a CW Type 316 SS baffle bolt from the Tihange 1 plant was characterized at three positions (1, 25, and 55 mm).[18] Although the loop densities were similar at all three positions, the size distribution at higher temperature (330-343°C) and lower flux at the 25- and 55-mm positions along the shank of the bolt shifted to larger sizes compared to that at the 1-mm position near the bolt head, which has the lowest temperature (320°C) and highest flux. The total dose at the three positions decreased from 19.2 dpa at the 1-mm position to 13.2 and 8.7 dpa at the 25- and 55-mm positions, respectively. Also, precipitates and cavities were found at all positions, but their density and size varied considerably. The cavities observed at the 1-mm position were less than 2 nm and not distributed homogenously throughout the matrix. The cavities observed at the 25- and 55-mm positions were faceted, indicating that they were voids and not He bubbles, and the average size was about 8 nm. The precipitates at the 25-mm position were identified as γ'phase.

Irradiation at temperatures above 320°C also leads to the formation of second phase particles. Such radiation-induced precipitates are similar to those that form during thermal aging and depend on material composition, thermo-mechanical treatment, and radiation conditions (neutron dose, temperature, and spectrum). Radiation can either enhance or retard the formation of some phases (e.g., Laves, σ and χ intermetallics, and MC, $M_{23}C_6$, and $M_6C$ carbides) and modify the composition of $M_6C$ and Laves phases.[42,43] The radiation-induced phases include γ' silicide ($Ni_3Si$), phosphides ($M_2P$ and $M_3P$), and G phase ($M_6Ni_{16}Si_7$). However, most of these observations are based on fast reactor irradiations at

temperatures above 350°C, and data obtained on materials irradiated under LWR irradiation conditions at 320-350°C are limited. The existing data suggest that radiation-induced precipitation is not a concern for LWRs at temperatures below 350°C. Metal carbides are the primary stable precipitate phase in 300-series stainless steels under LWR operating conditions, although RIS of Ni and Si to sinks in the matrix and grain boundaries may lead to the formation of γ' and G phases.

Because of the high displacement rates, fast reactors are an attractive alternative for irradiating test materials to dose ranges that cannot be achieved within a reasonable time in LWRs. However, the higher dose rates and differences in the thermal- and fast-neutron spectra may result in material microstructure and microchemistry that are not representative of LWR irradiations. Therefore, possible differences in material microstructure need to be examined.

The microstructural evolution in austenitic SSs irradiated in LWRs at 275-300°C has been compared with samples irradiated in the BOR-60 fast breeder reactor at 320°C (Fig. 6).[48] The results indicate that at 5-10 dpa the dislocation structure of commercial heats of austenitic SSs is comparable. Although the data show subtle variations in dislocation structure, the differences are minor. The loop density in these steels irradiated either in LWRs or the BOR-60 reactor is about 2 x $10^{23}$ $m^{-3}$; the saturation value was reached after about 2 dpa. The loop density is the same even in the ultra high-purity (UHP) heats of Type 304L (with or without minor additions of C, N, and Si) that have been irradiated to 20 dpa. However, there are some differences in the loop size of the irradiated steels. For the LWR-irradiated SSs, the Frank loop diameter in two high-purity heats (304-E and 316-F) is larger than that in the less pure heats.[44] Also, the loop size for the high-purity heats irradiated in BOR-60 reactor to 20 dpa is much lower than for the high-purity heats (Heats 304-E and 316-F) irradiated in LWRs to about 8 dpa; the average loop diameter is about 6 nm and 14 nm, respectively. Typically, stacking fault tetrahedra (SFT) are also observed in high-purity materials. The LWR-irradiated Heat 304-E contained some SFT in addition to the Frank loops, and the UHP 304 SS heat irradiated in the BOR-60 contained a high density of Frank loops and SFT. The existing data on microstructural evolution in irradiated SSs also indicate that addition of C increases the density of Frank loops and alters the tensile response of the steel, whereas addition of Si decreases the loop density as well as tensile hardening.[49] However, additions of C, Si, P

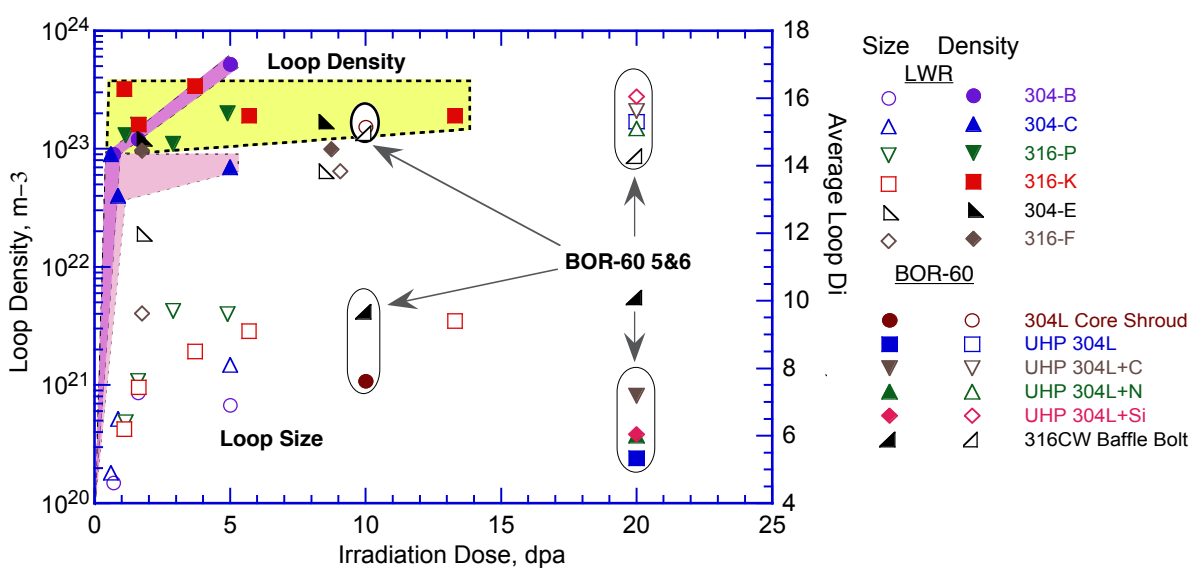


Figure 6. Results from the BOR-60 irradiation experiment with the data for austenitic stainless steels irradiated in a BWR (Ref. 48).

together and with other impurities appear to alter the evolution and type of microstructure of irradiated SSs in a complex way.

These results indicate that at irradiation temperatures of 275-320°C, the Frank loop microstructure appears to be relatively insensitive to the displacement rates between LWRs and fast reactors. The main difference between the two is the presence of He bubbles and cavities in materials irradiated to high dose levels under LWR irradiation conditions. Cavities were not observed in the BOR-60 materials. Also, He bubbles appear to form preferentially on the grain boundaries, which could lead to intergranular embrittlement of the material.[48] Additional data need to be obtained on reactor core internal materials irradiated to doses above 10 dpa and at temperatures of 300-350°C under LWR irradiation conditions.

### 2.1.2 Microchemistry

Neutron irradiation also changes the microchemistry of the material due to RIS. The migration of vacancies and self-interstitial atoms to sinks such as grain boundaries, dislocations, or precipitate surfaces leads to local compositional changes. Elements such as Si, P, and Ni that are believed to migrate by interstitial mechanisms are enriched near regions that act as sinks for the point defects, while elements such as Cr, Mo, and Fe that exchange more rapidly with vacancies are depleted near sinks.[2,4,14] The extent of segregation or depletion depends on the rate of generation and recombination of point defects (i.e., it depends on irradiation temperature and dose rate).

Typically, RIS peaks at intermediate temperatures. It is reduced at low temperatures because of reduced mobility and at high temperatures due to back diffusion. Also, for a specific neutron dose, RIS is greater at lower dose rate. At LWR temperatures (275-300°C), significant RIS is observed at irradiation doses as low as 0.1 to 5 dpa.[2-4,46] The grain boundary segregation/depletion profiles are extremely narrow at ≈300°C (≈572°F). The extent of segregation/depletion at grain boundaries is decreased, and the width of the profile is increased with an increase in irradiation temperature.[2] In low-C Type 316 SS, pre-segregation of Cr and Mo to grain boundaries in mill-annealed materials (without sensitization) promotes the formation of W-shaped profiles. At low doses, a narrow depleted region forms next to a grain boundary that is still higher than the matrix level. Dose levels above 3 dpa are needed to decrease the Cr level at the boundary below that in the matrix.[46] Dose levels greater than 6 dpa are needed to completely remove the W-shaped profiles and establish the typical V-shaped depletion profile. In general, lower doses are required to remove the W-shaped Cr profile in Type 304 SS (less than 3 dpa) compared with Type 316 SS. The depletion of Mo, particularly in Type 316 SS, is also controlled by pre-segregation of Mo to the grain boundary; it takes doses greater than 5 dpa to remove the W-shaped profile. Another minor alloying element Mn also shows significant depletion at the grain boundary after irradiation. However, quantitative measurements of the compositional profiles for Mn are not generally available because of the measurement difficulties in analyzing neutron-irradiated SSs by analytical transmission electron microscopy (ATEM).

The radiation-induced changes in Cr concentration at grain boundaries in several 300-series SSs irradiated in LWRs at 275-290°C are shown in Fig 7a as a function of neutron dose; additional data for Cr depletion from several studies at about 300°C are shown in Fig. 8. Most of the steels show a rapid decrease in Cr to about 13 wt.% at dose up to 5 dpa.[46] The data at dose levels above 10 dpa are limited, but they indicate that Cr content can decrease to 8-10 wt.% in some materials. Under similar irradiation conditions, grain-boundary Cr and Ni concentrations in most 300-series SSs irradiated in LWRs at 300-320°C up to 65 dpa are shown in Figs. 9a and b, respectively. The Cr concentrations measured by Fukuya et al.[50] in CW Type 316 SS PWR thimble tube materials are somewhat lower than those obtained

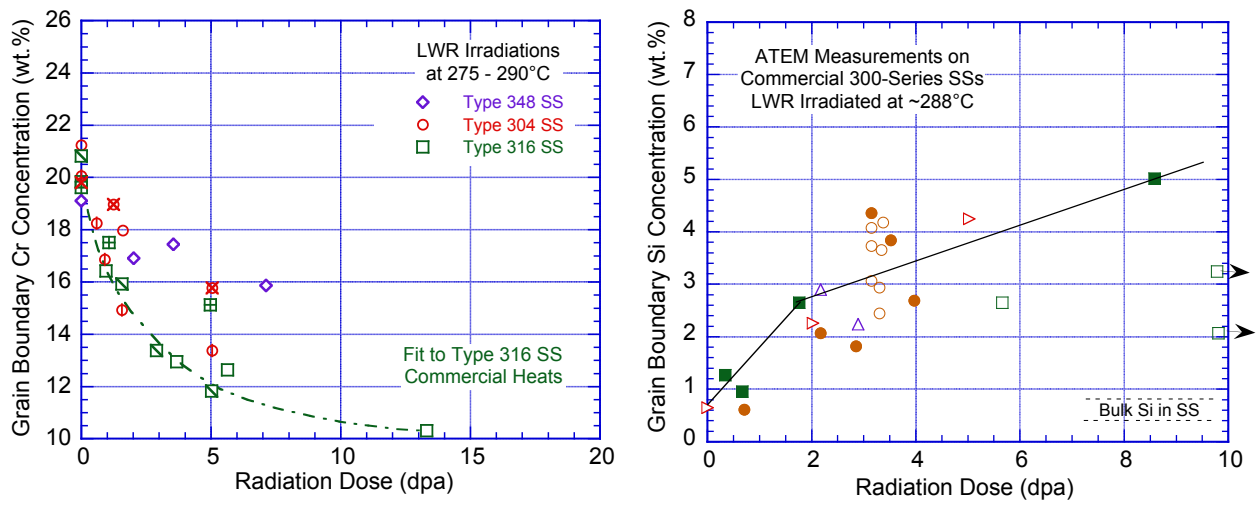


(a) (b)

Figure 7. Radiation-induced grain boundary (a) Cr and (b) Si concentration in 300-series stainless steels irradiated in LWRs at 275-290°C (Refs. 46,4).

by other investigators (e.g., Fujimoto et al.).[51] The irradiation temperature was comparable in the two studies (295-320°C), and the initial cold work was 10-12% and 15%, respectively.

The Si concentration in LWR-irradiated SSs is shown in Fig 7b as a function of neutron dose;[4] Si contents in SSs irradiated in LWRs at 300-320°C up to 65 dpa are shown in Fig. 9c. The results show a rapid increase in Si to about 4 wt.% at 5 dpa and a gradual increase to 5-6 wt.% at higher dose levels. Neutron irradiation should lead to enrichment of P; however, measurements of grain boundary P in neutron irradiated SSs have not yielded consistent results, but it appears that P does not segregate during LWR irradiations. The RIS behavior of other minor elements such as S, C, N, and B, all of which should segregate to the boundary, has not been established. These elements typically enrich grain boundaries but are difficult to measure. Existing data on LWR-irradiated SSs have not indicated significant segregation of these elements. However, these observations are for doses less than 15 dpa. Transmutation of Mn at higher doses may release S from MnS inclusions, which may lead to segregation.[46] Also, if B segregates to the boundaries, He produced by the transmutation reaction (from $^{10}B$ to form $^{4}He$ and $^{7}Li$) would enrich at grain boundaries, which may lead to intergranular embrittlement. The redistribution of S, C, N,

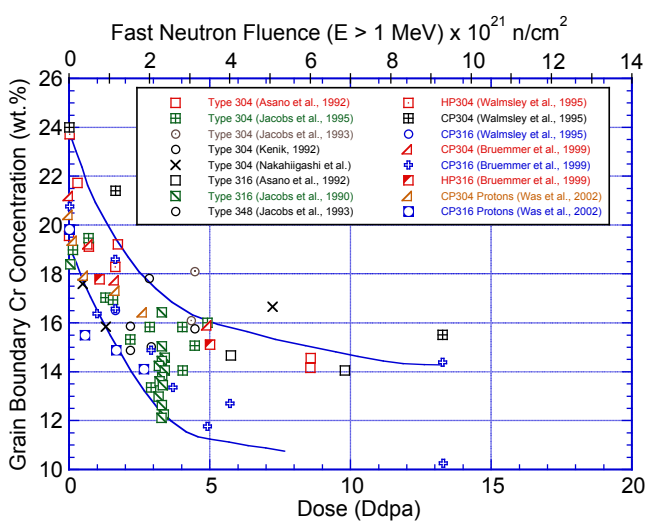


Figure 8. Dependence of grain boundary Cr concentration for several 300-series austenitic stainless steels irradiated at about 300°C on neutron dose (Ref. 3).

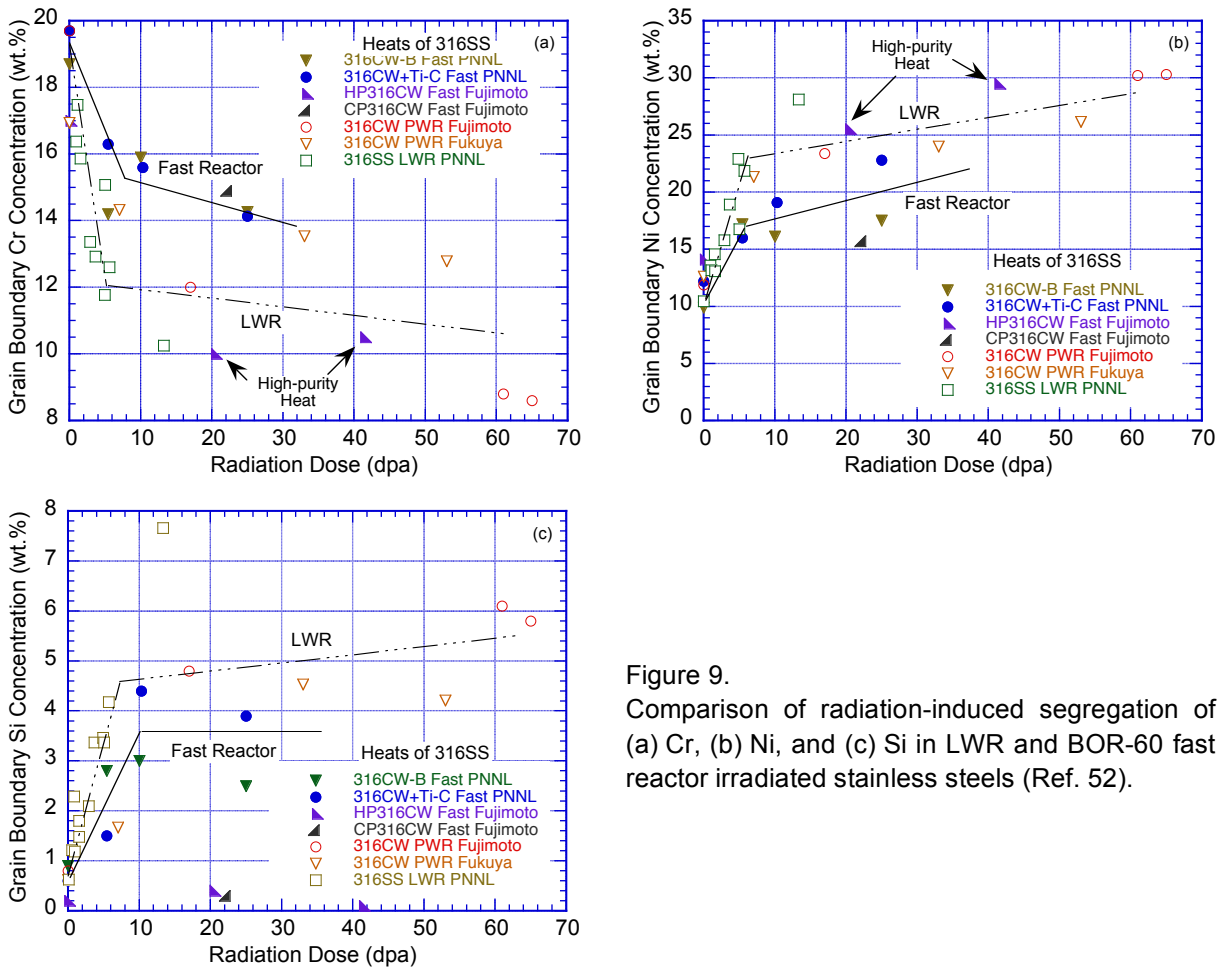


Figure 9.
Comparison of radiation-induced segregation of (a) Cr, (b) Ni, and (c) Si in LWR and BOR-60 fast reactor irradiated stainless steels (Ref. 52).

and B in austenitic SSs irradiated in LWR at dose levels above 15 dpa needs to be investigated to establish its significance on IASCC susceptibility and neutron embrittlement of SSs.

Measurements of RIS in SSs irradiated in LWRs at temperatures above 320°C are limited. Microchemical characterization of CW Type 316 SS materials taken from the Tihange 1 baffle bolt[18] showed that the Cr depletion and enrichment of Ni and Si in these materials were consistent with the data shown in Fig. 9 for SSs irradiated at 275-320°C. The Cr, Ni, and Si concentrations, respectively, were 10-12 wt.%, 24-27 wt.%, and about 4.5 wt.% at the 25-mm position (13.2 dpa at 343°C) and 15 wt.%, 16-21 wt.%, and 2 wt.% at the 55-mm position (8.7 dpa at 333°C).

The microchemical changes in irradiated material can result in the formation of various precipitates; the enrichment of Ni and Si at the grain boundaries may lead to the formation of γ' silicide or G phase. Although γ' precipitates have been observed in the matrix in SSs irradiated under LWR conditions and may affect radiation hardening, they have not been observed at the grain boundaries. The γ' precipitates were identified in the Tihange 1 baffle bolt at the 25-mm position.[18] The absence of γ' silicide ($Ni_3Si$) at the grain boundaries suggests that RIS of Ni and Si probably saturates at higher doses (the actual dose may vary with material composition and irradiation temperature).

As mentioned earlier, a large fraction of the high neutron dose data was obtained on materials irradiated in fast reactors. Therefore, possible differences in material microchemistry due to the higher

dose rates and differences in the thermal- and fast-neutron spectra need to be examined. The RIS of Cr, Ni, and Si in LWR- and BOR-60-irradiated austenitic SSs as a function of the neutron dose is shown in Fig. 9.[52] In all cases, the data from fast reactor irradiation fall below the lower limit of the data from LWR irradiation (i.e., Cr depletion and Ni and Si enrichment are less in the fast reactor irradiated materials). These differences may influence the IASCC susceptibility or radiation embrittlement of these materials. The results indicate that the RIS in the fast reactor irradiated materials may not be representative of that observed under LWR irradiation conditions.

### 2.1.3 Radiation Hardening

The point defect clusters and precipitates produced by irradiation act, to varying extent, as obstacles to a dislocation motion resulting in an increase in tensile strength and a reduction in ductility and fracture toughness of the material. In general, cavities (or voids) are strong barriers, large faulted Frank loops are intermediate barriers, and small loops and bubbles are weak barriers.[1] The yield strength of irradiated SSs can increase up to five times that of the nonirradiated material after a neutron dose of about 5 dpa.[3] The change in engineering stress vs. strain behavior of Type 304 and 316 SSs with neutron dose is shown in Fig. 10.[53] The yield and ultimate stresses increase and ductility decreases with irradiation.

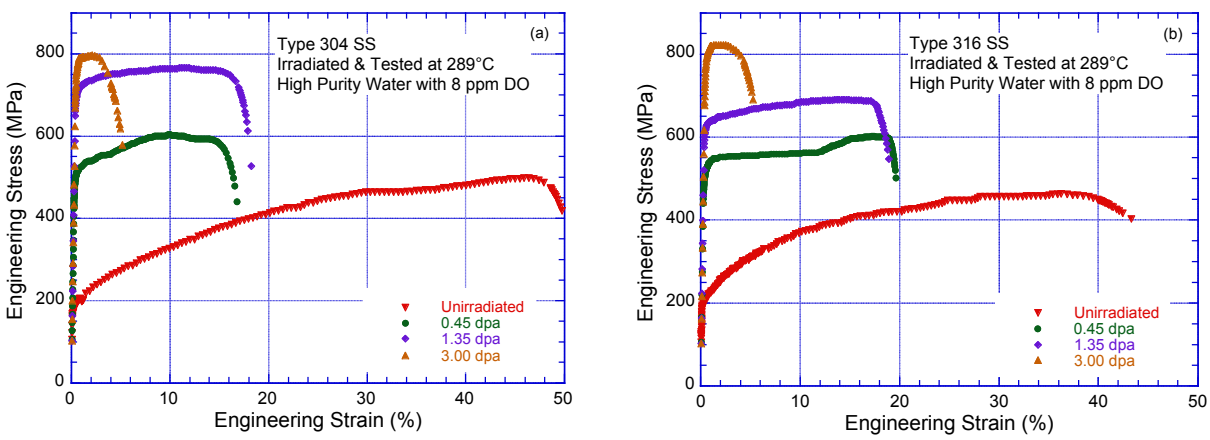


Figure 10. Engineering stress-strain curves at 289°C for (a) Type 304 SS and (b) Type 316 SS steel irradiated up to 3 dpa in the Halden reactor at 289°C. From SSRT tests in high-purity water containing 8 ppm dissolved oxygen (Ref. 53).

At high neutron doses, as the irradiated yield strength approaches the ultimate strength of the material, the deformation mode changes. Deformation by a planar slip mechanism is promoted and the material exhibits strain softening.[54] This process is also termed "dislocation channeling," whereby dislocation motion along a narrow band of slip planes clears the irradiation-induced defect structure, creating a defect-free channel that offers less resistance to subsequent dislocation motion or deformation. Nearly all SSs exhibit strain softening, and little or no uniform elongation, at neutron dose above 3-5 dpa. The enhanced planar slip leads to a pronounced degradation in the fracture toughness of austenitic SSs.[6] Such effects of irradiation on the fracture toughness of austenitic SSs appear to be strongly influenced by minor differences in the chemical composition of the steels;[1] the chemical composition can influence the stacking fault energy (SFE) and/or irradiation-induced microstructure. In general, a higher SFE enhances, and cold work inhibits, dislocation channeling.[1]

The change in yield strength of austenitic SSs correlates well with microstructural changes in the irradiated materials. As discussed in the previous section, under LWR operating conditions, the

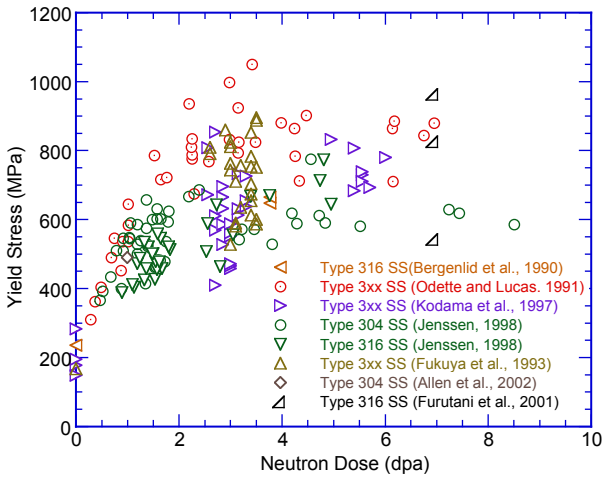


Figure 11.
The effects of neutron dose on measured tensile yield strength of 300-series stainless steels, irradiated and tested at about 300°C (Ref. 3).

microstructural and microchemistry of the irradiated material change rapidly at small neutron doses. The microstructure reaches saturation at about 5 dpa, and the changes in microchemistry are small above 5 dpa. The yield strength of the 300-series SSs irradiated under LWR conditions is plotted as a function of neutron dose in Fig. 11. The yield strength also appears to saturate at a neutron dose of 5 dpa.[54]

The extent of irradiation hardening and the increase in yield stress of austenitic SSs depend on the material composition and thermo-mechanical treatment, as well as the irradiation temperature. The effect of irradiation temperature on the yield strength and ductility of 20% CW Type 316 SS irradiated in fast reactors[55] is shown in Fig. 12. The effect of irradiation hardening and the loss of ductility are significantly more pronounced at 290°C (554°F), at least at low dose levels. Also, for a given neutron dose and irradiation temperature, the yield strength decreases with increasing test temperature. A similar behavior is observed for SSs irradiated under LWR conditions. The greatest increase in yield strength for a given irradiation dose occurs at irradiation temperatures near 300°C (572°F), which is in the temperature range of LWR operation.

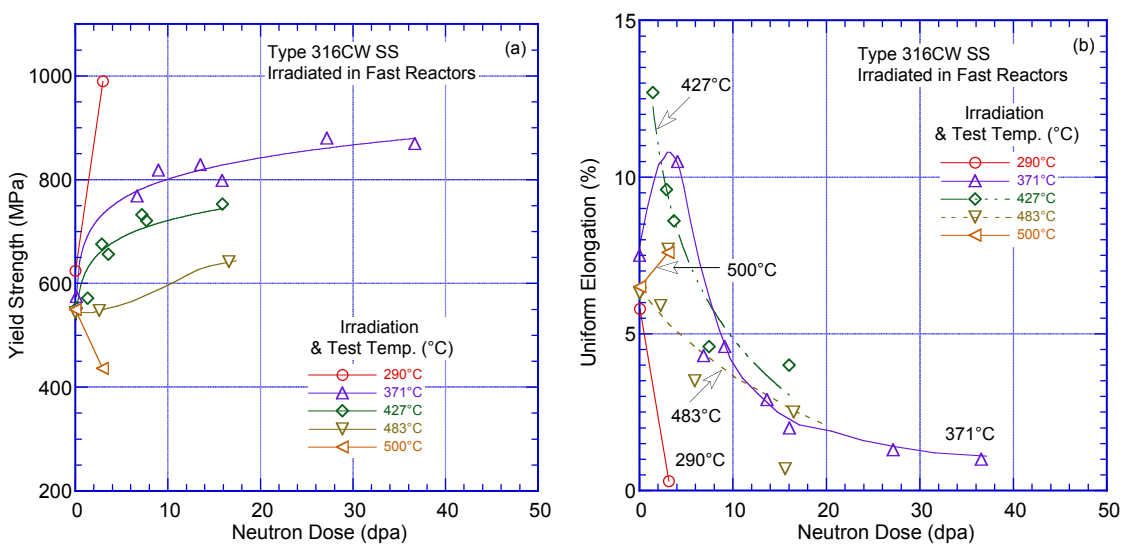


Figure 12. Effect of irradiation temperature on the (a) yield strength and (b) uniform elongation of CW Type 316 stainless steel irradiated in fast reactors at temperatures of 290-500°C and tested at the irradiation temperature (Ref. 55).

### 2.1.4 Tensile Properties

Tensile properties data have been obtained on solution-annealed and CW Type 304, 304L, 316, 316L, and 347 SSs, including weld HAZ material, Type 308 and 309 material, and CF-8 cast austenitic SSs, irradiated at temperatures of 300-400°C (572-752°F) in fast reactors and LWRs.[57-62] The 0.2% yield strength, ultimate tensile strength, uniform elongation, and total elongation at elevated temperatures are plotted in Figs. 13-15 as a function of neutron dose. Most data in these figures were obtained on materials irradiated in the BOR-60 fast reactor. Data on LWR-irradiated materials are limited, in particular, at high neutron dose.

The curves in these figures represent the Materials Reliability Program (MRP)-developed correlations[63] for estimating the tensile properties as a function of neutron dose. The 0.2% yield strength, ultimate tensile strength, uniform elongation, and total elongation data at 330°C were fitted to an exponential equation of the form:

$$\text{Property} = A_0 + A_1 (1-\exp(-d/d_0)), \quad (1)$$

where d is the neutron dose in dpa and the coefficients $A_0$, $A_1$, and $d_0$ for the irradiated material property equations are listed in Tables 1 and 2. The baseline reference tensile properties of nonirradiated materials are represented by a fourth-order polynomial[63] of the form:

$$\text{Property} = C_0 + C_1T + C_2T^2 + C_3T^3 + C_4T^4, \quad (2)$$

where T is the temperature (°C) and the coefficients for the different tensile property equations are listed in Table 3.

Table 1. Material property equations for irradiated CW Type 316 stainless steel.

| | | Property = $A_0 + A_1 (1-\exp(-d/d_0))$ | | |
|---|---|---|---|---|
| Property | Units | $A_0$ | $A_1$ | $d_0$ |
| 0.2% yield strength | MPa | 500 | 470 | 3 |
| Ultimate tensile strength | MPa | 650 | 330 | 3 |
| Uniform elongation | % | 10 | -9.7 | 2 |
| Total elongation | % | 18 | -11 | 5 |

Table 2. Material property equations for irradiated solution-annealed Type 304 stainless steel.

| | | Property = $A_0 + A_1 (1-\exp(-d/d_0))$ | | |
|---|---|---|---|---|
| Property | Units | $A_0$ | $A_1$ | $d_0$ |
| 0.2% yield strength | MPa | 200 | 600 | 3 |
| Ultimate tensile strength | MPa | 450 | 350 | 3 |
| Uniform elongation | % | 40 | -39.5 | 1 |
| Total elongation | % | 45 | -37 | 2.5 |

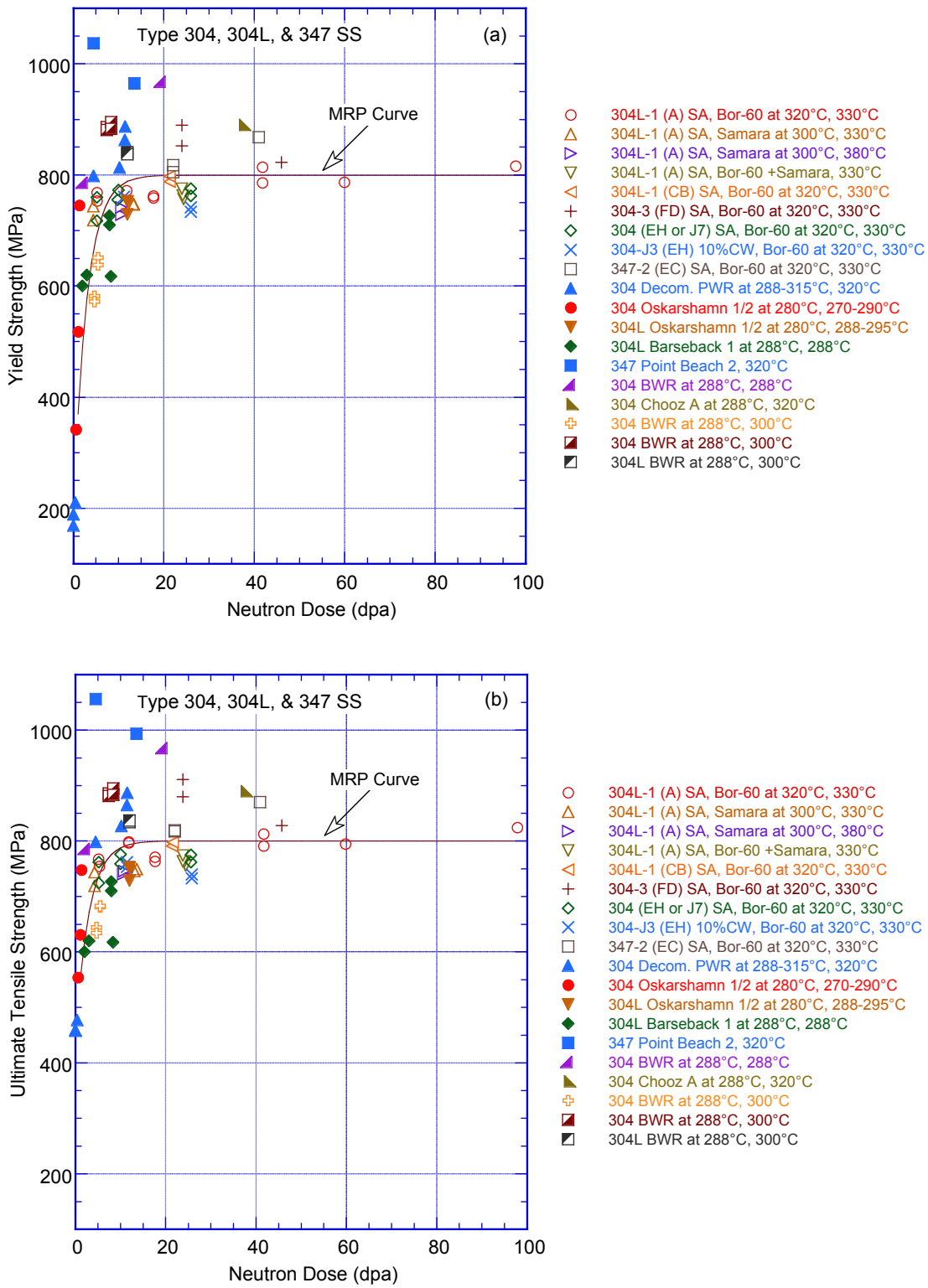


Figure 13. Change in (a) yield strength, (b) ultimate tensile strength, (c) uniform elongation, and (d) total elongation as a function of neutron dose for solution-annealed Type 304, 304L, and 347 stainless steels at elevated temperature (270-380°C) (Refs. 57-62).

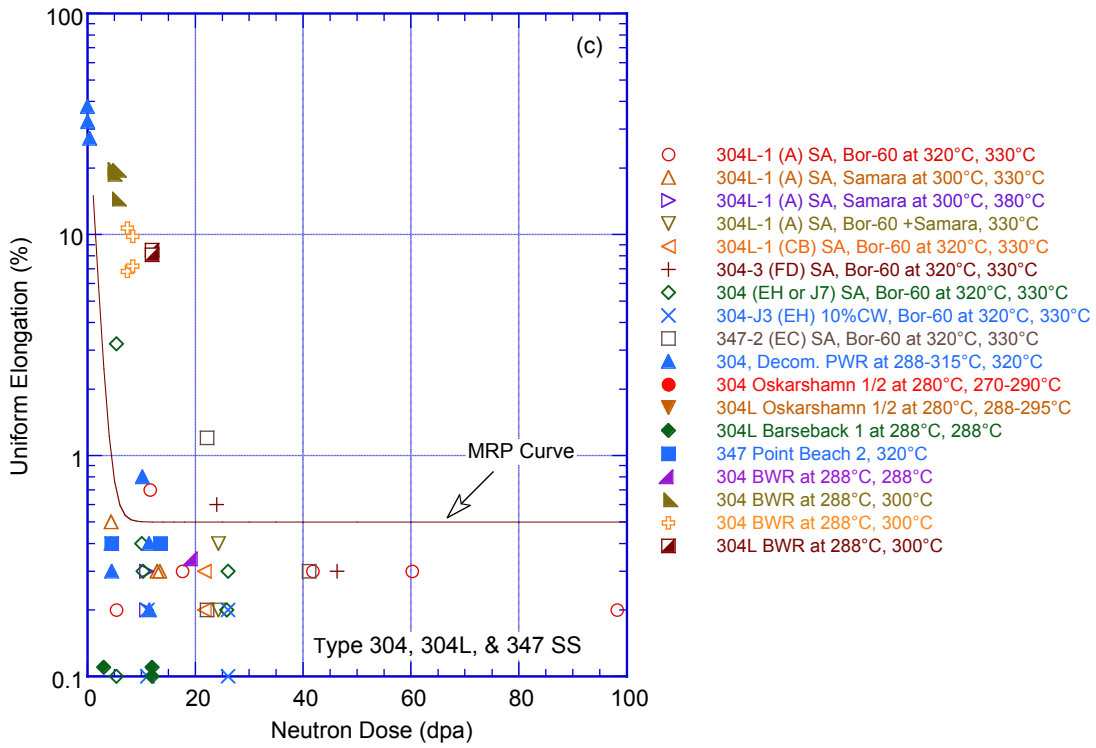


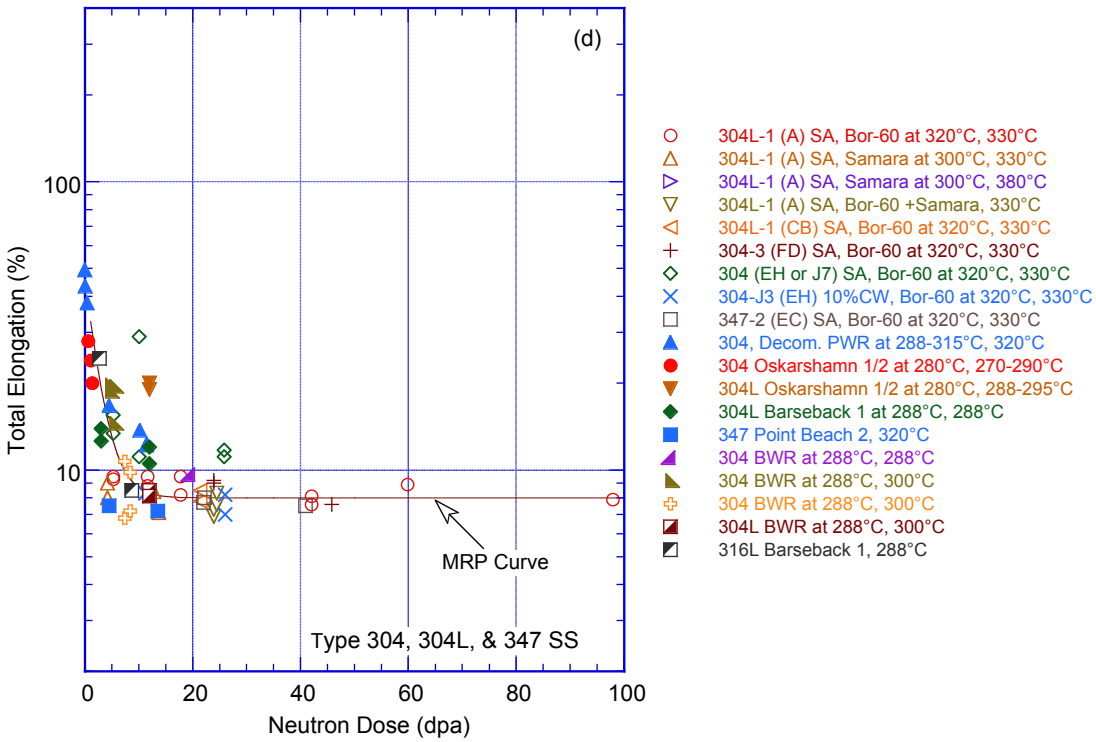


Figure 13. (Contd.)

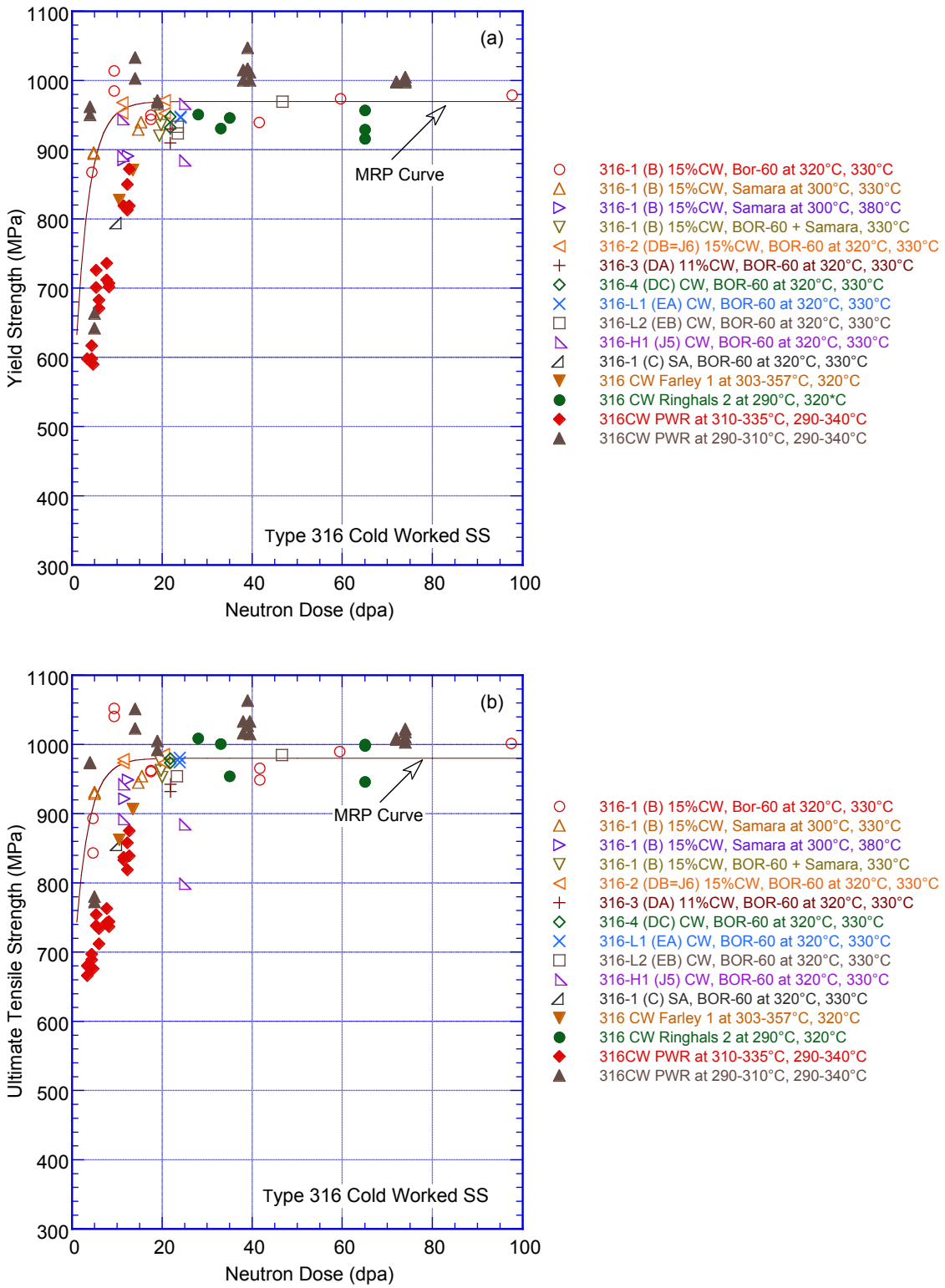


Figure 14. Change in (a) yield strength, (b) ultimate tensile strength, (c) uniform elongation, and (d) total elongation as a function of neutron dose for CW Type 316 stainless steel at elevated temperature (288-380°C) (Refs. 57-62).

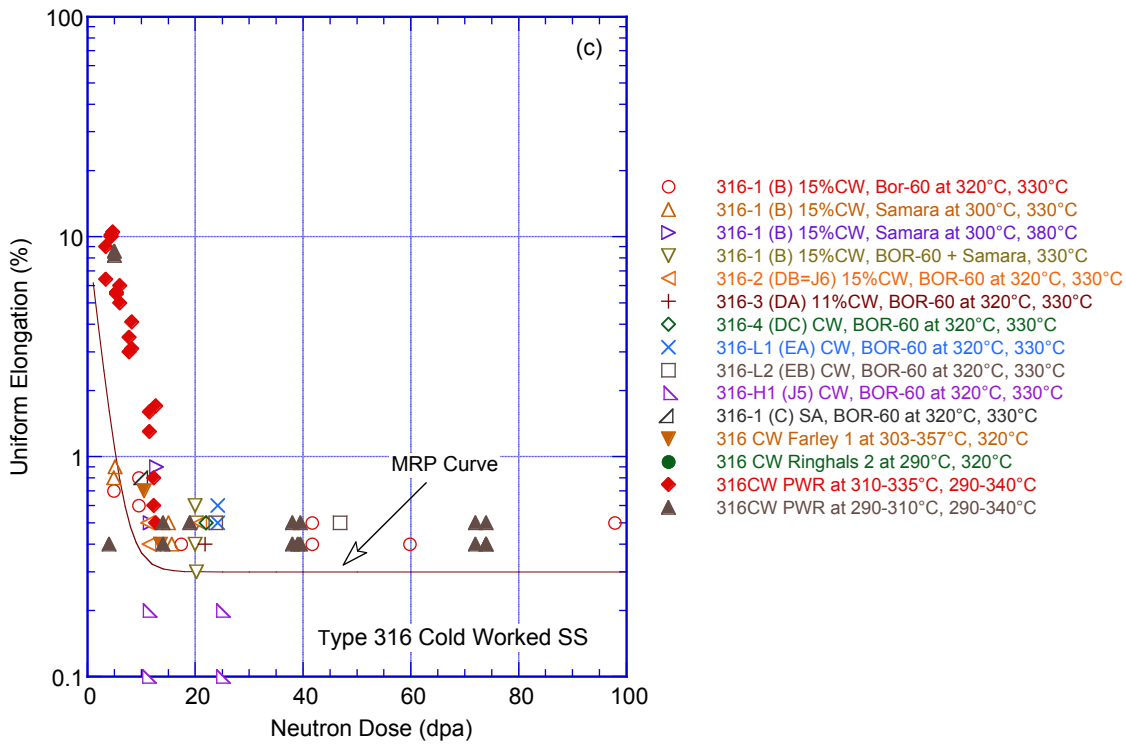


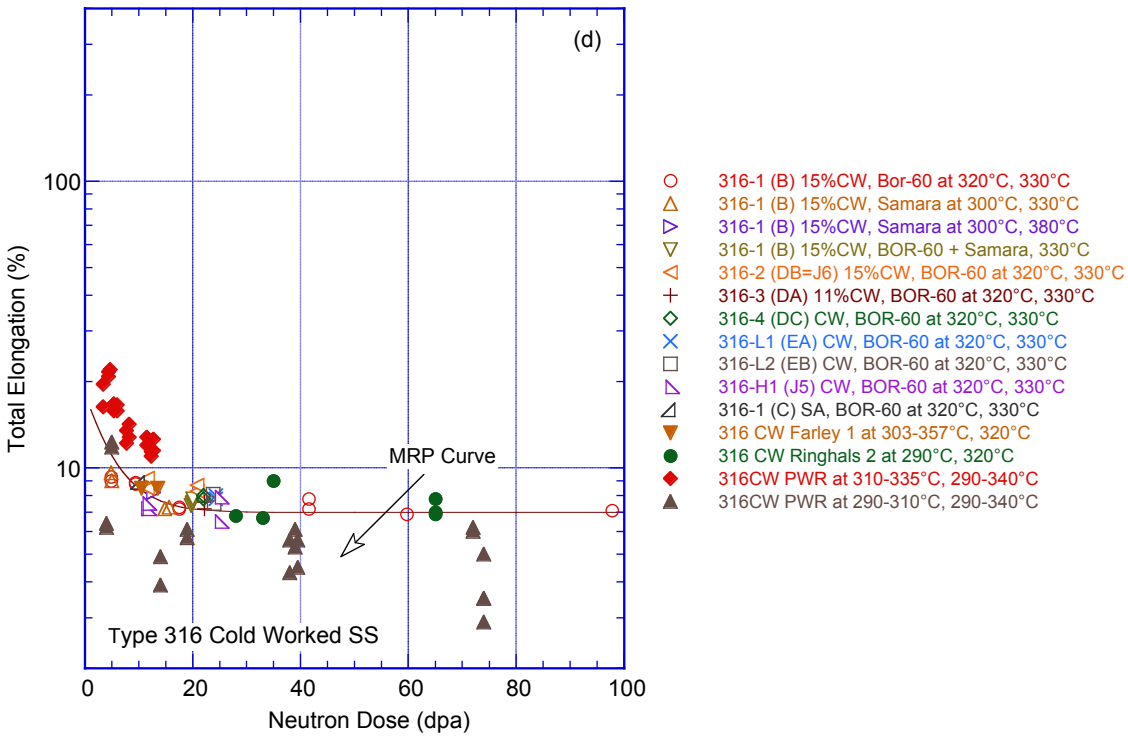


Figure 14. (Contd.)

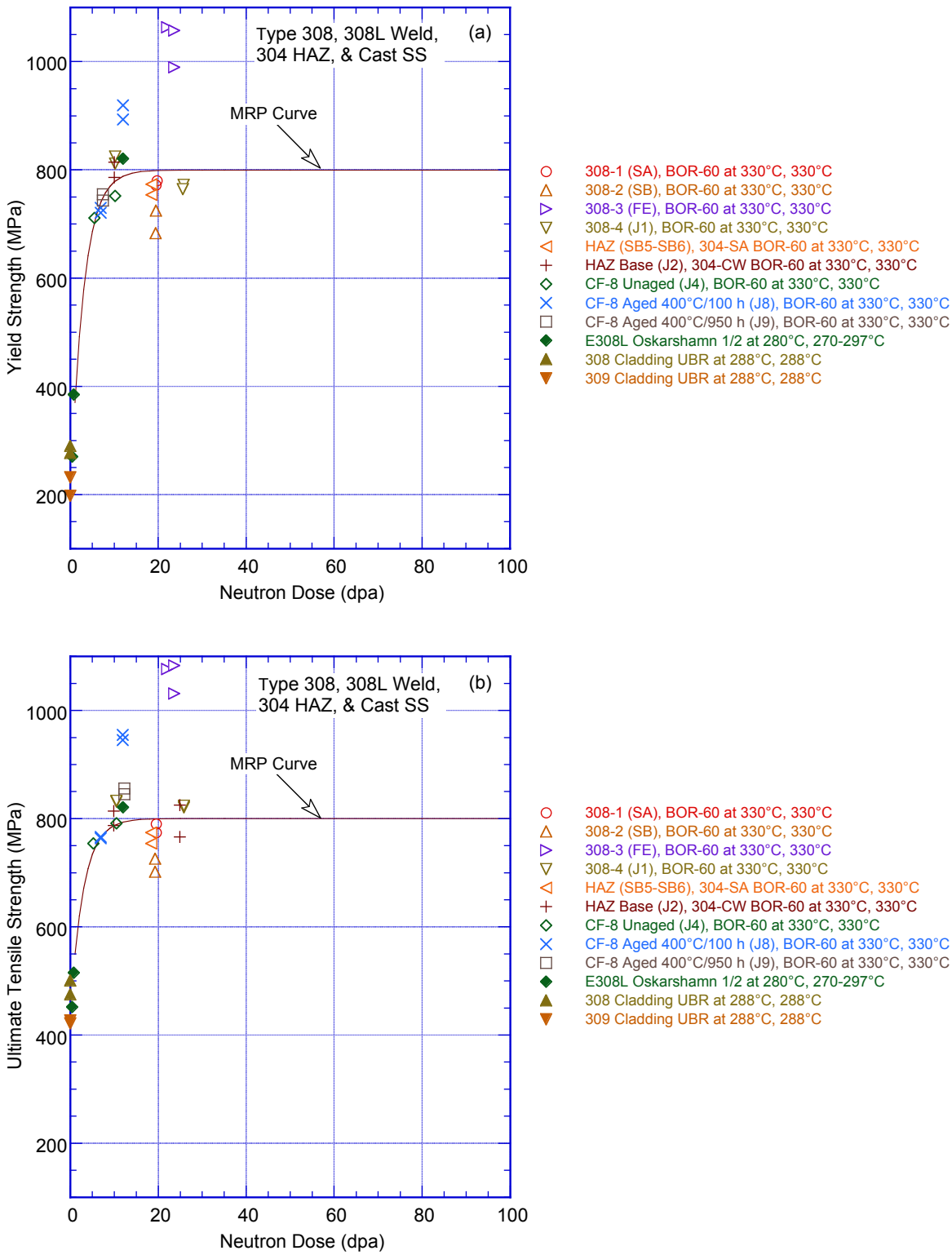


Figure 15. Change in (a) yield strength, (b) ultimate tensile strength, (c) uniform elongation, and (d) total elongation as a function of neutron dose for Type 308 and 309 weld metal, Type 304 HAZ, and CF-8 cast stainless steel at elevated temperature (270-330°C) (Refs. 57-62).

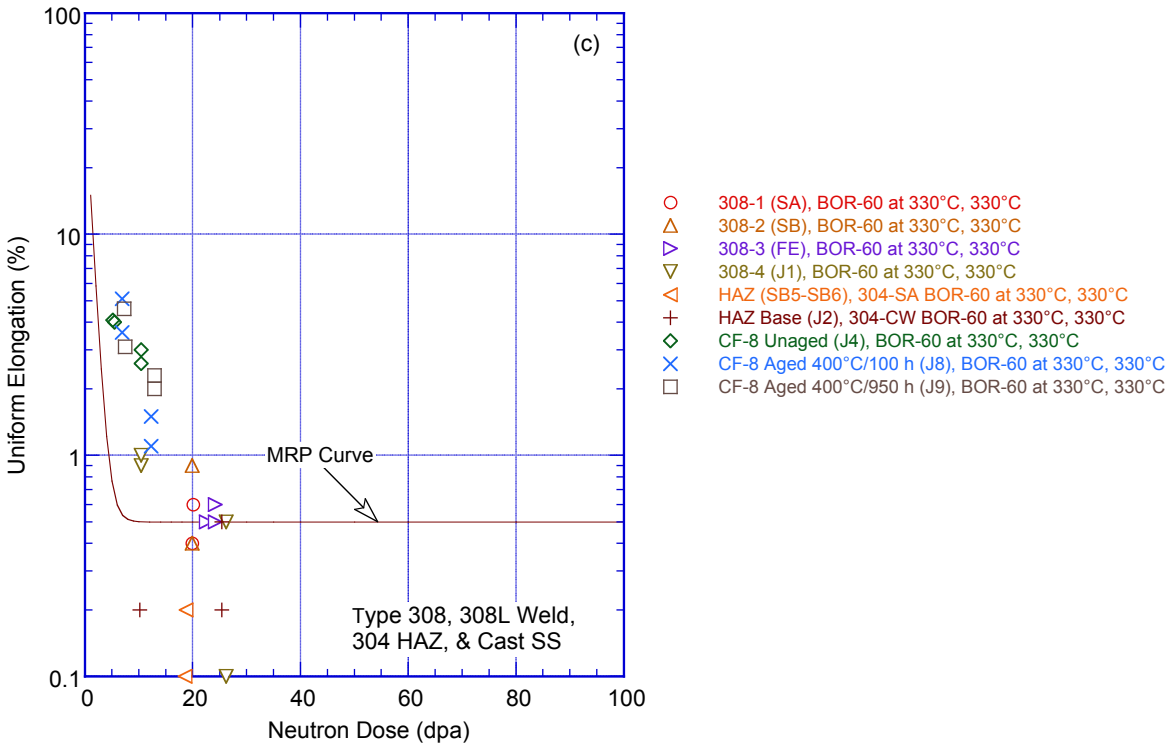


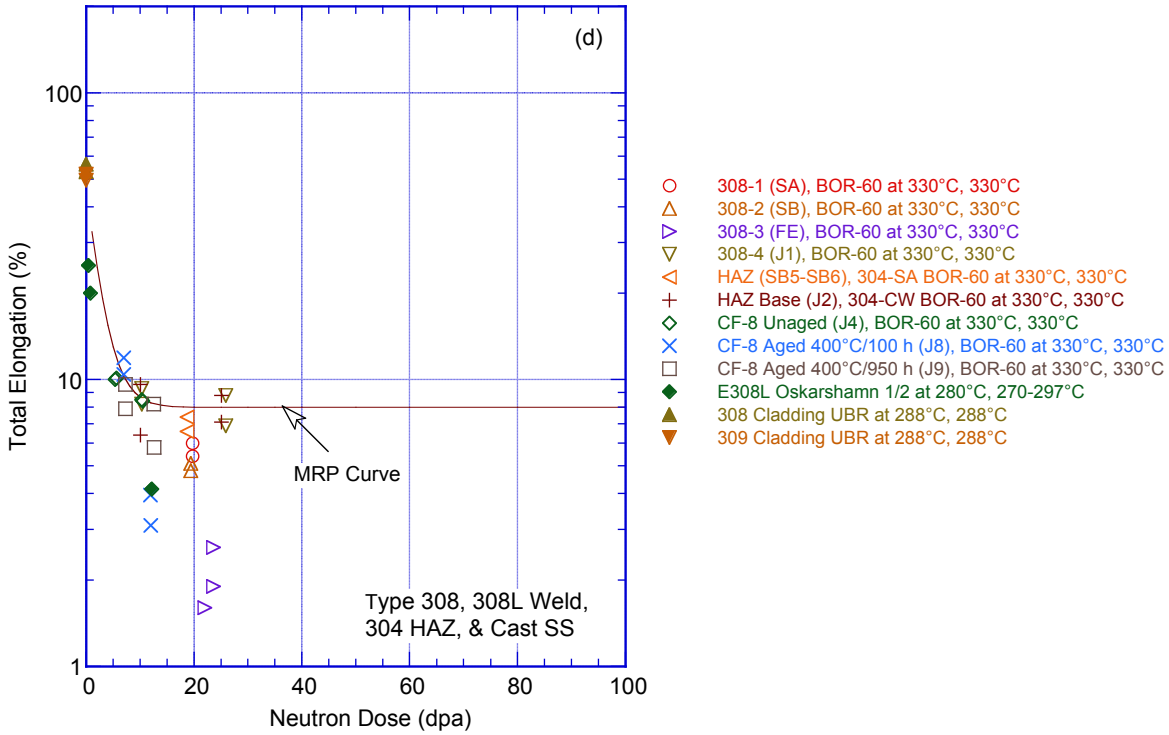


Figure 15. (Contd.)

Table 3. Material property equations for solution-annealed and nonirradiated Type 304 stainless steel.

| | | Property = $C_0 + C_1T + C_2T^2 + C_3T^3 + C_4T^4$ | | | | |
|---|---|---|---|---|---|---|
| Property | Units | $C_0$ | $C_1$ | $C_2$ | $C_3$ | $C_4$ |
| 0.2% yield strength | MPa | 270.09 | -0.5702 | 9.1162E-4 | -5.6198E-7 | |
| Ultimate tensile strength | MPa | 617.275 | -1.7750 | 7.0659E-3 | -1.0769E-5 | 4.8941E-9 |
| Uniform elongation | % | 55.8688 | -0.1893 | 5.3656E-4 | -4.5779E-7 | |
| Total elongation | % | 71.6321 | -0.1956 | 5.7562E-4 | -7.1266E-7 | 3.2172E-10 |

The results indicate that the tensile properties reach saturation at 5-20 dpa and do not change significantly at higher dose levels. Also, although the data on materials irradiated in LWRs are limited, the yield and ultimate strengths of the LWR-irradiated materials (solid symbols in Figs. 13 and 15) are consistently higher, and the uniform and total elongations are consistently lower than those for materials irradiated in fast reactors (open symbols in Figs. 13 and 15). The uniform elongation of some SSs can decrease to 0.1% at neutron dose levels of 5-10 dpa. The MRP correlations are primarily based on the fast reactor data and predict a saturated yield and ultimate strength value of 800 MPa for solution-annealed Type 304 SS and of 970 and 980 MPa, respectively, for CW Type 316 SS. However, most of the data for yield and ultimate strength of LWR-irradiated materials are above the MRP curve. Similarly, most of the data for uniform and total elongation of LWR-irradiated materials are below the MRP curve. Consequently, calculations of the tensile properties of irradiated austenitic SSs based on the MRP correlations underestimate irradiation hardening and loss of ductility in LWR conditions.

Additional data on austenitic SSs irradiated in LWRs to dose levels above 20 dpa are needed to better define the correlations for estimating tensile properties of these materials for LWR operating conditions. Also, the contribution of voids in these materials to irradiation hardening and loss of ductility should be investigated. The presence of voids is likely to degrade the ductility of irradiated SSs to the extent that a brittle fracture at room temperature may be a significant concern. The effect of voids on the tensile properties of SSs should be examined at LWR operating temperatures as well as at room temperature.

Other correlations have also been proposed to estimate the tensile properties of irradiated austenitic SSs. The most widely used equation for the yield stress of 300-series SSs irradiated in LWRs at about 300°C is that developed by Odette and Lucas.[64] The increase in yield stress (MPa) is expressed in terms of the neutron dose (dpa) by the relationship

$$\Delta\sigma_y = 670\ [1 - \exp(-\text{dpa}/2)]^{0.5}. \tag{3}$$

To help assess irradiation-induced degradation of fracture properties of BWR core internal components Electric Power Research Institute (EPRI) has proposed a correlation for estimating the flow stress of irradiated SSs as a function of fluence.[65] The correlation is based on BWR-irradiated base metal and welds tested at 150-300°C. The flow stress $\sigma_f$ (MPa), defined as the average of yield stress ($\sigma_y$) and ultimate stress ($\sigma_u$) [i.e., $(\sigma_y+\sigma_u)/2$], is expressed in terms of neutron fluence (n/cm$^2$) by a power law relationship:

$$\sigma_f = 113.67\ \ln(\text{fluence}) - 4952.8. \tag{4}$$

### 2.1.5 Yield Strength

The three elements that, in combination, influence the IGSCC of austenitic SSs in BWR environments are a susceptible (sensitized) material, a significant tensile stress, and an aggressive environment. The NRC staff technical recommendations to reduce the susceptibility to IGSCC included the use of low-carbon wrought austenitic SSs and weld metal, which are considered adequately resistant to sensitization by welding.[66] However, Andresen has shown that nonsensitized SSs are not immune to SCC; SSs with high yield strength (produced by cold work) are susceptible to IGSCC in ultra-high purity water.[15] The effect of yield strength on SCC growth rates in high-purity water at high and low potential is shown in Fig. 16. The CGRs increase with increasing yield strength. Increases in yield strength can originate from surface or bulk cold work, weld shrinkage strain, precipitation hardening, irradiation hardening, or oxide dispersion hardening; all of these increase SCC growth rates. At a given yield strength, a similar susceptibility to cracking is observed in high- and low-potential environments, although the CGRs in low-potential water are an order of magnitude lower. There is no significant difference among the different grades of SSs, as well as no effect of deformation-induced martensite on CGRs. However, SSs that are cold worked by rolling favor transgranular (TG) rather than intergranular (IG) crack morphology.[67]

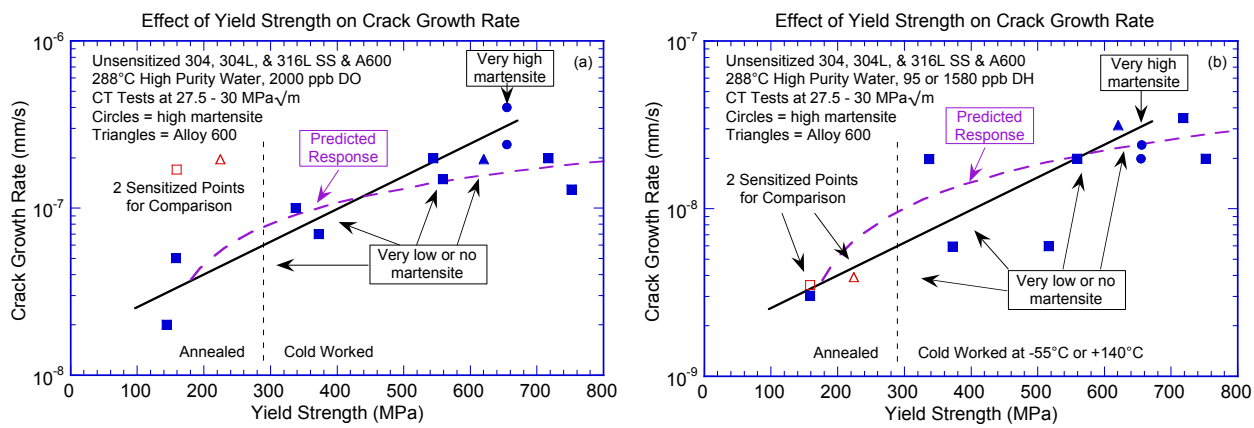


Figure 16. Effect of yield strength and martensite content on the SCC growth rate of stainless steels and Alloy 600 at 288°C in high-purity water (<0.10 mS/cm outlet) containing (a) 2000 ppb $O_2$ and (b) 95 or 1580 ppb $H_2$ (Ref. 15).

The increase in CGR with increasing yield strength has been explained by Andresen[15,39,68] and Shoji[69] on the basis of the redistribution of strain field ahead of an advancing crack. Under constant stress intensity factor K, the redistribution of stress and strain fields as the crack advances provides the dynamic deformation or strain rate at the crack tip, which leads to SCC. In high strength materials because the plastic zone at a given K is smaller, the strain gradient at the crack tip is higher.

The dependence of SCC growth rates on the yield strength of nonirradiated, cold-worked, 300-series austenitic SSs in an NWC BWR environment is shown in Fig. 17. In this figure, the curve was empirically determined to bound the available data. The results indicate a large increase in CGRs as the yield strength increased from 150 to 800 MPa and little or no increase at higher values. The available data also indicate that the SCC growth rates in the NWC BWR environment for sensitized SSs are higher than those for nonsensitized steels. Figure 18 shows CGR vs. yield strength for sensitized and nonsensitized SSs in the NWC BWR environment at 289°C and in the PWR environment at 340°C.[70,71] At yield strengths less than 800 MPa, the CGRs of sensitized materials are greater than those of

nonsensitized materials, but for yield strength values of 800 MPa or higher, the CGRs in the low- and high-potential environments may be comparable.

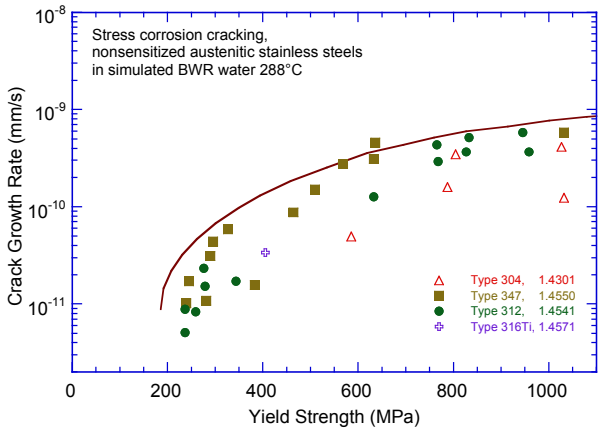


Figure 17.
Crack growth rates of nonirradiated, cold worked, 300-series austenitic SSs in NWC BWR environment as a function of yield strength (Ref. 3).

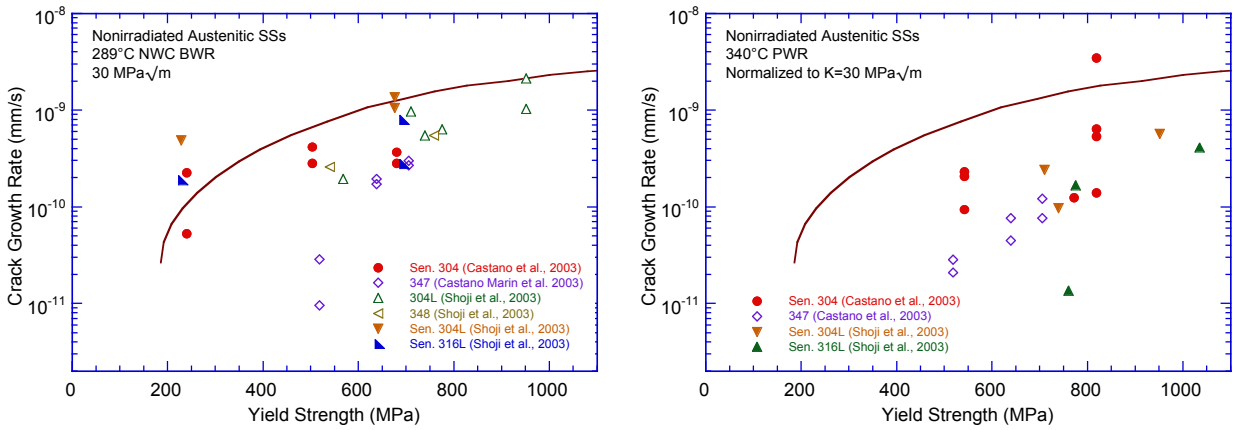


(a) (b)

Figure 18. Change in SCC growth rates of nonirradiated, sensitized and nonsensitized, stainless steels as a function of yield strength in (a) NWC BWR environment at 289°C and (b) PWR environment at 340°C (Refs. 70,71). The curve is replicated from Fig. 17.

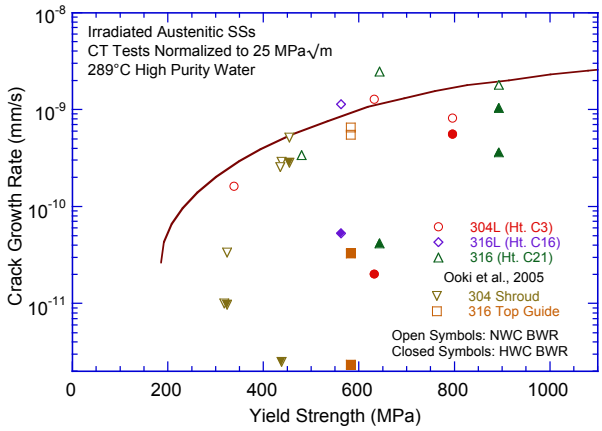


Figure 19.
Change in SCC growth rates at 289°C of LWR-irradiated austenitic stainless steels as a function of yield strength in NWC and HWC BWR environments (Refs. 11,72).

Similar behavior is observed in irradiated SSs, for which the increase in yield strength is due to irradiation hardening (Fig. 19). In the NWC BWR environment, CGRs in irradiated SSs increase rapidly

for yield strength values in the range of about 200 to 800 MPa. The rates are at least an order of magnitude lower in the HWC BWR environment. However, for yield strengths above 700 MPa (i.e., SSs irradiated above 3 dpa) the CGRs are comparable in both high- and low-potential (i.e., NWC BWR and HWC BWR or PWR) environments. The effect of yield strength on the SCC growth rates of irradiated austenitic SSs is discussed further in Section 2.2.2.1 of this report.

The SSRT tests on irradiated SSs show a different dependence on yield strength. The percent IGSCC in SSRT tests on austenitic SSs in high-DO water at 289°C is plotted as a function of yield strength in Fig. 20. As in the case of the CGR data, IASCC susceptibility, measured as the fraction of intergranular cracking, increases with yield strength, but the increase in percent IG fracture occurs at higher yield strength values of 400-800 MPa. These results suggest that irradiated SSs that have yield strengths of 150-400 MPa and are subject to SCC may not show an IG fracture mode.

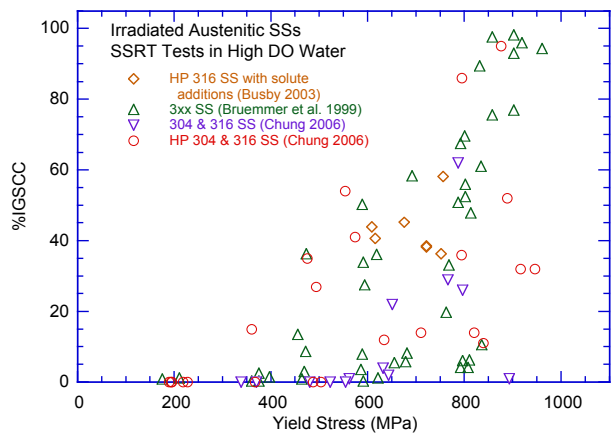


Figure 20.
Effect of yield strength on percent IGSCC in SSRT tests on irradiated 300-series stainless steels in high-DO water (Refs. 3,4,53).

### 2.1.6 Corrosion Potential

The increase in SCC susceptibility of SSs with an increase in corrosion potential is due to the effect of the corrosion potential on the crack-tip water chemistry. The CGR data demonstrate that decreasing the corrosion potential from that of an NWC BWR environment to that of HWC BWR or PWR environments decreases the CGRs for all nonirradiated SSs. Although SSs are not immune to SCC in low-potential environments, the SCC growth rates of nonirradiated SSs and SSs irradiated to moderate levels of neutron dose (less than 3 dpa) are more than an order of magnitude lower in such environments than those in high-potential environments.

The SCC growth rates of austenitic SSs irradiated to 1.0-2.5, 3.0-4.0, and more than 5 dpa are plotted as a function of the steel electrochemical potential (ECP) in Fig. 21.[11,15,60,73-79] The CGRs (da/dt) are expressed by a power law relationship with the stress intensity factor, K. The growth rates (m/s) for nonirradiated austenitic SSs are represented by the correlation given in the NRC report NUREG-0313, Rev. 2:[66]

$$da/dt = A1\ (K)^{2.161}, \tag{5}$$

where K is in MPa $m^{1/2}$, and the magnitude of the constant A1 depends on the water chemistry and composition and structure of the steel. A value for the constant of 2.1 x $10^{-13}$ was proposed in NUREG-0313 for sensitized SS in water with 8 ppm DO. For water with 0.2 ppm DO, the CGR is taken as one-third that of the value given in NUREG-0313; in this case A1 is 7.0 x $10^{-14}$. The value of constant A1 is

smaller in low-DO environments, such as HWC BWR or PWR environments. The CGRs plotted in Fig. 21 were corrected to a K value of 20 MPa $m^{1/2}$ by using the experimental value of the exponent of K, and if not known, using a value of 2.5. For nonirradiated SSs, the CGRs are typically corrected to 30 MPa $m^{1/2}$ to determine the effect of corrosion potential on SCC growth rates.[40,68]

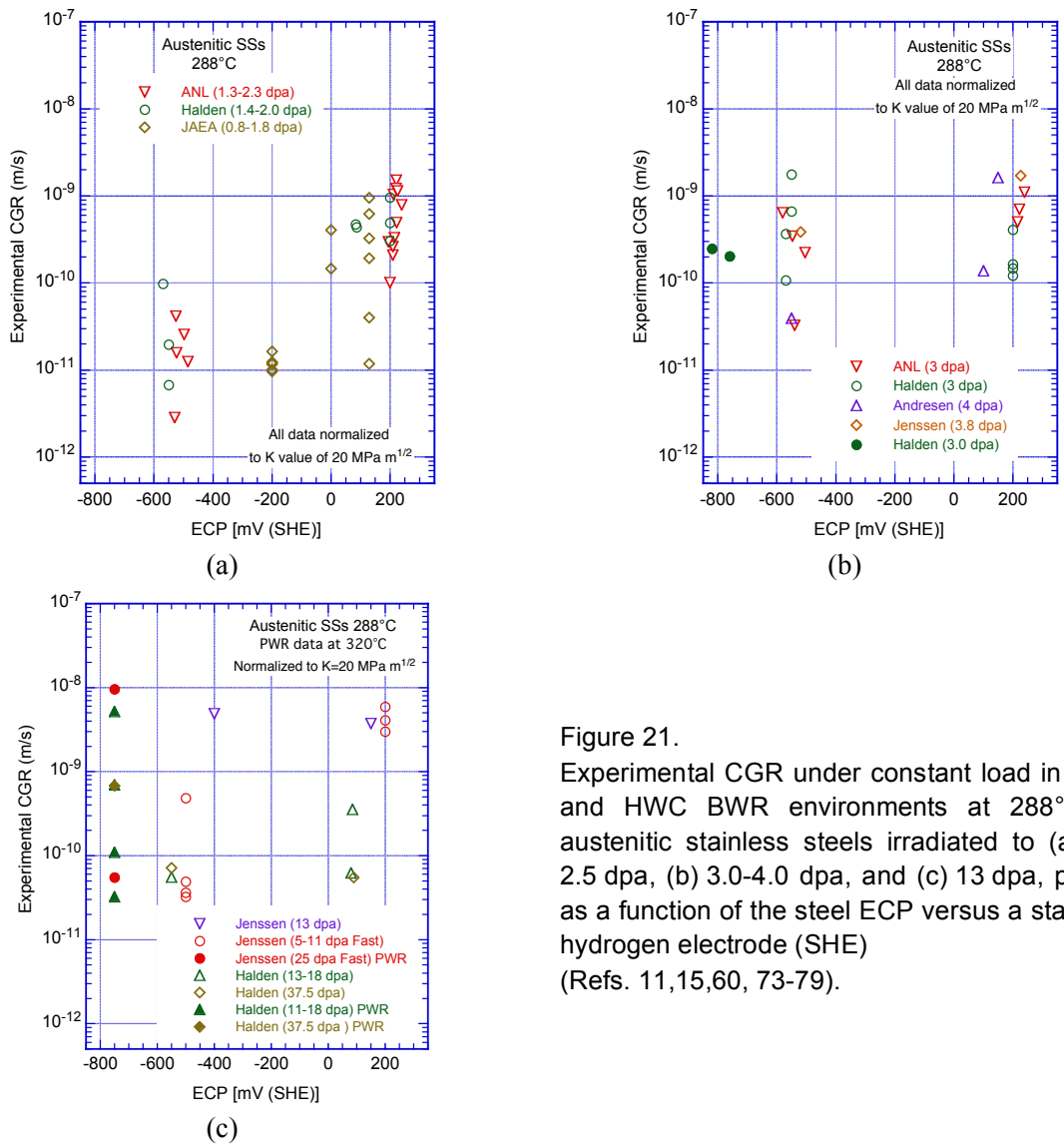


Figure 21.
Experimental CGR under constant load in NWC and HWC BWR environments at 288°C for austenitic stainless steels irradiated to (a) 1.0-2.5 dpa, (b) 3.0-4.0 dpa, and (c) 13 dpa, plotted as a function of the steel ECP versus a standard hydrogen electrode (SHE)
(Refs. 11,15,60, 73-79).

The effect of reduced corrosion potential on the CGRs of SSs that were irradiated to less than 3 dpa is seen clearly in these figures. Decreasing the corrosion potential has a beneficial effect on growth rates for all steels irradiated to 1.0-2.5 dpa (Fig. 21a), and for some steels irradiated to 3.0-4.0 dpa (Fig. 21b). Although the materials irradiated to about 4 dpa show some decrease in CGRs in the low-potential environment, the decrease is rather modest (about a factor of 5 lower growth rates). For these steels, the CGRs in the HWC BWR environment are greater than 3 x $10^{-10}$ m/s. The results also show that, except for the materials irradiated in fast reactor (BOR-60) to 5-11 dpa at 320°C,[79] none of the other materials irradiated in BWRs (at 289°C) showed a benefit of decreased corrosion potential on SCC growth rates. For SSs irradiated to 11-38 dpa in BWRs, the CGRs in NWC and HWC are comparable. However, the rates vary by more than an order of magnitude with neutron dose. The CGRs are, in fact, lower for SS

irradiated to 38 dpa compared to those irradiated to 11-13 dpa. The SSs irradiated in the BOR-60 reactor to 5-11 dpa at 320°C show more than an order of magnitude decrease in growth rate in the HWC BWR environment, compared to that in the NWC environment. The different behavior for the materials irradiated in BWRs and fast reactors may be attributed to differences in the material microstructure and microchemistry, as discussed in Sections 2.1.1 and 2.1.2, respectively. However, it is not clear whether these differences are due to differences in the irradiation temperature (320 versus 289°C) or neutron spectrum and flux. Data on SCC growth rates and microstructural characterization of SSs irradiated in PWRs (at 320°C or higher temperatures) are needed to establish the effect of irradiation temperature on IASCC susceptibility of austenitic SSs.

The SCC growth rates for SSs irradiated above 11 dpa in the PWR environment at 320°C show significant variation between different grades and heats of materials. The CGRs range from $5 \times 10^{-11}$ m/s for some steels to $5 \times 10^{-9}$ m/s for others. The differences have been explained on the basis of differences in the material microchemistry, in particular, the Si concentration at the grain boundaries.[60,76,79]

The CGR data also indicate that for some SSs a benefit of reduced potential is observed at low K values (<20 MPa $m^{1/2}$) but not at a higher K value.[11] The behavior could be explained on the basis of a loss of specimen constraint by exceeding the K/size criterion or may indicate some kind of threshold phenomenon. For example, loss of the beneficial effect of decreased corrosion potential seems to occur at a threshold growth rate of about $1 \times 10^{-9}$ m/s. At this threshold growth rate, the crack tip strain rate may be influenced by some mechanism that helps sustain the high growth rates, which are independent of corrosion potential and to some extent K. Under constant K, crack advance occurs by dynamic deformation or strain rate at the crack tip due to the redistribution of stress and strain fields as the crack advances. Any mechanism that enhances crack tip strain rate would facilitate SCC. A possible mechanism is the effect of hydrogen, generated from the oxidation/dissolution of the freshly exposed metal surface, on the crack tip strain rate. Hydrogen lowers the SFE, which promotes localized deformation and thereby influences the crack tip strain rate. The effect of SFE on IASCC susceptibility is discussed in Section 2.1.9.

The lack of an effect of reduced corrosion potential on CGRs for some SSs irradiated to 3-4 dpa[11] and nearly all SSs irradiated above 5 dpa[60,74-79] has often been explained on the basis of the loss of specimen constraint. The argument is that the specimen K/size criterion was exceeded at the high K values used in these tests. However, the basis for the proposed K/size criterion for irradiated materials is not well documented. Some recent studies have shown that the ASTM E399 size criterion is not exceeded in ½-T or ¼-T compact tension (CT) specimens of irradiated SSs that have yield stress above 600 MPa.[80,81] The effects of K/size criterion on SCC growth rates are discussed further in Section 2.2.1.3. Post-test metallographic evaluation of such test specimens does not suggest a loss of specimen constraint; the fracture morphology in these specimens is completely IG, and the fracture surface is normal to the stress axis.[11] The existing data suggest that some SSs may show IASCC susceptibility in low-potential environments at fluence levels as low as 3 dpa. Caution should be exercised in using a K/size criterion for irradiated SSs that screens out such experimental data simply because they do not agree with the current expectations for the IASCC behavior of austenitic SSs. Additional data on SSs irradiated to 3-8 dpa are needed to better determine the effect of low-potential environments on the CGRs of highly irradiated materials.

### 2.1.7 Silicon Segregation

The increased susceptibility to IASCC and the loss of benefit of reducing potential in highly irradiated SSs have been attributed to the segregation of Si at the grain boundaries. The Si segregation is

detrimental because at all relevant pH/potential conditions, Si oxidizes to $SiO_2$, which is highly soluble in hot water.

Unusually high CGRs have been observed in crack growth tests on CW SSs, containing 1.5 to 5 wt.% Si, in high-purity water with 2 ppm dissolved oxygen (DO), and the growth rates show no effect of corrosion potential and little effect of applied K.[82] Crack growth tests were conducted in high-purity water with 2000 ppb $O_2$ on Type 304L SS containing 5% Si (no Mo, Nb, or Ti additions) that had been cold worked to 15% at 220°C (yield strength about 500 MPa). The results yielded a CGR of 2.2 x $10^{-9}$ m/s at K of about 30 MPa $m^{1/2}$. The observed rate is a factor of 10 higher than the rates in most commercial SSs with similar levels of cold work/yield strength. More significant, the rate did not decrease when the environment was changed from high potential to low potential (95 ppb $H_2$). In addition, decreasing K at a rate of about 22 MPa $m^{1/2}$ per mm resulted in an initial decrease in CGR from 2.2 to 1 x $10^{-9}$ m/s but thereafter it remained constant as the K decreased from 30 to 15 MPa $m^{1/2}$ (Figs. 8 and 9 in Ref. 82).

A similar detrimental effect of Si, although not to the same extent, has been observed in custom heats of Type 304L SS with 3 or 1.5% Si, and elevated Ni and reduced Cr consistent with the segregation behavior expected in an irradiated material. The CGRs in these heats were nearly identical to those observed in the heat with 5% Si, but in this case a decrease in corrosion potential resulted in a modest decrease in growth rates. The CGR decreased from 2.1 to 1.2 x $10^{-9}$ cm/s in the heat with 3% Si to about 7 x $10^{-10}$ m/s in the heat with 1.5% Si. Also, for the 1.5%-Si heat, decreasing K from 30 to 16 MPa $m^{1/2}$ decreased the CGR by a factor of 9. The effect of Si concentration on SCC growth rates in these custom heats of Type 304L SSs in various water chemistries and at various stress intensity factors is summarized in Fig. 22.

The effect of bulk Si content on the SCC behavior of Type 316L SS has also been evaluated. Crack growth tests were performed on heats of Type 316L with 2 and 4% Si.[82] None of these heats showed elevated growth rates. The reason for the different behavior in Type 316L compared with Type 304L is not clear. It is possible that molybdenum silicides form in Type 316L SS thereby removing the effect of Si on SCC susceptibility.

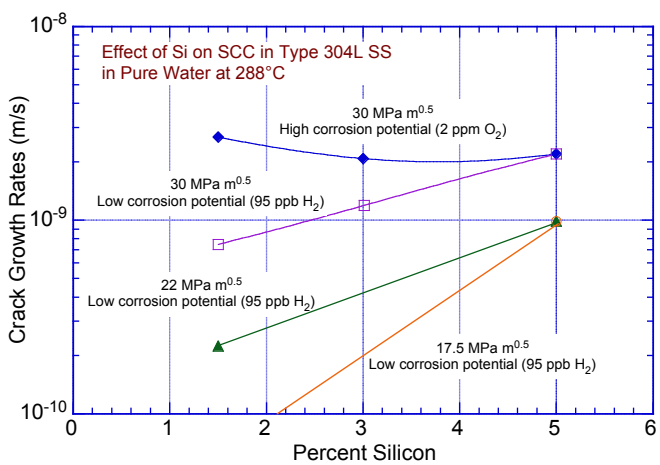


Figure 22.
Crack growth rates versus Si concentration in custom heats of Type 304L stainless steel simulating expected grain boundary microchemistries for high and low corrosion potentials and at various stress intensity factors (Ref. 82).

Tests with irradiated austenitic SSs have shown behavior similar to that observed in the tests on the model alloys, i.e., a relatively low K dependence and no benefit of decreased corrosion potential on SCC growth rates. For example, CGRs in BWR control-rod blade material (Type 304L SS) irradiated to about 12 dpa were one to two orders of magnitude higher than those in the same material irradiated to 3 dpa.[76]

The material irradiated to 12 dpa contained a high concentration of Si (~3 wt.%) at the grain boundary. Also, a cold-worked Type 316+Ti SS baffle bolt material, irradiated to 25 dpa in the BOR-60 reactor at 320°C, showed growth rates that were two orders of magnitude higher than those observed in cold-worked Type 316 SS baffle bolt material irradiated under the same conditions. The Ni and Si concentrations at the grain boundary were higher in the Type 316+Ti SS.[79] However, the validity of these tests is considered questionable because either the stress intensity factors exceeded the allowed values based on the proposed K/size criterion for irradiated materials or the duration of the test period was inadequate. The effects of K/size criterion are discussed in Section 2.2.1.3.

A common feature among the tests on high-Si SSs and irradiated SSs is that they all seem to have a relatively high growth rate (i.e., about 1 x $10^{-9}$ m/s or higher). As discussed in the previous section, this rate could be associated with some kind of threshold phenomenon that influences the crack tip strain rate.

In contrast to the increased susceptibility of high-Si materials indicated by crack growth tests on CT specimens, SSRT test data on several laboratory heats of irradiated Type 304 and 316 SSs with 0.5 to 1.8 wt.% Si show the opposite behavior. For the same fluence level, steels with 1.5 to 1.8 wt.% Si showed less irradiation hardening and greater elongation than steels containing 0.5 wt.% Si.[53] The percent IG cracking was not significantly different in the low- or high-Si heats of SSs. The addition of Si to pure austenitic SSs without Mo has been shown to promote dislocation loop nucleation. The presence of Mo negates the effect of Si on loop nucleation by trapping Si atoms and preventing them from binding with SIAs; Mo-Si clusters form instead.[83]

Because most commercial SSs contain about 0.5% Si, its effect on irradiation hardening is not likely to be significant. The tests on model alloys certainly suggest that high concentrations of Si at grain boundaries due to RIS could greatly increase susceptibility to IASCC. However, the absence of γ' silicide ($Ni_3Si$) at the grain boundaries suggests that RIS of Ni and Si probably saturates at higher doses; the actual dose and saturation concentrations may vary with material composition and irradiation temperature. The significance of Si segregation at grain boundaries on the SCC behavior of irradiated SSs is not clear, but the available results suggest that this segregation could be important. Crack growth tests should be conducted on irradiated material from commercial heats of SSs with similar compositions but different Si contents to establish the role of Si segregation on the IASCC susceptibility of irradiated SSs.

### 2.1.8 Sulfur Content

Based on SSRT tests, for several commercial heats of Type 304 and 316 SS that contain S concentrations of ≤0.002 wt.%, excellent resistance to IASCC is observed for neutron fluence up to ≈3 dpa.[53] As the S content is increased above 0.003 wt.%, IASCC susceptibility (expressed as percentage IGSCC) increased drastically as shown in Fig. 23 for irradiated Types 304, 304L, 316, and 316L SS in high-DO water at 289°C.[53]

The IASCC susceptibility of Type 304 or 316 SSs has been represented by a two-dimensional map of bulk S and C contents in the steel to show the range in which these steels are either resistant or susceptible to IASCC in the NWC BWR environment. An S-C content map for Type 304 and 316 SS in BWR-like oxidizing environments is shown in Fig. 24. At sufficiently low concentrations of S (≤0.002 wt.%), a high concentration of C suppresses the deleterious effect of S. However, when S concentration is high (≥0.003 wt.% in Type 304 and 316 SS, and ≥0.01 wt.% for Type 348 SS), the deleterious effect of S is so dominant that the effect of C is negligible or insignificant, even at high concentrations. Typically, in-service cracking of BWR core internal components occurs at >2 dpa and is

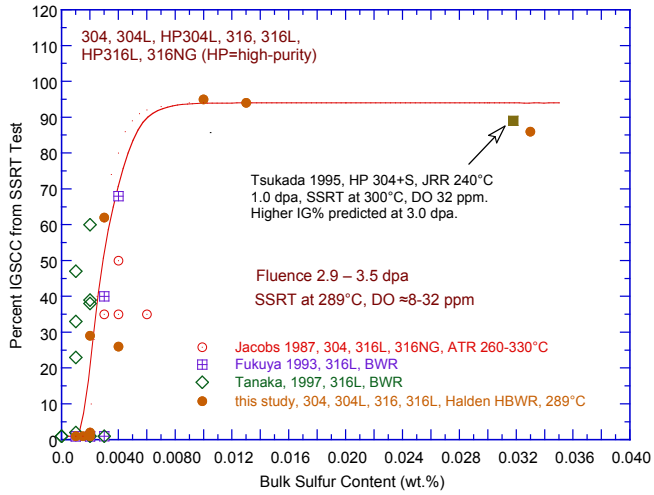


Figure 23.
Effect of bulk S content on IASCC susceptibility (percent IGSCC) of commercial heats of Type 304, 304L, 316, and 316L tested in high DO water at 289°C (Ref. 53).

characterized by a virtually full intergranular fracture surface, sometimes accompanied by a small amount of TG fracture surface. In constructing Fig. 24, Chung and Shack determined the resistance to IASCC based on the negligible IGSCC observed in SSRT tests conducted in high-DO (8-32 ppm) water with fluence levels of 3 dpa or greater. Limited data indicate a similar behavior of the effect of S and C contents on IASCC susceptibility in the PWR environment. The S-C content map for austenitic SSs in the PWR environment is shown in Fig. 25.

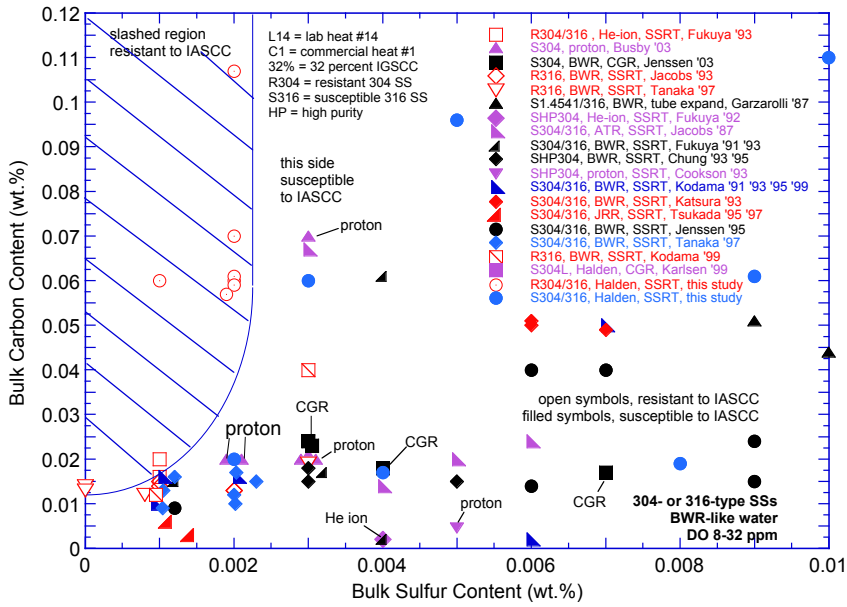


Figure 24. Range of bulk S and C contents, in which Type 304 or 316 stainless steels are resistant or susceptible to IASCC, in BWR-like oxidizing water (Ref. 53).

### 2.1.9 Stacking Fault Energy

As discussed earlier, irradiation hardening promotes dislocation channeling and localized deformation. The SFE of the material is an important parameter that determines the deformation mode. In SSs, the SFE increases with increased Ni content. Slow strain rate tensile test results have shown that high-Ni alloys have good resistance to IASCC. Alloys with Ni concentration >18 wt.% are highly

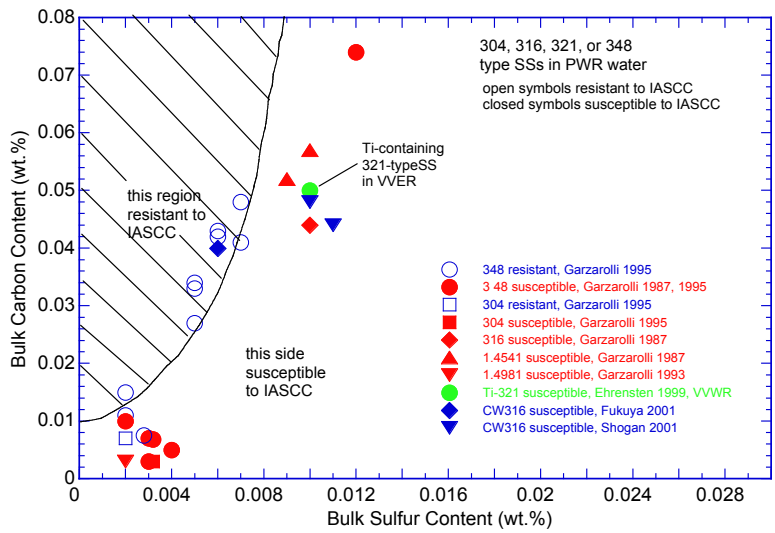


Figure 25. Range of bulk S and C contents, in which Type 304, 316, 321, or 348 stainless steels are resistant or susceptible to IASCC, in PWR water.

resistant to IASCC compared to Type 304 SS with 8 wt.% Ni.[3] Alloys with low SFE, such as SSs with 8 wt.% Ni, deform entirely by planar slip, whereas there is no evidence of planar slip in alloys with high SFE (i.e., alloys with >20 wt.% Ni). The deformation microstructure of low-SFE materials consists of well-defined slip bands or dislocation channels. As the Ni content increases, the cross slip increases. The deformation microstructure of high-SFE materials consists of dislocation tangles.

The effect of SFE on IASCC susceptibility (measured by percent IG cracking) of austenitic SSs is shown in Fig. 26. The results indicate a high susceptibility to IGSCC for materials with low SFE. Typically, Type 3xx SSs have relatively low SFE. In such materials, partial dislocations are widely separated and cannot readily combine; this condition reduces cross slip and promotes planar slip and localized deformation. The higher resistance of Type 316 SS compared to Type 304 SS may be explained on the basis of differences in the deformation mode because of the higher SFE in Type 316 SS.

A model for IASCC, based on the deformation mode, has been proposed.[3] In the model, IASCC susceptibility of SSs is explained in terms of two processes. In the first, the pileup of dislocations in the

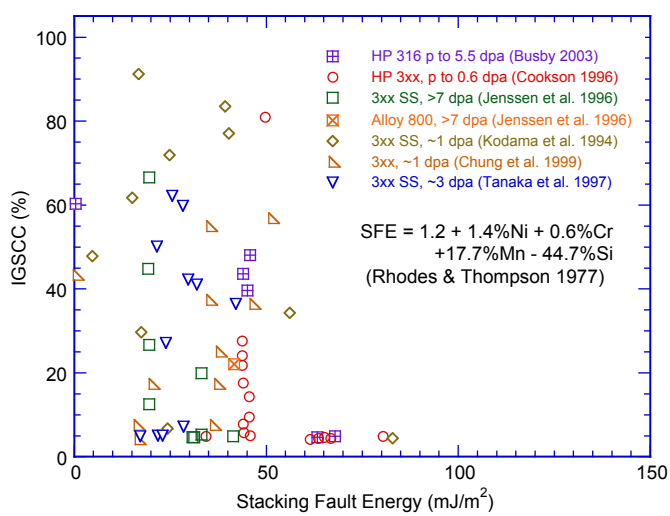


Figure 26.
IASCC susceptibility as measured by percent IG cracking as a function of stacking fault energy (Ref. 3).

slip bands or channels intersecting the grain boundaries creates progressively higher stresses at the grain boundary at the head of the pileup. When the stress exceeds a critical value, separation of the boundary may occur by a wedge cracking mechanism. This process does not depend on the environment and may be the mechanism for IG cracking observed in highly irradiated SSs in an inert environment. Susceptibility at lower fluences results from a second process. In this case, stress at the grain boundary can change the crack tip strain rate by rupturing the oxide film, thereby exposing bare metal surface and leading to oxidation/dissolution and crack extension. Alternatively, absorption of dislocations at the grain boundaries may cause grain boundary sliding ahead of the crack tip, resulting in crack extension and IASCC. The role of the localized deformation mode on IASCC of austenitic SSs and the possible contribution of SFE should be further investigated.

#### 2.1.10 LWR vs. Fast Reactor Irradiations

Comparison of data on materials irradiated in fast reactors and LWRs indicates that the fast reactor irradiations may not be prototypic of LWRs, particularly at fluence levels above 5 dpa. The differences in the neutron spectrums could lead to higher defect survival rates in LWRs compared to fast reactors, whereas the differences in flux and temperature could lead to lower defect survival rates in LWRs compared to fast reactors. In addition to possible differences in RIS and radiation hardening, differences in helium generation, because helium can migrate to grain boundaries, could play an important role in IASCC of PWR core internals. As discussed in Section 2.1.2, microchemistry characterization indicated that the RIS is greater in SSs irradiated in LWRs than in fast reactors. Also, for similar irradiation conditions, small cavities (probably He bubbles) are observed in LWR irradiated materials.

The effect of accelerated irradiation and helium generation on the IASCC susceptibility of SSs in PWR environment has been evaluated by comparing the results for materials irradiated in a fast reactor to 40 dpa with those irradiated in actual PWRs to 65 dpa.[51] Although the tensile properties were not significantly different for the materials irradiated in a fast reactor or a PWR, the fast-reactor-irradiated materials showed less helium and lower IASCC susceptibility compared to the PWR-irradiated materials. Also, IG cracking was observed in highly irradiated materials tested in an inert environment.

Slow strain rate tensile test results from another study also indicate that fast reactor irradiations may not be representative of LWR irradiations.[*] In Fig. 27, the yield strength (YS) and uniform elongation (UE) measured from SSRT tests on several heats of Types 304 and 304L SS irradiated in the Halden reactor at ~290°C to 3 dpa are compared with those measured on the same heats of SSs irradiated in the BOR-60 fast breeder reactor at 320°C to 4.8 dpa. The results indicate that although the total dose for the Halden materials is lower than that of the BOR-60 materials, their YS is higher, and their UE is lower. However, it cannot be ascertained whether these differences are due to the differences in irradiation temperature or flux and energy spectrum for the two irradiations. Additional studies are needed to validate the applicability of the fast reactor data to LWRs.

## 2.2 Crack Growth Rates

Experimental data have been obtained from studies sponsored by the NRC at Argonne, the Halden Reactor Project in Norway, the Cooperative IASCC Research (CIR) program, industry sponsored programs such as the BWR Vessel and Internals Project (BWRVIP) and Materials Reliability Program (MRP), and studies conducted at various institutions in Japan, EdF/Framatome in France, and Studsvik in

---

[*]Yiren Chen, Argonne National Laboratory, private communications, "Evaluation of the Causes and Mechanisms of IASCC in PWRs – Preliminary Results of IASCC Study on BOR-60 Materials," Sept. 2007.

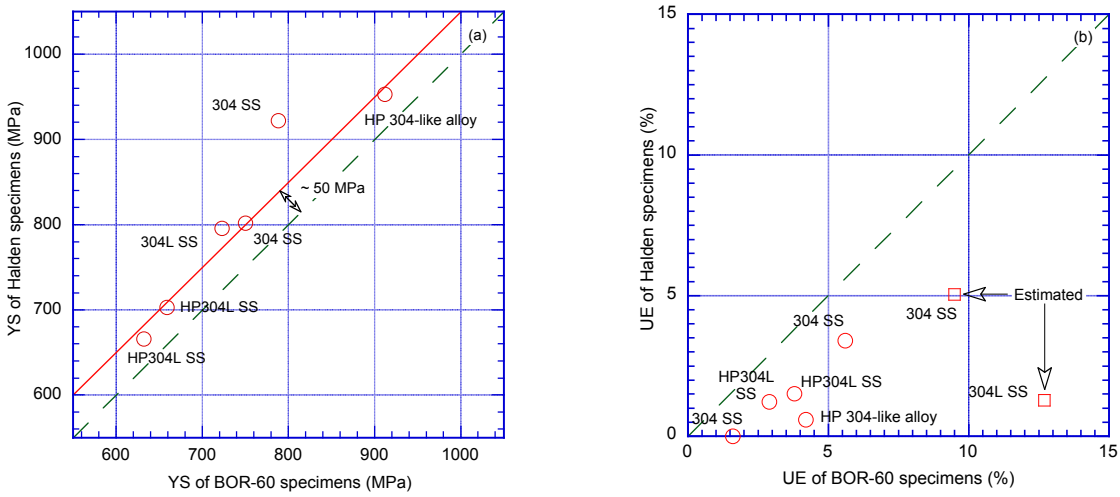


Figure 27. Measured (a) yield strength and (b) uniform elongation for several heats of Type 304 and 304L stainless steels irradiated in the Halden reactor at 290°C to 3 dpa and in BOR-60 fast breeder reactor at 320°C to 4.8 dpa.

Sweden. The data were obtained from specimens either machined from materials from LWR core internal components (mostly BWR components) or irradiated, after machining, under LWR irradiation conditions. However, some of the high neutron dose data have been obtained on materials irradiated in fast reactors (e.g., nearly all of the data obtained under the CIR program have been on specimens irradiated in the BOR-60 reactor in Russia). The applicability of the fast-reactor data for estimating irradiation effects under LWR operating conditions needs to be evaluated.

As discussed previously, SCC is a complex phenomenon that is dependent on several parameters such as material composition and processing, irradiation effects, water chemistry and electrochemistry, loading condition, and temperature. In addition, these parameters interact with each other such that their effect on growth rates is not always the same. For example, low-potential HWC BWR or PWR environments reduce susceptibility in SSs irradiated up to about 5 dpa, but not in SSs irradiated to higher dose levels. Sensitization (Cr depletion) due to thermal treatment or irradiation, as well as the presence of chlorides or sulfates in water, is known to have a strong effect on SCC susceptibility of austenitic SSs in the high-potential NWC BWR environment but little effect on SCC in low-potential HWC BWR or PWR environments.[82] As a result of these complexities and uncertainties in experimental measurements, the CGR vs. K data in LWR environments show significant variability (up to 1000X), and it is not yet possible to determine specific effects of these parameters on SCC growth rates with high confidence under all conditions of interest. Therefore, most investigators have emphasized the importance of high quality data and used caution in interpreting the results.

Crack growth rates have been obtained on irradiated wrought and cast austenitic SSs as well as SS weld metal and weld HAZ materials. There is little or no CGR data on irradiated Ni alloys, such as Alloy 600 or X750, that are used for some core internal components.

The quality of the CGR data has been evaluated or screened according to the following factors: (a) test procedures that closely reproduce the loading and environment conditions for reactor core internal components, (b) data acquisition and analysis system that provides accurate measurements and reproducible results, and (c) well-characterized material. These concerns and problems regarding the quality of experimental data for CGR are discussed further in the following section. The potential sources of uncertainty in experimental measurements and data scatter are also discussed.

### 2.2.1 Quality of Crack Growth Rate Data

#### 2.2.1.1 Test Procedures

Nearly all of the recent CGR data on irradiated materials in simulated BWR and PWR environments have been obtained on CT specimens (1/4-T or 1/2-T CT) or four-point bend specimens. The tests are performed in accordance with American Society for Testing and Materials (ASTM) E-647, "Standard Test Method for Measurement of Fatigue Crack Growth Rates," and ASTM E-1681, "Standard Test Method for Determining a Threshold Stress Intensity Factor for Environment-Assisted Cracking of Metallic Materials under Constant Load."

The specimens are fatigue pre-cracked (typically in air) to create a starter crack and are actively loaded in the environment of interest at constant K or constant load to determine the SCC growth rates and under cyclic loading to measure fatigue CGRs. The fatigue CGR tests are conducted with a triangular or slow/fast saw-tooth waveform with rise times up to 10,000 s and load ratio R between 0.2 and 0.9, and the SCC growth rate tests are conducted under constant K with or without periodic partial unloading. The stress intensity factor for SCC tests (and maximum stress intensity factor $K_{max}$ for fatigue tests) is in the range 3-40 MPa $m^{1/2}$. Also, the reversing direct-current (DC) potential difference method is used to monitor crack extension. The crack extensions determined from the DC potential drop method are corrected to match the final optically measured crack length. In most studies, crack lengths obtained from the DC potential drop method have shown good agreement with post-test fractography measurements; typically crack lengths measured by the potential drop method are 5-20% smaller.

During each test period (i.e., a specific loading and environmental condition), the crack extension is at least 10 times the resolution of the DC potential drop method (typically ≈5 μm). Thus, crack extensions are at least 50 μm and range up to 500 μm. The CGRs are determined from the slope of the corrected crack length (a) vs. time (t) plots. For cyclic loading, the CGR can be expressed in terms of a time-based growth rate (da/dt) or a growth rate per cycle (da/dN). However, the method for calculating da/dt varies among different investigators. Crack growth studies on austenitic SSs by Shack and Kassner[84] in the simulated BWR environment, and by Tice et al.[85,86] in the PWR environment have used a saw-tooth waveform (where the rise time was more than 85% of the period of the cycle) and da/dt was determined by dividing the crack advance per cycle by the rise time for the cycle.

Other investigators have used triangular or sinusoidal waveforms and determined CGRs by dividing the da/dN by the total time period for the cycle. In some studies, to account for the effects of surface oxide, crack closure, and roughness between the edges of the crack, an effective time of loading, $t_{eff}$, is used instead of the total time period t.[87] Thus, da/dt is determined from the relationship

$$\frac{da}{dt} = \frac{1}{t_{eff}}\left(\frac{da}{dN}\right), \tag{6}$$

where the $t_{eff}$ for loading cycle ranges from 0.6t, at R = 0.1, to t, at R = 0.7 or greater.

#### 2.2.1.2 Intergranular Starter Crack

A major source for variability in measured SCC growth rates is crack morphology. Typically, SCC of austenitic SSs in high-temperature water is IG, whereas the starter crack for SCC tests is produced by fatigue cycling the specimen in air, which creates a TG crack. Depending on the susceptibility of the material to SCC, the TG crack may not transition to an IG crack during the test or may transition only

along a portion of the specimen width. This behavior results in an irregular or finger-like crack front. Even if precracking is carried out in simulated LWR environments, an IG crack is not guaranteed. Under the more rapid cyclic loading typically used for precracking, the crack growth is dominated by mechanical fatigue, which nearly always creates a TG crack.

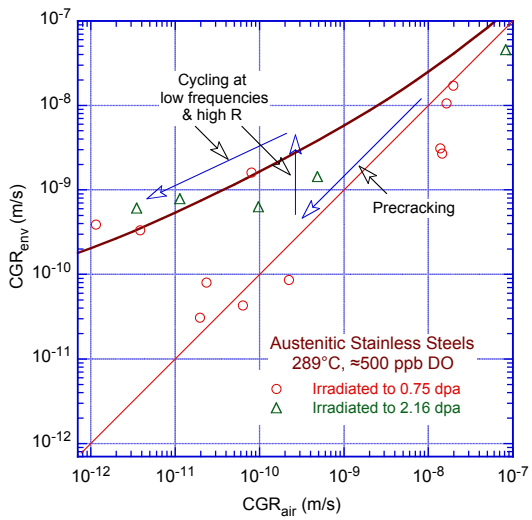


Figure 28.
Plot of CGR in water vs. CGR in air showing environmental enhancement of growth rates in high-purity water at 289°C (Refs. 10,11).

The specimens are, therefore, subsequently subjected to gentle cycling (to reduce the contribution of mechanical fatigue compared to corrosion fatigue or SCC) and facilitate the transition of a TG crack to an IG crack. To achieve this, the loading frequency is gradually decreased, and the load ratio R is increased above 0.3. This behavior is illustrated in Fig. 28, where CGRs in the environment are plotted as a function of the estimated CGRs in air under the same loading conditions. In this plot, since the CGRs of austenitic SSs in air are independent of frequency, the data points that lie along the diagonal represent predominantly mechanical fatigue, and those that lie above the diagonal indicate environmentally enhanced crack growth. Under gentle cycling as the frequency is decreased and R is increased, the CGRs first decrease along the diagonal, as shown by the curve denoted "Precracking" in Fig. 28, then jump to new, higher environmentally enhanced growth rates. Once environmental enhancement is achieved, the crack morphology for austenitic SSs is IG, and the crack front in test specimens is relatively straight. Environmental enhancement of growth rates is readily achieved for materials that are susceptible to SCC, as seen for the material irradiated to 2.16 dpa, whereas materials less susceptible to SCC (e.g., SS irradiated to 0.75 dpa) take much longer and often require some coaxing, i.e., very gradual reductions in the cyclic loading. For austenitic SSs, at $K_{max}$ = 15–18 MPa $m^{1/2}$, environmental enhancement typically occurs at R ≥ 0.5 and rise times ≥ 30 s.[10]

An example of enhanced growth rates for irradiated Type 304L SS in the simulated NWC BWR environment at 289°C is shown in Fig. 29.[9] The change in crack length is plotted as a function of time. For this specimen, environmental enhancement occurred after ≈170 h, when the load ratio and rise time, respectively, were changed from 0.5 and 60 s to 0.7 and 300 s. For the new loading condition, although the predicted CGR in air decreased by a factor of ≈15, the measured rate in the environment increased by a factor of ≈3.

#### 2.2.1.3 K/Size Criteria

Fracture mechanics is a correlative technology and does not attempt to describe the mechanisms that are occurring at the crack tip. It correlates the behavior of components with that of specimens

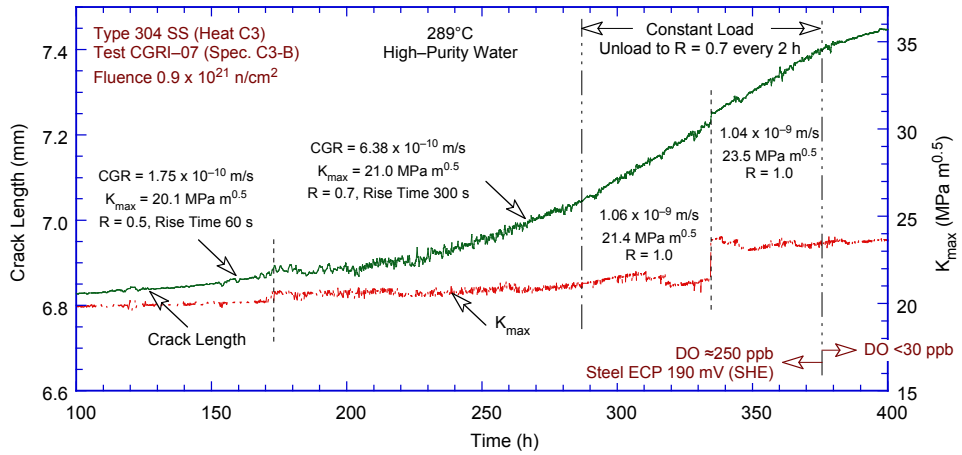


Figure 29. Plot of crack length vs. time for irradiated Type 304 stainless steel in high-purity water at 289°C (Ref. 9).

through the use of the K parameter. If two cracks have the same K, then they have the same strains and stresses in a region near the crack tip. For this correlation between specimen and component to work, K has to characterize the stresses and strains at the crack tip in the process zone. Mathematically, it can be shown that this observation is true if the plastic zone size is "small enough." The K/size criteria are combined theoretical and empirical results that have been found to ensure the plastic zone is small enough and K is controlling. The ASTM specifications for specimen K/size criteria are intended to ensure the applicability and transferability of the cracking behavior of a component or specimen of a given thickness under a specific loading condition to a crack associated with a different geometry, thickness, and loading condition. For constant load tests, ASTM E 1681 requires that

$$B_{eff} \text{ and } (W - a) \geq 2.5\ (K/\sigma_y)^2, \tag{7}$$

and for cyclic loading, ASTM 647 requires that

$$B_{eff} \text{ and } (W - a) \geq (4/\pi)\ (K/\sigma_y)^2, \tag{8}$$

where K is the applied stress intensity factor, $\sigma_y$ is the yield stress of the material, a is crack length, and the $B_{eff}$ is the specimen effective thickness, defined as $(B\ B_N)^{0.5}$. Thus, the specimen thickness or remaining ligament ahead of the advancing crack is at least a factor of 8 greater than the plastic zone size for tests conducted in accordance with the K/size criterion of Eq. 7. For high strain-hardening materials [i.e., ratio of ultimate stress to yield stress $(\sigma_u/\sigma_y) \geq 1.3$], both criteria allow the use of the flow stress defined as $\sigma_f = (\sigma_u + \sigma_y)/2$ rather than the yield stress.

At the present time, the database for defining the K/size criteria for irradiated materials is inadequate. The K/size criteria were developed for materials that show work hardening and, therefore, may not be applicable for materials irradiated to fluence levels where, on a local level, they do not strain harden. This lack of strain hardening, termed "strain softening," is most dramatic when dislocation channeling occurs at high fluences. For moderate to highly irradiated material, Andresen[15] has suggested an effective yield stress, defined as the average of the nonirradiated and irradiated yield stresses [$\sigma_{eff} = (\sigma_{yirr} + \sigma_{ynonirr})/2$]; this discounts the irradiation-induced increase in yield stress by a factor of 2.

Jenssen et al.[78] obtained crack growth data in simulated BWR environments on Type 304L SS irradiated to ≈13 dpa and investigated the specimen K/size criterion for CGR testing of irradiated

austenitic SSs. They concluded the following from a finite element study: if the strain softening found in highly irradiated materials is taken into account, and if the K/size criterion is defined as $\sigma_{eff} = (\sigma_{yirr} + \sigma_{ynonirr})/2$, there is a significant amount of plastic deformation in the plane of the growing crack. The authors argue that as a result of an increased tendency for "highly irradiated material" to deform by dislocation channeling, a K/size criterion based on the sum of irradiated and nonirradiated yield stress divided by 3 [i.e., $\sigma_{eff} = (\sigma_{yirr} + \sigma_{ynonirr})/3$] fits the crack growth behavior better.[78]

Thus, in these proposed K/size criteria, the irradiation-induced increase in yield stress is discounted by a factor of 2 for moderately irradiated materials and by a factor of 3 for highly irradiated materials.

These proposed criteria were not developed based on analyses of crack tip plastic strain or experimental comparisons of specimens with different degrees of constraint. Rather they seem to be based on an implicit assumption that if the benefit of reduced corrosion potential on CGRs is effective at one K level and is not effective at a higher K level, then the difference must be due to a violation of the K/size criterion. The argument being that since austenitic SSs irradiated above approximately 3 dpa exhibit strain softening, the K/size criterion based on the measured yield strength of the irradiated material is inadequate for such materials. It is not clear whether due consideration has been given to the possibility of other effects. As discussed later in this section, strain softening in highly irradiated austenitic SSs is rarely more than 10-15%.

Nakamura et al.[80] investigated the validity of a K/size criterion based on the effective yield stress instead of the measured yield stress of the material. They conducted crack growth tests with ½-T CT specimens of irradiated Type 304L SS in simulated BWR environments. The material was from a BWR control rod irradiated to $2.5 \times 10^{21}$ n/cm$^2$ (3.5 dpa), and the yield stress of the material at 288°C was 600 MPa. The CGRs were obtained in BWR environments at K values of 23-35 MPa m$^{1/2}$. The authors concluded that their results did not support a K/size criterion based on an effective yield stress rather than the measured yield stress. The crack growth behavior was relatively stable even after K exceeded the upper limit based on a small-scale yielding condition with effective yield stress for the irradiated material.[80] The plastic zone, evaluated on the basis of the microstructure and hardness distribution around the crack tip, was estimated to be 0.2-0.4 mm at K = 30 MPa m$^{1/2}$. For the same loading condition, the plastic zone size was estimated to be ≈0.8 mm for a material with 600-MPa yield stress, and ≈2.0 mm if the effective yield stress proposed by Andresen is considered.

Another study,[81] evaluated the validity of the K/size criterion for irradiated materials by comparing the plastic strain distribution in a ½-T CT specimen estimated from finite element method calculations with experimentally observed plastic deformation area. The results indicate that for a Type 316L SS material irradiated to $3 \times 10^{21}$ n/cm$^2$ in the Japan Materials Test Reactor, the appropriate K for SCC growth rate tests is at least 30 MPa m$^{1/2}$ for a 5.8-mm-thick ½-T CT specimen.

Pettersson* has presented three arguments against the proposed reduced effective stresses. First, he suggests that the strain softening in irradiated austenitic SSs is rarely more than 10-15%. This behavior is clearly demonstrated in the engineering stress vs. strain curves shown in Fig. 30 for Type 304 SS irradiated to 3.0 dpa in the Halden reactor at 288°C and tested in air at 289 and 325°C.[53] Secondly, in most of the plastic zone the plastic strains are so low that the material never passes the maximum tensile stress, so that it is effectively not a strain-softening material. Third, finite element analyses indicate that the difference is marginal between the strain distributions ahead of an advancing crack in a strain-

*Kjell Pettersson, Matsafe AB, private communication, "Some Aspects of Specimen Size Validity and Crack Tip Strain Rate," Nov. 2006.

hardening versus a strain-softening material (Fig. 31). These calculations do not support the suggestion that the nonirradiated yield strength should be involved in any calculations of specimen sizes for obtaining valid data.

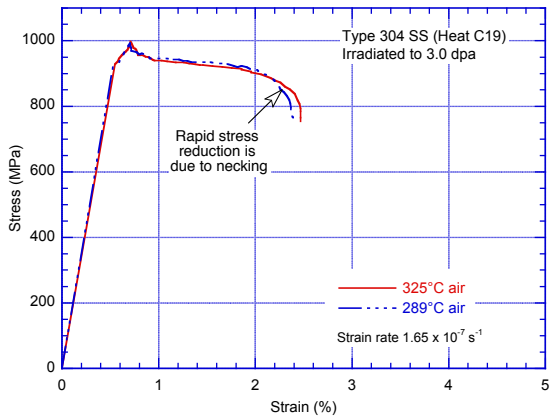


Figure 30.
Engineering stress vs. strain curve for Type 304 stainless steel irradiated to 3.0 dpa and tested in air at 289 and 325°C (Ref. 53).

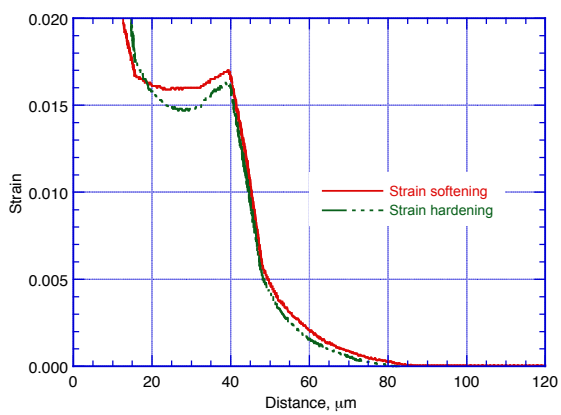


Figure 31.
Strain distribution of a moving crack in a strain-softening and a strain-hardening material (Ref. 11).

The adequacy of the proposed K/size criterion has also been evaluated by examining the effect of loss of specimen constraint on fracture morphology and crack growth behavior.[11] The experimental data for CGRs obtained under loading conditions that either meet or exceed the K/size criterion proposed by Andresen are shown in Fig. 32; the numbers next to the data points in Fig. 32b represent the value (in percentages) by which applied K exceeded the allowed value.

In Fig. 32b, although the applied K exceeds the value allowed by the K/size criterion proposed by Andresen by up to ≈40%, the CGRs measured from these tests are consistent with the results from tests shown in Fig. 32a that meet the criterion. Also, the K dependence for these tests is consistent with that observed for valid tests (e.g., the data yield an exponent of ≈2.1). Furthermore, in high-DO water, the CGR did not increase during the test period (for up to 200 h). Typically, the CGR increases rapidly when the applied load exceeds the specimen K/size criterion. For example, for a 1/2-T CT specimen of Type 304 SS irradiated to 4.0 dpa, the CGR increased by a factor 5 over a period of 40 h in high-DO water at 288°C and $K_{max}$ of 29-34 MPa $m^{1/2}$.[15]

The two data points obtained in a low-DO environment on Type 304L and 316 SS irradiated to 3.0 dpa and tested at 25-30 MPa $m^{1/2}$ (solid triangle and solid right-angle triangle in Fig. 32b) did not show the expected decrease in CGR when the DO level in the environment was decreased. The change in crack length and $K_{max}$ with time for Type 304L SS irradiated to 2 x $10^{21}$ n/cm$^2$ is shown in Fig. 33. The

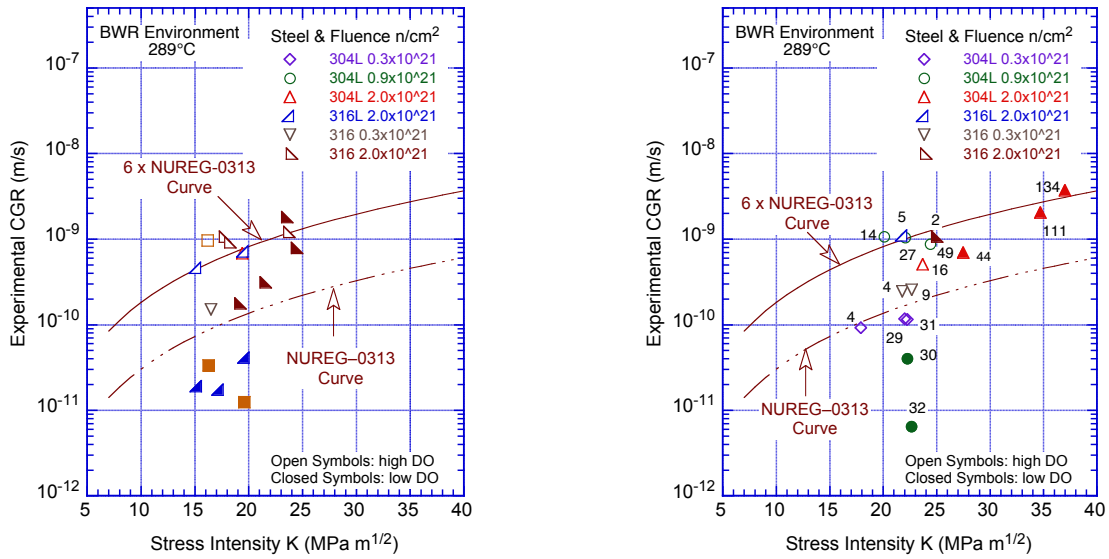


(a) (b)

Figure 32. Crack growth rates for irradiated stainless steels in BWR environments under loading conditions that (a) meet or (b) exceed the proposed K/size criterion. The numbers next to the data points represent the percentage difference between the applied and allowed K (Ref. 11).

results indicate no change in CGR for more than 300 hours when the DO level was decreased from 400 ppb to about 20 ppb. A similar behavior was observed for Type 316 SS. It can be argued that because the expected decrease in growth rate is not observed for these tests, the loading conditions must have exceeded the specimen K/size criterion, but it is not clear whether this behavior should be attributed to loss of specimen constraint. If specimen constraint had been lost, the growth rate should have rapidly increased in high-DO water.

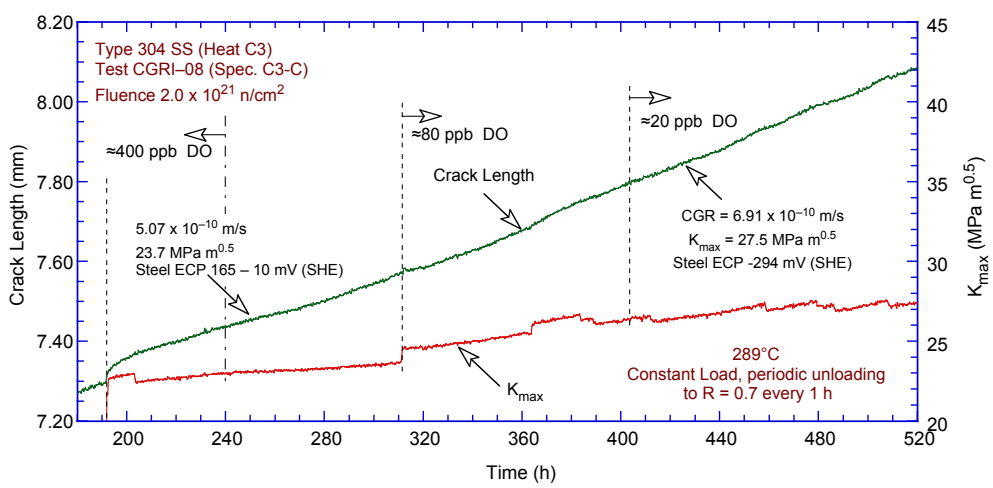


Figure 33. Crack length and K vs. time for Type 304L SS in high-purity water at 289°C (Ref. 11).

The specimen constraints based on Eq. 7 were lost for the two tests on irradiated Type 304L SS in low-DO water at K levels above 35 MPa $m^{1/2}$ (solid triangles in Fig. 32b), as evidenced by the unusually high growth rates. This behavior was verified by fractographic examination of the specimen; under these loading conditions, the crack propagation was away from the normal plane.

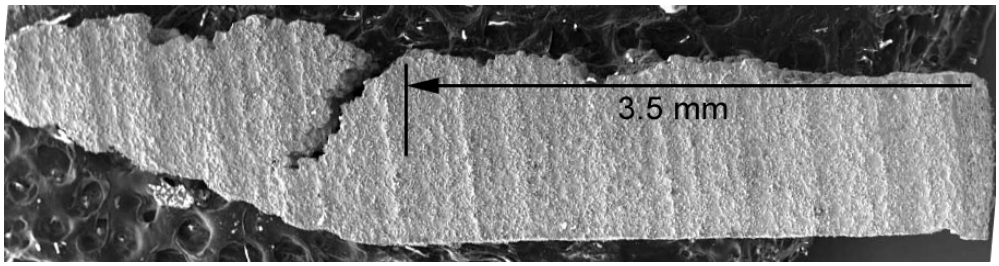


Figure 34. Side view of the first slice cut from Type 304L SS Specimen C3-C (Ref. 11).

A loss of specimen constraint should influence the fracture mode and morphology. For example, if the thickness criterion is exceeded, the crack plane is typically out-of-normal near the edges of the specimen, and if the specimen ligament criterion is exceeded, the crack propagates away from the normal plane at an angle of 45°. The fracture surface of Specimen C3-C was examined to investigate any change in fracture morphology and/or change in the fracture plane. Figure 34 shows a side view of a 1-mm-wide slice of the fracture surface (along the entire crack advance) cut from Specimen C3-C. The fracture surface is toward the top, in a plane perpendicular to the picture. (Although precautions were taken to ensure that the specimen was square to the movement of the electrical discharge machine wire, the cuts were not always straight; the bottom surface of this slice had an uneven cut.) The profile of the fracture surface indicates that the fracture plane is relatively straight and normal to the stress axis for the initial ≈3.5-mm crack extension. The DO level was decreased from ≈400 to 20 ppb at ≈1.7-mm crack extension, which is equivalent to the middle of the relatively straight crack extension. The fracture plane is out-of-normal for crack extensions greater than 3.5 mm. A secondary crack propagated at an angle of ≈45° to the original fracture plane. This region corresponds to the crack advance for the two tests for Type 304L SS at K levels of about 35 MPa $m^{1/2}$, which are represented as solid triangles in Fig. 32b; the CGRs during these periods were unusually high.

In addition, the fracture morphology did not change when the DO level was decreased from 400 to 20 ppb. After the initial TG fracture during fatigue precracking, the fracture morphology during all other test periods was completely IG. These results do not show any fractographic indication of a loss in constraint in the specimen (i.e., the fracture morphology did not change, and the fracture plane was straight and normal to the stress axis). Furthermore, the growth rate was constant for the entire duration when the DO level was decreased.

The results in Fig 32 indicate that some SSs may show IASCC susceptibility in low-potential environments at fluence levels as low as 3 dpa. Caution should be exercised to not propose a K/size criterion for irradiated SSs that screen out such experimental data simply because they do not agree with the current understanding of the IASCC behavior of austenitic SSs. The specimen size criteria for nonirradiated materials could be validated experimentally by using different size specimens. Such an approach is extremely difficult for irradiated materials, but more rigorous finite element studies of crack tip behavior may be helpful in developing appropriate validity criteria. In any case, the potentially conflicting results currently available indicate that additional data on SSs irradiated to 3-8 dpa are needed to accurately establish the threshold for IASCC susceptibility in low-potential PWR environments.

#### 2.2.1.4 Rising K or dK/da Effects

Another factor that can influence measurements of CGRs, under conditions that are relevant for LWRs, is a variation in K as the crack advances. In LWR components, K can increase as the crack depth, a, increases with crack advance, and can increase and then decrease due to the through-wall weld residual stress profile, which is usually U-shaped. Consequently, as the crack advances through the wall, K can

increase, remain relatively constant, or decrease depending on the residual stress profile. Initially, when the crack depth is small, K could increase very rapidly because it is proportional to the square root of crack depth ($K \alpha \sigma\sqrt{a}$). Studies on austenitic SSs and Ni alloys in high-purity water with 2000 ppb $O_2$ at 288°C have shown that rising K (+dK/da) at K values that are relevant for LWR components can increase the CGRs significantly, whereas decreasing K (-dK/da) has little or no effect.[88] Under rising K conditions, growth rates can be more than two orders of magnitude higher than those under constant K conditions.

As discussed by Andresen and Morra,[88] dynamic strain at the crack tip is an important element of crack advance under constant K loading conditions. As the crack advances, the process of stress and strain redistribution sustains crack growth. It leads to slip offset, which ruptures the surface oxide film, and the crack advances due to oxidation/dissolution of the metal. Thus, there is an inherent synergy between crack advance and growth rate itself (or dK/da as the crack advances). The data presented by Andresen and Morra[88] indicate that when changes in K are controlled by dK/da, very different responses can be seen for increasing versus decreasing K conditions with crack propagation. For example, increasing K results in an increased growth rate, which causes faster increase in K, which is a positive feedback. Decreasing K, on the other hand, yields negative feedback. These results indicate that CGR data obtained from tests where K was allowed to increase during the test or was decreased too fast may give erroneous results for the K dependence of SCC growth rates. Caution should be exercised while interpreting such results.

#### 2.2.1.5 Reloading Effects

For some irradiated austenitic SS materials, small increases in the stress intensity factor K due to either load perturbations or the reloading portion of the partial unload/reload cycle during an SCC growth rate test result in a rapid or step-like crack extension.[60] The growth rates during such periods are as high as $10^{-7}$ m/s. Such reloading effects produce a classic staircase appearance in the crack length vs. time plots. Similar behavior has been observed in nonirradiated CW SSs with high yield strength.[39] This behavior has often been attributed to the breaking of uncracked ligaments in the material, and is believed to occur in materials with an uneven crack front. The significance and cause for this behavior should be investigated.

### 2.2.2 Stress Corrosion Cracking Growth Rates

Most of the CGR data on irradiated materials have been obtained under BWR operating conditions (i.e., relatively low neutron dose in NWC or HWC BWR environments). Consequently, the data in BWR environments are discussed first.

#### 2.2.2.1 BWR Environments

*Dependence of Stress Intensity Factor K*

The majority of the SCC growth rate tests in BWR environments have been conducted at constant K with or without periodic partial unloading to R = 0.5-0.7. A few tests were performed using a trapezoidal waveform with rise and return times up to 5000 s. For these tests, the experimental data can be adjusted to account for the contribution of corrosion fatigue by using the cyclic CGR data; the details are discussed in Section 2.2.3. The SCC growth rates reported in the literature for various grades and heats of austenitic SSs irradiated from $5 \times 10^{20}$ n/cm$^2$ to $2.5 \times 10^{22}$ n/cm$^2$ (0.75 to 37.5 dpa) in NWC BWR and HWC BWR environments are shown in Figs. 35a-c and Figs. 36a-c, respectively. Crack

growth rates in submerged arc (SA) weld and shielded metal arc (SMA) weld HAZ materials as well as sensitized SSs are included in the figures. Also included are the K vs. CGR disposition curves proposed in NUREG-0313 for nonirradiated sensitized austenitic SSs in high-purity water containing 8 ppm DO (Eq. 5) and the curve proposed by EPRI for austenitic SS BWR core internal components.[89] The EPRI disposition curve for use in BWR core environments is expressed as

$$da/dt\ (m/s) = A2\ (K)^{2.5}, \tag{9}$$

where K is in MPa $m^{1/2}$, and the constant A2 is $4.564 \times 10^{-13}$ in NWC and $1.512 \times 10^{-13}$ in HWC BWR environments. The EPRI correlations are based on two datasets: General Electric (GE)/Japan Power Engineering and Inspection Corp. (JAPEIC) data for SSs irradiated to $2.7 \times 10^{21}$ n/cm$^2$ (4.0-4.5 dpa),[89]

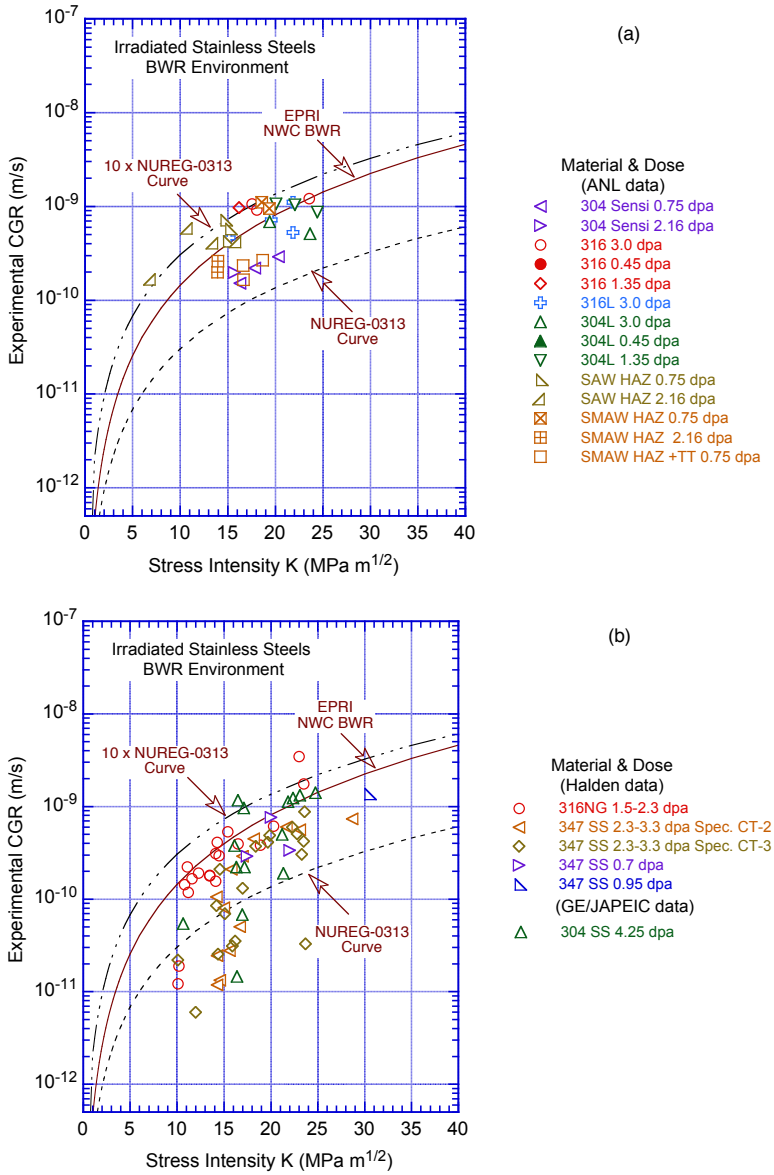


Figure 35. Experimental SCC growth rates in NWC BWR environment of austenitic stainless steels irradiated to (a) 0.75-3.0 dpa (Refs. 9,11), (b) 0.7-4.25 dpa (Refs. 74,75,77,89) and (c) 5.5-37.5 dpa (Refs. 74,75,77,79,78).

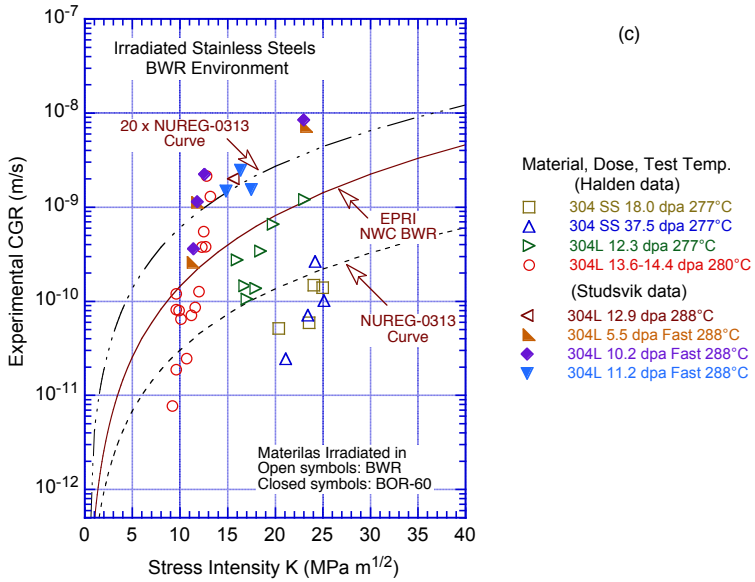


Figure 35. (Contd.)

and the Halden IFA data (639 test series) for Type 304, 347, and 316NG SSs that were irradiated to 9.0, 1.5, and 0.9 x $10^{21}$ n/cm$^2$ (13.5, 2.25, and 1.35 dpa).[74] The significant results in NWC and HWC BWR environments are summarized as follows.

1. In the NWC BWR environment, the SCC growth rates of austenitic SSs irradiated to 5 dpa could be a factor of 10 higher than the NUREG-0313 disposition curve for nonirradiated SSs in 8 ppm water, and those irradiated to 10-12 dpa could be a factor of 25 higher than the NUREG-0313 curve. Furthermore, as seen in Figs. 35a and b, for the end-of-60-year-life fluence level (3 x $10^{21}$ n/cm$^2$ or 4.5 dpa), the CGRs of some SSs materials could be significantly higher than the CGR disposition curve proposed by EPRI. In Fig. 35a, the data for SA weld HAZ materials irradiated to 0.75 or 2.16 dpa[11] are a factor of 2 above the EPRI curve. The results also indicate that the SCC growth rates for SSs irradiated in BWRs to 18 dpa or higher are below the NUREG-0313 disposition curve for nonirradiated SSs. The reasons for the low CGRs obtained for these highly irradiated BWR materials in the high-potential BWR environment are not clear.

2. A CGR disposition curve a factor of 10 higher than the NUREG-0313 curve bounds nearly 80% of the data obtained in the NWC BWR environment for SSs irradiated up to 4.25 dpa (Fig. 35b). The EPRI curve is about a factor of 6 higher than the NUREG-0313 curve, although the K dependence is higher (i.e., the exponent is 2.5 for the EPRI curve and 2.161 for the NUREG-0313 curve).

3. In general, CGR data obtained using test procedures in which the specimen was precracked in air and then transferred to the autoclave for the SCC test show much more variability at K values of 8-15 MPa m$^{1/2}$ (Halden data in Figs 35b and c) than data obtained using test procedures in which the specimen was precracked in the NWC environment and the TG fatigue crack was transitioned to an IG crack using slow fatigue cycling in the same environment before starting the SCC test [Argonne National Laboratory (ANL) data in Fig. 35a and Studsvik data in Figs. 35b and c]. This difference does not appear to be due to differences in material or irradiation conditions because data obtained at Halden and Studsvik on the same heat of Type 304L SS BWR control-rod blade material irradiated to comparable neutron dose [e.g., the two horizontal triangles (▷ and ◁) in Fig. 35c for Type 304L

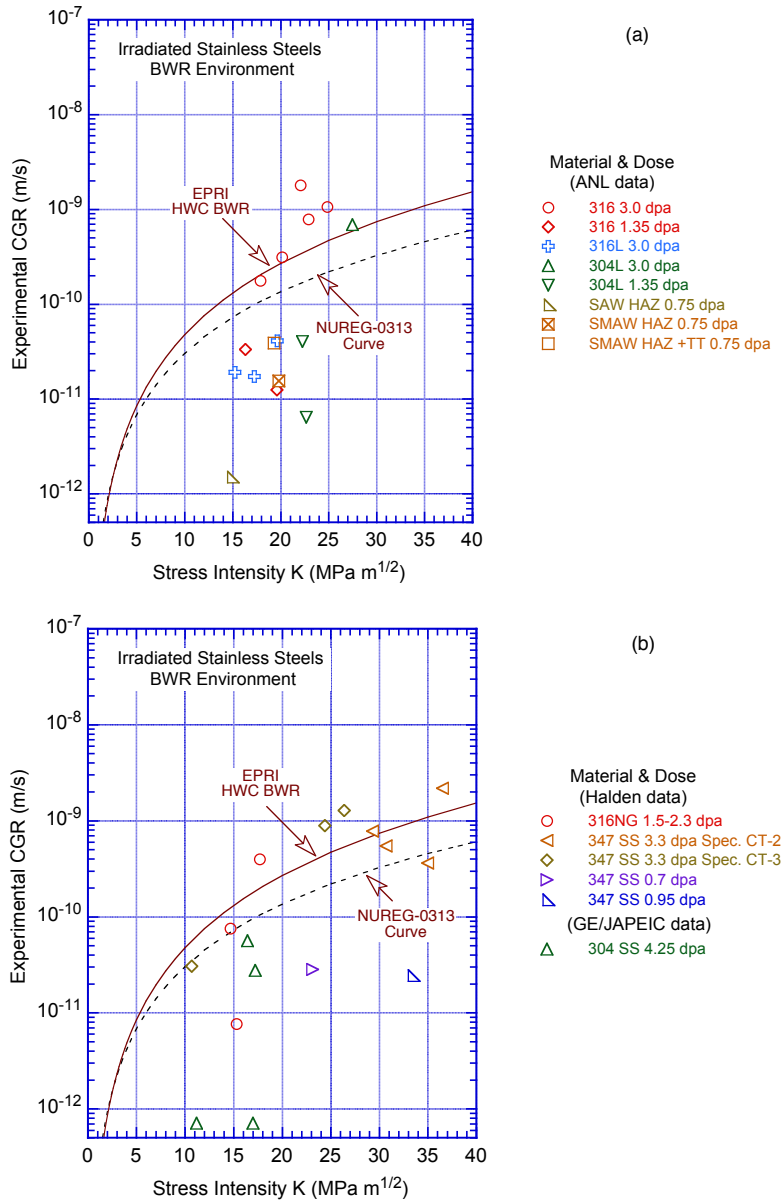


Figure 36. SCC growth rates in HWC BWR environment of austenitic stainless steels irradiated to (a) 0.75-3.0 dpa (Refs. 9,11), (b) 0.7-4.25 dpa (Refs. 74,75,77,89), and (c) 5.5-37.5 dpa (Refs. 74,75,77,79,78).

irradiated to 12.3 and 12.9 dpa, respectively] show more than a factor 10 higher growth rates for the material tested at Studsvik than for the material tested at Halden.

The difference is also not related to failure mode differences, since post-test fractography of the Halden specimens showed that the fracture morphology was always IG as in the ANL and Studsvik testing. Finally, for the loading sequence used in the tests at ANL and Studsvik, the CGRs at K values of 3-11 MPa $m^{1/2}$ were obtained by decreasing K from 14-20 MPa $m^{1/2}$ to the low values. Thus, the cracks were growing at a rate $\geq 7 \times 10^{-10}$ m/s before K was decreased, whereas, in the Halden data, tests were started at low K and the CGRs were $<1 \times 10^{-10}$ m/s as K was allowed to increase during the test. As discussed in Sections 2.1.6 and 2.1.7, the relatively weak K dependence

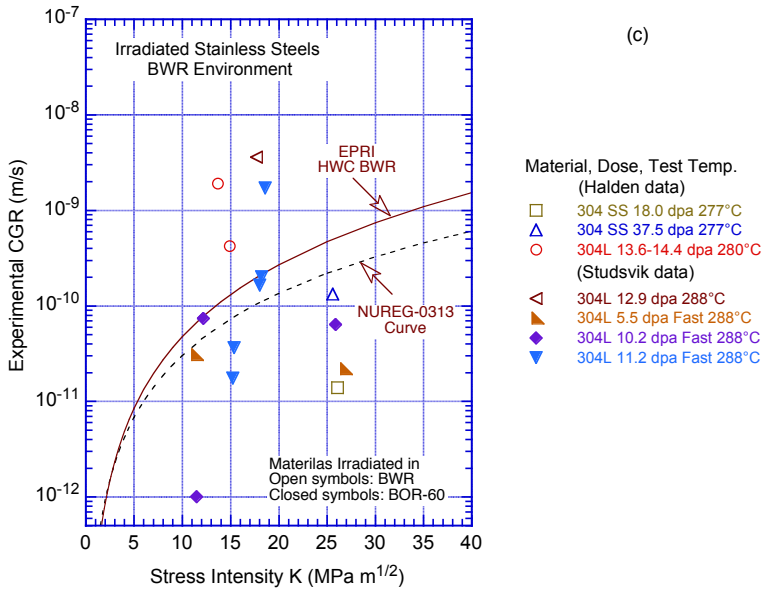


Figure 36. (Contd.)

of CGRs may be associated with a threshold growth rate (e.g., about 1 x $10^{-9}$ m/s) that influences the crack tip strain rate. Therefore, differences between the CGR appear to be due to the differences in the loading sequence and not to differences in materials, failure mode, or irradiation fluence.

4. For the tests where the fatigue TG crack was transitioned to an IG crack by slow fatigue cycling in the environment, periodic unloading during the SCC test at constant K had little or no effect on growth rates; the CGRs obtained with periodic unloading are comparable to those obtained without unloading. However, periodic unloading seems to have a significant effect on growth rates for some tests that did not use slow fatigue cycling to transition the fatigue TG crack to an IG crack. In these tests, for low dose materials (e.g., less than 5 dpa), the CGRs obtained with periodic unloading are comparable to those obtained without periodic unloading in the NWC BWR environment but are typically higher than those obtained without periodic unloading in the HWC BWR environment. This difference is associated with uncracked ligaments in the material. Also, for the Type 304 SS irradiated to 18.0 or 37.5 dpa (Fig. 35c), stable CGRs could be established only with periodic unloading and not under constant K. Both materials came from a decommissioned PWR. It is possible that this behavior is unique to the material microstructure and microchemistry.

5. The K dependence of growth rates shows some variability. The exponent of K, in Eq. 5, was typically between 1.7 and 2.7 for SSs irradiated up to about 5 dpa. For the Halden data, the exponent was about 2 for the IFA-639 test series and about 2.5 for the IFA-658 test series. Exponents between 1.5 and 2.0 were observed for the ANL data sets. For SSs irradiated to higher dose levels, depending on the test procedure, the exponent could be as high as 7. As discussed above, the higher K dependence may be due to the effect of the loading sequence. However, as discussed above, for the SSs irradiated to 18.0 or 37.5 dpa, stable CGRs were observed only with periodic unloading, and the rates were relatively insensitive to changes in K.

6. The cracking behavior of various grades and heats of SSs irradiated to the same dose level seems to be the same. For example, in the Halden study, the CGRs for Type 316NG and 347 SSs irradiated to 2.0-3.5 dpa are similar.[74] Similarly, in the ANL study, the CGRs of Type 304L, 316L, or 316 SSs irradiated to 1.35-3.0 dpa are comparable.[11] However, the rates for weld HAZ materials are slightly

higher than those for solution-annealed materials (Fig. 35a). The higher rates most likely are due to weld residual strains, which could be as high as 30% of room-temperature tensile strain.[40] Typically, residual strains are the highest at the root of the weld and near the weld fusion line. The significance of cold work in increasing SCC susceptibility is well known, and has been discussed in Section 2.1.5.

Figure 37 gives the SCC growth rates for two irradiated specimens of CF-8M cast SS in the NWC BWR environment. The specimens were aged for 10,000 h at 400°C before irradiation. The large difference between the measured CGRs for the two specimens is because sustained crack growth was not achieved in Specimen 75-11TT under constant K loading (i.e., without periodic unloading). The results for the other specimen are comparable to the data obtained on solution-annealed SSs and weld HAZ materials irradiated to similar dose levels. The CGRs are a factor of 2-6 above the values predicted by the NUREG-0313 curve for nonirradiated austenitic SSs.[66]

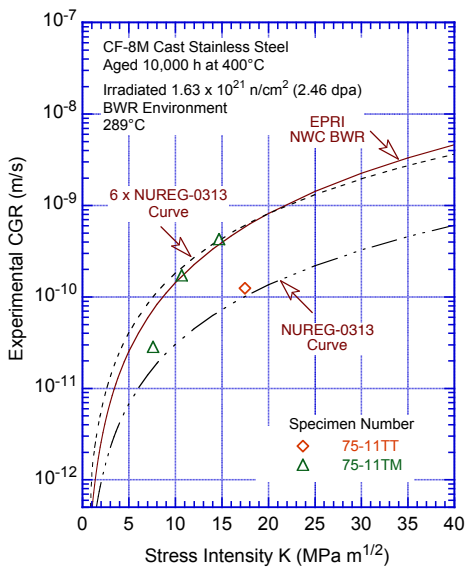


Figure 37.
CGR under constant load for thermally aged and irradiated CF-8M cast stainless steel specimens in BWR environment at 289°C (Ref. 11).

*Effect of Corrosion Potential*

The data in Fig. 36 for SCC growth rates in the HWC BWR environment show a significant decrease in growth rates relative to those in the NWC BWR environment for SSs irradiated to less than 3 dpa; little or no reduction for some heats of SSs irradiated to 3-4 dpa, at least at K values above 18 MPa $m^{1/2}$; and no decrease for all SSs irradiated 12-14.5 dpa. The materials irradiated to 18 or 37.5 dpa also did not show any benefit of decreased corrosion potential on CGRs, but a sustained crack advance was not observed in these materials under constant K. In these materials, growth rates were established with periodic unloading, and the rates even in the NWC BWR environment were below the NUREG-0313 curve for nonirradiated SSs. A significant feature of the cracking behavior of high dose materials was the "staircase" effect or reloading effect discussed in Section 2.2.1.5. In the HWC BWR environment, each unloading/reloading cycle was accompanied by a step or "jump" in crack length, creating a staircase or stepped crack growth. Although this behavior is often attributed to breaking of uncracked ligaments or straightening of the crack front, it is not clear why it should occur only in the HWC environment. Additional data in the HWC BWR or PWR environments are needed on high-dose materials to better understand the IASCC behavior of austenitic SSs.

The data for the 3-4 dpa materials (e.g., circles in Fig. 36a and diamonds and horizontal triangles in Fig. 36b) are often considered invalid because of the high K values that exceeded the proposed K/size

criterion for irradiated materials (i.e., the irradiation-induced increase in yield stress is discounted by a factor of 2). As discussed in some detail in Section 2.2.1.3, the arguments against the validity of the data do not seem to have a well-developed technical basis. The results in Figs. 32 and 36 indicate that the benefit of low-potential environments on SCC growth rates may be lost for some heats of SSs irradiated to fluence levels as low as 3 dpa. Some internal consistency checks can be used to demonstrate the validity of the Halden data for Type 347 SS irradiated to 2.3-3.3 dpa (diamonds in Figs. 35b and 36b). The growth rates observed (not corrected) during the test time from 720 to 840 h for two identical specimens (CT-2 and CT-3) of this material tested in the NWC BWR environment were 7.32 x $10^{-10}$ m/s at 28.7 MPa $m^{1/2}$ and 8.75 x $10^{-10}$ m/s at 23.6 MPa $m^{1/2}$.[74] The environment was then changed to HWC and the rates for the two specimens during test time 840 to 950 h were 7.77 x $10^{-10}$ m/s at 29.3 MPa $m^{1/2}$ and 8.9 x $10^{-10}$ m/s at 24.4 MPa $m^{1/2}$. The growth rates for both specimens did not decrease after the corrosion potential was decreased. Also, note that the applied K for specimen CT-2 in NWC was higher than that for specimen CT-3 in HWC. If the measured CGR for specimen CT-3 is invalid in HWC, it should also be invalid for specimen CT-2 in NWC. The experimental data or the post-test fractography of these samples do not show any indication that the specimen constraints were exceeded for these specimens.

Some investigators seem to dismiss such results simply because they do not agree with the current understanding of the IASCC behavior of austenitic SSs. The feature that is common between specimens CT-2 and CT-3 is that although the K values are different, the growth rates for the specimens are comparable and may represent a threshold rate above which CGRs are relatively insensitive to changes in stress intensity factor or corrosion potential. As discussed previously, additional data on SSs irradiated to 3-8 dpa are needed to accurately establish the threshold for IASCC susceptibility in low-potential PWR environments.

*IASCC Growth Rate Disposition Curve for BWR Core Internals*

The IASCC growth rate vs. K disposition curves proposed by EPRI for BWR core internal components are based primarily on two datasets: GE/JAPEIC and Halden data for austenitic SSs irradiated up to 13 dpa. The database does not include results obtained at ANL on weld HAZ materials or at Studsvik on BWR-irradiated Type 304L SS, which show SCC growth rates that are a factor of 2-3 higher than the EPRI disposition curve. Therefore, the EPRI disposition curves in NWC and HWC environments should be revaluated in light of recent data. The curve is clearly not bounding, and an updated estimate of the fraction of the population of CGR data that are encompassed by the curve is needed. Additional data should be obtained on austenitic SSs, including Type 304L SS and weld HAZ materials, in HWC to better define the threshold fluence for IASCC susceptibility in low-potential environments.

*Effect of Neutron Fluence*

For the various grades and heats of austenitic SSs shown in Figs. 35 and 36, the SCC growth rates in the NWC BWR and HWC BWR environments at 288°C and K = 20 MPa $m^{1/2}$ are plotted as a function of neutron dose in Figs. 38a and b, respectively. The materials were irradiated in BWRs at 280-300°C and in a fast reactor at 320°C. For each data set, the CGR at 20 MPa $m^{1/2}$ was determined using Eq. 5; the actual value of the exponent was used when known. In the NWC BWR environment, the CGR increases above the NUREG-0313 level for doses >0.5 dpa, and it also increases with dose to about 10 dpa, although there is variability in the data. In the HWC BWR environment, the CGRs do not exceed the NUREG-0313 levels until the fluence is ≥3.0 dpa. The CGRs for materials irradiated >5 dpa are comparable to those observed in the NWC BWR environment. As noted previously, there are some

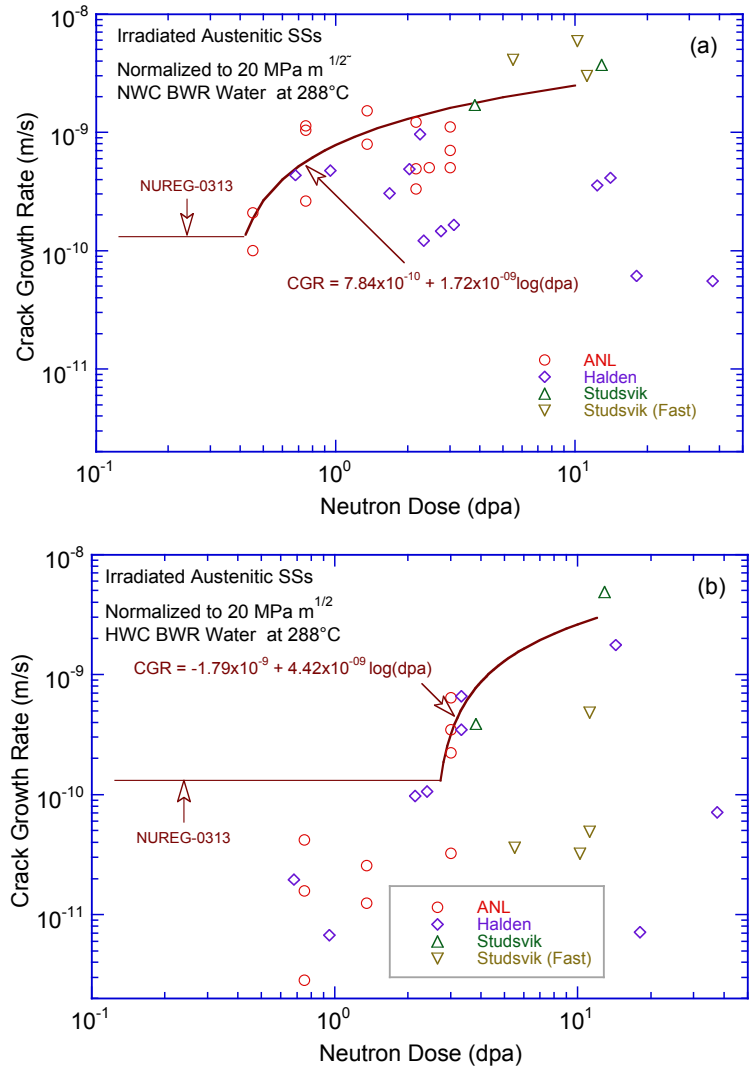


Figure 38. Crack growth rates of irradiated austenitic stainless steels in (a) NWC and (b) HWC BWR environments at 288°C and K of 20 MPa $m^{1/2}$ plotted as a function of neutron dose.

anomalously low data at 18 and 38 dpa. The curves shown in Fig. 38 bound approximately the 75th percentile of the data in the NWC environment and greater for the HWC environment. The curves assume a threshold dose of 0.45 dpa and 2.7 dpa (or 3 x $10^{20}$ and 1.8 x $10^{21}$ n/$cm^2$) in the NWC and HWC environment, respectively. The curves assume that the value for the constant A1 in the NUREG-0313 disposition curve (Eq. 5) varies with neutron dose. In the NWC environment A1 is taken as

$$A1 = 1.21 \times 10^{-12} + 2.65 \times 10^{-12} \log(\text{dpa}), \tag{10}$$

and in the HWC environment as

$$A1 = 2.76 \times 10^{-12} + 6.82 \times 10^{-12} \log(\text{dpa}). \tag{11}$$

Note that because Eqs. 10 and 11 define the constant A1 in Eq. 5, these values must be multiplied by $(20)^{2.161}$ to obtain the expression for the CGR curves shown in Fig. 38.

*Effect of Yield Strength*

The effect of neutron dose on SCC growth rates may also be determined from the change in CGRs as a function of material yield strength (measured at temperatures of 280-300°C). The data shown in Figs. 38a and 38b are plotted as a function of material yield stress in Figs. 39a and 39b for CGRs in NWC and HWC environments, respectively. The results show an increase in CGRs with an increase in yield stress due to irradiation hardening. The increase in growth rates occurs at about 300 MPa in the NWC environment and at about 550 MPa in the HWC environment. However, the correlation between yield stress and CGR is not as good as that for cold-worked, nonirradiated austenitic SSs (in Fig. 16 or 17). For example, the yield stress of SSs irradiated to 0.45 or 0.75 dpa is 500-550 MPa, but the growth rates vary by a factor of 7-10 for these materials. Although data scatter and material variability contribute to the large differences in the CGRs, the results for irradiated materials suggest that in addition to irradiation hardening, other factors such as the RIS of Cr and Si at the grain boundaries are also important.

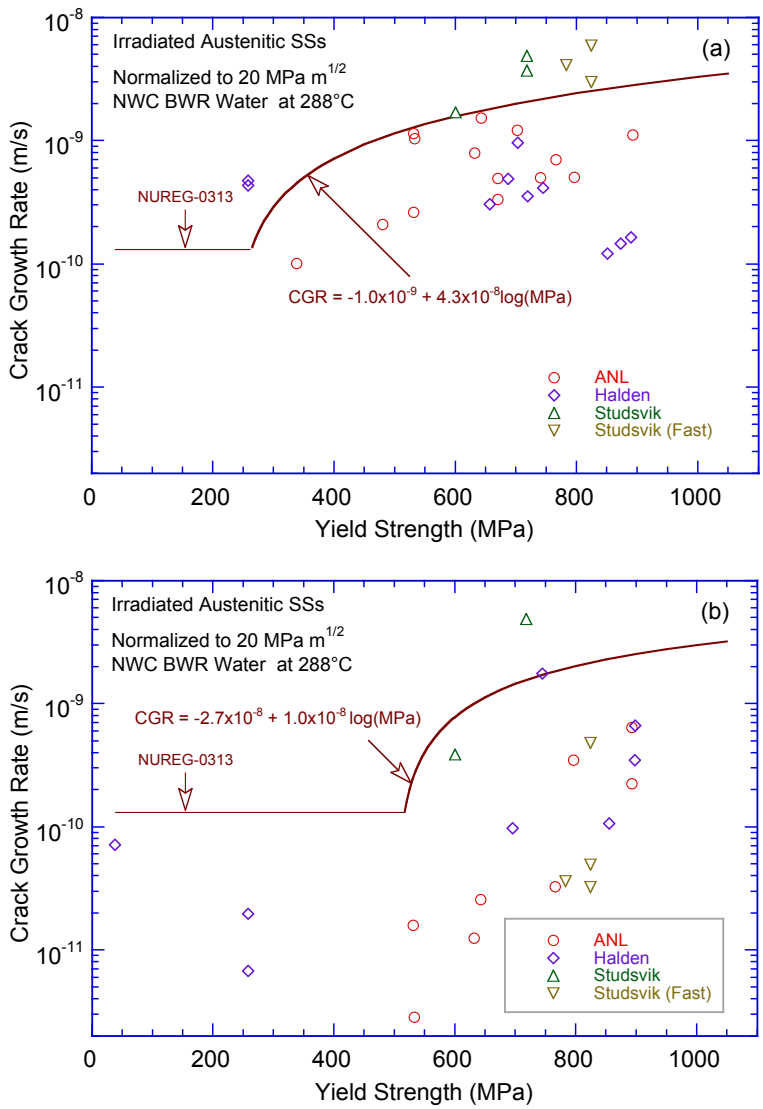


Figure 39. Crack growth rates of irradiated austenitic stainless steels in (a) NWC and (b) HWC BWR environments at 288°C and K of 20 MPa $m^{1/2}$ plotted as a function of yield stress.

### 2.2.2.2 PWR Environments

Data on the SCC growth rate for irradiated austenitic SSs in the PWR environment have been obtained at Halden[60,76] on BWR irradiated materials, at Studsvik[79] on BOR-60 irradiated materials, and from EPRI-sponsored studies on BWR and PWR irradiated materials. The total irradiation dose for these materials was in the range of 3.0-37.5 dpa, with test temperatures of 288-340°C. The measured growth rates in various grades and heats of austenitic SSs in the PWR environment are shown in Fig. 40. There is a great deal of variability in the reported data. For a given material and irradiation condition, the variability is on the order of a factor of 10. The variability between materials and irradiation conditions is on the order of 1000.

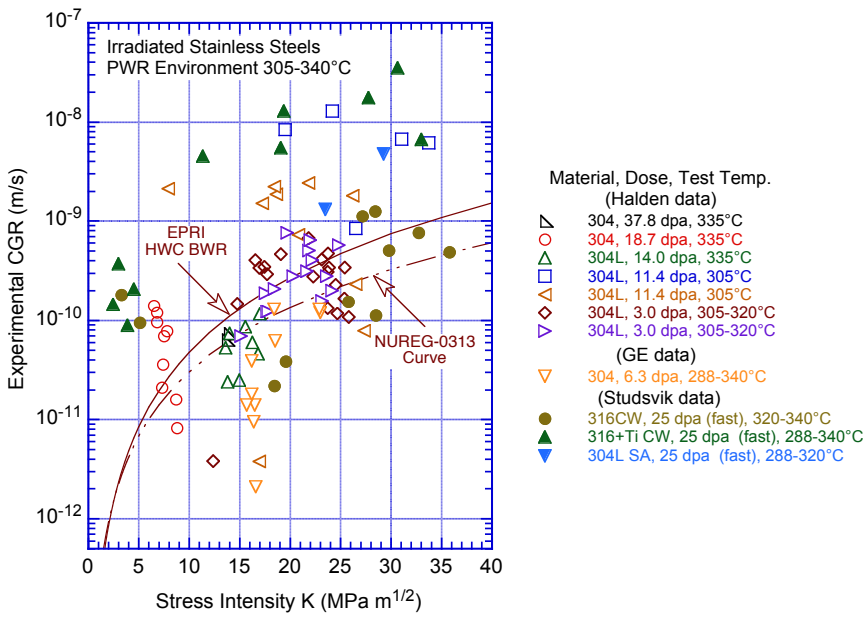


Figure 40. SCC growth rates of austenitic stainless steels irradiated to 3.0-37.8 dpa in PWR environment (Refs. 60,76,79,90).

Tests conducted on the same material at different temperatures indicate that the CGRs increase with increasing temperature. The temperature dependence of the SCC growth rates in irradiated and nonirradiated austenitic SSs yields activation energies between 60 and 150 kJ/mol. The experimental data for CGRs[79] of irradiated CW Type 316+Ti SS in PWR are plotted as a function of inverse temperature in Fig. 41. The data yield an activation energy of 105 kJ/mol. An activation energy of 100 kJ/mol was used to normalize the data shown in Fig. 40 to a temperature of 320°C; the normalized CGRs are shown in Fig. 42 for materials irradiated to (a) 3 dpa, (b) 11-25 dpa, and (c) 6-38 dpa. Note that normalization does not significantly decrease the overall data scatter in Fig. 42 compared to Fig. 40. The normalization process changes only the magnitude of CGRs for a specific data set.

The following observations were made from the normalized CGRs:

1. In general, in the PWR environment at 320°C, the SCC growth rates of materials irradiated up to 12 dpa are above the EPRI disposition curve for the HWC BWR environment at 288°C. More than half the data points for Type 304L SS irradiated to 3 dpa are above the EPRI curve (Fig. 42a). The CGRs for Type 304L SS irradiated to 11.4 dpa and for fast-reactor-irradiated materials (except cold-worked Type 316 SS) irradiated to 25 dpa are about two order of magnitude higher than the NUREG-

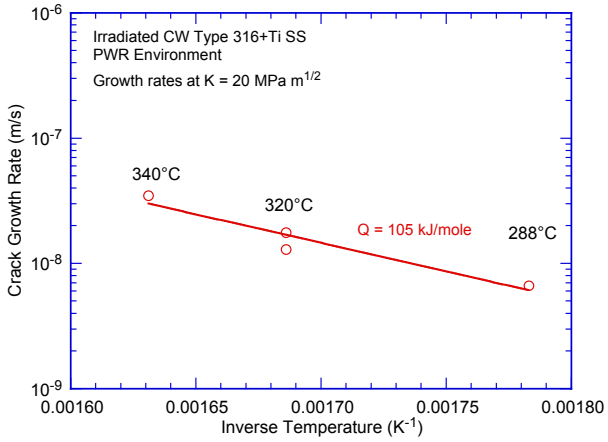


Figure 41.
Temperature dependence of SCC growth rates in irradiated CW Type 316+Ti stainless steel in PWR environment (Ref. 79).

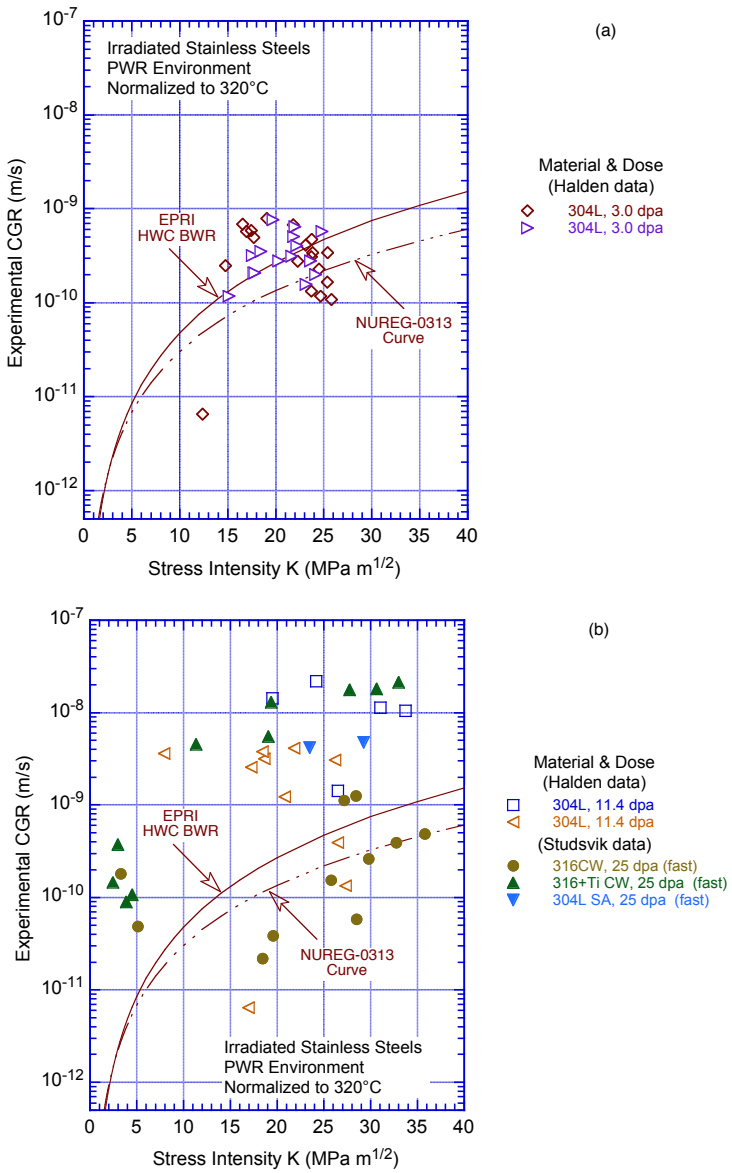


Figure 42. Normalized SCC growth rates in PWR environment for austenitic stainless steels irradiated to (a) 3 dpa, (b) 11-25 dpa, and (c) 6-38 dpa (Refs. 60,76,79).

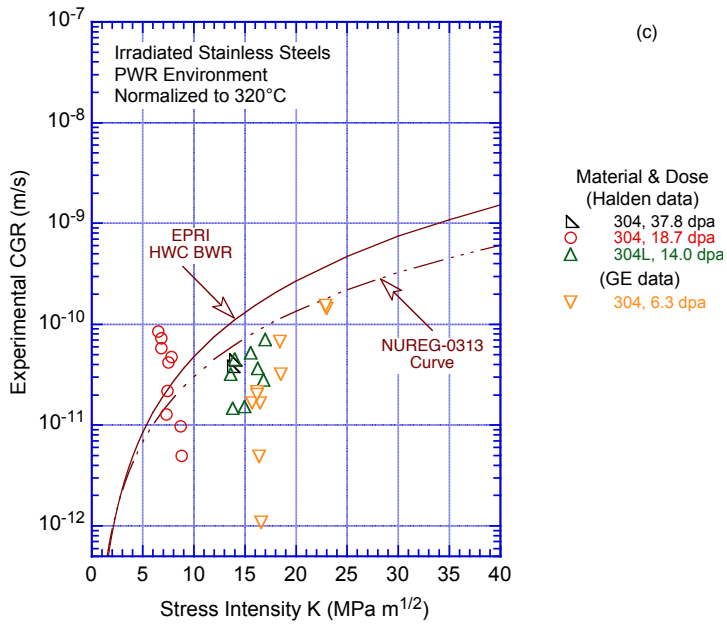


Figure 42. (Contd.)

0313 curve (Fig. 42b). The high growth rates in the 11.4 dpa material have been explained on the basis of possible effects of short test duration, high K values, and high grain-boundary Si concentration. Figure 42c shows that, as observed earlier for the NWC BWR environment, CGRs in non-CW SSs irradiated to 14 dpa or higher are mostly below the NUREG-0313 curve for nonirradiated SSs.

2. The data presented in Fig. 42c show that the CGRs for a Type 304 SS irradiated to only 6.3 dpa[90] are also below the NUREG-0313 curve. The low growth rates measured for this material might be due to the test procedure. These tests were conducted at constant K but, before initiation of the SCC growth rate test at constant K, the TG fatigue precrack was not transitioned to an IG crack by slow fatigue cycling in the environment.

3. Figure 43 shows the SCC growth rates in the PWR and HWC BWR environments for austenitic SSs irradiated to 0.7-4.25 dpa. The rates in the PWR environment were normalized to 288°C by using an activation energy of 100 kJ/mol. Except for the CGRs for the 3.0 dpa materials the growth rates of most materials are bounded by the EPRI CGR curve for the HWC BWR environment.

Figure 44 shows the SCC growth rates as a function of neutron dose for various grades and heats of austenitic SSs that had been irradiated to 0.7-37.5 dpa in the HWC BWR water at 288°C or the PWR environment at 320°C, with K = 20 MPa $m^{1/2}$. All materials except those irradiated in a fast reactor were irradiated in BWRs at temperatures of 280-300°C; the fast reactor irradiations were at 320°C. The data for the HWC BWR or PWR environments may be represented by the bounding curves shown in the figure. The curve represents a variation of A1 in the NUREG-0313 disposition curve (Eq. 5) with neutron dose that is expressed by Eq. 11.

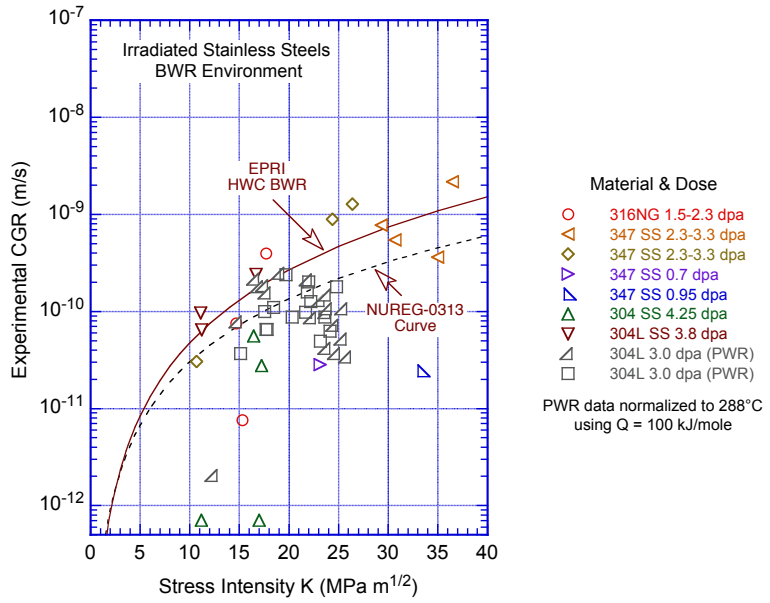


Figure 43. Normalized SCC growth rates of austenitic stainless steels irradiated to 0.7-4.25 dpa in HWC BWR and PWR environments at 288°C (Ref. 74-79).

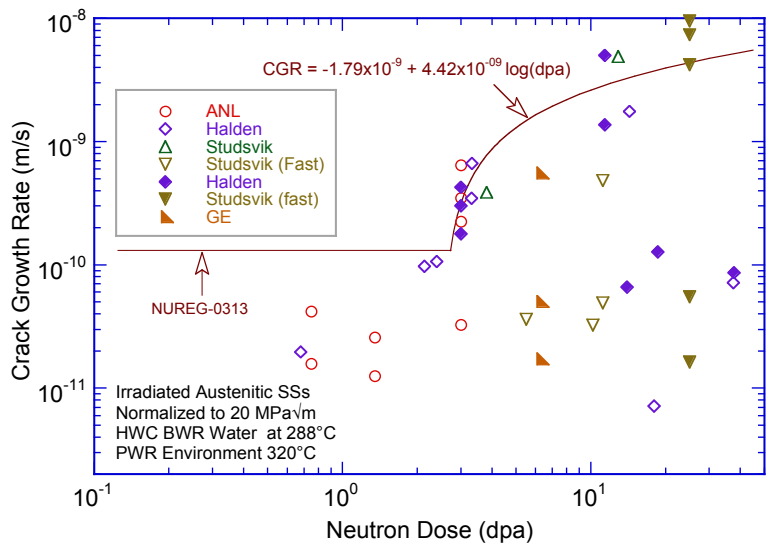


Figure 44. Crack growth rates for irradiated austenitic stainless steels in HWC BWR water at 288°C or PWR environment at 320°C plotted as a function of neutron dose.

As noted previously, the available SCC growth rate data for irradiated austenitic SSs in PWR environments show significant variability. The reason for the high CGRs for some heats irradiated to 11.4 dpa and the unusually low growth rates in SSs irradiated above 18 dpa is not known. Also, most of the data in the PWR environment were obtained either on BWR irradiated material or materials irradiated in the BOR-60 fast reactor. The possible effects of differences in neutron spectrum and flux (fast vs. LWR) or irradiation temperature (288°C for BWRs vs. >320°C for PWRs) cannot be determined from the existing data. Additional data on PWR irradiated materials and materials irradiated at different temperatures (e.g., between 300 and 350°C) are needed to better understand the IASCC susceptibility of austenitic SSs in PWR environments.

### 2.2.3 Fatigue Crack Growth Rates

Cyclic CGRs tests have been conducted with either a triangular or slow/fast sawtooth waveform. The values of load ratio, R, are ≤0.3 for the triangular waveform tests and 0.3-0.8 for the sawtooth waveform tests. The reported time-based CGRs (da/dt) were determined by using only the rise time for the fatigue cycle. Corresponding CGRs in air, under the same loading conditions, were determined from the correlations developed by James and Jones[91] for solution-annealed SSs.

Under cyclic loading in a test environment, the CGR (m/s) can be expressed as the superposition of the rate in air (i.e., mechanical fatigue) and the rates due to corrosion fatigue and SCC, given as

$$CGR_{env} = CGR_{air} + CGR_{cf} + CGR_{scc}. \tag{12}$$

The $CGR_{air}$ (m/s) was determined from the James and Jones correlations:[91]

$$CGR_{air} = C_{SS}\, S(R)\, \Delta K^{3.3}/t_r\,, \tag{13}$$

where R is the load ratio ($K_{min}/K_{max}$), $\Delta K$ is $K_{max}$ - $K_{min}$ in MPa $m^{1/2}$, $t_r$ is the rise time (s) of the loading waveform, and the function S(R) is expressed in terms of the load ratio R as follows:

$$\begin{aligned} S(R) &= 1.0 && R < 0 \\ S(R) &= 1.0 + 1.8R && 0 < R < 0.79 \\ S(R) &= -43.35 + 57.97R && 0.79 < R < 1.0. \end{aligned} \tag{14}$$

In Eq. 13, $C_{SS}$ is a function of temperature, which is expressed by James and Jones in terms of a third-order polynomial in temperature T (°C):

$$C_{SS} = 1.9142 \times 10^{-12} + 6.7911 \times 10^{-15}\, T - 1.6638 \times 10^{-17}\, T^2 + 3.9616 \times 10^{-20}\, T^3. \tag{15}$$

Shack and Kassner[84] have investigated the effects of LWR coolant environments on the fatigue CGR of nonirradiated austenitic SSs. In the absence of any significant contribution of SCC to growth rate, the CGRs in water with ≈0.3 ppm DO were best represented by the expression

$$CGR_{env} = CGR_{air} + 4.5 \times 10^{-5}\, (CGR_{air})^{0.5}, \tag{16}$$

and in water with ≈8 ppm DO by the expression,

$$CGR_{env} = CGR_{air} + 1.5 \times 10^{-4}\, (CGR_{air})^{0.5}. \tag{17}$$

In Eq. 12, the SCC growth rates, $CGR_{scc}$, are represented by the NUREG-0313 (Rev. 2)[66] correlation shown in Eq. 5 for nonirradiated materials, and by Eq. 9 for irradiated materials. For fatigue loading, contributions from mechanical fatigue, and to some extent, from corrosion fatigue are always present for austenitic SSs and Ni alloys in LWR environments. The SCC contribution may not be significant for nonirradiated materials in low-potential HWC BWR or PWR environments.

The only data on the effect of neutron irradiation on fatigue crack growth have been obtained under the fast breeder reactor program. The data were obtained on austenitic SSs irradiated in fast reactors (primarily EBR-II) at temperatures of 370-450°C and tested at 427-593°C. For Type 304 and 316 SS irradiated at 405-410°C to 1.2 x $10^{22}$ n/$cm^2$ (E>0.1 MeV) (6.0 dpa), the CGRs at 427°C are less than a

factor of 2 higher than those for nonirradiated material at ΔK values less than 44 MPa $m^{1/2}$ (40 ksi $in.^{1/2}$), and CGRs are comparable or lower at higher ΔK values.[92] A similar behavior is observed for Type 316 weld.[93] Fatigue CGR data on Type 304 and 20% CW Type 316 SSs irradiated in the EBR-II reactor at slightly higher temperatures, 455-477°C, to 1.3 and 9.0 x $10^{21}$ n/$cm^2$ (E>0.1 MeV) (0.65 and 4.5 dpa), showed no effects on growth rates at 427°C, and slightly lower growth rates at 538°C.[94,95] Also, tests on Type 304 and 316 SS irradiated in a thermal reactor, the Advanced Test Reactor (ATR), at 288°C to 1.8 x $10^{21}$ n/$cm^2$ (E>0.1 MeV) and tested at 427°C had crack growth rates that were less than a factor of 2 lower than those for nonirradiated materials.[96] These results indicate no significant effect of irradiation on the fatigue CGRs for austenitic SSs at these temperatures and K values.

The measured values of fatigue CGRs in air of SS weld HAZ materials irradiated to ≈2.16 dpa are plotted in Fig. 45 as a function of the CGRs estimated from the James and Jones[91] correlations for nonirradiated austenitic SSs under the same loading conditions. Once again, the results indicate no significant effect of irradiation on the fatigue CGRs for weld HAZ in air.

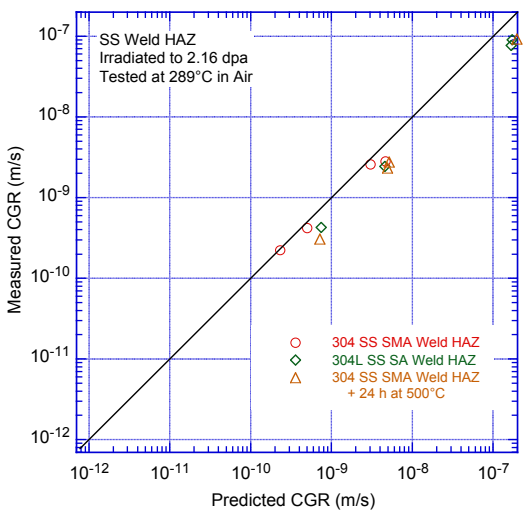


Figure 45.
CGR data under cyclic loading for irradiated SS weld HAZ materials in air at 289°C (Ref. 11).

### 2.2.3.1 Solution-Annealed Materials

Under continuous cyclic loading, experimental data for CGR for solution-annealed Type 304 and 316 SSs irradiated up to 3 dpa and tested in high- and low-DO environments are plotted in Fig. 46 as a function of CGRs predicted in air for the same loading conditions.[9] The curves in the figures are based on the superposition model (Eq. 12). The cyclic CGRs in air ($CGR_{air}$) were determined from Eq. 13, which was developed by James and Jones for nonirradiated materials.[91] The corrosion fatigue contribution ($CGR_{cf}$) was determined from the Shack/Kassner model for nonirradiated SSs in high-purity water with either 8 or 0.2 ppm DO (Eqs. 16 and 17, respectively),[84] and the SCC contribution ($CGR_{scc}$) was determined from Eq. 5.[66] The SCC growth rate in SSs irradiated to >0.75 dpa was assumed to be a factor of six higher than that predicted by Eq. 5; as a result, the constant A in the equation was taken to be 1.26 x $10^{-12}$ for irradiated SSs. For cyclic loading using either a triangular or a slow/fast sawtooth waveform, $CGR_{scc}$ is determined by considering the contribution of SCC during the slow rise time of the cycle; an equivalent K is computed to determine the contribution of SCC. The average values of K used in calculating the superposition curves are given in Fig. 46.

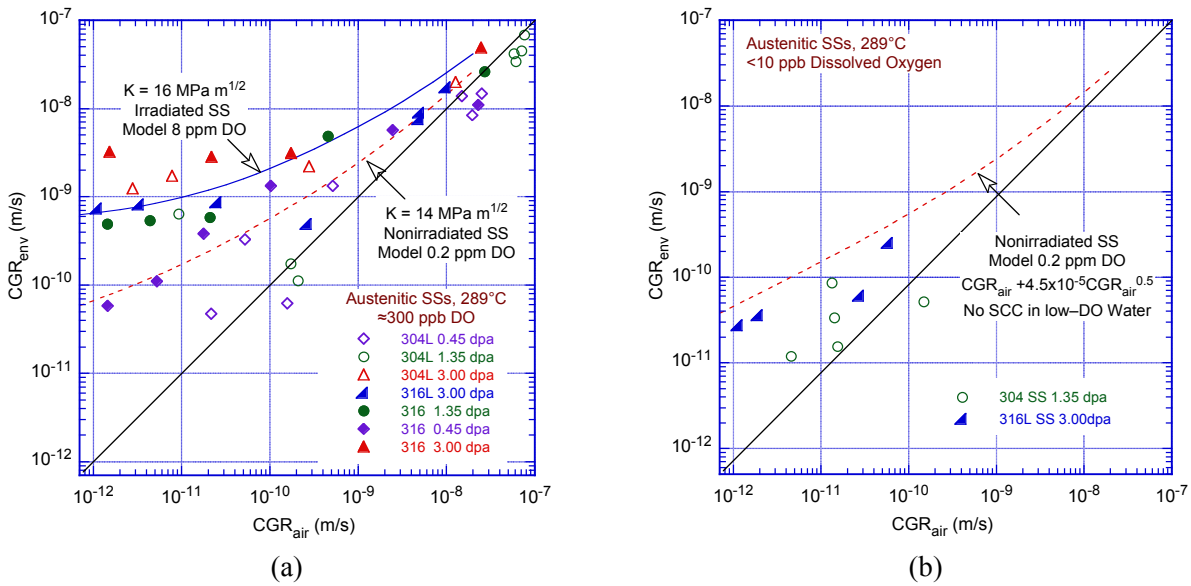


(a) (b)

Figure 46. CGR for irradiated specimens of austenitic SSs under continuous cycling at 289°C in high-purity water with (a) ≈300 ppb and (b) <30 ppb dissolved oxygen (Refs. 9,11).

In Fig. 46, the data points that lie along the diagonal represent predominantly mechanical fatigue, and those that lie close to the model curve indicate environmentally enhanced crack growth. Austenitic SS irradiated to 0.45 dpa shows very little environmental enhancement of CGRs in high-DO water (open and closed diamonds in Fig. 46a). For austenitic SSs irradiated to less than 0.5 dpa, the fatigue CGRs in water with ≈ 300 ppb DO may be represented by superposition of the NUREG-0313 curve for nonirradiated SSs[66] and by the Shack/Kassner model for nonirradiated austenitic SSs in high-purity water with 0.2 ppm DO.[84]

The results for SSs irradiated to 1.35 or 3.0 dpa indicate significant enhancement of the CGRs in high-DO water under cyclic loading with long rise times. For austenitic SSs irradiated to 0.75-3.0 dpa, the fatigue CGRs in water with ≈ 300 ppb DO may be represented by superposition of the SCC curve for irradiated SSs (i.e., six times the NUREG-0313 curve) and by the Shack/Kassner model for nonirradiated SSs in high-purity water with 8 ppm DO.[84]

For continuous cyclic loading, decreasing the DO level has a beneficial effect on the CGRs of irradiated SSs; for example, decreasing the DO from ≈300 ppb DO to <30 ppb DO lowers the CGR by a factor of 25. At 289°C, the fatigue CGRs for irradiated austenitic SSs in water with <30 ppb DO are lower than those predicted by the Shack/Kassner model for nonirradiated austenitic SSs in high-purity water with 0.2 ppm DO (Fig. 46b);[84] there is no contribution of SCC in low-DO water.

### 2.2.3.2 Stainless Steel Weld HAZ Materials

The experimental data for CGRs of nonirradiated SS weld HAZ materials in high-DO water[10] are plotted in Fig. 47 as a function of those predicted in air for the same loading conditions. The curve (dotted and dashed line) is based on the superposition model. For the nonirradiated HAZ materials, the growth rate did not increase readily when the load ratio and rise time were increased. A large number of data points lie along or below the diagonal in Fig. 47. The applied $K_{max}$ had to be increased for environmental enhancement. The fatigue CGRs of nonirradiated SS weld HAZ materials may be conservatively represented by superposition of the SCC curve for nonirradiated SSs and the

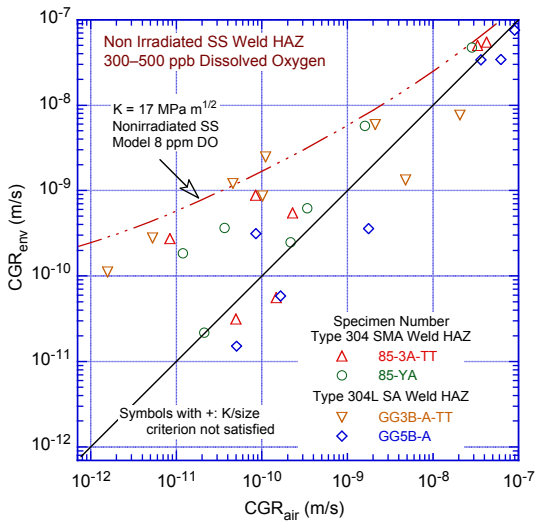


Figure 47.
CGR data under cyclic loading for nonirradiated SS weld HAZ materials in high-purity water at 289°C (Ref. 11).

Shack/Kassner model for austenitic SSs in high-purity water with 8 ppm DO.[84] The results also indicate that thermal treatment of the material for 24 h at 500°C has little or no effect on growth rates.

Experimental data for CGRs of irradiated GG Type 304L SA weld HAZ from the Grand Gulf (GG) core shroud and laboratory-prepared Type 304 SMA weld HAZ in high-DO water are plotted as a function of those predicted in air for the same loading conditions in Figs. 48a and 48b, respectively. The curves in the figures are based on the superposition model (Eq. 12). The results indicate significant environmental enhancement of CGRs for HAZ materials irradiated to 0.75 or 2.16 dpa. The CGRs of the GG Type 304L weld HAZ are slightly lower than those of the Type 304 SMA weld HAZ. The fatigue CGRs of SS weld HAZ materials irradiated to 0.75-2.16 dpa in water containing ≈ 500 ppb DO can be represented by superposition of the SCC curve for irradiated SSs (i.e., six times the NUREG-0313 curve) and the Shack/Kassner model for nonirradiated austenitic SSs in high-purity water with 8 ppm DO.[84] The estimates may be somewhat conservative for Type 304L weld HAZ materials.

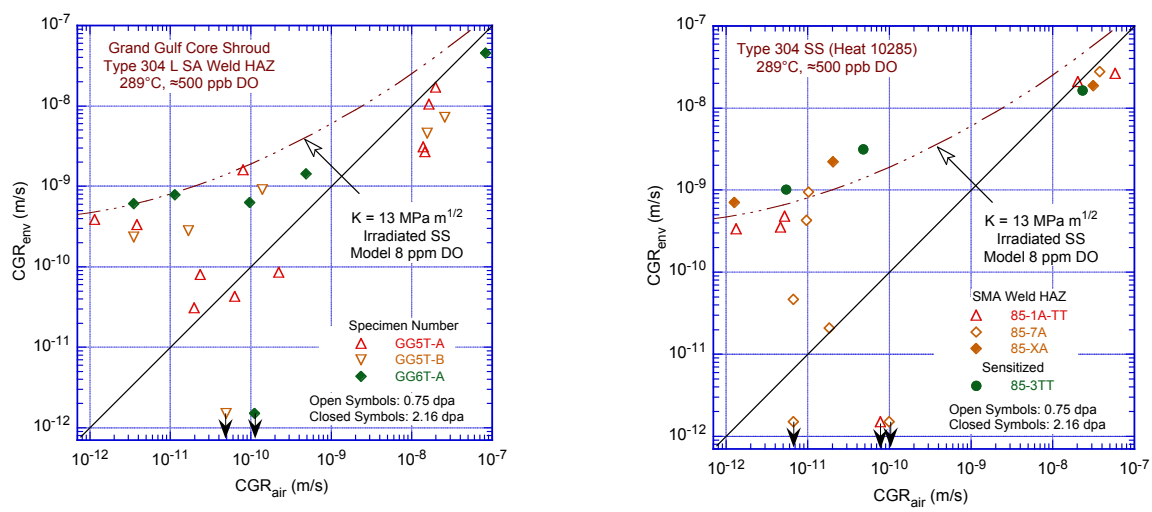


(a) (b)

Figure 48. CGR for irradiated specimens of (a) Type 304L SA weld HAZ from the Grand Gulf core shroud and (b) laboratory-prepared Type 304 SS SMA weld HAZ under continuous cycling in high-purity water at 289°C (Ref. 11).

### 2.2.3.3 Cast Austenitic Stainless Steels

Experimental data for CGRs of CF-8M cast austenitic SS under continuous cycling in the NWC BWR environment are plotted in Fig. 49 as a function of those predicted for austenitic SSs under the same loading conditions in air. The two curves in the figure are based on the superposition model for different DO levels. The material was thermally aged for 10,000 h at 400°C and then irradiated to 2.46 dpa at ≈300°C. As seen before (Fig. 47) for nonirradiated HAZ materials, environmental enhancement of CGRs did not occur readily for Specimen 75-11TT when the load ratio and rise time were increased; for this specimen, a large number of data points lie along the diagonal in Fig. 49. The applied $K_{max}$ had to be increased for environmental enhancement.

Under similar loading and environmental conditions, the fatigue CGRs of CF-8M cast austenitic SS appear to be lower than those of wrought SSs or SS weld HAZ materials. The limited data available indicate that the fatigue CGRs of SS weld HAZ materials irradiated to 0.75-2.46 dpa in water containing ≈ 300 ppb DO can be represented by superposition of the SCC curve for irradiated SSs (i.e., six times the NUREG-0313 curve) and the Shack/Kassner model for nonirradiated austenitic SSs in high-purity water with 0.2 ppm DO.[84]

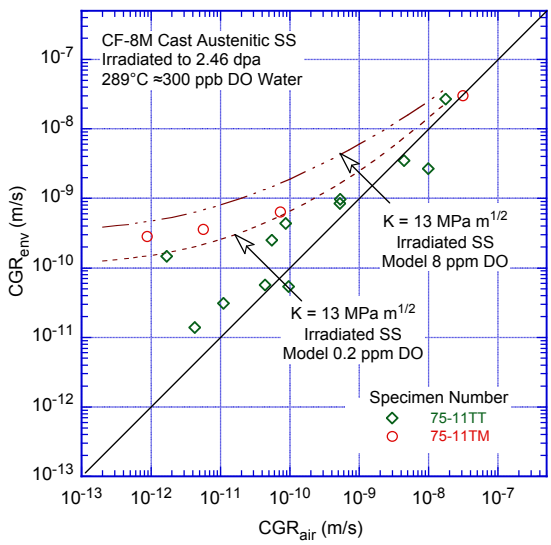


Figure 49.
CGR data under cyclic loading for two irradiated specimens of CF-8M cast austenitic SS in high-purity water at 289°C (Ref. 11).

## 2.3 Initiation of Irradiation-Assisted Stress Corrosion Cracking

As discussed previously, IASCC is an irradiation-induced increase in susceptibility of materials to SCC with increasing neutron fluence. The SCC of materials in high-temperature, high-pressure water depends on material susceptibility, high stresses, and an aggressive environment. However, the mechanism of IASCC in the PWR environment and the individual effect of various material and environmental parameters on IASCC are still not well understood. Although the degradation of tensile and fracture properties of austenitic SSs appears to saturate at 5-20 dpa, the susceptibility of these materials to IASCC continues to increase with neutron fluence. Both solution-annealed and cold-worked austenitic SSs are susceptible to cracking in the PWR environment, but there is significant heat-to-heat variability. In general, the irradiation-induced degradation of fracture properties of austenitic SSs is slower in cold-worked than solution-annealed materials because the cold-worked materials have a high dislocation density, which slows irradiation hardening and damage and suppresses void nucleation and swelling. However, at high neutron fluence levels (i.e., above 10-20 dpa or $6.7 \times 10^{21}$ n/cm$^2$ to

1.3 x $10^{22}$ n/cm$^2$, E>1.0 MeV), there is little or no difference in IASCC susceptibility of these materials in PWR environments.

For all wrought and cast austenitic SSs and their welds there appears to be a threshold value of neutron fluence below which the materials can be considered not susceptible to IASCC in a PWR environment. Current estimates of a threshold value have been based on laboratory SSRT data. The following values have been proposed: a conservative threshold fluence of approximately 6.7 x $10^{20}$ n/cm$^2$ (1 dpa),[101] which represents the fluence at which IASCC can occur in a material after extremely high strains, and a more realistic value of 2 x $10^{21}$ n/cm$^2$ (3 dpa),[100,101] which represents the fluence at which IASCC can be initiated at above the yield stress of the material. For materials irradiated above this threshold, IASCC initiation data have also been used to define for a given neutron dose, an apparent stress threshold below which IASCC initiation will not occur in a PWR environment. The SCC initiation data were obtained by conducting constant-load SCC initiation tests in a simulated PWR environment on O-ring, C-ring, or tensile specimens of irradiated materials.[61,62,97-101] The specimens were tested as a function of fluence and applied stress.

The constant-load IASCC initiation results plotted as stress (as percent of irradiated yield stress) versus time are shown in Fig. 50. The open symbols represent specimens that did not fail, and the closed symbols represent failed specimens. The same data are plotted as a function of neutron dose in Fig. 51. The results indicate that under a high enough stress, crack initiation in highly irradiated materials can occur quite rapidly (i.e., within 500 h). Furthermore, 80% of these failures occurred within 150 h. The results also indicate a stress threshold below which cracks did not initiate even after several thousands of hours. Data on CW Type 316 SS flux thimble tubes removed from commercial PWRs show that, at 26 dpa, cracks initiated at stresses above approximately 62% of the irradiated yield stress.[97] In Fig. 51, for SSs irradiated to very high fluence levels, the stress threshold has been defined as 50% of the irradiated yield stress, although two data points fall below this threshold. The IASCC initiation data also indicate significant scatter with respect to failure vs. non-failure, and the time to failure. For example, in a set of six identical specimens simultaneously tested, four failed and two did not. Also, of the four

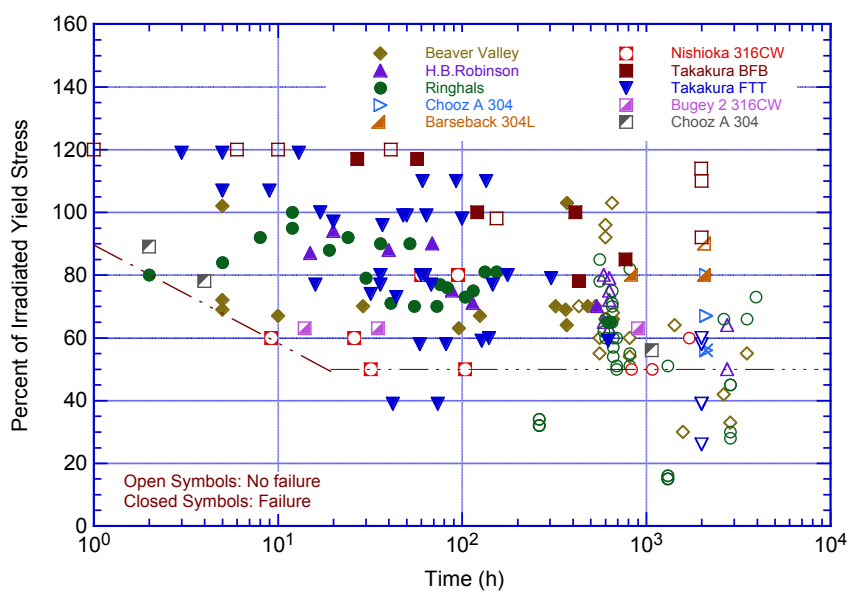


Figure 50. Stress as percent of irradiated yield stress vs. time data for IASCC flaw initiation in austenitic stainless steels in a PWR environment (Refs. 61,62,97-101).

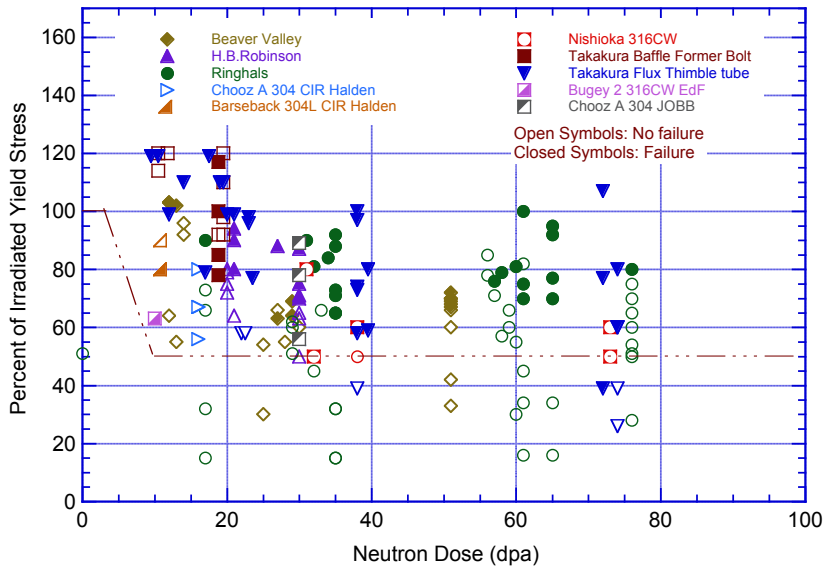


Figure 51. Stress as percent of irradiated yield stress vs. neutron dose for IASCC flaw initiation in austenitic stainless steels in a PWR environment (Refs. 61,62,97-101).

specimens that did fail, time to failure varied from 29 to 483 h. Therefore, sufficiently large numbers of specimens have been tested to identify valid data trends.

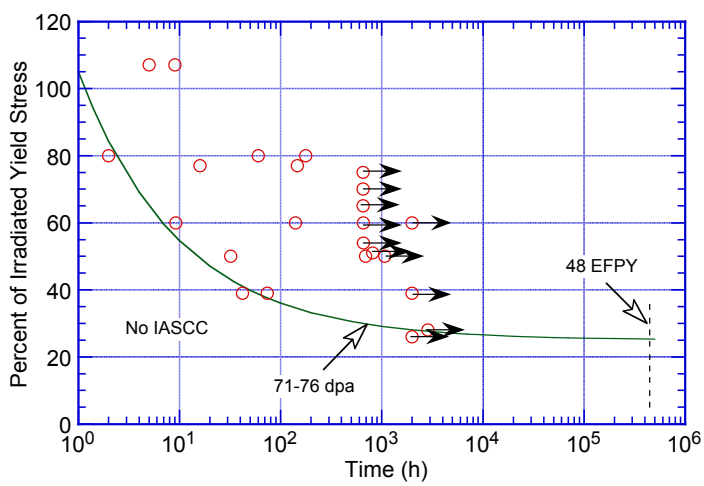


Figure 52. Percent of irradiated yield stress vs. time for IASCC flaw initiation in a PWR environment, for an austenitic stainless steel irradiated to 71-76 dpa (Ref. 62,97,98).

The IASCC initiation data have been used to estimate, for a given neutron dose, a lower bound stress vs. time-to-failure curve for austenitic SSs irradiated to 71-76 dpa. The curve in Fig. 52 represents for a specific irradiated material, the shortest time to initiate IASCC at a given stress in the PWR environment. These curves are extrapolated to 40-y or 60-y reactor life [i.e., 32 or 48 effective full power year (EFPY)] to define an apparent stress threshold below which IASCC initiation will not occur for that material within a specified time, say, the reactor lifetime. Such results are used to develop the curves for stress vs. neutron fluence threshold that predict time for IASCC initiation as a function of stress and fluence.

Figure 53 presents two curves that define the approximate stress and neutron fluence for IASCC initiation in a relatively short time (i.e., 100 h) and after a very long time. The latter may be used as the lower bound for stress and fluence below which IASCC is not likely to occur within the lifetime of the reactor. However, the data that were used to develop these curves do not account for the effect of material composition, material variability between heats, or the differences between solution-annealed or cold-worked material. To account for material variability and uncertainty due to data scatter, MRP has proposed a screening curve, shown in Fig. 53, for IASCC initiation of austenitic SSs. This curve is used to divide various PWR core internal components into different categories of aging management strategies during the initial screening process.

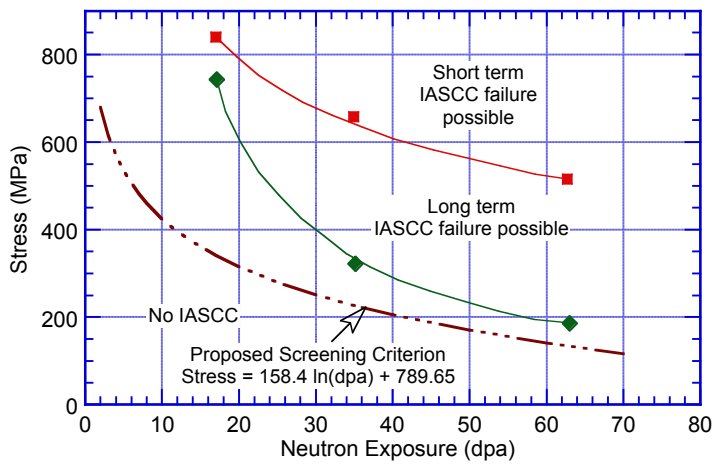


Figure 53. Time for initiation of IASCC in irradiated austenitic stainless steels as a function of stress (Ref. 61,101).

Such an approach for defining neutron dose/applied stress thresholds for austenitic SSs is limited by the adequacy of the database used for developing the screening curve. First of all, insufficient data are currently available to adequately define an IASCC initiation curve correlating stress and neutron fluence. Considerably more data are needed to account for uncertainties due to data scatter, material variability, irradiation temperature, neutron spectrum effects, and water chemistry. As more information has been added to the IASCC initiation database, the threshold stress below which IASCC is considered not likely to occur during a 60-y reactor lifetime has been decreased from an initial value of 62% to 50% and now possibly 40% of the irradiated yield stress. Although a threshold fluence of 3 dpa has been defined for IASCC in the PWR environment, there are no IASCC initiation data on austenitic SSs irradiated between 3 and 9.5 dpa. Thus, in Fig. 51, for materials irradiated to 3-10 dpa, the threshold stress for IASCC initiation is defined arbitrarily by a straight line between 3 and 10 dpa. In addition, the existing database for IASCC initiation does not consider the effects of the following parameters that are known to influence IASCC susceptibility:

1. *Material Type, Composition, and Condition*: The available IASCC initiation data have been obtained primarily on CW Type 316 SS and data on solution-annealed Type 304, 304L, or 316 SS are limited. Also, there are no data on cast austenitic SSs, SS welds, and weld HAZ materials. Additional IASCC initiation data should be obtained on these materials irradiated to neutron fluence levels relevant for PWR core internals.

   Also, the increased susceptibility to IASCC and the loss of benefit of reduced corrosion potential on IASCC susceptibility in highly irradiated SSs are often attributed to the segregation of Si at the grain

boundaries. Initiation data should be obtained on irradiated material from commercial heats of SSs with similar compositions but different Si contents to establish the role of Si segregation on the IASCC susceptibility of irradiated SSs.

2. *Irradiation Temperature*: Nearly all of the high fluence (above 20 dpa) data and the majority of the low fluence data on IASCC initiation have been obtained on materials irradiated below 325°C. Consequently, the database does not include the potential effects of additional precipitate phases, voids, and cavities, which are observed in SSs irradiated to high fluence levels at temperatures above 320°C. Also, He bubbles have been observed in SSs irradiated in reactors with high thermal neutron fluxes and could also influence IASCC initiation.

3. *Neutron Spectrum*: The current IASCC initiation data include some tests on austenitic SS irradiated in the BOR-60 fast reactor. Several studies have shown that materials irradiated in fast reactor show lower susceptibility to IASCC than those irradiated in LWRs. Such data have not been included in Figs. 50 and 51. Caution should be exercised when using fast reactor data to assess the degradation of LWR core internal materials.

4. *Water Chemistry*: The addition of $H_2$ to the reactor water greatly reduces the effect of radiolysis by scavenging the radiolysis products. Because PWR coolants typically contain 2 ppm $H_2$ (30 cc/kg), radiolysis has no effect on the corrosion potential in PWRs. However, in reactor core internal components, IASCC is likely to occur under creviced conditions (i.e., under off-normal water chemistry). Nearly all of the IASCC initiation tests have been conducted in the normal PWR environment, and the possible effects of impurities on initiation have not been investigated.

This page is intentionally left blank.

# 3 Neutron Embrittlement

Neutron irradiation can decrease the fracture toughness of austenitic SSs significantly, and failure may occur without general yielding. In such instances, a fracture mechanics methodology, such as elastic-plastic fracture mechanics (EPFM) or linear-elastic fracture mechanics (LEFM), is needed for analysis of structural integrity and development of inspection guidelines. The former involves the J integral-resistance (J-R) curve approach and is used where failure is caused by plastic deformation. The J integral is a mathematical expression used to characterize the local stress-strain field at the crack tip region (parameter J represents the driving force for crack propagation), and the J-R curve characterizes the resistance of the material to stable crack extension. The fracture toughness of such materials is represented by fracture mechanics parameters such as $J_{Ic}$, the value of J near the onset of crack extension, and the tearing modulus, T, which characterizes the slope of the J-R curve:

$$T = \frac{dJ}{da}\frac{E}{\sigma_f^2}, \tag{18}$$

where E is the elastic modulus, a is the crack length, and $\sigma_f$ is the flow stress defined as the average of the yield stress ($\sigma_y$) and ultimate stress ($\sigma_u$). The LEFM methodology is used where failure involves negligible plastic deformation. The fracture toughness of such materials is represented by the parameter $K_{Ic}$ (i.e., plane strain fracture toughness), which characterizes the resistance of the material to unstable crack extension. Under EPFM conditions, the equivalent critical stress intensity factor, $K_{Jc}$, can be determined from the saturation $J_{Ic}$ value using the relationship

$$K_{Jc} = \left(E' J_{Ic}\right)^{1/2}, \tag{19}$$

where $E' = E/\left(1-\upsilon^2\right)$, E is the elastic modulus, and $\upsilon$ is the Poisson ratio.

The fracture toughness of austenitic SSs has been divided into three broad categories.[6] Category III corresponds to high toughness materials with $J_{Ic}$ above 150 kJ/cm$^2$ (857 in.-lb/in.$^2$). In these materials, fracture occurs after stable crack extension at stresses well above the yield stress. Category II corresponds to materials with intermediate toughness with $J_{Ic}$ in the range of 30-150 kJ/cm$^2$ (171-857 in.-lb/in.$^2$). In these materials, fracture occurs by stable or unstable crack extension at stress levels close to the yield stress. Category I corresponds to low-toughness materials with $K_{Ic}$ less than 75 MPa m$^{1/2}$ (68.2 ksi in.$^{1/2}$) [$J_{Ic}$ < 30 kJ/cm$^2$ (< 171 in.-lb/in.$^2$)]. In these materials, fracture occurs by unstable crack extension at stress levels well below the yield stress.

Nonirradiated wrought and cast austenitic SSs and their welds fall in Category III. The $J_{Ic}$ values for Type 304 and 316 SS at temperatures up to 125°C (257°F) vary between 169 and 1660 kJ/cm$^2$ (965 and 9479 in.-lb/in.$^2$), with a median value of 672 kJ/cm$^2$ (3837 in.-lb/in.$^2$).[6] The $J_{Ic}$ values at 400-550°C (752-1022°F) are ≈35% lower, with a median value of 421 kJ/cm$^2$ (2404 in.-lb/in.$^2$). Fracture in such high-toughness materials is by the nucleation and coalescence of microvoids and is characterized by a dimpled fracture morphology.

Although cast austenitic SSs and SS welds also exhibit ductile fracture at temperatures up to 550°C (1022°F), their fracture toughness is lower than that of the wrought SSs. A dimpled fracture morphology is also observed in SS welds.[102] Because of a high density of inclusions in the weld, the dimples are

relatively small and shallow. Also, dimples are often associated with an inclusion and are initiated by decohesion of the particle/matrix interface. The overall fracture toughness of cast austenitic SSs and SS welds is controlled by the density and morphology of second-phase inclusions in these materials and varies with the cast or weld process. For example, static cast products have lower fracture toughness than centrifugally cast pipes. Gas tungsten arc (GTA) welds exhibit the highest toughness; SMA welds have intermediate toughness; and SA welds have the lowest toughness.[6] The median value of $J_{Ic}$ is 492 kJ/cm$^2$ (2809 in.-lb/in.$^2$) for GTA welds and 147 kJ/cm$^2$ (839 in.-lb/in.$^2$) for SA welds at temperatures up to 125°C (257°F).

Welding of austenitic SSs results in a HAZ adjacent to the fusion zone, where the material microstructure and microchemistry are greatly altered because of the precipitation of Cr-rich carbides at the grain boundaries. The formation of the carbides depletes Cr from the grain-boundary region, thereby creating a region that is susceptible to SCC. However, the fracture toughness of HAZ material is generally superior to that of the weld metal and may be comparable to that of the base metal.

## 3.1 Fracture Toughness of Irradiated Austenitic Stainless Steels

Neutron irradiation can degrade fracture toughness of austenitic SSs to the level of Category II or I. Until recently, most of the published experimental data on neutron embrittlement of austenitic SSs had been obtained on materials irradiated in high-flux fast reactors.[103-119] In these studies, the embrittlement of the materials has been characterized in terms of tensile properties, Charpy-impact properties, and fracture toughness. The tensile properties of Type 304, 316, and 347 SSs and their weld metals and HAZ materials, as well as CF-8 cast austenitic SSs irradiated in fast reactors or LWRs, have been discussed in Section 2.1.4 of this report.

Fracture toughness is typically characterized by the initiation toughness $J_{Ic}$ and tearing modulus T for materials that fail after substantial plastic deformation (for EPFM analysis) and by the critical stress intensity factor $K_{Ic}$ for materials that fail after little or no deformation (for LEFM analysis). Typically, fracture toughness data for irradiated materials have been obtained from compact tension (CT) or single edge bend [SE(B)] specimens and, in some cases, from Chevron notch short rod (CNSR) specimens. To reduce activity and facilitate handling, small specimens (e.g., ≈8-mm thick ¼-T CT) have been used in several studies. For these specimens, J values above 150 kJ/m$^{1/2}$ and crack extensions beyond about 1.2 mm are above the validity limits based on ASTM Specification E 1820-06. However, comparison of fracture toughness data obtained on 1-T CT and small-size CT or SE(B) specimens shows comparable J vs. Δa values even beyond the ASTM defined validity limits. The small specimens yield equivalent J-R curve data at least for materials with $J_{Ic}$ values up to about 300 kJ/m$^{1/2}$ and, maybe, even higher.

Plots of $J_{Ic}$ or $K_{Ic}$ and $K_{Jc}$ as a function of neutron dose are used for developing screening criteria for neutron embrittlement. In ASTM Specification E 1820-06, $J_{Ic}$ is determined from the intersection of the best-fit power-law J-R curve with the 0.2-offset line parallel to the blunting line, provided the specimen size criterion of Eq. 7 is satisfied. The blunting line is defined as

$$J = M\sigma_f\Delta a, \tag{20}$$

where $\sigma_f$ is the flow stress, Δa is crack extension, and the constraint factor M is 2 or a value determined from the best fit of the experimental data. However, the analysis procedures described in the ASTM specifications for $J_{Ic}$ determination are not applicable to austenitic SSs because of their extremely high toughness, ductility, and strain hardening ability. The main difference concerns the expression for the crack-tip blunting line. For austenitic SSs, a value of 2 for M significantly overpredicts the crack

extension due to crack tip blunting, and, therefore, it yields a non-conservative value of $J_{Ic}$.[6,120] For austenitic SSs, a value of 4 for M better defines the blunting line.

The constraint factor M, which relates J to the crack tip opening displacement (CTOD) given by the expression

$$J = M\sigma_y(\text{CTOD}). \tag{21}$$

The use of a higher value for M in Eq. 20 is consistent with the expected variation of M and $\sigma_f$ with strain hardening. The factor M is 1 for materials with intermediate to high strength and low strain hardening, and 2 for materials with low strength and high strain hardening, such as austenitic SSs. For the latter, the yield strength is approximately two-thirds of the flow stress, and the crack extension associated with blunting is approximately one-third of CTOD.[6] Thus, for such materials, the crack tip blunting line is given by

$$J = M\sigma_y(\text{CTOD}) \approx 2(2\sigma_f/3)(3\Delta a) = 4\sigma_f\Delta a, \tag{22}$$

i.e., Eq. 20 with M = 4. This relationship has been used to determine $J_{Ic}$ in most investigations on neutron embrittlement.[11,59] A value of 2 for M has also been used by several investigators.[58] The latter typically yields a higher value of $J_{Ic}$ for Category III materials (i.e., $J_{Ic}$ above 150 kJ/cm). However, the difference in $J_{Ic}$ values determined using values of M of 2 or 4 is insignificant for Category II materials (i.e., $J_{Ic}$ <100 kJ/cm$^2$). Since it is primarily the cases in which the fracture toughness of irradiated austenitic SSs is reduced to Category II levels that are of interest, the effect of differences in the procedure to determine $J_{Ic}$ is likely to be insignificant.

Another factor that may influence the reported values of $J_{Ic}$ is when an effective yield stress is used instead of the measured yield stress. As discussed in Section 2.2.1.3, the K/size criteria were developed for materials that show work hardening and, therefore, may not be applicable for materials irradiated to fluence levels where, on a local level, they do not strain harden. An effective yield stress, in which the irradiation-induced increase in yield stress is discounted by a factor of 2 for moderately irradiated materials and by a factor of 3 for highly irradiated materials, has been proposed to define K/size criteria for moderate to highly irradiated materials. Some studies have used such a yield stress to determine $J_{Ic}$.[11] Because $J_{Ic}$ is a measure of fracture toughness at instability without significant stable crack extension, the measured yield or flow stress of the irradiated materials seems more appropriate for $J_{Ic}$ determinations. Nevertheless, the choice of measured or effective yield stress is likely to have an insignificant effect on the measured $J_{Ic}$ of materials with poor fracture toughness.

### 3.1.1 Fracture Toughness $J_{Ic}$

The effect of neutron exposure (in dpa) on the fracture toughness $J_{Ic}$ at 25-427°C (77-842°F) of austenitic SSs irradiated at 90-450°C (194-842°F) up to 90 dpa in fast reactors is shown in Fig. 54.[103-119] The irradiation and test temperatures were 100-155°C and 125°C for the data obtained by Sindelar et al.,[114] 90-250°C and 25-250°C for the data obtained by Alexander et al.,[113] and 325°C and 25°C for the data obtained by Kim et al.[119] The rest of the data were obtained on materials irradiated at 350-427°C and tested at 300-427°C. The fast reactor data show a rapid decrease in fracture toughness at a neutron dose of 1-2 dpa; the neutron dose at the onset of the rapid decrease varies with the chemical composition and heat treatment of the steel. The effects of irradiation may be divided into three regimes: little or no loss of toughness below an exposure of ≈1 dpa, substantial decrease in toughness at exposures of 1-10 dpa, and no further reduction in toughness above a saturation exposure of 10 dpa. The degradation in

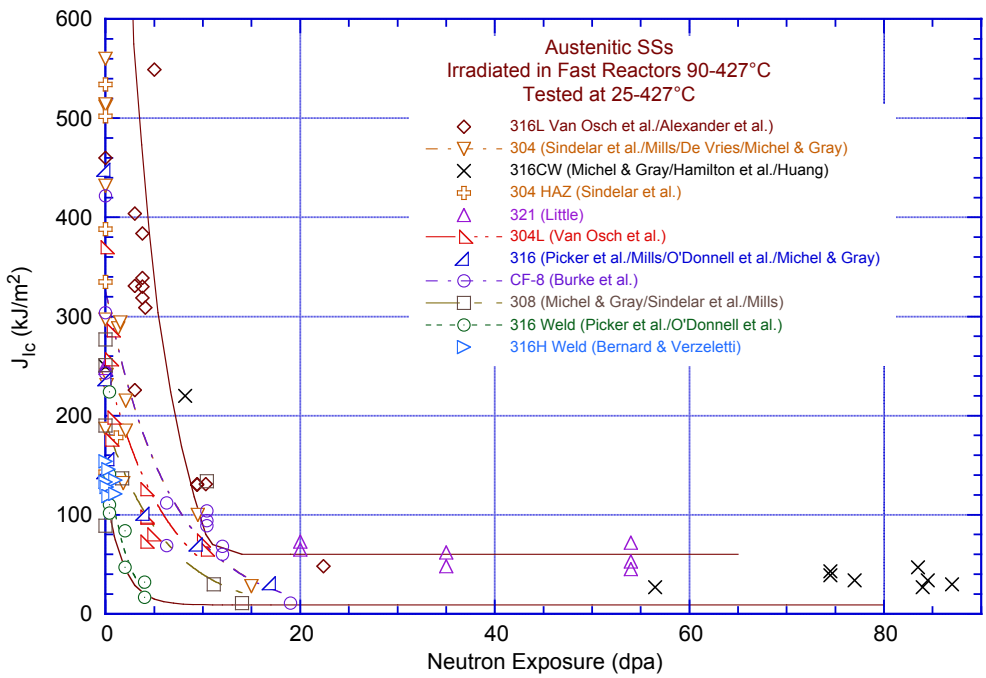


Figure 54. Change in fracture toughness $J_{Ic}$ as a function of neutron exposure for austenitic SSs irradiated in fast reactors. Solid lines represent the scatter band for the fast reactor data on austenitic SSs (Refs. 104-119).

fracture properties saturates at a $J_{Ic}$ value of ≈30 kJ/m$^2$ (171 in.-lb/in.$^2$) [i.e., $K_{Jc}$ of 75 MPa m$^{1/2}$ (68.2 ksi in.$^{1/2}$)]. Also, the failure mode changes from dimple fracture to channel fracture.

The fracture toughness trend for the LWR data[5,11,57-59,65,121,122] is similar to that observed for fast reactor data (Fig. 55). Most of the fracture toughness $J_{Ic}$ values for austenitic SSs irradiated in LWRs [288-316°C (550-601°F)] fall within the scatter band of the data obtained on materials irradiated in fast reactors, even though the LWR irradiations were at lower temperatures. There are only minor differences in the fracture toughness of the various wrought and cast austenitic SS materials. For the same irradiation conditions, the fracture toughness of thermally aged cast SS and weld metal is lower than that of HAZ material, which, in turn, is lower than that of solution-annealed materials. A similar behavior is also observed for the fast reactor data in Fig. 54. The $J_{Ic}$ values of welds and HAZ materials are consistently lower than those for the solution-annealed and even CW materials. The data for CF-8 cast SS were obtained at room temperature and, therefore, are relatively high; the $J_{Ic}$ values are expected to be lower at LWR operating temperatures.

Some materials irradiated above 4 dpa at LWR temperatures show very poor fracture toughness; their $J_{Ic}$ values are below the lower bound curve for the fast reactor data. For a Type 304 SS irradiated to 4.5-5.3 dpa (shown as cross in Fig. 55), nine out of ten CT specimens showed no ductile crack extension, and the $K_{Ic}$ values were 52.5-67.5 MPa m$^{1/2}$ (47.7-61.4 ksi in$^{1/2}$).[57] The lowest fracture toughness, with $K_{Ic}$ or $K_{Jc}$ values in the range of 36.8-40.3 MPa m$^{1/2}$ (33.5-36.6 ksi in$^{1/2}$), was for a Type 347 SS irradiated to 16.5 dpa in a PWR[57] and for a Type 304 SS irradiated to 7.4-8.4 dpa in a BWR.[122]

Another significant result is a strong orientation effect on fracture toughness. Fracture toughness J-R tests and microstructural and microchemistry characterization were performed on a Type 304 control-rod and Type 304L top guide materials irradiated to 4.7-12 dpa in a BWR, and on Type 304 control-rod

material irradiated to 7.4 and 8.4 dpa in another BWR. All materials consistently showed lower fracture toughness in the T-L orientation than in the L-T orientation,[58] and these toughness values were lower than the limiting fracture toughness $K_{Ic}$ of 55 MPa $m^{1/2}$ (50 ksi in.$^{1/2}$) that has been proposed by industry for flaw tolerance evaluation in austenitic SSs irradiated above 4.5 dpa (3 x $10^{-21}$ n/cm$^2$).[58,65] The lower fracture toughness along the T-L orientation has been attributed to the presence of stringers consisting of long, narrow particles oriented in the rolling direction, which result in a long and narrow quasi-cleavage structure parallel to the crack advance, thereby accelerating the crack advance.[58] In addition, the Type 304 control-rod material (7.4-8.4 dpa) showed very poor fracture toughness ($J_{Ic}$ of 40 kJ/m$^2$ in L-T and 7.5 kJ/m$^2$ in T-L orientation). The authors concluded that the low $J_{Ic}$ of this material might be considered a special case of materials containing a high density of particles aligned in the rolling direction. Nonetheless, these results show that very low fracture toughness values are possible for irradiated austenitic SSs. Microstructural characterization of the Type 304 control-rod material showed a fine distribution of γ' phase with size in the range of 2-10 nm and an average size of 4.4 nm.[58] The density was 1-3 x $10^{22}$ $m^{-3}$. This phase was not observed in the Type 304 top guide material, and may influence the fracture toughness of these materials. The γ' phase has been observed at dose levels above 4 dpa in CW Type 316 SS irradiated under the PWR condition.[123] The contribution of additional precipitate phases, voids, and cavities on fracture toughness needs to be investigated.

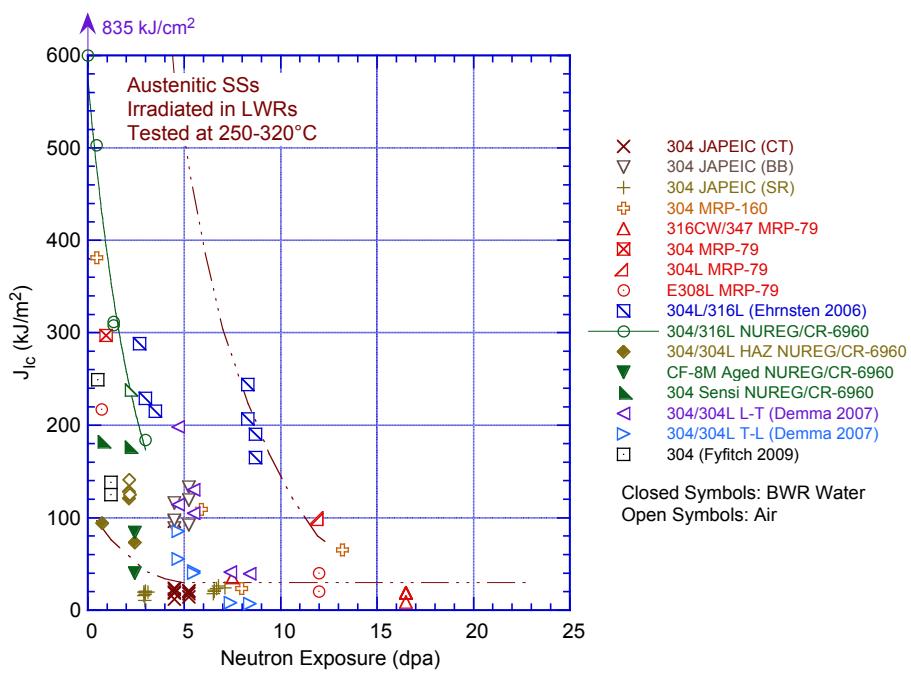


Figure 55. Change in fracture toughness $J_{Ic}$ as a function of neutron exposure for irradiated austenitic SSs. Dashed lines represent the scatter band for the fast reactor data on austenitic SSs irradiated at 350-450°C (662-843°F) (Refs. 5,11,57-59,65,121,122).

### 3.1.2 Fracture Toughness J-R Curve

Fracture toughness J-R curve data have been obtained for the following materials: Type 304, 304L, and 316L SSs; SS weld materials and HAZs; and CF-3, CF-8, and CF-8M cast austenitic SSs. Data are available for materials irradiated in LWRs up to about 14 dpa,[11,57-59,65,121,122] and in fast reactors to much higher dose levels. The change in the J-R curve with neutron dose is shown in Fig. 56. The decrease in fracture toughness is quite rapid up to about 6 dpa, and the toughness continues to decrease

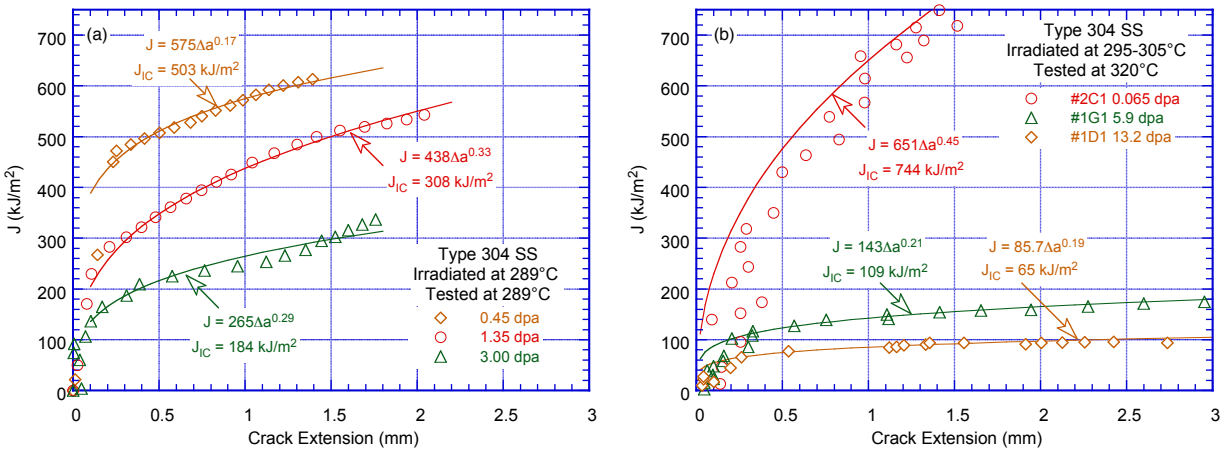


Figure 56. Change in fracture toughness $J_{IC}$ as a function of neutron exposure for SSs (Refs. 11,122).

moderately at higher dose levels. The effects of various parameters such as material type and heat treatment, test and irradiation temperature, and neutron energy spectrum, flux, and dose are discussed below.

*Irradiation Conditions:* Fast reactor irradiations are at fluxes and temperatures higher than those typically observed in LWRs and have a different spectrum. Until recently, most of the high neutron exposure data were from fast reactor irradiations at temperatures above 350°C (662°F) (Fig. 54). An accurate determination of the effects of neutron spectrum, flux, and temperature on the fracture properties of these materials requires data on the same heat of material irradiated in a fast reactor and an LWR to comparable neutron dose. Such information is not available. Although the general data trends appear to be similar for fast reactor and LWR irradiations, the tensile property data discussed in Section 2.1.4 indicate that tensile strength is higher and ductility is lower for the BWR-irradiated materials than materials irradiated in fast reactors. However, the existing data are inadequate to determine the individual contributions of irradiation temperature, flux, and energy spectrum to the degradation of fracture properties in irradiated austenitic SSs. Therefore, additional fracture toughness data should ideally be obtained on the same heat of material that has been irradiated in both fast and thermal reactors to comparable fluence levels at the same temperature. Only such carefully controlled data can be used to accurately assess the applicability of fast reactor data to LWR irradiation conditions.

*Material Type:* Most of the J-R curve data on LWR-irradiated austenitic SSs have been obtained on Type 304 and 304L SS. Data on Type 316, 316L, 316CW, and 347 SSs are very limited. Also, the only data for SS welds are on Type 308L material irradiated to <1 dpa or 12 dpa. Similarly, there are only a few J-R curve tests on weld HAZ materials and CF-8M cast SS irradiated to 2.1-2.5 dpa. Some differences in the fracture toughness data trends appear for the various grades of wrought austenitic SSs, but these differences may be artifacts of the limited data. For example, the heat-to-heat variation for a particular grade may be comparable to the apparent differences between grades in the current data. The results for different heats of Type 304 SS indicate little or no effect of sensitization treatment (green open circles and green-filled right-angle triangles in Fig. 55, respectively). Also, for the same irradiation conditions, the fracture toughness of the weld HAZ materials is lower than that of the solution-annealed materials (olive-filled diamonds and green open circles in Fig. 55, respectively), and the toughness of the thermally aged cast SS is lower than that of the HAZ material (Fig. 57).

Although the fracture toughness of nonirradiated CW steels is lower than that of nonirradiated solution-annealed steels, the decrease in toughness of CW steels with neutron exposure is lower and the

$J_{Ic}$ value at saturation is higher than those of irradiated solution-annealed steels (Fig. 54). However, the data for CW steels are from fast reactor irradiations at relatively high temperatures, 400-427°C (752-800°F). The saturation $J_{Ic}$ for CW SSs is likely to be lower for irradiations at LWR operating temperatures [i.e., 290-320°C (554-608°F)], and the differences may be small.

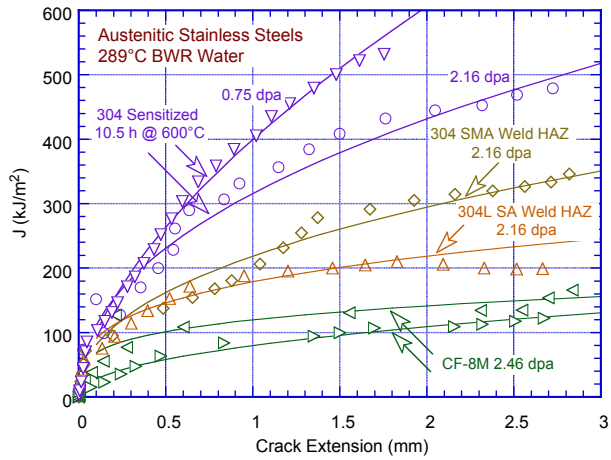


Figure 57.
Fracture toughness J-R curves for sensitized Type 304 SS, weld HAZ materials of Type 304 and 304L SS, and CF-8M cast SS in high-purity water at 289°C (Ref. 8).

Nonirradiated weld metals and thermally aged cast SSs have lower fracture toughness than wrought austenitic SSs, and their fracture toughness generally decreases more rapidly with neutron exposure than that of solution-annealed material. However, the saturation toughness for the welds is not significantly different from that of solution-annealed SSs, and the same bounding curve for $J_{Ic}$ appears to be applicable to both wrought materials and welds and cast austenitic SSs. Although LWR core internals are typically constructed of CF-8 or CF-3 steels, the only data for LWR irradiation of cast SS are for CF-8M steel. The data for thermally aged CF-8 cast SS shown in Fig. 54 are for materials that were irradiated in the BOR-60 fast reactor, and may be non-conservative for LWR irradiation conditions. Furthermore, the data were obtained at room temperature; as discussed below in this section, fracture toughness at higher temperatures is expected to be lower. For thermal embrittlement of cast SSs the fracture toughness of CF-8M steel represents the worst-case scenario.[102,124] It thus might also represent a bounding case also for the synergistic effects of irradiation and thermal aging.

*Test Environment:* Nearly all of the existing fracture toughness data have been obtained from tests in air and on specimens that were fatigue precracked at relatively low load ratios (typically 0.1-0.2) in room-temperature air. However, in reactor core components, cracks are initiated primarily by SCC and have IG morphology, whereas the fatigue precracks in fracture toughness tests are always TG. Also, the corrosion/oxidation reaction could influence fracture toughness. For example, hydrogen generated from the oxidation reaction could diffuse into the material and change the deformation behavior by changing the stacking-fault energy of the material.

To investigate the possible effects of the BWR coolant environment on fracture toughness (e.g., the effect of the corrosion/oxidation reaction during crack extension or use of specimens with an IG rather than the TG fatigue crack generally employed in nearly all fracture toughness tests), J-R curve tests have also been conducted in a BWR NWC environment.[11] The J-R curve data on irradiated SS weld HAZ materials (Fig. 58) indicate that an NWC BWR environment has little or no effect on the fracture toughness. The J-R curves for irradiated Type 304L SA weld HAZ in air and water environments are essentially identical (Fig. 58b), and, although the complete J-R curve could not be obtained for Type 304 SMA weld HAZ in air, ductile crack extension occurred at approximately the same value of J in air and water environments (Fig. 58a).

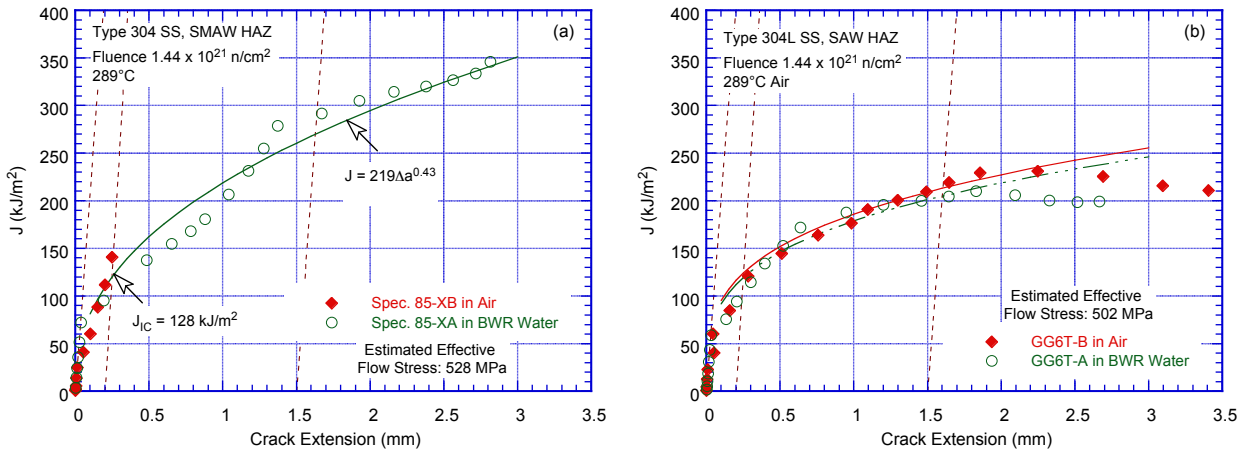


Figure 58. Fracture toughness J-R curves for irradiated specimens of (a) Type 304 SS SMA weld HAZ and (b) Type 304L SA weld HAZ in air and NWC BWR environment (Ref. 8).

The J-R curves for a sensitized Type 304 SS in air and water environments are shown in Fig. 59. The results indicate slightly lower fracture toughness in water. Also, the material tested in water was sensitized for a shorter time than the material tested in air. Therefore, for materials with identical sensitization treatment, the difference between the J-R curves in air and water environments may be greater than that indicated by Fig. 59.

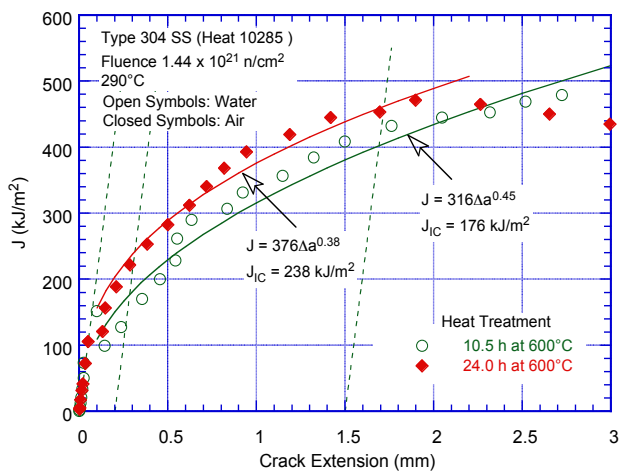


Figure 59.
Fracture toughness J-R curves for sensitized Type 304 SS in air and NWC BWR water at 289°C (Ref. 8).

The J-R curves and the load vs. load-line displacement curves for the two tests on thermally aged and irradiated CF-8M cast SS in NWC BWR water are shown in Fig. 60. Companion tests in air have not been conducted on this material. In both tests, large load drops, accompanied by crack extensions up to 0.5 mm in Specimen 75-11TM and 1.0 mm in Specimen 75-11TT, were observed at the onset of crack extension. Such load drops are not typically observed during tests in air.[124] The fracture surfaces of these specimens have not been examined to establish the fracture morphology. Additional tests on irradiated cast SSs or SS welds in air and water environments should be conducted to determine the possible effect of LWR coolant environments on their fracture toughness.

*Irradiation Temperature:* The available data are inadequate to establish accurately the effects of the irradiation temperature on the fracture toughness of austenitic SSs. However, tensile data for austenitic SSs indicate that irradiation hardening is highest, and ductility loss is maximum, at an irradiation

temperature of ≈300°C (≈572°F).[54] Thus, the $J_{Ic}$ values for all of the data at neutron exposures greater than 20 dpa shown in Fig. 62 may overestimate the toughness of materials irradiated at temperatures of 290-320°C (554-608°F) because the irradiation temperatures for these data were above 350°C (662°F).

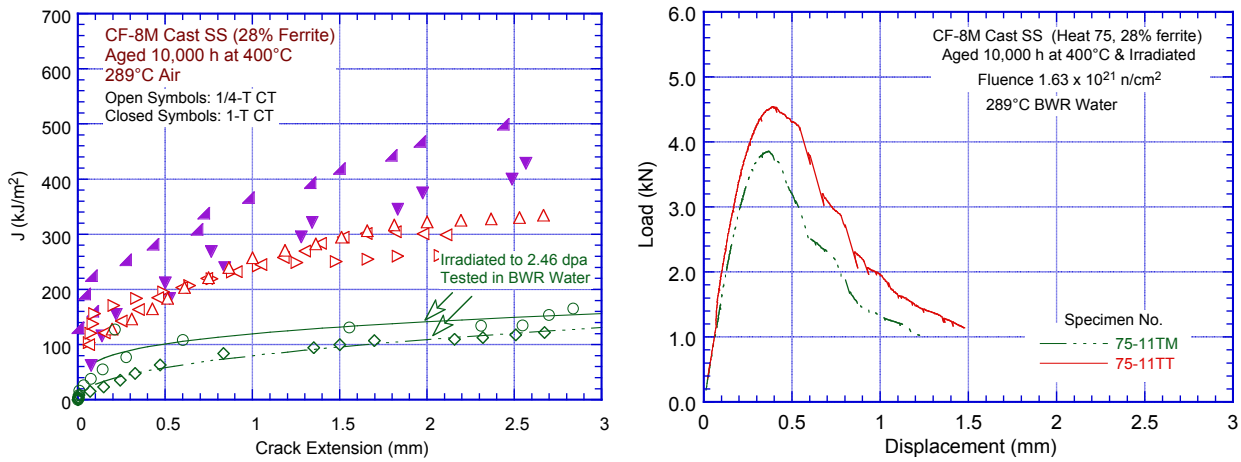


Figure 60. Fracture toughness J-R curves and load vs. loadline displacement curves for thermally aged and irradiated CF-8M cast SS (Ref. 8).

*Test Temperature:* The fracture toughness of nonirradiated austenitic SSs is known to decrease as the test temperature is increased. The change in the $J_{Ic}$ of irradiated SSs as a function of test temperature is plotted in Fig. 61 for several grades of SSs and welds irradiated in LWRs and fast reactors. The fracture toughness of steels irradiated to relatively low dose (less than 5 dpa) decreases with increasing test temperature in most cases. However, for steels irradiated to more than 12 dpa, test temperature has little effect on fracture toughness. The data on materials irradiated in LWRs or fast reactors exhibit similar trends. It should be noted that, at this fluence level, the toughness value is already low, which makes it difficult to discern definitive trends.

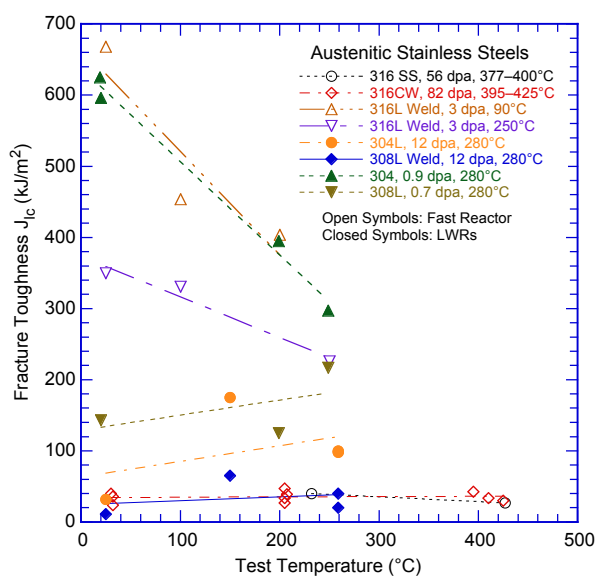


Figure 61.
Fracture toughness $J_{Ic}$ of irradiated austenitic stainless steels and welds as a function of test temperature (Ref. 11).

The effect of test temperature is also reflected in the fracture morphology of highly irradiated materials. At temperatures above 230°C (446°F) the failure mode is predominantly channel fracture

characterized by a faceted fracture surface. It is associated with highly localized deformation along a narrow band of slip planes whereby the initial dislocation motion along the narrow band clears away the irradiation-induced defect structure, creating a defect-free channel that offers less resistance to subsequent dislocation motion. The localization of the deformation ultimately leads to channel failure.

## 3.2 Fracture Toughness Trend Curve

The change in initiation toughness $J_{Ic}$ of wrought austenitic SSs (including weld HAZ materials and sensitized SSs) and cast SSs and weld metals is shown in Fig. 62 as a function of neutron dose. The fracture toughness data from both fast reactor and LWR irradiations are included. The irradiation temperatures range from 90 to 427°C (194-800°F) and test temperatures generally from 250 to 427°C (212-800°F). Only the data for CF-8 cast SS irradiated in a fast reactor to 10-11 dpa (inverted triangles in the figure) were obtained at room temperature. The data in Fig. 61 indicate little or no effect of test temperature for materials irradiated to 12 dpa or higher, although the toughness values are already quite low above 12 dpa. Also, as discussed previously in Section 3.1, the procedures for determining $J_{Ic}$ vary

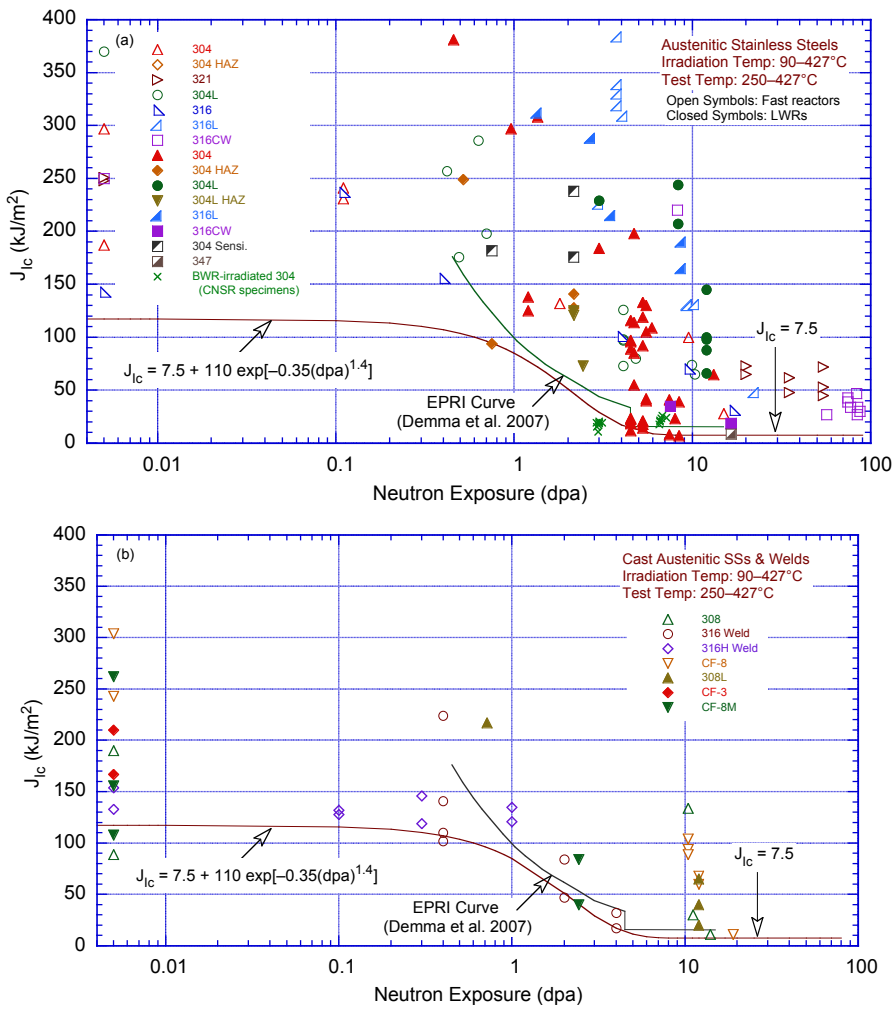


Figure 62. The change in initiation toughness $J_{Ic}$ of (a) wrought austenitic SSs and (b) cast austenitic SSs and weld metals as a function of neutron exposure. The data points plotted at 0.005 dpa are for nonirradiated materials.

among these studies. For example, in earlier studies a bilinear J-R curve was used to fit the data, whereas a power-law curve was used in the more recent studies. Different expressions have also been used for the blunting line. Overall, the results indicate little or no change in toughness below 0.5 dpa, a rapid decrease between 1 and 5 dpa, and no further change (saturation) beyond 10 dpa.

There appear to be some differences in behavior between subsets of the data in Fig. 62a. The threshold dose and the dependence of the decrease in fracture toughness $J_{Ic}$ on neutron dose seem to vary for different grades of materials. The average $J_{Ic}$ of the Type 304 SS drops from above 150 kJ/m$^2$ (857 in.-lb/in.$^2$) at 1 dpa to 12-24 kJ/m$^2$ (69-137 in.-lb/in.$^2$) at about 5 dpa. For Type 316L SS the decrease appears to occur at a somewhat higher fluence range (3 dpa to 10 dpa), and for Type 304L SS it appears to occur at a somewhat lower fluence. Therefore, the decrease in toughness with increasing fluence appears earliest in Type 304L SS, followed by Type 304 SS and then Type 316 SS.

The fracture toughness data in Fig. 62b for cast SSs and welds are lower than those of the wrought SSs for all dose levels less than the 10-dpa saturation level. However, the available fracture toughness data for irradiated SS welds and cast austenitic SSs are extremely limited. There are no data on any of these materials for fluences above 20 dpa, and little or no data on cast austenitic SSs for fluences below about 2 dpa. The existing data for welds suggest that ≈0.3 dpa may be considered a threshold neutron dose below which irradiation has little or no effect on fracture toughness of SS welds. However, this threshold does not consider the possible synergistic effects of thermal and neutron embrittlement of welds.

The existing data for cast austenitic SSs are inadequate to define a threshold dose for irradiation effects on fracture toughness. First, there are no fracture toughness data for dose levels of 0.1-2.0 dpa; second, the potential synergistic interactions of thermal aging and neutron irradiation embrittlement of cast austenitic SSs and SS welds[124-128] have yet to be addressed.

Although wrought SSs are typically completely austenitic, welded and cast SSs have a duplex microstructure consisting of austenite and ferrite phases. The ferrite phase increases the tensile strength and improves resistance to SCC, but it is susceptible to thermal embrittlement after extended service at reactor operating temperatures. Thermal aging of cast SSs at 250-400°C (482-752°F) leads to precipitation of additional phases in the ferrite (e.g., formation of Cr-rich $\alpha'$ phase by spinodal decomposition; nucleation and growth of $\alpha'$; precipitation of a Ni- and Si-rich G phase, $M_{23}C_6$ carbide, and $\gamma_2$ austenite; and additional precipitation and/or growth of existing carbides at the ferrite/austenite phase boundaries).[129-132] The formation of the Cr-rich $\alpha'$ phase by spinodal decomposition of ferrite is the primary mechanism for thermal embrittlement; it strengthens the ferrite phase by increasing strain hardening and the local tensile stress. Thermal aging has little or no effect on the austenite phase. Thus, thermal aging of cast SSs and SS welds leads to the development of a material with a brittle phase dispersed in a ductile matrix.

Embrittlement of the ferrite phase due to neutron irradiation occurs much faster than for austenitic SSs; at reactor operating temperatures of 288-343°C (550-650°F), a shift in the nil-ductility transition (ΔNDT) temperature of up to 150°C (302°F) has been observed in pressure vessel steels after neutron exposures of 0.07-0.15 dpa (0.5-1.0 x $10^{20}$ n/cm$^2$).[133] The irradiation temperature is an important factor in establishing the extent of embrittlement of ferritic steels. Although both the thermal aging embrittlement of ferrite and the neutron irradiation embrittlement of ferrite are well characterized, the synergistic effect of thermal aging and neutron irradiation on the embrittlement of SS welds and cast SSs has not been investigated yet. The concurrent exposure to high neutron fluence levels could result in a synergistic effect wherein the service-degraded fracture toughness is reduced from the levels predicted

independently for either of the two mechanisms. The possible synergistic effects of thermal aging and neutron irradiation embrittlement of SS welds and cast SSs are discussed further in Section 3.3.

The two curves shown in Fig. 62 represent a disposition curve proposed by EPRI[58] and a fracture toughness trend curve that bounds the existing data. The trend curve takes into consideration: (a) a threshold neutron exposure for radiation embrittlement of austenitic SSs and a minimum fracture toughness for these materials irradiated to less than the threshold value, (b) a saturation neutron exposure and a saturation fracture toughness for materials irradiated to greater than this value, and (c) a description of the change in fracture toughness between the threshold and saturation neutron exposures. As shown in Fig. 62, the fracture toughness $J_{Ic}$ curve that bounds the existing data for $J_{Ic}$ as a function of neutron dose (in dpa) may be represented by

$$J_{Ic} = 7.5 + 110 \exp[-0.35(\text{dpa})^{1.4}]. \tag{23}$$

This lower bound curve represents a threshold dose of 0.3-0.5 dpa for neutron embrittlement, a minimum fracture toughness $J_{Ic}$ of ≈118 kJ/m$^2$ below the threshold dose, a saturation threshold of 5 dpa beyond which the fracture toughness of these materials appears to saturate, a saturation fracture toughness $J_{Ic}$ of 7.5 kJ/m$^2$ (or $K_{Ic}$ or $K_{Jc}$ of 38 MPa m$^{1/2}$), and a description of the change in toughness between 0.3 and 5 dpa. The $J_{Ic}$ value of ≈118 kJ/m$^2$ below the threshold dose is appropriate for thermally aged and unaged cast SSs and SS flux welds. A value higher than 118 kJ/m$^2$ maybe considered for the minimum fracture toughness $J_{Ic}$ for wrought austenitic SSs irradiated below the threshold dose for neutron embrittlement. The description of the change in fracture toughness below 1.5 dpa will change accordingly. The lower bound trend curve given by Eq. 23 is consistent with the MRP lower bound model proposed for PWRs.[121] The MRP model is expressed in terms of a lower bound $K_{Jc}$ (MPa m$^{1/2}$) curve. It bounds all the fracture toughness data from fast reactors, BWRs, and PWRs as a function of the neutron dose (in dpa) and is given by the expression,

$$K_{Jc} = 180 - 142[1-\exp(-\text{dpa})]. \tag{24}$$

Both Eqs. 23 and 24 predict a saturation fracture toughness $K_{Ic}$ of 38 MPa m$^{1/2}$. For materials irradiated below the threshold dose for irradiation embrittlement, Eq. 23 predicts a minimum $K_{Jc}$ of about 151 MPa m$^{1/2}$, but the MRP expression predicts fracture toughness values that for some materials, such as SS welds or weld HAZ, may be higher than the minimum toughness of the materials in the nonirradiated condition. The disposition curve proposed by EPRI for BWRs is not bounding for the existing data for BWR-irradiated austenitic SSs. For example, at neutron doses <0.7 dpa, the $J_{Ic}$ values based on the EPRI curve are higher than the minimum $J_{Ic}$ of nonirradiated SS welds (particularly flux welds), some heats of wrought SSs, and most thermally aged cast austenitic SSs with >15% ferrite.[124] The saturation $K_{Ic}$ of 55 MPa m$^{1/2}$ at 4.5 dpa for the EPRI curve is also higher than the value of 38 MPa m$^{1/2}$ previously proposed by MRP for PWRs.[121] The saturation $K_{Ic}$ for the EPRI curve was based on data for which the specimen orientation was unknown. Recent data indicate that fracture toughness in the transverse orientation is nearly half of that in the longitudinal orientation.[58] Therefore, the bounding $K_{Ic}$ values above 4.5 dpa are likely to be lower than 55 MPa m$^{1/2}$. Also, as seen in Fig. 62b, some of the data for SS welds irradiated to 2-4 dpa are also below the EPRI curve.

A fracture toughness J-R curve may be used to analyze material behavior for loading beyond $J_{Ic}$. The J-R curve is expressed in terms of the J integral and crack extension ($\Delta a$) by the power law $J = C(\Delta a)^n$. At dose levels below the threshold dose for saturation (i.e., at dose levels less than ≈5 dpa), the effect of neutron irradiation on the fracture toughness of austenitic SSs can also be represented by a decrease in the coefficient C of the power-law correlation for the J-R curve with neutron dose. The

variation of C for wrought and cast SSs and welds as a function of neutron dose is shown in Fig. 63. Except for the results for CF-3 (closed diamond in Fig. 63b) and CF-8 irradiated in BOR-60 reactor (open inverted triangle in Fig. 63b), the remaining data were obtained at temperatures above 250°C. Based on the data trends in Fig. 61, test temperature should have little or no effect on the data for CF-8 cast SS. However, the constant C for CF-3 cast SS may be more than a factor of two lower at LWR operating temperatures. The two curves in Fig. 63 represent the disposition curve proposed by EPRI for BWRs,[65] and a trend curve for coefficient C that bounds the existing data.

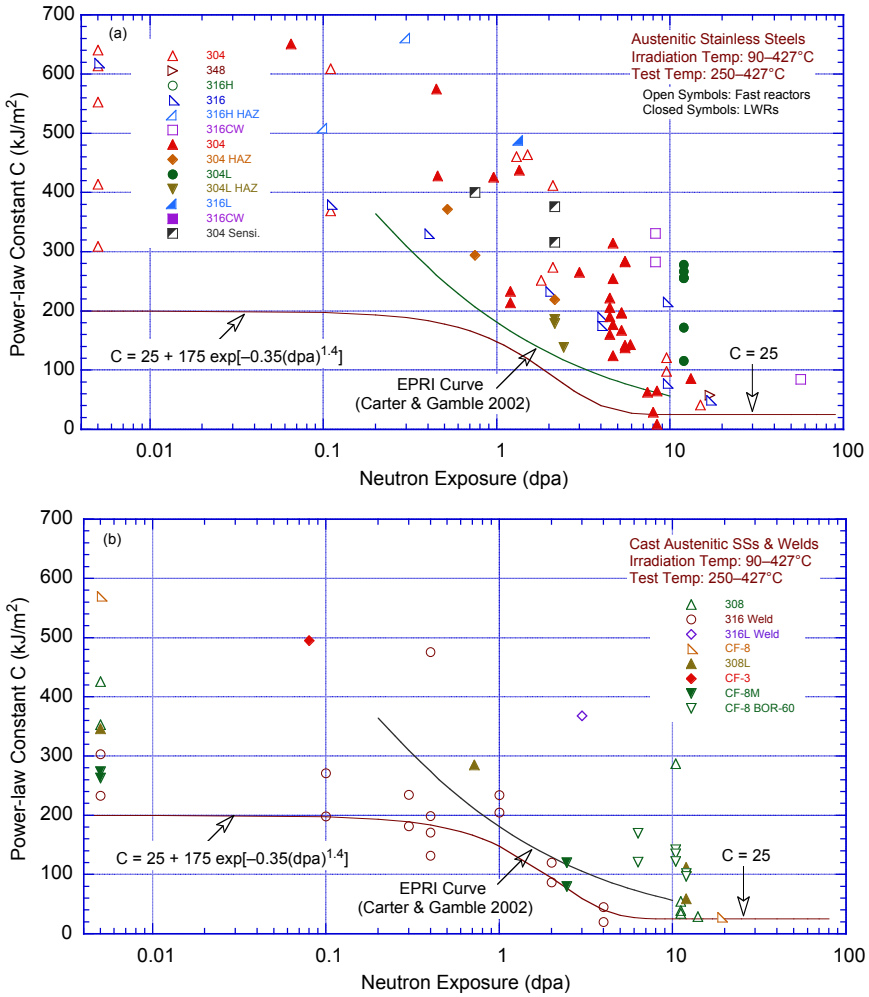


Figure 63. Change in coefficient C of the power-law J-R curve for (a) wrought austenitic SSs and (b) cast austenitic SSs and weld metals as a function of neutron exposure.

Even for fluence levels above 10 dpa, most heats of wrought austenitic SSs show ductile crack extension in the toughness tests. Under similar irradiation conditions, the coefficient C for cast SSs and welds is lower than that for wrought SSs. However, since most of the data are from irradiations in fast reactors and at temperatures of 370-427°C (698-800°F), the values for the power-law coefficient C are likely to be lower for irradiations at LWR operating temperatures. As mentioned previously, fracture toughness data are limited on materials irradiated in LWRs to neutron dose levels of 0.1-1.0 dpa or above 10 dpa. Therefore, it is not possible to define accurately the lower bound trend curve for the power-law coefficient C as a function of neutron dose. For fluences less than 5 dpa, as shown in Fig. 63, the existing fracture toughness data can be bounded by the following expression for C:

$$C = 25 + 175 \exp[-0.35(\text{dpa})^{1.4}], \quad (25)$$

and an exponent n equal to 0.37 (the median value of the experimental data). The exponent n of the power-law curve typically ranges from 0.35 to 0.70 for nonirradiated materials and 0.16 to 0.65 for irradiated materials. Unlike the behavior for thermally aged cast austenitic SSs, where exponent n typically decreases with a decrease in fracture toughness,[124] no obvious trend of n with fluence is evident. For irradiated materials, the median value of n is 0.37. Equation 25 yields a C value of ≈200 kJ/m$^2$ (1285 in.-lb/in.$^2$) for materials irradiated to less than 0.1 dpa and ≈31 kJ/m$^2$ (≈160 in.-lb/in.$^2$) for materials irradiated to ≈5 dpa. These values yield $J_{Ic}$ values of 125 and 17 kJ/m$^2$, respectively, for materials irradiated to <0.1 and 5 dpa. These values are consistent with the $J_{Ic}$ trend curve of Fig. 62. The $J_{Ic}$ at 5 dpa is also consistent with the data for the CT specimens of Type 304 SS irradiated to ≈4.5 dpa in a BWR (closed triangles in Fig. 62a).

As noted previously, ductile crack extension was also not observed for some specimens of a 20% CW Type 316 SS irradiated to 74-88 dpa in a fast reactor at 410-425°C (770-797°F). The specimens failed by a quasi-cleavage fracture believed to be an indirect consequence of the onset of void swelling in the material. The $K_{Ic}$ values were 74-90 MPa m$^{1/2}$ (67-82 ksi in.$^{1/2}$).

## 3.3 Synergistic Effect of Thermal and Neutron Irradiation

An issue that has been a concern for reactor core internal components is the possibility of a synergistic interaction between irradiation embrittlement and thermal embrittlement of cast austenitic SSs and SS weld metals. The effect of neutron irradiation on the fracture toughness of wrought and cast SSs and welds has been discussed in Section 3.1, and the change in fracture toughness $J_{Ic}$ and coefficient C of the power-law J-R curve with neutron dose is shown in Figs. 62 and 63, respectively. Thermal aging of cast austenitic SSs and SS welds at reactor operating temperatures of 280-350°C (536-662°F) can lead to degradation of their fracture properties.[102,124-126] Welded and cast SSs have a duplex structure consisting of austenite and ferrite phases. Formation of Cr-rich $\alpha'$ phase in the ferrite is the primary mechanism for thermal embrittlement of these materials;[124-132] thermal aging has no effect on the austenite phase.

Thermal aging increases the tensile strength, hardness, and Charpy-impact transition temperature, and it decreases the ductility, fracture toughness, and impact strength.[124-127] For cast austenitic SSs, the extent of mechanical-property degradation is essentially determined by the chemical composition of the steel, the casting process used to construct the component, the ferrite content and ferrite morphology of the steel, and the time and temperature of service for the component.[124] Cast SSs with high levels of Mo (e.g., CF-8M) show greater susceptibility to thermal embrittlement than steels with low Mo content (e.g., CF-3 or CF-8). Static cast steels are more susceptible to thermal embrittlement than centrifugally cast components.[124] The screening criteria to determine the susceptibility of cast SS components to thermal aging embrittlement are outlined in Table 4.

For cast austenitic SSs, the minimum fracture toughness that can occur due to thermal embrittlement depends strongly on the ferrite content and morphology. A globular ferrite morphology in which the brittle ferrite phase is isolated in an austenitic matrix will have a higher fracture toughness than a lacy morphology in a material with greater than 9% ferrite, where a continuous fracture path through the brittle ferrite is possible. The minimum toughness due to thermal aging occurs when the ferrite is fully embrittled, and the remaining toughness depends on the toughness provided by the ductile matrix surrounding the embrittled phase. Based on an ANL study,[124] the predicted saturation J-R curves for the various cast SSs in the thermally aged condition (i.e., the lowest fracture toughness that could be achieved

Table 4. Screening criteria for thermal-aging susceptibility of cast austenitic stainless steels (Ref. 134).

| Mo Content (wt.%) | Casting Method | Ferrite Content | Susceptibility Determination |
|---|---|---|---|
| High (2.0-3.0) | Static | ≤14% | Not susceptible |
| | | >14% | Potentially susceptible |
| | Centrifugal | ≤20% | Not susceptible |
| | | >20% | Potentially susceptible |
| Low (0.5 max.) | Static | ≤20% | Not susceptible |
| | | >20% | Potentially susceptible |
| | Centrifugal | All | Not susceptible |

for the steel after thermal aging) are expressed as $J \approx 264\ \Delta a^{0.35}$, $\approx 251\ \Delta a^{0.34}$, and $\approx 167\ \Delta a^{0.31}$, respectively, for CF-3, CF-8, and CF-8M steels at 290°C (554°F).

The results for SS welds indicate that the decrease in fracture toughness due to aging depends on the ferrite content and initial toughness of the weld.[102] Differences in the fracture toughness of SS welds arise from differences in the density and size of inclusions in the material. Failure occurs by the formation and growth of microvoids near hard inclusions. Welds with relatively high fracture toughness (e.g., GTA or tungsten inert gas weld) show a significant decrease due to thermal aging whereas welds with poor fracture toughness (e.g., SA, SMA, or manual metal arc welds) show minimal change. In the latter, failure primarily occurs by the formation and growth of microvoids. Such processes are relatively insensitive to thermal aging. The existing data indicate that at 280-350°C, the fracture toughness $J_{Ic}$ of thermally aged welds can be as low as 40 kJ/m$^2$. A conservative estimate of the J-R curve for aged SS welds[102] is given by $J = 40 + 83.5\ \Delta a^{0.643}$.

Reactor core internal components are subject to thermal and concurrent exposure to neutron irradiation. This condition could result in a synergistic effect wherein the service-degraded fracture toughness can be less than that predicted for either thermal embrittlement or neutron irradiation embrittlement independently.

For license renewal, to account for the effects of thermal aging and neutron irradiation embrittlement on the fracture toughness of reactor core internal components, the NRC staff has proposed that for cast austenitic SS components that have a fluence of greater than $1 \times 10^{17}$ n/cm$^2$ (0.00015 dpa) or are determined to be susceptible to thermal aging embrittlement, an aging management program should be implemented. This program should consist of either a supplemental examination of the affected components as part of the applicant's 10-year inservice inspection program during the license renewal term, or a component-specific evaluation to determine the susceptibility to loss of fracture toughness.[134] Furthermore, the program should consider the synergistic loss of fracture toughness due to neutron irradiation embrittlement and thermal aging embrittlement.

An EPRI report on thermal aging embrittlement of cast SS components proposed the use of the J value at a crack extension of 2.5 mm (0.1 in.), $J_{2.5}$, to differentiate between nonsignificant and potentially significant reductions in fracture toughness of cast austenitic SSs.[135] Flaw tolerance evaluations were presented in Appendices A and B of the EPRI report to support the choice of a threshold value of $J_{2.5} = 255$ kJ/m$^2$ (1456 in.-lb/in.$^2$). The NRC staff has found that using $J_{2.5} = 255$ kJ/m$^2$ is an acceptable screening approach for fracture toughness of cast SSs.[134] This concept can be extended to irradiated materials. However, the applicability of the flaw tolerance evaluations in Appendices A and B of the EPRI report would have to be demonstrated to support the use of the $J_{2.5}$ parameter for evaluating the toughness of irradiated SSs.

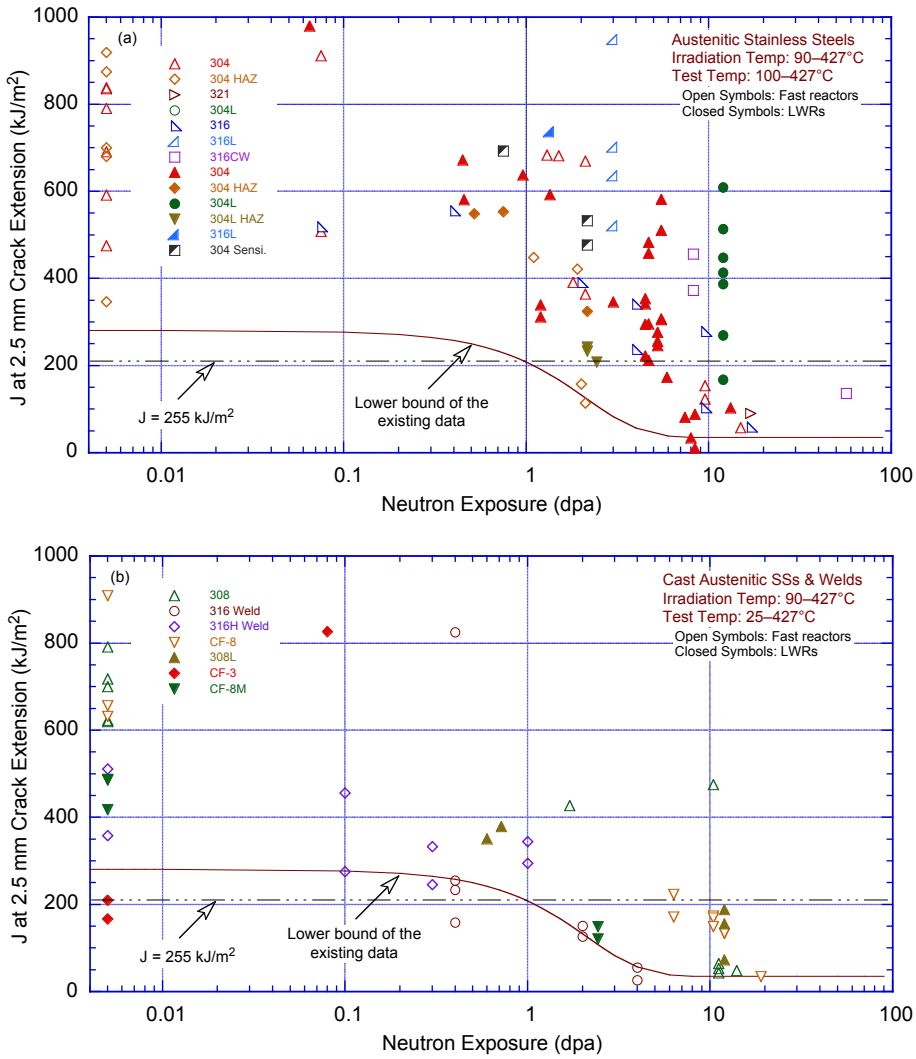


Figure 64. Experimental values of J-integral at a crack extension of 2.5 mm for (a) wrought austenitic SSs and (b) cast austenitic SSs and weld metals plotted as a function of neutron exposure.

For the wrought and cast austenitic SSs and welds listed in Fig. 63, the experimental J-integral values at a crack extension of 2.5 mm are plotted as a function of neutron dose in Fig. 64. The solid curve in Fig. 64 represents the predicted values of J at 2.5-mm crack extension that are expected to bound the existing experimental data shown in Fig. 63. The curve was obtained using the power-law J-R curve relationship, with coefficient C determined from Eq. 25 and an exponent n of 0.37. The lower bound curve indicates that for cast SSs and welds irradiated up to 1.0 dpa, the predicted J at 2.5 mm is above the screening value of 255 kJ/m$^2$ (1456 in.-lb/in.$^2$). However, additional fracture toughness data on irradiated SS welds and cast SSs, particularly at 0.1-2.0 dpa, are needed to better define the threshold dose when the fracture toughness of austenitic SSs begins to significantly decrease.

This evaluation does not consider the synergistic interaction of neutron irradiation embrittlement and thermal aging embrittlement. Embrittlement of ferrite phase from neutron irradiation occurs at lower dose levels than does embrittlement of the austenite phase. A shift in the NDT temperature of up to 150°C (302°F) has been observed in pressure vessel steels irradiated to 0.07-0.15 dpa.[133] Thus, embrittlement of ferrite is expected to occur at 0.05-1.0 dpa, whereas, as discussed in Section 3.1, any

significant effect of neutron irradiation on embrittlement of the austenite phase occurs only above ≈0.5 dpa (Fig. 62).

In addition to possibly altering the threshold dose for neutron embrittlement, synergistic effects of neutron irradiation and thermal aging embrittlement could decrease the saturation fracture toughness of irradiated welded and cast SSs and accelerate the change in fracture toughness between the threshold and saturation neutron exposures. Unfortunately, limited data are available to assess such effects. Figure 64 shows the results of two tests on a CF-8M steel that was thermally aged for 10,000 h at 400°C and then irradiated to well above the threshold dose for neutron embrittlement (inverted triangles in Fig. 64). The resulting toughness is bounded by the curve for other SSs irradiated to a similar level, i.e., thermal aging does not seem to lower the toughness below that expected for irradiation alone at these neutron dose levels.

Additional fracture toughness data are needed to better establish the potential for synergistic loss of toughness in these materials in the transition dose range from 0.05 to 2 dpa. A program is being conducted at ANL on fracture toughness characterization of CF-3, CF-8, and CF-8M cast SS and SS welds irradiated in the Halden reactor in Norway at 315°C and doses of $5 \times 10^{19}$ n/cm$^2$ (0.075 dpa) and $2 \times 10^{21}$ n/cm$^2$ (3.0 dpa). Although cast CF-8M SSs are not used in LWR core internal components because of the difficulty of testing irradiated materials, it may be helpful to study this material as a "worst-case" in lieu of testing a number of heats of CF-3 and CF-8.

This page is intentionally left blank.

# 4. Void Swelling

## 4.1 Background Information

Void swelling refers to the volume change of materials under neutron irradiations. Void swelling was first observed in the late 1960s in austenitic SSs irradiated in fast reactors to neutron exposures above $1 \times 10^{23}$ n/cm$^2$ at temperatures of 370-650°C (698-1202°F).[17] As discussed in Section 2.1.1, neutron irradiation damages materials by displacing atoms from their lattice position. Such displacements create vacancies and interstitials, most of which are annihilated by recombination. The surviving defects lead to microstructural changes as they rearrange into more stable configurations. Because of the relatively large strain field that surrounds interstitials, there is a strong interaction between interstitials and dislocations, which results in a preferential flux of interstitials toward dislocations. The remaining vacancies cannot annihilate by recombining with interstitials, and this condition leads to the nucleation of cavities or microvoids. Under certain conditions of temperature and dose rate, these cavities or microvoids can eventually grow to larger sizes. Fission products such as He and H also play an important role in void formation. By combining with these gas atoms, void nucleation is facilitated through reduction of the surface energy of vacancy clusters. The fundamental driving force of void formation, however, remains the excess vacancy flux toward voids.

The formation of a large number of voids results in an increase in the volume of the material; this process is referred to as void swelling. The volume changes from void swelling are normally isotropic and occur in all directions. However, there are always constraints on swelling, both internally due to gradients of temperature and dose rate within the component, and externally from neighboring components. Such constraints result in anisotropic swelling and stress fields within the components that activate irradiation creep in unconstrained directions, producing dimensional distortions and misfits that can compromise the functional integrity of the reactor core internal components.

Most void swelling data have been obtained from materials irradiated in fast breeder reactors at temperatures above 385°C (725°F) and at dose rates that are orders of magnitude higher than those in PWRs, and extrapolation of these results to estimate the void swelling behavior for PWR end-of-life or extended life conditions introduces substantial uncertainties.

The void swelling process is divided into two regimes: a transient regime followed by a steady-state swelling rate. All materials regardless of material composition and thermo-mechanical condition, stress state, neutron flux and spectrum, or irradiation temperature (above 300°C) are believed to reach a steady-state swelling rate of ~1%/dpa.[17] However, the duration of the transient regime varies with the various material, stress, and irradiation parameters. In general, higher neutron flux and stress accelerate, and cold work in the material delays, the onset of the steady-state swelling rate. To achieve steady-state swelling rate within the life time of PWRs may require irradiation tempertures above 400°C. Significant effects of various material and environmental parameters on void swelling are as follows:

*Irradiation Temperature*: In the temperature range for fast reactors, void swelling shows a strong dependence on irradiation temperature. For 20% CW Type 316 SSs a steady-state swelling rate of 1%/dpa is observed in fast reactor data at 427°C (800°F) or higher temperatures.[18] As discussed in Section 2.1.1, voids typically appear in austenitic SSs at temperatures above 340°C. The PWR coolant temperatures do not exceed 345°C (653°F), although gamma heating of thick section components near the reactor core could increase the local temperature within the component to 370°C (698°F) or even higher. The lower irradiation temperatures, typical of LWRs, extend the transient regime to much longer times

and result in the formation of a higher density of smaller voids. However, depending on the irradiation temperature, dose, and dose rate, voids can form under PWR operating conditions within the reactor lifetime. Voids have been observed in austenitic SSs irradiated at temperatures as low as 300°C (572°F).[136]

*Material Composition*: Reactor core internal components are primarily constructed of austenitic SSs. These materials have a face-centered cubic crystal structure and are more susceptible to void swelling (i.e., swelling occurs earlier and at a higher rate) than ferritic steels, which have a body-centered cubic crystal structure. The material composition can influence the transient regime for void swelling. The most important factor is the Ni content in the steel. In the 300-series SSs, swelling decreases rapidly with increasing Ni content up to about 30-40%.[137] In contrast, Cr has the opposite effect; it decreases the transient regime and increases swelling.[137] However, at low temperatures typical of LWRs, swelling is not expected to change significantly over the range of Cr found in the 300-series SSs used for nuclear service. Because of compositional differences, Type 304 SS typically swells more than Type 316 SS under similar thermal-mechanical conditions.

The effect of minor trace elements on void swelling is sensitive to material and environmental conditions and, therefore, is less predictable. Similar to the effect of Ni, P contents above 0.01 wt.% and Si contents above 0.2 wt.% decrease swelling in the 300-series SSs.[138,139] The effect of these solutes at small concentrations may be different at lower temperatures typical of PWRs. However, since most SSs used for the construction of LWR core internals typically contain 0.03-0.04 wt.% P and ~0.5 wt.% Si, these elements are expected to decrease void swelling. Both change the effective diffusivity of vacancies and thereby the vacancy supersaturation. Minor differences in the concentration of these minor elements and their distribution due to differences in thermal-mechanical history may explain the large differences in the swelling behavior sometimes observed in essentially identical heats of SSs.[101]

*Phase Changes during Irradiation*: As discussed in Section 2.1.1, irradiation at higher temperatures, particularly above 340°C, leads to the formation of second phase particles. The radiation-induced formation of γ' silicide ($Ni_3Si$), phosphides ($M_2P$ and $M_3P$), and G phase ($M_6Ni_{16}Si_7$) can remove Ni, P, and Si from the alloy matrix, and thereby increase void swelling. However, radiation-induced precipitation of second phases is strongly dependent on both temperature and displacement rate.[17]

*Material Condition*: Cold work in the material prolongs the transient regime for void swelling in austenitic SSs. The high dislocation density produced by the cold work provides additional recombination sites for vacancies and interstitials, thereby decreasing supersaturation of vacancies in the material and delaying void nucleation. The high dislocation density also interferes with diffusion of minor elements and, therefore, delays or prevents the formation of second phase particles, which remove elements (such as Ni, Si, or P) that are known to suppress void swelling. However, the benefit of cold work is short lived because absorption of vacancies increases the mobility of the dislocations, permitting them to interact and decline in density to levels similar to those achieved in solution-annealed materials with comparable irradiation doses. In solution-annealed Type 304 SS, voids nucleate easily, and the transient regime is characterized by a slowly increasing rate of swelling with increasing neutron dose. In CW Type 316 SS, void nucleation is difficult or does not occur for some time, but the transient regime ends, and the steady-state swelling rate starts abruptly.[18]

*Stress and Stress History*: In general, stress accelerates void swelling and decreases the transient regime. The sign of the stress state, tensile or compressive, does not matter; it is the shear component and not the hydrostatic component that accelerates swelling.[17] As discussed above, constraints due to

gradients in temperature and/or dose rate and from adjoining components lead to anisotropic swelling and buildup of stresses within the component. These stresses, however, are limited by irradiation-induced creep and will relax in time; the rate of relaxation is proportional to the swelling rate. Therefore, the swelling-induced stresses often vary with time, increasing due to swelling and component constraints, and decreasing with creep relaxation. The interaction of swelling and irradiation creep relaxation plays an important role in evaluation of swelling in PWR core internal components. The deformation due to irradiation creep is in the direction that relieves the shear component of the applied stress. In a bolt, the primary stress is tensile along the bolt axis. Thus, the bolt would creep to increase its length and decrease the diameter. However, if the plate in which the bolt is embedded swells at a greater rate, the stress in the bolt would be reestablished. In the case of the hot spot in the former plate behind the reentrant baffle plate corner, the local stresses that are generated because of external and internal constraints would redirect swelling in the vertical direction.[101] Another effect of stress is that a high swelling region within a component would produce stresses in an adjacent lower swelling region, thereby increasing their swelling rate. Therefore, calculations of swelling based on stress-free material would tend to overestimate swelling gradients in a component.

*Displacement Rate*: Void swelling data on annealed Type 304L SS irradiated to ~30 dpa at 390°C in fast reactors indicate that swelling increases as the displacement rate is decreased.[140] This finding suggests that estimates of void swelling based on high flux fast reactor data could yield nonconservative results for PWR core internal components. In other words, under comparable irradiation temperatures and neutron dose levels, the lower displacement rates typical of PWRs could result in higher swelling. However, the exact mechanism by which displacement rate affects swelling is not well understood. Initially, it was believed to be due to an upward shift in the temperature range for void swelling with increases in displacement rate. Such a temperature shift is observed under ion bombardment in pure metals.[141] At low temperatures, the displacement rate effect is believed to arise from displacement-rate-dependent changes in point defect concentration and their effect on vacancy-interstitial recombination. At high temperatures, the higher production rate of vacancies and interstitials at the high dose rates is balanced by the enhanced defect migration rate so that the point defects that survive recombination are comparable in number to those surviving from the low displacement rate neutrons. Such an argument explains the change in swelling in terms of a change in void growth rate rather than a change in void nucleation. However, several studies on austenitic SSs irradiated in EBR-II at 373-444°C (703-831°F) indicate that the effect of displacement rate on swelling is due to its effect on the transient regime and not void growth.[142] The data also indicate that the displacement rate effect in solution-annealed materials is similar to that in cold-worked materials.

*Helium Production*: Under neutron irradiation, He can be produced by the $^{10}B$ reaction to form $^{4}He$ and $^{7}Li$, and also from the two-step production of $^{59}Ni$ from $^{58}Ni$ by thermal neutrons [i.e., $^{58}Ni(n,\gamma)^{59}Ni(n,\alpha)\ ^{56}Fe$]. In the latter, the He generation rate is proportional to the $^{59}Ni$ content and the thermal neutron flux. In PWRs, transmutations can produce both He and H. Hydrogen is produced from the two-step reaction $^{58}Ni(n,\gamma)^{59}Ni(n,p)\ ^{59}Co$ with thermal neutrons as well as from other non-transmutation sources. The nucleation of microvoids due to migration and condensation of vacancies produced by neutron displacements can be stabilized by the transmuted gas atoms (He or H), thereby increasing void swelling. A fine dispersion of He bubbles has been observed in SSs irradiated in LWRs at 300-340°C, especially in reactors with high thermal flux.[48,51] However, the effect of He on swelling is not as strong as that on Ni or P contents in the steel. Most of the earlier studies have focused on the effects of He on swelling. Studies on the effects of H are limited.

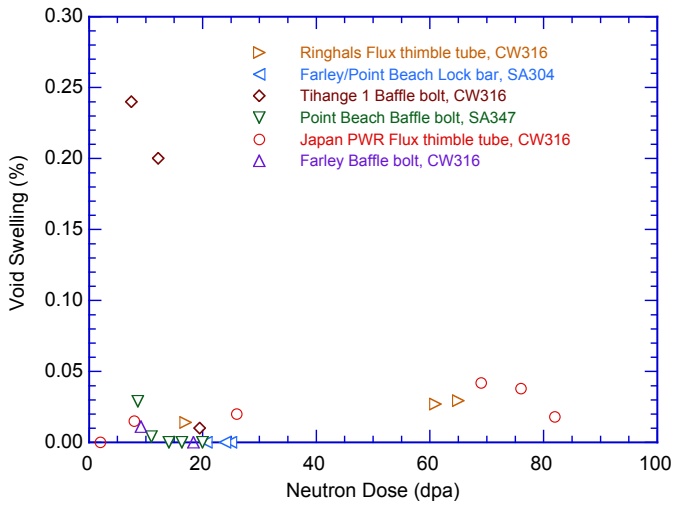


Figure 65. Void swelling of PWR materials plotted as a function of neutron dose (Refs. 20,143,144).

## 4.2 Assessment of Void Swelling in PWR Core Internal Components

The void swelling measured in PWR internal components, such as the flux thimble tubes and baffle bolts,[20,143,144] is plotted as a function of neutron dose in Fig. 65. Except for two data points that show 0.2-0.25% swelling, void swelling in these SSs irradiated up to 80 dpa is insignificant. However, the irradiation temperature for the low-swelling materials was less than 330°C (626°F). A review of the existing void swelling data on austenitic SSs irradiated in fast reactors and the limited data available on PWR-irradiated materials indicated that they all can reach the steady-state swelling rate of ~1%/s. The duration of the transient regime to reach this steady-state rate depends on material composition and thermal-mechanical condition, stress state, irradiation temperature, and neutron displacement rate. The state of the knowledge on the effects of these variables is discussed next.

1. *Temperature*: Although PWR coolant temperatures do not exceed 345°C (653°F), gamma heating can increase the local temperature in thick sections of reactor core components to values as high as 420°C (788°F). However, as shown in Fig. 66, most of the void swelling data on PWR-irradiated materials

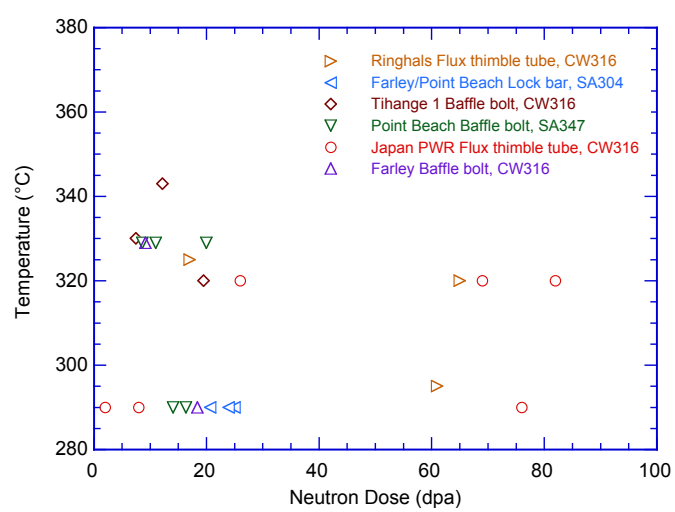


Figure 66. Irradiation temperature and neutron dose for the void swelling data shown in Fig. 65.

are at temperatures below 330°C, where swelling is minimal. There are no swelling data at 370-420°C (698-788°F), where swelling is expected to be the highest. Estimates of void swelling in PWR components are based on materials irradiated in fast reactors at temperatures above 370°C (698°F).

2. *Displacement Rate*: Typical displacement rates in PWRs are 0.3-9.0 x $10^{-8}$ dpa/s, whereas rates used in the void swelling studies are 0.3-10.0 x$10^{-7}$ dpa/s. Void swelling data on annealed and CW austenitic SSs irradiated in fast reactors at 373-444°C (703-831°F) indicate that swelling increases as the displacement rate is decreased. The displacement rate effect is primarily due to its effect on the transient regime. In other words, the dose required to achieve the 1%/dpa steady-state swelling rate is lower for austenitic SSs irradiated at the lower dose rate. These results suggest that under comparable irradiation temperatures and neutron dose levels, the lower displacement rates typical of PWRs would result in higher swelling. Limited void swelling data on PWR-irradiated materials are consistent with this prediction, which is based on fast reactor data at temperatures relevant for PWR internals and at displacement rates below 5.0 x $10^{-8}$ dpa/s.

3. *Stress State*: In general, irrespective of whether it is tensile or compressive, applied stress or swelling-induced stress accelerates void swelling. Secondary stresses due to thermal gradients and geometric constraints, however, are limited by irradiation creep and relax rather quickly. Therefore, the interaction of swelling and irradiation creep relaxation plays an important role in evaluation of swelling in PWR core internal components. Also, another stress-related effect is that stresses produced by a high swelling region in an adjacent lower swelling region force the lower swelling region to try to catch up with the faster growing regions. Thus, estimates of swelling based on stress-free material would tend to overestimate swelling gradients in a component.

4. *Material Composition and Condition*: The data on LWR-irradiated materials are inadequate to establish the differences in the swelling behavior of austenitic SSs under LWR and fast reactor irradiation conditions. The material composition can influence the transient regime for void swelling. In general, an increase in Ni, P, or Si content decreases swelling by increasing the transient regime. In contrast Cr has an opposite effect. Under PWR irradiation conditions, void swelling is not expected to change significantly with minor differences in the Cr content. Cold work also increases the transient regime for swelling but does not affect the steady-state swelling rate. Based on the fast reactor data on CW Type 316 SS, which indicate that the steady-state swelling rate of 1%/s is not reached after very high fluence and a temperature of 400°C (750°F), Byrne et al. concluded that it is unlikely that the 1%/dpa swelling rate would ever be attained in commercial PWR core internal materials.[18] However, their assessment is for 60-year operation; a steady-state swelling rate could eventually be attained in PWR internal materials during extended operation beyond 60 years. The differences between LWR and fast reactor irradiations need to be investigated.

5. *Phase Change*: As discussed above, radiation-induced formation of second phases can remove elements such as Ni, P, and Si, which are known to decrease swelling, from the alloy matrix. This effect increases void swelling. The precipitation of second phases is strongly dependent on material composition and thermal-mechanical condition as well as temperature, dose, and dose rate. However, another aspect of precipitation of second phase particles may tend to decrease swelling. Typically, irradiation-induced precipitation at PWR operating temperatures is extremely small (i.e., a few to several tens of nanometers), and the precipitate density is large. Therefore, at low temperatures, precipitation creates very large internal surfaces (i.e., interfaces between the precipitates and the metal matrix), which would act as sinks for vacancies, thereby suppressing the accumulation and condensation of vacancies to form voids. This behavior has been well known to occur in vanadium

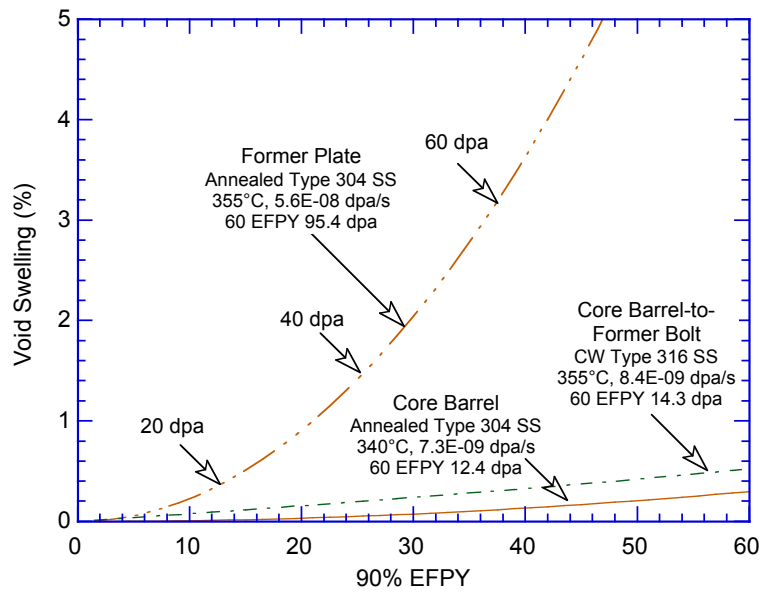


Figure 67. Void swelling of PWR materials plotted as a function of effective full power years (Refs. 20,143,144).

alloys.[20] The role of precipitation on void swelling in austenitic SSs under PWR irradiation conditions needs to be investigated.

Most of the void swelling data on LWR-irradiated materials have been obtained on CW Type 316 SS, and data on solution-annealed Type 304 SS are limited. As discussed above, because of the higher Ni content, void swelling in Type 316 SS is less than that in Type 304 SS. Also, cold work further reduces swelling in CW Type 316 SS. Therefore, additional data are needed on PWR-irradiated annealed Type 304 SS. Also, it is important to develop a technical basis for extrapolating the fast reactor data and the limited PWR data to predict void swelling in PWR core internal components. Although extrapolation of these results suggests that void swelling will not be a significant problem during the first license extension period, investigations are still needed on the effects of irradiation temperature (particularly above 370°C), displacement rate, and stress on void swelling, including the interaction of swelling and irradiation creep relaxation.

Stress-free swelling equations have been developed by the MRP for annealed Type 304 and CW Type 316 SSs used in PWR core internal components.[63] The swelling rate SR (%/dpa) is expressed in terms of the temperature T (°C), neutron dose $\phi$ (dpa), and dose rate $\dot{\phi}$ ($10^{-7}$ dpa/s). The swelling rate for annealed Type 304 SS is given by

$$SR_{SA304} = 2\phi\dot{\phi}^{-0.731}\exp\left(22.106 - \frac{18558}{T + 273.15}\right), \tag{26}$$

and the swelling rate for CW Type 316 SS by

$$SR_{CW316} = 0.9\left[10 + 2\phi\left(1 - \exp\left(-0.01\phi\right)\right)\right]\dot{\phi}^{-0.731}\exp\left(22.106 - \frac{18558}{T + 273.15}\right). \tag{27}$$

Equation 27 predicts a slightly higher swelling rate for Type 316 SS than that for annealed Type 304 SS up to 10 dpa and a lower swelling rate for higher dose levels. The predicted void swelling for Type 304 SS core barrel and former plate and for CW Type 316 SS core barrel-to-former bolt for a 60-y life at 90% EFPY is shown in Fig. 67. Note that the effect of temperature is much stronger than that of dose rate. For the core barrel, although the dose rate is low, the 60-y end-of-life void swelling is quite low because the total dose is only 12.4 dpa.

An expression to correlate stress-enhanced swelling has also been developed. The incremental stress-enhanced swelling, ΔS (%), is given by

$$\Delta S = S'\Delta\phi\left(1 + 0.005\bar{\sigma}\right), \tag{28}$$

where $S'$ is stress free swelling rate $SR_{SA304}$ or $SR_{CW316}$, $\Delta\phi$ is the increment of neutron dose, and $\bar{\sigma}$ is the von Mises effective stress (MPa). As discussed previously, any stress state, negative or positive, will accelerate the swelling rate.

Equations 26-28 are based on isothermal irradiation, and the maximum swelling rate is limited to 1%/s.

## 4.3 Embrittlement due to Void Swelling

As the volume of voids in the material continues to increase beyond 3-5%, the size and distribution of voids essentially control the fracture properties of the material. Several studies have shown that austenitic SSs irradiated at ≤400°C to neutron dose levels that produce ≥10% void swelling suffer from severe embrittlement.[144-147] Furthermore, the critical swelling level required to induce an extremely brittle state decreases with decreasing irradiation temperature.[145] A Type 316 SS irradiated in the EBR-II fast reactor at 400°C to 130 dpa, producing 14% void swelling, fractured during handling at room temperature.[146] Also, a Russian SS, EI-847, irradiated in the BN-350 fast reactor in the annealed condition to 73 dpa at 335°C and in the CW condition to 82 dpa at 365°C had more than 10% void swelling, and was found to be exceptionally brittle.[147]

In austenitic SSs with ≥10% void swelling, the high embrittlement has been attributed to a process that involves stress concentration between voids, Ni segregation at void surfaces, and a tendency toward martensite formation when the steel is deformed at room temperature.[145] As discussed previously, the removal of Ni and Si from the metal matrix to form γ' or G phase promotes void nucleation and swelling. Once voids form, Ni segregates to void surfaces due to the inverse Kirkendall effect, in which the slowest diffusing elements segregate. This further depletes Ni from the matrix. The loss of Ni and relative increase of Cr in the matrix in the region between the voids decrease the SFE substantially, which promotes planar slip and formation of martensite during room-temperature deformation. The austenite/martensite boundaries provide a low-energy crack propagation path, resulting in a brittle, quasi-cleavage fracture at room temperature.[146,147] At higher temperatures, the effect of Ni segregation on SFE is much less pronounced, and large levels of flow localization are required for failure, which occurs along the flow localization path, and is referred to as channel fracture.[115]

There are few quantitative data correlating the void swelling with fracture toughness of the material. A Fe-14Cr-16Ni-1.5Mo SS (D9) irradiated in the Fast Flux Test Facility (FFTF) at 390°C (734°F) to 114 dpa showed a $K_{Ic}$ of about 30 MPa $m^{1/2}$ measured at 410°C and zero tearing modulus.[148] Although the void swelling was not measured for this material, it is expected to be above 10%. Swelling

in the same material irradiated at 410°C to 175 dpa showed about 30% void swelling, and 20% CW Type 316 SS irradiated at 410°C to 170 dpa showed 18-23% swelling.

The fracture toughness of highly irradiated SSs with >10% swelling is lower than that observed in Type 304 or 316 SS irradiated to 4.5-8.5 dpa in BWRs (at 290°C). As discussed in Section 3.1.2, a $K_{Ic}$ of 55 MPa $m^{1/2}$ has been reported for BWR control blade material irradiated to 4.5 dpa, and 37 MPa $m^{1/2}$ in material irradiated to about 8 dpa. The latter value is currently defined as the saturation fracture toughness for irradiated austenitic SSs. The results for high swelling suggest that the fracture toughness of PWR core internal components of austenitic SS could be lower than the saturation value ($K_{Ic}$=38 MPa $m^{1/2}$) proposed by MRP.[121] The embrittlement of austenitic SSs due to void swelling under PWR irradiation conditions should be further investigated.

# 5. Stress Relaxation and Creep

Loss of preload for bolted joints and redistribution of stresses in components due to stress relaxation are other aging degradation concerns that need to be addressed to assure the functional integrity of the reactor core internal components. Stress relaxation represents plastic deformation that occurs with time under constant strain below the yield point of the material. In other words, stress relaxation may be considered as creep that occurs under constant strain instead of constant load or stress. It can occur either by thermal creep[21] or neutron-irradiation-assisted creep.[23,24]

Thermal creep is represented by primary (or transient), secondary (or steady-state), and tertiary creep stages. For most metals and alloys, at temperatures below 0.4 or 0.5 of their melting temperature (in degrees kelvin), creep under constant load is characterized by only primary creep with decreasing creep rates, and steady-state creep is insignificant. For the 300-series austenitic SSs and Ni alloys used in LWR core internal components, this temperature is about 394°C (740°F), which is higher than the typical temperature range for PWR core components. Only a few locations close to the core may be above this temperature due to gamma heating. Thus, for PWR internals, the contribution to total strain due to steady-state thermal creep under constant load is likely to be relatively small.

Stress relaxation data are generally obtained from tests performed in accordance with ASTM Specification E 328-86 under tension, compression, torsion, or bending to reflect the stress state imposed on the component. Most of the available data are for stress relaxation tests that have been conducted under tension (for bolted joints) and bending (for leaf springs). The stress state behavior of coil springs is more complex, and there are no stress relaxation data for coil springs in the open literature. In general, the thermal stress relaxation of coil springs appears to be much larger and depends on the coil design geometry.[101]

The existing data on thermal stress relaxation have been obtained from short-term tests (less than 1000 h) at 260-705°C (500-1300°F) on Type 304 SS as a function of cold work, thermo-mechanical condition, and stress level.[22] The results indicate that the percentage of stress relaxation increases with increasing initial stress and levels off at about 207 MPa (30 ksi). At PWR operating temperatures, stress relaxation saturates within 100 h with a maximum decrease of 10-20% of the initial preload stress depending on the thermal-mechanical treatment of the material.[101]. At temperatures below 315°C (600°F), for the same initial stress, the extent of stress relaxation decreases with increasing amount of cold work in the material. The effect of cold work is less significant at temperatures above 371°C (700°F). Stress relaxation reaches saturation in the short-term tests because only two components, anelastic strain and microplastic strain, contribute to the total time-dependent strain (or creep strain). Secondary or steady-state creep is insignificant in these tests at relatively low temperatures (i.e., less than 394°C). However, over the reactor lifetime, even a rather low steady-state creep rate could lead to greater stress relaxation than anticipated from the short-term tests. For example, at 350°C (662°F), the steady-state creep rate for Type 304 SS is estimated to be $5.2 \times 10^{-13}$ /s, which corresponds to 0.049% strain over 30 y or a total stress relaxation of 76.5 MPa (11.1 ksi).[21]

Neutron-irradiation-enhanced creep can greatly increase the plastic strain by increasing both the primary creep and steady-state creep rates. Unlike thermal creep, neutron irradiation can result in significant creep strain at PWR temperatures. Irradiation creep can be divided into three stages: transient, steady-state, and void-swelling-induced creep. The magnitude of both transient creep and steady-state creep is essentially proportional to the applied stress level. Transient creep is typically short and, although its magnitude depends on material condition and structure and irradiation temperature, the

contribution to total creep strain is relatively small (e.g., PWR fuel rods show <0.05% transient creep);[17] the steady-state creep rate is independent of these parameters. Figure 68 plots the thermal creep and irradiation-enhanced creep of 20% CW Type 316 SS in the EBR-II fast reactor at 454°C (850°F) and under an uniaxial stress of 138 MPa (20 ksi).

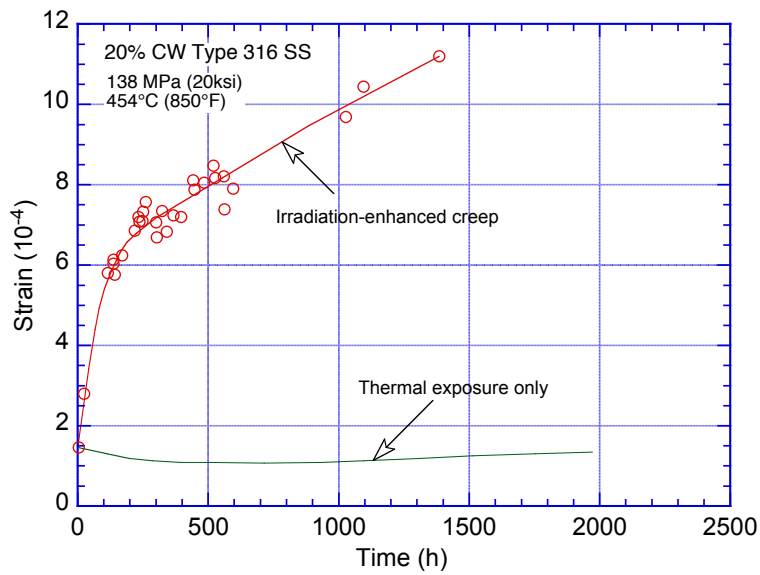


Figure 68. Thermal creep and irradiation-enhanced creep of a 20% CW Type 316 stainless steel irradiated in EBR-II (Ref. 101).

Empirical models have been developed for irradiation creep using data obtained from fast reactors. Because of the relatively weak dependence of steady-state creep on dose rate or temperature, the fast reactor data have been used to estimate irradiation creep at PWR operating temperatures.[101] The existing data are inadequate to determine the effects of cold work or material composition on irradiation-enhanced steady-state creep.

Initially, void-swelling-induced creep was not considered to be significant for PWR core internal components. However, as discussed in Section 4.2, void swelling could be significant for PWR core internals because of the low dose rates, which could lead to considerable creep strain. A detailed evaluation based on typical temperature/dose rate information for core components is needed to estimate the contribution of void-swelling-induced creep.

As discussed previously, stress relaxation is creep that occurs at constant strain. It follows the trends observed in thermal and irradiation creep. Initially, there is a sharp decrease in stress representing transient creep, followed by a gradual decrease in stress due to essentially steady-state irradiation creep. Empirical equations have been developed from the irradiation creep data to estimate stress relaxation as a function of initial stress and neutron dose, and the constants in the equations were derived by regression fitting to the available stress relaxation data. One such curve representing stress relaxation (%) as a function of neutron dose is given by,[101]

$$\frac{\sigma}{\sigma_o} = \exp\left\{-0.774\left(1-\exp\left(-23f\right)\right)-0.688f\right\}, \tag{29}$$

where f is the accumulated neutron fluence in dpa, and $\sigma$ and $\sigma_o$ are the remaining and initial stress. The first term [i.e., 0.774(1 - exp(-23f))] in the equation represents stress relaxation due to irradiation-enhanced transient creep, and the second term [i.e., 0.688f] represents stress relaxation due to steady-state creep. The screening trend curve obtained with the available stress relaxation data is shown in Fig. 69. The curve bounds all available test data for Type 304 SS, 20% CW Type 316 SS, and Alloy X-750.[23-25] The results indicate approximately 60% stress relaxation at a neutron dose of 0.2 dpa (or 1.3 x $10^{20}$ n/cm$^2$ E >1 MeV). Based on the screening trend curve in Fig. 69, all bolted PWR internals locations or spring component items that require preload for functionality and reach 0.2 dpa or higher are identified for further evaluation.[101]

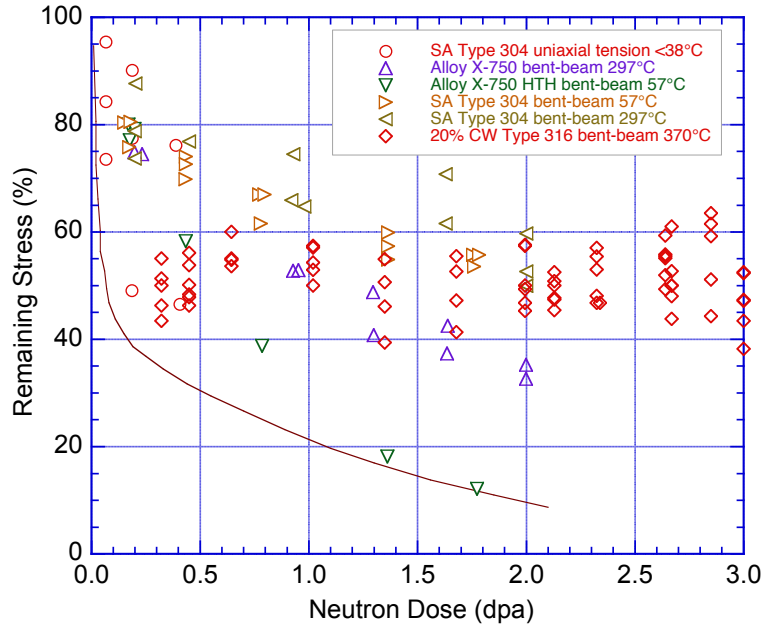


Figure 69. Trend line for screening irradiation-induced stress relaxation based on available test data (Refs. 23-25,101).

However, most of the existing data on irradiation-enhanced stress relaxation/irradiation creep have been from fast reactor irradiations, and data obtained under PWR irradiation conditions is limited. Therefore, the effects of neutron spectrum and He production rate are not known.

Contributions from other mechanical factors related to washers, gaskets, O-ring, or cycling loading, including vibrations, need to be considered in evaluating stress relaxation of bolted joints.

This page is intentionally left blank.

# 6. Summary

The existing data on the effect of neutron irradiation on PWR core internal materials have been reviewed to evaluate the susceptibility of structural materials to irradiation effects such as IASCC, neutron embrittlement, void swelling, and irradiation-induced stress relaxation. The results are used to (a) define threshold fluence for irradiation effects, (b) develop disposition curves for crack growth rates for reactor core internal materials, and (c) assess the significance of void swelling and irradiation creep relaxation on the structural and functional integrity of reactor internal components.

## 6.1 Susceptibility to IASCC

A review of the literature has identified the following key material and environmental parameters that influence the susceptibility of LWR core internals materials to IASCC susceptibility.

*Microstructure*: Neutron irradiation of austenitic SSs creates point defects that rearrange into more stable configurations such as dislocation loops, network dislocations, precipitates, and cavities (or voids). Such changes in the microstructure of austenitic SSs vary with material composition, irradiation temperature, neutron fluence and flux, and energy spectrum. At temperatures below 300°C, the material microstructure primarily consists of "black spot" defect clusters and faulted dislocation loops, whereas large faulted loops, network dislocations, cavities/voids (clusters of vacancies and/or gas bubbles), and precipitates are observed above 300°C. At LWR operating temperatures (i.e., 275-300°C), the loop density saturates at a relatively low dose (about 1 dpa), and the average loop diameter saturates at 5 dpa. Alloying elements can affect the material microstructure (e.g., P, Ti, and Nb increase the loop density and decrease loop size). Cavities or voids have not been observed in SSs irradiated below 300°C.

The loop size increases and loop density decreases with increasing irradiation temperature. At temperatures of 300-350°C, the microstructure primarily consists of large Frank loops and a network of tangled dislocations. Cavities and voids form at high doses and high temperatures. High irradiation temperatures also lead to the formation of second phase particles. However, radiation-induced precipitation is not a concern at temperatures below 350°C. Metal carbides are the primary stable precipitates in 300-series SSs under LWR conditions, although RIS of Ni and Si to sinks may lead to the formation of γ' phase ($Ni_3Si$) and G phase ($M_6Ni_{16}Si_7$).

Most of the studies under LWR conditions have been conducted on BWR components such as control-rod blades or top guides irradiated at 290°C to up to 13 dpa. Studies on PWR materials such as flux thimble tubes or baffle bolts are limited, particularly on materials irradiated at 320-350°C. Additional microstructural data, including the distribution of voids/cavities and second phase particles, should be obtained on austenitic SSs irradiated in PWRs above 10 dpa and at temperatures above 300°C.

*Microchemistry*: The microchemistry of the material is also changed due to RIS. Elements such as Si, P, and possibly Ni are enriched at regions such as grain boundaries that act as sinks for point defects, while Cr, Mo, and Fe are depleted. The extent of segregation or depletion depends on the rate of generation and recombination of point defects (i.e., irradiation temperature and dose rate). Typically, RIS peaks at intermediate temperatures. It is reduced at low temperatures because of reduced mobility and at high temperatures due to back diffusion. For a given neutron dose, RIS increases at lower dose rate. At LWR temperatures, significant segregation is observed at irradiation dose of 0.1 dpa, and the effect either saturates or changes very slowly beyond ≈5 dpa. Although measurements of RIS in austenitic SSs irradiated in LWRs at temperatures above 320°C are limited, the available data indicate that Cr content at

grain boundaries can decrease to 8 wt.%, and Si and Ni contents can increase to 6 and 30 wt.%, respectively, at high dose levels. Such enrichment of Ni and Si at the grain boundaries may lead to the formation of γ' silicide or G phase.

As discussed above for material microstructure, additional studies are needed to characterize the microchemistry of austenitic SSs irradiated in PWRs above 10 dpa and at temperatures above 300°C. Also, the redistribution of S, P, C, N, and B in austenitic SSs irradiated in LWRs at dose levels above 15 dpa needs to be investigated to establish its significance on IASCC susceptibility and neutron embrittlement of SSs.

*Radiation Hardening*: The point defect clusters and precipitates act, to varying extent, as obstacles to a dislocation motion that leads to matrix strengthening, resulting in an increase in tensile strength and a reduction in ductility and fracture toughness of the material. The yield strength of irradiated SSs can increase up to 5 times that of the non-irradiated material after a neutron dose of about 5 dpa. In general, cavities (or voids) are strong barriers, large faulted Frank loops are intermediate barriers, and small loops and bubbles are weak barriers to dislocation motion. For austenitic SSs, the greatest increase in yield strength for a given irradiation level occurs at LWR operating temperatures. The change in yield strength correlates well with microstructural changes in the material. The yield strength of solution-annealed SSs saturates at 3-5 dpa. At higher neutron dose (above 3 dpa) as the yield strength approaches the ultimate strength of the material, deformation by planar slip is promoted, and the material exhibits strain softening, also termed "dislocation channeling." The enhanced planar slip leads to a pronounced degradation in the fracture toughness of austenitic SSs.

*Tensile Properties*: Irradiation at LWR operating temperatures increases the tensile strength and decreases the ductility of wrought and cast austenitic SSs and their welds. The tensile properties reach saturation at 5-20 dpa and do not seem to change significantly at higher dose levels. Uniform elongation of some LWR-irradiated SSs can decrease to 0.1% at neutron dose levels of 5-10 dpa. Correlations have been developed by MRP for estimating tensile yield and ultimate strengths and uniform and total elongation of austenitic SSs as a function of neutron dose. However, the majority of the data are for materials irradiated in a fast reactor, and data on LWR-irradiated materials are limited, in particular, above 10 dpa. The available data for the LWR-irradiated materials indicate that the yield and ultimate strengths are typically higher, and the uniform and total elongations lower, than those for materials irradiated in fast reactors. Consequently, estimates of the tensile properties of irradiated austenitic SSs based on the MRP correlations are likely to be non-conservative for LWR operating conditions.

Additional data on austenitic SSs irradiated in LWRs to dose levels above 20 dpa are needed to better define the correlations for estimating the tensile properties of these materials for LWR operating conditions. Also, the contribution of voids and second phase particles in these materials to irradiation hardening and loss of ductility should be investigated. Voids and second phase particles may not affect the tensile strength, but depending on whether they form preferentially at the grain boundaries, fracture toughness and ductility and IASCC susceptibility could be affected significantly.

*Yield Strength*: It is well known that a susceptible material, significant tensile stress, and an aggressive environment, in combination, can increase the IGSCC of austenitic SSs in BWR environments. The susceptibility to IGSCC is decreased for low-C SSs and weld metal, which are considered resistant to sensitization by welding. However, nonirradiated, nonsensitized, austenitic SSs with high tensile strength are susceptible to IGSCC in ultra-high purity water. Increases in yield strength can originate from surface or bulk cold work, weld shrinkage strain, and precipitation or irradiation hardening; all of these increase SCC susceptibility.

*Corrosion Potential*: For nonirradiated SSs, decreasing the corrosion potential from that of an NWC BWR environment to that of HWC BWR or PWR environments decreases the CGRs. Although SSs are not immune to SCC in low-potential environments, the CGRs of nonirradiated SSs and SSs irradiated to a neutron dose of less than 3 dpa are more than an order of magnitude lower in such environments than those in high-potential environments. The results also indicate that the beneficial effect of decreased corrosion potential on CGRs is lost for most SSs irradiated above 10 dpa and some heats of SSs irradiated to dose levels as low as 3-5 dpa. Furthermore, for some SSs, the benefit of reduced potential is observed at K values less than 20 MPa $m^{1/2}$ but not at higher K values.

*Silicon Segregation*: The increased susceptibility to IASCC and the loss of benefit of reducing potential in highly irradiated SSs have often been attributed to the segregation of Si at the grain boundaries. The Si segregation is detrimental because at all relevant pH/potential conditions, Si oxidizes to $SiO_2$, which is highly soluble in hot water. The possible effect of Si segregation is based on crack growth studies on CW Type 304L SS containing 3-5 wt.% Si. Unusually high CGRs were observed in these materials in high-purity water with 2000 ppb DO, and the rates did not decrease when the environment was changed from high to low potential, or K was decreased from 30 to 15 MPa $m^{1/2}$. However, in contrast to the increased susceptibility of high Si materials indicated by crack growth tests on CT specimens, SSRT test data on irradiated Type 304 and 316 SSs with 0.5 to 1.8 wt.% Si show the opposite behavior. For the same fluence level, steels with 1.5 to 1.8 wt.% Si showed less irradiation hardening and greater elongation than steels containing 0.5 wt.% Si.

The significance of Si segregation at grain boundaries on the SCC behavior of irradiated SSs is not clear, but it could be important. Crack growth tests should be conducted on irradiated material from commercial heats of SSs with similar compositions but different Si contents to establish the role of Si segregation on the IASCC susceptibility of irradiated SSs.

*Sulfur Content*: Several commercial heats of Types 304 and 316 SS with ≤0.002 wt.% S show excellent resistance to IASCC in the NWC BWR environment at neutron dose up to ≈3 dpa. At sufficiently low concentrations of S (≤0.002 wt.%), a sufficiently high concentration of C suppresses the deleterious effect of S. However, when S concentration is high (≥0.003 wt.%), the deleterious effect of S is so dominant that the effect of C is negligible or insignificant, even at high concentrations. Limited data indicate a similar behavior of the effect of S and C contents on IASCC susceptibility in the PWR environment.

*Stacking Fault Energy*: The SFE is an important parameter that determines the deformation mode. Alloys with high SFE (e.g., Ni concentration >18 wt.%) are highly resistant to IASCC compared to Type 304 SS with 8 wt.% Ni. Alloys with low SFE, such as SSs with 8 wt.% Ni, deform entirely by planar slip, whereas there is no evidence of planar slip in alloys with high SFE (with >20 wt.% Ni). The increased susceptibility to IASCC is attributed to absorption of dislocations at the grain boundaries that may cause grain boundary sliding ahead of the crack tip, resulting in crack extension and IASCC. Alternatively, progressively higher stresses at the grain boundary can change the film rupture frequency, thereby exposing bare metal surface and leading to oxidation/dissolution and crack extension. However, the role of the localized deformation mode on IASCC of austenitic SSs, and the possible contribution of SFE, should be further investigated.

*LWR vs. Fast Reactor Irradiations*: Fast reactors are an attractive alternative for irradiating materials to high dose levels because of the higher displacement rates. However, differences in the thermal- and fast-neutron spectra result in differences in microstructure and microchemistry that may not be representative of LWR irradiations. At 275-320°C, although the loop microstructure appears to be

relatively insensitive to displacement rates, the main difference in the microstructure is the presence of He bubbles and cavities in materials irradiated to high dose levels in LWRs. Also, Cr depletion and Si and Ni enrichment are less in fast reactor irradiated materials. These differences are likely to influence neutron embrittlement and IASCC susceptibility of PWR core internal materials. Caution should be exercised when using fast reactor data to determine the effects of neutron irradiation on the fracture properties of LWR core internal components.

## 6.2 IASCC Growth Rates

Irradiation-assisted SCC is a complex phenomenon. It is dependent on several parameters that interact with each other such that their effect on growth rates is not always the same. As a result of these complexities and uncertainties in experimental measurements, the SCC crack growth rate data in LWR environments show significant variability (up to 1000X), and specific effects of these parameters on growth rates cannot be accurately determined under all conditions of interest. Therefore, the SCC crack growth data have been typically screened to ensure: (a) well-characterized material, (b) test procedures that closely reproduce the loading and environmental conditions for reactor core internal components, and (c) data acquisition and analysis system that provides accurate measurements and reproducible results.

Crack growth rate data on irradiated wrought and cast austenitic SSs, as well as SS weld metal and weld HAZ materials in LWR environments, have been compiled and evaluated to define the threshold fluence for IASCC and to develop disposition curves for cyclic and IASCC growth rates for reactor core internal materials. The significance of test procedures, importance of IG starter crack and specimen K/size criterion, and effects of rising K and reloading are discussed.

Data on the SCC growth rate have been obtained for NWC and HWC BWR environments as well as the PWR environment on wrought and cast austenitic SSs and weld HAZ materials irradiated up to 38 dpa in LWRs or fast reactors. In the NWC BWR environment, neutron irradiation up to 0.45 dpa ($3 \times 10^{20}$ n/cm$^2$) has no effect on CGRs; the SCC growth rates are below the NUREG-0313 CGR disposition curve for nonirradiated materials in high-purity water containing 8 ppm DO. The CGRs in the NWC BWR environment for materials irradiated to higher neutron dose levels can be up to factor of 40 higher than the NUREG-0313 CGR disposition curve. The growth rates for some materials irradiated to 5-8 dpa (corresponding to a 60-y end-of-life neutron dose for BWRs) are a factor of 20 higher than the NUREG-0313 curve and 2-3 higher than the EPRI disposition curve for BWR core internal components. In NWC, the cracking behavior of various grades and heats of SSs irradiated to the same dose level seems to be the same. However, the rates for weld HAZ materials are slightly higher than those for solution-annealed SSs, most likely due to weld residual strains.

The CGR data for highly irradiated materials (greater than 18 dpa) show unusual behavior. For SSs irradiated in a PWR to 18 or 37.5 dpa, SCC growth rates in the NWC BWR environment are below the NUREG-0313 disposition curve for nonirradiated SSs. The reasons for the low CGRs observed for these highly irradiated BWR materials in the high-potential BWR environment are not clear. The low growth rates may be an artifact associated with the test procedure used in obtaining these results. In general, the SCC growth rate data obtained using test procedures in which the specimen was precracked in air and then transferred to the autoclave for the SCC test in the test environment show much more variability at K values of 8-15 MPa m$^{1/2}$ than the data obtained using test procedures in which the specimen was precracked in the test environment and the TG fatigue crack was transitioned to an IG crack by using slow fatigue cycling before starting the SCC test. The data on the high irradiation dose materials were obtained by a procedure that did not involve slow cycling in the environment. Also, CGRs are lower by a factor of

10 for the same heat of BWR control-rod blade material tested using a procedure that did not include slow cycling to transition the TG crack into an IG crack compared with a procedure that included slow cycling.

The SCC growth rates in the HWC BWR environment consistently show the following effects: a significant decrease in growth rates relative to those in the NWC BWR environment for SSs irradiated to less than 3 dpa. However, some heats of SSs irradiated to dose levels as low as 3-4 dpa show little or no reduction, at least at K values above 18 MPa $m^{1/2}$. No decrease has been observed for any SS irradiated to 12-14.5 dpa. The CGRs for some of the materials irradiated to 3-4 dpa are above the CGR disposition curve proposed by EPRI for the HWC BWR environment. Some investigators seem to screen out the 3-4 dpa data that do not show the benefit of the reduced corrosion potential on growth rates on the premise that they exceeded a proposed K/size criterion for irradiated materials (i.e., an irradiation-induced increase in yield stress is discounted by a factor of 2 or 3). However, the arguments against the validity of the data do not seem to have a well-developed technical basis. Additional CGR data on SSs irradiated to 3-8 dpa are needed to accurately establish the threshold for IASCC susceptibility in low-potential environments.

The results also indicate a threshold dose of $3 \times 10^{20}$ and $1.8 \times 10^{21}$ n/cm$^2$ (or 0.45 and 2.7 dpa) in the NWC and HWC environments, respectively, above which the CGRs of austenitic SSs are greater than the NUREG-0313 curve for nonirradiated materials. The CGR data on irradiated austenitic SSs have been used to develop correlations for determining the constant A1 in the CGR disposition curve as a function of neutron dose. These correlations could be used to determine the CGR disposition curve for irradiated austenitic SSs in NWC and HWC BWR environments. However, the existing database is quite limited, and additional CGR data should be obtained on SA and SMA SS welds and weld HAZ materials in BWR environments to better define the CGR disposition curve for BWRs.

For the 3-5 dpa materials, the lack of an effect of reduced corrosion potential on growth rates has often been explained on the basis of the loss of specimen constraint by exceeding the K/size criterion. However, the basis for the proposed K/size criterion for irradiated materials is not well documented. Some recent studies have shown that the ASTM E399 size criterion is not exceeded in ½-T or ¼-T CT specimens of irradiated SSs that have yield stress above 600 MPa. The loss of the beneficial effect of decreased corrosion potential in some cases may be an indication of a threshold phenomenon. For example, the loss seems to occur under conditions that result in a growth rate of about $1 \times 10^{-9}$ m/s. At this threshold growth rate, the crack tip strain rate may be influenced by an alternative mechanism that helps sustain the high growth rates, which are independent of corrosion potential. Additional data on SSs irradiated to 3-8 dpa are needed to better determine the effect of low-potential environments on the CGRs of highly irradiated materials.

The SCC growth rates have been obtained in the PWR environment at 288-340°C on austenitic SSs irradiated to 3.0-37.5 dpa in LWRs or fast reactors. The CGRs for the same material and irradiation conditions increase with increasing temperature. The temperature dependence of growth rates may be represented by an activation energy of 100 kJ/mol. In PWR water at 320°C, most of the CGR data for SSs irradiated to 3 dpa are up to a factor of 5 above, and those for SSs irradiated to 11-25 dpa are nearly two orders of magnitude above, the NUREG-0313 curve for nonirradiated materials. Also, as observed earlier in HWC BWR water tests, the CGRs in the PWR environment of SSs irradiated above 18 dpa are below the NUREG-0313 curve for nonirradiated SSs. The results also indicate that in the PWR environment at 320°C, the SCC growth rates of materials irradiated up to 12 dpa are above the EPRI disposition curve for the HWC BWR environment at 288°C.

The SCC growth rates in the PWR environment show significant variability. The reason for the high CGRs for some SSs irradiated to 11.4 dpa, as well as the unusually low CGRs in SSs irradiated to 18 and 39 dpa, is not known. The available CGR data in the PWR environment at 320°C could also be represented by the same expressions used to represent CGRs in the HWC BWR environment. Additional data on materials irradiated at different temperatures (e.g., between 300 and 350°C) are needed to better understand the IASCC susceptibility of austenitic SSs in PWR environments.

The SCC growth rate data show rapid increase in CGRs as the yield strength of the material increases from 150 to 600 MPa, and only a moderate increase at higher yield strengths. At yield strength below 800 MPa, a similar growth rate behavior is observed for different grades of SSs, although the CGRs in low-potential water are up to an order of magnitude lower. Also, in a high-potential environment, the CGRs of sensitized materials are higher than those for nonsensitized materials. However, at yield strengths of 800 MPa or higher, the CGRs in low- and high-potential environments are comparable. The significance of material yield strength on IASCC susceptibility is not well established and should be further investigated, particularly in the PWR environment.

## 6.3 Fatigue Crack Growth Rates

The limited fatigue CGR data in air on austenitic SSs irradiated to 2 dpa indicate little or no effect of neutron irradiation on growth rates. Additional data on austenitic SSs irradiated to higher neutron doses have been obtained on materials irradiated in fast reactors at 400-482°C. The results at 427°C show only slightly higher CGRs (up to a factor of 2 higher) for $\Delta K$ less than 44 MPa $m^{1/2}$ (40 ksi $in.^{1/2}$). Also, tests on Type 304 and 316 SS irradiated in a thermal reactor at 288°C to 2.7 dpa and tested at 427°C exhibited no significant adverse effects of irradiation on crack growth rate. In fact, the crack growth rates of the irradiated materials were actually 25 to 50% lower than those for the same heats of nonirradiated 304 and 316 SS materials.

Fatigue CGRs have been obtained in NWC and HWC BWR environments on wrought and cast austenitic SSs and weld HAZ materials irradiated up to 3 dpa. In the NWC BWR environment, the cyclic CGRs of SSs irradiated to 0.45 dpa ($3 \times 10^{20}$ n/cm$^2$) are the same as those for nonirradiated materials, whereas the CGRs of SSs irradiated to 0.75-3.0 dpa are higher. Limited data indicate that the growth rates of irradiated CF-8M cast SS are lower than those of wrought materials irradiated to the same neutron dose. The cyclic CGRs at low frequencies are decreased by more than an order of magnitude when the DO level is decreased by changing from NWC to HWC. A superposition model has been used to represent the cyclic CGRs of austenitic SSs. The CGR in the test environment is expressed as the superposition of the rate in air (mechanical fatigue) and the rates due to corrosion fatigue and SCC. The calculated results indicate that the higher fatigue CGRs for the irradiated materials are primarily due to the SCC component of crack growth. The correlations for the various material and environmental conditions are listed in Table 5. The fatigue CGRs for irradiated SSs in the NWC BWR environment can be described by superposition of the Shack/Kassner model for nonirradiated SSs in high-purity water with 8 ppm DO and by the SCC curve for irradiated SSs. Note that although irradiation had no significant effect on fatigue CGRs in air, both fatigue and SCC growth rates for austenitic SSs irradiated above 0.45 dpa are higher than those for nonirradiated SSs or SSs irradiated below 0.45 dpa.

Fatigue CGR data on wrought and cast austenitic SSs and their welds irradiated in LWRs to high neutron dose levels and tested in BWR or PWR environments are not available. Additional fatigue crack growth data under these material and environmental conditions are needed to develop fatigue CGR correlations for BWR and PWR core internal components. The new reactor designs minimize use of cast austenitic SSs for reactor core internal components to avoid loss of toughness due to thermal aging effects

and difficulties encountered in performing nondestructive examination of cast SSs and their welds. However, such information would be used to address the license renewal issues for operating reactors.

Table 5. Fatigue CGR correlations for wrought and cast austenitic stainless steels in BWR environments at 289°C.

| CGR (m/s) | Correlations | Material & Environmental Conditions |
|---|---|---|
| $CGR_{air}$ | $CGR_{air} = da/dt_{air} = C_{SS}\,S(R)\Delta K^{3.3}/t_{rise}$<br>$C_{SS} = 1.9142x10^{-12} + 6.7911x10^{-15}T - 1.6638x10^{-17}T^2 + 3.9616x10^{-20}T^3$<br>$S(R) = 1.0$ $R < 0$<br>$S(R) = 1.0 + 1.8R$ $0 < R < 0.79$<br>$S(R) = -43.35 + 57.97R$ $0.79 < R < 1.0$ | Nonirradiated or irradiated |
| $CGR_{CF}$ | | Nonirradiated and irradiated <0.45 dpa |
| | $CGR_{CF} = 4.5x10^{-5}(CGR_{air})^{0.5}$ | 0.3 ppm DO |
| | $CGR_{CF} = 1.5x10^{-4}(CGR_{air})^{0.5}$ | 8.0 ppm DO |
| | | Irradiated >0.5 & ≤3.0 dpa |
| | $CGR_{CF} = 1.5x10^{-4}(CGR_{air})^{0.5}$ | 0.2 - 0.5 ppm DO[a] |
| $CGR_{SCC}$ | | Nonirradiated and irradiated <0.45 dpa |
| | $CGR_{SCC} = 2.1x10^{-13}(K)^{2.161}$ | 8.0 ppm DO |
| | $CGR_{SCC} = 7.0x10^{-14}(K)^{2.161}$ | 0.2 ppm DO |
| | | Irradiated >0.45 dpa & ≤12 dpa |
| | $CGR_{SCC} = \left[1.21x10^{-12} + 2.65x10^{-12}\log(dpa)\right](K)^{2.161}$ | Normal water chemistry BWR |
| | $CGR_{SCC} = \left[2.76x10^{-12} + 6.82x10^{-12}\log(dpa)\right](K)^{2.161}$ | Hydrogen water chemistry BWR |

[a]Correlation may yield conservative estimates of CGR for cast austenitic SSs and low-C Type 304L SS weld HAZ materials.

## 6.4 IASCC Initiation

All wrought and cast austenitic SSs and their welds, irradiated below a threshold neutron fluence are considered not susceptible to IASCC in a PWR environment. Based on laboratory SSRT data and PWR operating experience, a threshold fluence of $2 \times 10^{21}$ n/cm$^2$ (3 dpa) has been proposed. For materials irradiated above this threshold, IASCC initiation data have been used to define for a given neutron dose, an apparent stress threshold below which IASCC initiation will not occur in a PWR environment. The existing IASCC initiation data have been reviewed to evaluate the adequacy of the database for developing screening criteria for the IASCC susceptibility of PWR core internal components. The following conclusions are reached:

1. Most of the IASCC data have been obtained on CW Type 316 SS, while data on solution-annealed Type 304, 304L, or 316 SS are limited. Also, there are no data on cast austenitic SSs, SS welds, and weld HAZ materials.

2. Although a threshold fluence of 3 dpa has been defined for IASCC in the PWR environment, no IASCC initiation data are available on austenitic SSs irradiated between 3 and 9.5 dpa.

3. Nearly all of the high fluence (>20 dpa) data and the majority of the low fluence data are for materials irradiated below 325°C and, therefore, do not include the potential effects of additional precipitate phases, voids/cavities, and He generation rate on IASCC.

4. In reactor core internal components, IASCC is likely to occur under creviced conditions. Nearly all of the IASCC initiation tests have been conducted in the normal PWR environment

5. Several studies indicate that materials irradiated in fast reactors show lower susceptibility to IASCC than those irradiated in LWRs. The current IASCC initiation database, however, includes some tests on austenitic SS irradiated in the BOR-60 fast reactor.

## 6.5 Neutron Embrittlement

The fracture toughness of austenitic SSs has been divided into three broad categories. Category III materials with $J_{Ic}$ >150 kJ/cm$^2$ fracture after stable crack extension at stresses well above the yield stress. Category II materials with $J_{Ic}$ of 30-150 kJ/cm$^2$ fracture at stress levels close to the yield stress by stable or unstable crack extension. Category I materials with $K_{Ic}$ <75 MPa m$^{1/2}$ fracture at stress levels well below the yield stress by unstable crack extension. Nonirradiated wrought and cast austenitic SSs and their welds fall in Category III. The fracture toughness of cast austenitic SSs and SA and SMA welds is generally lower than that of the wrought SSs. Neutron irradiation can degrade fracture toughness of austenitic SSs to the level of Category II or I.

Fracture toughness data on irradiated wrought and cast austenitic SSs and their welds have been compiled and evaluated to define the threshold neutron dose above which the fracture toughness of these materials is reduced significantly. Fracture toughness is typically characterized by the initiation toughness $J_{Ic}$ and tearing modulus for materials that fail after substantial plastic deformation (EPFM analysis) and by the critical stress intensity factor $K_{Ic}$ for materials that fail after little or no deformation (LEFM analysis). To reduce activity and facilitate handling, small specimens have been used in most studies. The validity of the J-R curve data and the different methods for determining $J_{Ic}$ is discussed. The fracture toughness data obtained on different size specimens show that small specimens yield valid J-R curve data, at least for materials with $J_{Ic}$ below 300 kJ/m$^{1/2}$.

Until recently, most published experimental data on the neutron embrittlement of austenitic SSs were obtained on materials irradiated at 350-427°C in high-flux fast reactors and tested at 300-427°C. The effects of fast reactor irradiation are divided into three regimes: little or no loss of toughness below an exposure of ≈1 dpa, substantial and rapid decrease in toughness at exposures of 1-10 dpa, and no further reduction in toughness above a saturation exposure of 10 dpa. The degradation in fracture properties saturates at a $J_{Ic}$ value of ≈30 kJ/m$^2$ or an equivalent $K_{Jc}$ of 75 MPa m$^{1/2}$ (68.2 ksi in.$^{1/2}$). The fracture toughness trend for the LWR data is similar to that observed for fast reactor data. However, the tensile property data discussed in Section 2.1.4 indicate that tensile strength is higher and ductility is lower for the LWR-irradiated materials than those for materials irradiated in fast reactors. Additional fracture toughness data obtained on austenitic SS, preferably the same heat of material, irradiated under comparable conditions in fast and thermal reactors are needed to determine the applicability of fast reactor data to LWR irradiation conditions.

Most of the J-R curve data on LWR-irradiated austenitic SSs have been obtained on Type 304 and 304L SSs, and similar data on SS welds, cast SSs, or weld HAZ materials are limited. The available data indicate minor differences in the fracture toughness of the various wrought and cast austenitic SS materials. For the same irradiation conditions, the fracture toughness of thermally aged cast SS and weld

metal is lower than that of HAZ material, which, in turn, is lower than that of solution-annealed materials. Available data indicate a strong orientation effect on fracture toughness. Tests performed on Type 304 or 304L SS irradiated to 4-12 dpa in BWRs consistently show lower fracture toughness in the T-L than in the L-T orientation. Some SSs irradiated above 4 dpa in BWRs show $K_{Ic}$ or $K_{Jc}$ values in the range of 36.8-40.3 MPa $m^{1/2}$ (33.5-36.6 ksi $in^{1/2}$). Several J-R curve tests on Type 304 SS control-rod blade material irradiated to 4.5-5.5 dpa showed no ductile crack extension.

Fracture toughness J-R curve tests have also been conducted in a BWR NWC environment to investigate the possible effects of the coolant environment and crack morphology on fracture toughness. Nearly all of the existing fracture toughness data have been obtained from tests in air and on specimens that were fatigued to produce a crack that has TG morphology. In reactor core components, cracks initiate primarily by SCC and have IG morphology. Limited data suggest that the BWR environment has little or no effect on materials with poor fracture toughness, whereas materials with relatively high fracture toughness may be decreased in the test environment. In particular, the effect of environment on the fracture toughness of cast SS and welds should be investigated.

The available data are inadequate to establish accurately the effects of the irradiation temperature on the fracture toughness of austenitic SSs. However, tensile data for austenitic SSs indicate that irradiation hardening is the highest, and ductility loss is maximum, at an irradiation temperature of ≈300°C (≈572°F). Additional data should be obtained on austenitic SSs irradiated to similar dose levels at temperatures between 290 and 340°C to establish the effects of the irradiation temperature.

The material fracture toughness can vary with test temperature. In general, the fracture toughness of nonirradiated austenitic SSs is known to decrease as the test temperature is increased. The fracture toughness of steels irradiated to relatively low dose (less than 5 dpa) shows the same trend. However, for steels irradiated to more than 12 dpa, test temperature has little effect on fracture toughness.

The existing fracture toughness data have been used to develop a fracture toughness trend curve that includes (a) a threshold neutron exposure for radiation embrittlement of austenitic SSs and a minimum fracture toughness for these materials irradiated to less than the threshold value, (b) a saturation neutron exposure and a saturation fracture toughness for materials irradiated to greater than this value, and (c) a description of the change in fracture toughness between the threshold and saturation neutron exposures. These trend curves describe the change in either $J_{Ic}$ or the coefficient C of the power-law J-R curve as a function of neutron dose (Eqs. 23 and 25, respectively). The results indicate that the saturation fracture toughness proposed by MRP for PWRs is consistent with the existing data. However, the saturation fracture toughness proposed by EPRI for BWR internal materials irradiated above 4.5 dpa is higher than that observed for several materials irradiated to 4.5-8.5 dpa.

A review of the existing data indicated the following: (a) limited data on materials irradiated in LWRs to neutron dose levels of 0.1-1.0 dpa or above 10 dpa, and (b) little or no data on LWR-irradiated cast austenitic SSs and welds. As discussed in Section 6.3, the new reactor designs minimize use of cast austenitic SSs for reactor core internal components. However, this information would be used to address license renewal issues for operating reactors. Also, a fine distribution of γ' phase is often associated with BWR-irradiated materials with poor fracture toughness. The contribution of additional precipitate phases, voids, and cavities on the fracture toughness of these materials needs to be investigated.

## 6.6 Synergistic Effects of Thermal and Neutron Embrittlement

Cast and welded austenitic SSs have a duplex structure consisting of austenite and ferrite phases. Formation of Cr-rich $\alpha'$ phase in the ferrite is the primary mechanism for thermal embrittlement of these materials; thermal aging has no effect on the austenite phase. Embrittlement of the austenite phase from neutron irradiation under LWR operating conditions occurs at dose levels above 0.5 dpa, and that of the ferrite phase occurs at lower dose levels (above 0.07 dpa). However, for reactor core internal components, concurrent exposure to neutron irradiation could result in a synergistic effect wherein the service-degraded fracture toughness can be less than that predicted for either thermal embrittlement or neutron irradiation embrittlement independently.

The screening criteria are discussed for thermal-aging susceptibility of cast austenitic SSs and estimates of the saturation J-R curve for specific grades of cast SSs as well as for aged SS welds. A methodology is also presented for determining the threshold neutron dose for irradiation embrittlement of wrought and cast austenitic SSs and welds. The available fracture toughness data indicate a threshold dose of about 0.3 dpa for these materials. However, the data are inadequate to evaluate the synergistic effects of thermal and neutron embrittlement on the threshold dose for embrittlement. Additional fracture toughness data are needed to better establish the potential for synergistic loss of toughness in these materials in the transition dose range from 0.05 to 2 dpa.

## 6.7 Void Swelling

Void swelling refers to the volume change of materials under neutron irradiations. Voids form in the material when vacancies produced by the displacements migrate and accumulate to form small cavities, which eventually grow to large sizes. The fundamental driving force of void formation, however, remains the excess vacancy flux toward voids. Most of the void swelling data have been obtained from materials irradiated in fast breeder reactors at temperature above 385°C (725°F) and at dose rates that are orders of magnitude higher than those in PWRs. Therefore, caution should be exercised in extrapolation of the fast reactor data to estimate the void swelling behavior for PWR end-of-life or extended life conditions.

Void swelling is divided into two regimes: a transient regime followed by a steady-state swelling rate. All materials are believed to reach a steady-state swelling rate of ~1%/dpa. The time to reach the steady-state rate (i.e., the transient regime) depends on the material composition and thermo-mechanical condition, stress state, neutron flux and spectrum, and irradiation temperature (above 300°C). The existing data were reviewed to assess void swelling in PWR core internal components and to evaluate the effects of key material and environmental parameters.

Reactor core internal components are primarily constructed of austenitic SSs and some of Ni alloys, both of which have a face-centered cubic crystal structure. These materials are more susceptible to void swelling than ferritic steels, which have a body-centered cubic crystal structure. The material composition can influence void swelling, in particular, the Ni content. In the 300-series SSs, void swelling decreases with increasing Ni content. Increases in the Si and P contents also decrease swelling. Thus, under similar thermal-mechanical conditions, Type 304 SS typically swells more than Type 316 SS. However, radiation-induced precipitation of second phase particles can remove Ni, P, and Si from the alloy matrix, and thereby increase void swelling. In addition, cold work prolongs the transient regime for void swelling in austenitic SSs. The high dislocation density produced by the cold work provides additional recombination sites for vacancies and interstitials, thereby decreasing supersaturation of vacancies in the material, which retards void nucleation.

Void swelling in the 300-series austenitic SSs is typically observed at irradiation temperatures above 340°C (644°F), and shows a strong dependence on temperature. However, the low temperatures typical of LWRs extend the transient regime to much longer times and result in the formation of a higher density of smaller voids. Nonetheless, depending on the irradiation temperature, dose, and dose rate, voids can form under PWR operating conditions within the reactor lifetime. The displacement rate also influences void swelling; swelling increases as the displacement rate is decreased. Available data obtained in fast reactors at 373-444°C and displacement rates of 0.3-10.0 x $10^{-7}$ dpa/s suggest that under comparable irradiation temperatures and neutron dose levels, the lower displacement rates typical of PWRs would result in higher swelling.

Applied or swelling-induced stress, irrespective of whether it is tensile or compressive, accelerates void swelling. These stresses, however, are limited by irradiation creep relaxation. Therefore, the interaction of swelling and irradiation creep relaxation plays an important role in evaluation of swelling in PWR core internal components. Another stress-related effect is that a high swelling region produces stresses in the adjacent lower swelling region, forcing it to try to catch up. Thus, estimates of swelling based on stress-free material tend to overestimate the swelling gradients in a component.

Most of the void swelling data have been obtained on materials irradiated in fast reactors at temperatures and dose rates that are higher than those typical for LWRs. Also, data on PWR-irradiated materials and on CW Type 316 SS are limited. It is important to develop a technical basis for extrapolating the fast reactor data and the limited PWR data to predict void swelling in PWR core internal components. Although a reasonable extrapolation of these results suggests that void swelling will not be a significant problem during the first license extension period, the effects of irradiation temperature (particularly above 370°C), displacement rate, and stress on void swelling, including the interaction of swelling and irradiation creep relaxation, should be investigated.

Stress-free swelling equations, including stress-enhanced swelling, have been developed by the MRP for solution-annealed Type 304 and CW Type 316 SSs. These equations correlate the swelling rate in PWR core internal components with irradiation temperature, neutron dose, and dose rate.

Embrittlement of SS materials due to voids is also discussed. Typically, austenitic SSs irradiated at ≤400°C to neutron dose levels to produce ≥10% void swelling suffer from severe embrittlement, particularly at room temperature. This behavior has been attributed to a second-order process, which involves stress concentration between voids, Ni segregation at void surfaces, and a resultant tendency toward martensite formation when the steel is deformed at room temperature. At room temperature, the austenite/martensite boundaries provide a low-energy crack propagation path, resulting in a brittle quasi-cleavage fracture. At higher temperatures, the effect of Ni segregation on SFE is much less pronounced, and failure occurs along flow localization path, referred to as channel fracture. However, few quantitative data correlate void swelling with fracture toughness of the material. A heat of SS irradiated in the FFTF at 390°C (734°F) to 114 dpa showed $K_{Ic}$ of 30 MPa $m^{1/2}$ at 410°C. This value is slightly lower than the saturation $K_{Ic}$ of 38 MPa $m^{1/2}$ for several SSs irradiated in BWRs to 5-8 dpa. However, these results suggest that the fracture toughness of PWR core internal SS components could be lower than the saturation value ($K_{Ic}$=38 MPa $m^{1/2}$) proposed by MRP. The embrittlement of austenitic SSs due to void swelling under PWR irradiation conditions should be further investigated.

## 6.8 Irradiation Creep Relaxation

Loss of preload for bolting and springs due to stress relaxation is another aging degradation effect that needs to be addressed to assure the functional integrity of the reactor core internal components.

Stress relaxation represents plastic deformation that occurs under constant strain below the yield point of the material. It is caused by either primary creep (thermal stress relaxation) or a flux of high-energy neutrons (irradiation creep). Thermal stress relaxation data have been obtained from short-term tests (less than 1000 h). At PWR operating temperatures, stress relaxation saturates within 100 h with a maximum decrease of 10-20% of the initial preload stress. The extent of relaxation depended on thermal-mechanical treatment of the material; it increased with increasing initial stress and saturated at about 207 MPa (30 ksi). For PWRs, plastic strains resulting from thermal stress relaxation were considered to be insignificant and not a concern for the dimensional change of core internal components. Although steady-state creep is insignificant at PWR operating temperatures, over the reactor lifetime it could lead to appreciable stress relaxation not anticipated in the short-term tests.

However, neutron-irradiation-enhanced creep at PWR temperatures can greatly increase the plastic strain by increasing both the transient creep and steady-state creep rates. The magnitude of transient creep and steady-state creep is essentially proportional to the applied stress level. Transient creep is typically short and, although its magnitude depends on material condition and structure and irradiation temperature, the contribution to total creep strain is relatively small; the steady-state creep rate is independent of these parameters. Empirical models have been developed for irradiation creep using data obtained from fast reactors. The results have been used to develop an expression for estimating stress relaxation as a function of initial stress and neutron dose.

# 7. Gaps in Available Data

## 1. Applicability of Fast Reactor Data to LWRs

The following subtopics are related to the applicability of fast reactor data to LWRs.

### *1a. Material Microstructure and Microchemistry*

A large fraction of the high neutron dose data has been obtained on materials irradiated in fast reactors. Therefore, possible differences in material microstructure and microchemistry due to higher dose rates and differences in the thermal- and fast-neutron spectra need to be examined. A significant difference between the two is the presence of He bubbles and cavities in materials irradiated to high dose levels under LWR irradiation conditions. Also, data on material microchemistry indicate that RIS in the fast reactor irradiated materials may not be representative of LWR irradiation conditions; Cr depletion and Ni and Si enrichment are less in the fast-reactor-irradiated materials. These differences are likely to influence neutron embrittlement and IASCC susceptibility of LWR core internal materials. Additional studies are needed to validate the applicability of fast reactor data to LWRs.

### *1b. Irradiation Hardening and Tensile Properties*

Correlations have been developed by industry for estimating tensile yield and ultimate strengths and uniform and total elongation of austenitic SSs as a function of neutron dose. However, most data have been obtained on materials irradiated in a fast reactor and data on LWR-irradiated materials are limited, in particular above 10 dpa. Additional data on austenitic SSs irradiated in LWRs to dose levels above 20 dpa are needed to better define the correlations for estimating the tensile properties of these materials for LWR operating conditions. Also, the influence of voids and second phase particles on irradiation hardening and loss of ductility should be investigated.

### *1c. Fracture Toughness Database for Irradiated LWR Core Internal Materials*

Although the general trends for the fracture toughness data for austenitic SSs appear to be similar for fast reactor and LWR irradiations, the significant differences in irradiation hardening and tensile properties indicate the need for fracture toughness data on materials irradiated in LWRs. A review of the existing fracture toughness database indicated the following: (a) limited data on materials irradiated in LWRs to neutron dose levels of 0.1-1.0 dpa or above 10 dpa, and (b) little or no data on LWR-irradiated cast austenitic SSs and welds. Also, the contribution of additional precipitate phases, voids, and cavities on the fracture toughness of these materials needs to be investigated.

### *1d. Void Swelling*

Most of the void swelling data have been obtained on materials irradiated in fast reactors at temperatures and dose rates that are higher than those typical for LWRs. Data on PWR-irradiated materials are limited, and predominantly on CW Type 316 SS. To develop a technical basis for extrapolating the fast reactor data and the limited PWR data to predict void swelling in PWR core internal components, additional void swelling data should be obtained to establish the effects of irradiation temperature (particularly above 370°C), displacement rate, and stress on void swelling.

### *1e. Irradiation Creep Relaxation*

Most of the existing data on irradiation-enhanced stress relaxation/irradiation creep have been from fast reactor irradiations, and data under PWR irradiation conditions are limited. Therefore, the effects of neutron spectrum and He production rate, are not known.

## 2. Microstructure and Microchemistry Characterization of PWR-Irradiated Materials

Most of the studies on characterization of the microstructure and microchemistry of irradiated austenitic SSs have been on BWR components such as control-rod blades or top guides irradiated at 290°C up to 13 dpa. Studies on PWR materials such as flux thimble tube or baffle bolts are limited, particularly on materials irradiated at 320-350°C. Additional microstructural and microchemistry data, including the distribution of voids/cavities and second phase particles, should be obtained on austenitic SSs irradiated in PWRs to neutron dose levels above 10 dpa and at temperatures above 300°C. Also, the redistribution of S, P, C, N, and B in austenitic SSs irradiated in LWRs at dose levels above 15 dpa needs to be investigated to establish its significance on IASCC susceptibility and neutron embrittlement of SSs.

## 3. Effect of Si Segregation on IASCC Susceptibility

The increased susceptibility to IASCC and the loss of benefit of reduced corrosion potential on IASCC susceptibility in highly irradiated SSs have often been attributed to the segregation of Si at the grain boundaries. However, this proposition is based on data for nonirradiated cold-worked materials. The significance of Si segregation at grain boundaries on the SCC behavior of irradiated SSs is not clear, but it could be important. Crack growth tests should be conducted on irradiated material from commercial heats of SSs with similar compositions but different Si contents to establish the role of Si segregation on the IASCC susceptibility of irradiated SSs.

## 4. Validity of Proposed K/Size Criteria

The existing data suggest that some SSs may show IASCC susceptibility in low-potential environments at fluence levels as low as 3 dpa. However, such data are often screened out simply because they do not agree with the current expectations for the IASCC behavior of austenitic SSs. The justification is that the applied K for these tests may have exceeded the K/size criteria that have been proposed for irradiated austenitic SSs to account for strain softening in the material. These proposed K/size criteria could be validated experimentally by using different size specimens. Such an approach would be extremely difficult for irradiated materials, but more rigorous finite element studies of crack tip behavior may be helpful in developing appropriate validity criteria. In any case, the potentially conflicting results currently available indicate that additional data on SSs irradiated to 3-8 dpa are needed to accurately establish the threshold for IASCC susceptibility in low-potential PWR environments.

## 5. IASCC Crack Growth Rate Disposition Curve for PWR Core Internals

The available crack growth data on irradiated austenitic SSs in the PWR environment show significant variability. Also, crack growth data on austenitic SSs irradiated above 12 dpa have been obtained on materials that were either from a decommissioned PWR or were irradiated in the BOR-60 fast reactor. The SCC growth rate tests on the PWR-irradiated material show anomalous results (i.e., the CGRs on material irradiated to 18 or 38 dpa are lower than the growth rates for nonirradiated material). Additional data on austenitic SSs, including SS welds and weld HAZ materials, irradiated in LWRs at 300-350°C, should be obtained in PWR environments to better define a CGR disposition curve for PWRs.

## 6. Fatigue Crack Growth Rates

The available fatigue crack growth data for irradiated austenitic SSs are limited to materials irradiated under BWR operating conditions to neutron doses up to 3 dpa. Additional fatigue crack growth data on irradiated wrought and cast austenitic SSs and their welds in BWR and PWR environments are needed to develop fatigue CGR correlations for LWR core internal components.

## 7. IASCC Initiation

The screening criteria used to disposition various PWR core internal components into different categories for aging management strategies define for a given neutron fluence above a threshold value (i.e., 3 dpa) an apparent stress threshold below which IASCC will not occur in a PWR environment. The fluence threshold of 3 dpa is based on incidents of IASCC failures in operating PWRs and on SSRT test results in a PWR environment. The stress thresholds are based upon the IASCC initiation data. However, the database used for defining neutron dose/applied stress thresholds for austenitic SSs is inadequate to evaluate the variability between different grades of SSs, or the differences between solution-annealed or cold-worked material, or the effect of irradiation temperature. Most of the data are on cold-worked Type 316 SS irradiated at temperatures below 310°C. Also, although the fluence threshold for IASCC is defined as 3 dpa, there are no IASCC initiation data on materials irradiated below 10 dpa. Furthermore, in reactor core internal components, IASCC is likely to occur under creviced conditions (i.e., under off-normal water chemistry). The variability and uncertainties due to these factors need to be addressed in developing threshold and screening criteria for IASCC in reactor core internal materials. Additional data should be obtained to determine the possible effects of material condition and composition, irradiation temperature, water chemistry, and neutron fluence below 10 dpa on IASCC initiation in a PWR environment.

## 8. Effect of Irradiation Temperature on Fracture Toughness

The tensile data for austenitic SSs indicate that irradiation hardening is the highest, and ductility loss is maximum, at an irradiation temperature of ≈300°C (≈572°F). However, the existing data are inadequate to establish accurately the effects of the irradiation temperature on the fracture toughness of austenitic SSs. Additional data should be obtained on austenitic SSs irradiated to similar dose levels at temperatures between 290 and 340°C to establish the effects of the irradiation temperature.

## 9. Lower Bound Fracture Toughness of Irradiated Austenitic Stainless Steels

The existing data indicate a strong orientation effect on fracture toughness. Tests performed on Type 304 or 304L SS irradiated to 4-12 dpa in BWRs consistently show lower fracture toughness in the T-L than in the L-T orientation. In addition, some SSs irradiated above 4 dpa in BWRs show poor fracture toughness; the $K_{Ic}$ is 36.8-40.3 MPa $m^{1/2}$. Several J-R curve tests on Type 304 SS control-rod blade materials irradiated to 4.5-5.5 dpa showed no ductile crack extension. The lower bound fracture toughness curve proposed by industry for BWR and PWR core internal components does not consider this data. The lower bound curve should be updated to include these results.

## 10. Void Swelling and its effect on Fracture Toughness

Most of the void swelling data have been obtained on materials irradiated in fast reactors, and data on PWR-irradiated matereials are quite limited. Additional void swelling data on PWR-irradiated materials should be obtained to establish the effects of irradiation temperature, diaplacement rate, and

stress on void swelling. In addition, austenitic SSs with ≥10% void swelling suffer from severe embrittlement. There are few quantitative data correlating void swelling with fracture toughness of the material. Limited data indicate $K_{Ic}$ values that are slightly lower than the saturation value of 38 MPa $m^{1/2}$ proposed by the MRP for austenitic SSs irradiated to a very high neutron dose in PWRs. However, these results indicate the importance of void swelling on fracture toughness. The embrittlement of austenitic SSs due to void swelling under PWR irradiation conditions should be further investigated

## 11. Effect of Coolant Environment on Fracture Toughness

Limited data suggest a possible effect of reactor coolant environment and crack morphology on the fracture of LWR structural materials. Nearly all fracture toughness tests are conducted on specimens containing a TG fatigue crack, whereas core internal components are likely to be IG SCC cracks. Fracture toughness J-R curve data should be obtained in LWR environments to evaluate the possible effects of coolant environment, in particular, for cast austenitic SSs and SS welds.

The priorities for addressing the various data gaps in the current understanding of irradiation effects on LWR core internal materials are assessed based on the effect of these knowledge gaps on the following criteria:

1. The basic mechanism of the degradation process,

2. The application and use of these materials for LWR core internal components, and

3. The performance of the component as the material ages.

Based on these criteria, the assessed priorities are given in Table 6.

Table 6. Data gaps in the current understanding of irradiation effects on LWR core internal materials.

| Item | Description | Priority |
|---|---|---|
| 1 | Applicability of fast reactor data to LWRs | |
| | a. Material microstructure and microchemistry | M |
| | b. Irradiation hardening and tensile properties | M |
| | c. Fracture toughness database for irradiated LWR core internal materials | H |
| | d. Void swelling | L |
| | e. Irradiation creep relaxation | L |
| 2 | Microstructure and microchemistry characterization of PWR-irradiated material | M |
| 3 | Effect of Si segregation on IASCC susceptibility | L |
| 4 | Validity of proposed K/size criterion | H |
| 5 | IASCC crack growth rate disposition curve for PWR core internals | H |
| 6 | Fatigue crack growth rates | M |
| 7 | IASCC initiation | H |
| 8 | Effect of irradiation temperature on fracture toughness | H |
| 9 | Lower bound fracture toughness of irradiated austenitic stainless steels | H |
| 10 | Embrittlement due to void swelling | M |
| 11 | Effect of coolant environment on fracture toughness | L |

Priority: H → high, M → medium, and L → low

## References


1. Bruemmer, S. M., et al., "Critical Issue Reviews for the Understanding and Evaluation of Irradiation-Assisted Stress Corrosion Cracking," EPRI TR-107159, Electric Power Research Institute, Palo Alto, CA, 1996.

2. Scott, P., "A Review of Irradiation Assisted Stress Corrosion Cracking," J. Nucl. Mater. **211**, 101-122, 1994.

3. Was, G. S., and P. L. Andresen, "Stress Corrosion Cracking Behavior of Alloys in Aggressive Nuclear Reactor Core Environments," Corrosion **63**, 19-45, 2007.

4. Bruemmer, S. M., E. P. Simonen, P. M. Scott, P. L. Andresen, G. S. Was, and J. L. Nelson, "Radiation-Induced Material Changes and Susceptibility to Intergranular Failure of Light-Water-Reactor Core Internals," J. Nucl. Mater. **274**, 299-314, 1999.

5. Herrera, M. L., et al., "Evaluation of the Effects of Irradiation on the Fracture Toughness of BWR Internal Components," Proc. ASME/JSME 4th Intl. Conf. on Nucl. Eng. (ICONE-4), Vol. 5, A. S. Rao, R. M. Duffey, and D. Elias, eds., American Society of Mechanical Engineers, New York, pp. 245-251, 1996.

6. Mills, W. J., "Fracture Toughness of Type 304 and 316 Stainless Steels and Their Welds," Intl. Mater. Rev. **42**, 45-82, 1997.

7. Kanasaki, H., I. Satoh, M. Koyama, T. Okubo, T. R. Mager, and R. G. Lott, "Fatigue and Stress Corrosion Cracking Behaviors of Irradiated Stainless Steels in PWR Primary Water," Proc. 5th Intl. Conf. on Nuclear Engineering, ICONE5-2372, pp. 1-7, 1997.

8. Chopra, O. K., E. E. Gruber, and W. J. Shack, "Fracture Toughness of Irradiated Wrought and Cast Austenitic Stainless Steels in BWR Environment," Proc. 13th Intl. Conf. on Environmental Degradation of Materials in Nuclear Power Systems - Water Reactors, T. R. Allen, P. J. King, and L. Nelson, eds., Canadian Nuclear Society, Toronto, Canada, Paper No. 115, 2007.

9. Chopra, O. K., E. E. Gruber, and W. J. Shack, "Fracture Toughness and Crack Growth Rates of Irradiated Austenitic Stainless Steels," NUREG/CR-6826, ANL-03/22, 2003.

10. Chopra, O. K., B. Alexandreanu, E. E. Gruber, R. S. Daum, and W. J. Shack, "Crack Growth Rates of Irradiated Austenitic Stainless Steel Weld Heat Affected Zone in BWR Environments," NUREG/CR-6891, ANL-04/20, 2006.

11. Chopra, O. K., and W. J. Shack, "Crack Growth Rates and Fracture Toughness of Irradiated Austenitic Stainless Steels in BWR Environments," NUREG/CR-6960, ANL-06/58, March 2008.

12. Chopra, O. K., E. E. Gruber, and W. J. Shack, "Crack Growth Rates of Irradiated Austenitic Stainless Steels in BWR Environments at 289°C," Proc. of the 2007 ASME Pressure Vessels and Piping Divisions Conf., San Antonio, TX, July 22-26, 2007, Paper No. PVP2007-26659, 2007.

13. Chopra, O. K., B. Alexandreanu, E. E. Gruber, and W. J. Shack, "Crack Growth Behavior of Irradiated Austenitic Stainless Steel Weld Heat Affected Zone Material in High-Purity Water at 289°C," Proc. 12th Intl. Conf. on Environmental Degradation of Materials in Nuclear Power Systems - Water Reactors, T. R. Allen, P. J. King, and L. Nelson, eds., Minerals, Metals & Materials Society, Warrendale, PA, pp. 289-298, 2005.

14. Andresen, P. L., F. P. Ford, S. M. Murphy, and J. M. Perks, "State of Knowledge of Radiation Effects on Environmental Cracking in Light Water Reactor Core Materials," Proc. 4th Intl. Symp. on Environmental Degradation of Materials in Nuclear Power Systems - Water Reactors, NACE, Houston, TX, pp. 1.83-1.121, 1990.

15. Andresen, P. L., "Similarity of Cold Work and Radiation Hardening in Enhancing Yield Strength and SCC Growth of Stainless Steel in Hot Water," Corrosion/02, NACE, Houston, TX, Paper No. 02509, 2002.

16. Jenssen, A., and L. G. Ljungberg, "Irradiation Assisted Stress Corrosion Cracking of Stainless Alloys in BWR Normal Water Chemistry and Hydrogen Water Chemistry," Proc. Sixth Intl. Symp. on Environmental Degradation of Materials in Nuclear Power Systems - Water Reactor, R. E. Gold and E. P. Simonen, eds., Minerals, Metals & Materials Society, Warrendale, PA, pp. 547-553, 1993.

17. Garner, F. A., "Irradiation Performance of Cladding and Structural Steels in Liquid Metal Reactors," in Materials Science and Technology: A Comprehensive Treatment, Vol. 10A, VCH Publishers, pp. 419-543, 1994.

18. Byrne, S., F. A. Garner, S. Fyfitch, and I. L. Wilson, "Application of Void Swelling Data to Evaluation of Pressurized Water Reactor Components," Proc. 10th Intl. Conf. on Environmental Degradation of Materials in Nuclear Power Systems - Water Reactors, NACE/ANS/TMS, Aug. 5-9, 2001, Lake Tahoe, NV.

19. Edwards, D. J., E. P. Simonen, F. A. Garner, L. R. Greenwood, B. M. Oliver, and S. M. Bruemmer, "Influence of Irradiation Temperature and Dose Gradients on the Microstructural Evolution in Neutron-Irradiated 316SS," J. Nucl. Mater. **317**, 32-45, 2003.

20. Chung, H. M., "Assessment of Void Swelling in Austenitic Stainless Steel Core Internals," NUREG/CR-6897, ANL-04/28, 2006.

21. Manjoine, M. J., and H. R. Voorhees, "Compilation of Stress-Relaxation Data for Engineering Alloys," ASTM Data Series Publication DS 60, ASTM Philadelphia, PA, 1982.

22. Manjoine, M. J., "Stress Relaxation Characteristics of Type 304 Stainless Steel," Conference Publication C165/73, Institute of Mechanical Engineers, 1973.

23. Kenfield, T. A., H. J. Busboom, and W. K. Appleby, "In-reactor Stress Relaxation in Bending of 20% Cold-Worked 316 Stainless Steel," J. Nucl. Mater. **66**, 238-243, 1977.

24. Causey, A. R., G. J. C. Carpenter, and S. R. MacEwen, "In-reactor Stress Relaxation of Selected Metals and Alloys at Low Temperatures," J. Nucl. Mater. **90**, 216-223, 1980.

25. Foster, J. P., E. R. Gilbert, K. Bunde, and D. L. Porter, "Relationship Between In-reactor Stress Relaxation and Irradiation Creep," J. Nucl. Mater. **252**, 89-97, 1998.

26. Brown, K. S., and G. M. Gordon, "Effects of BWR Coolant Chemistry on the Propensity for IGSCC Initiation and Growth in Creviced Reactor Internals Components," Proc. Third Intl. Symp. on Environmental Degradation of Materials in Nuclear Power Systems - Water Reactor, Metallurgical Society, Warrendale, PA, pp. 243-248, 1987.

27. Gordon, G. M., and K. S. Brown, "Dependence of Creviced BWR Component IGSCC Behavior on Coolant Chemistry," Proc. 4th Intl. Symp. on Environmental Degradation of Materials in Nuclear Power Systems - Water Reactor, Daniel Cubicciotti, ed., NACE, Houston, TX, pp. 14.46-14.61, 1990.

28. Garzarolli, F., D. Alter, and P. Dewes, "Deformability of Austenitic Stainless Steels and Nickel-Base Alloys in the Core of a Boiling and a Pressurized Water Reactor," Proc. Intl. Symp. on Environmental Degradation of Materials in Nuclear Power Systems - Water Reactor, American Nuclear Society, Lagrange, IL, pp. 131-138, 1986.

29. Kodama, M., et al., "IASCC Susceptibility of Austenitic Stainless Steels Irradiated to High Neutron Fluence," Proc. Sixth Intl. Symp. on Environmental Degradation of Materials in Nuclear Power Systems - Water Reactor, R. E. Gold and E. P. Simonen, eds., Minerals, Metals & Materials Society, Warrendale, PA, pp. 583-588, 1993.

30. Kodama, M., et al., "Effects of Fluence and Dissolved Oxygen on IASCC in Austenitic Stainless Steels," Proc. Fifth Intl. Symp. on Environmental Degradation of Materials in Nuclear Power Systems - Water Reactor, American Nuclear Society, Lagrange, IL, pp. 948-954, 1991.

31. Clark, W. L., and A. J. Jacobs, "Effect of Radiation Environment on SCC of Austenitic Materials," Proc. First Intl. Symp. on Environmental Degradation of Materials in Nuclear Power Systems - Water Reactor, NACE, Houston, TX, p. 451, 1983.

32. Jacobs, A. J., G. P. Wozadlo, K. Nakata, T. Yoshida, and I. Masaoka, "Radiation Effects on the Stress Corrosion and Other Selected Properties of Type-304 and Type-316 Stainless Steels," Proc. Third Intl. Symp. on Environmental Degradation of Materials in Nuclear Power Systems - Water Reactor, Metallurgical Society, Warrendale, PA, pp. 673-681, 1987.

33. Chung, H. M., R. V. Strain, and R. W. Clark, "Slow-Strain-Rate-Tensile Test of Model Austenitic Stainless Steels Irradiated in the Halden Reactor," in Environmentally Assisted Cracking in Light Water Reactors Semiannual Report July 2000 - December 2000, NUREG/CR-4667, Vol. 31, ANL-01/09, pp. 22-32, 2002.

34. Chung, H. M., R. V. Strain, and R. W. Clark, "Slow-Strain-Rate-Tensile Test of Model Austenitic Stainless Steels Irradiated in the Halden Reactor," in Environmentally Assisted Cracking in Light Water Reactors Semiannual Report January-December 2001, NUREG/CR-4667, Vol. 32, ANL-02/33, pp. 19-28, 2003.

35. Andresen, P. L., and F. P. Ford, "Irradiation Assisted Stress Corrosion Cracking: From Modeling and Prediction of Laboratory & In-Core Response to Component Life Prediction," Corrosion/95, NACE, Houston TX, Paper No. 419, 1995.

36. R. Stoenescu, M. L. Castano, S. van Dyck, A. Roth, B. van der Schaaf, C. Ohms, and D. Gavillet, "Irradiation-Assisted Stress Corrosion Cracking of Heat-Affected Zones of Austenitic Stainless Steel Welds," Proc. 12th Intl. Conf. on Environmental Degradation of Materials in Nuclear Power System - Water Reactors, T. R. Allen, P. J. King, and L. Nelson, eds., Minerals, Metals, & Materials Society, pp. 267-275, 2005.

37. Jenssen, A., and L. G. Ljungberg, "Irradiation Assisted Stress Corrosion Cracking: Post Irradiation CERT Tests of Stainless Steels in a BWR Test Loop," Proc. Seventh Intl. Symp. on Environmental Degradation of Materials in Nuclear Power Systems - Water Reactor, G. Airey et al., eds., NACE, Houston, TX, pp. 1043-1052, 1995.

38. Ford, F. P., and P. L. Andresen, "Corrosion in Nuclear Systems: Environmentally Assisted Cracking in Light Water Reactors," in Corrosion Mechanisms, P. Marcus and J. Ouder, eds., Marcel Dekker, pp. 501-546, 1994.

39. P. L. Andresen, "Emerging Issues and Fundamental Processes in Environmental Cracking in Hot Water," Proc. Research Topical Symposium on Environmental Cracking, Corrosion/07, NACE, 2007.

40. Andresen, P. L. and M. M. Morra, "Emerging Issues in Environmental Cracking in Hot Water," Proc. 13th Intl. Conf. on Environmental Degradation of Materials in Nuclear Power Systems - Water Reactors, T. R. Allen, P. J. King, and L. Nelson, eds., Canadian Nuclear Society, Toronto, Canada, Paper No. P0124, 2007.

41. Maziasz, P. J., and C. J. McHargue, "Microstructural Evolution in Annealed Austenitic Steels during Neutron Irradiation," Int. Met. Rev. **32**, 190, 1987.

42. Maziasz, P. J., "Overview of Microstructural Evolution in Neutron-Irradiated Austenitic Stainless Steels," J. Nucl. Mater. **205**, 118-145, 1993.

43. Zinkle, S. J., P. J. Maziasz, and R. E. Stoller, "Dose Dependence of the Microstructural Evolution in Neutron-Irradiated Austenitic Stainless Steels," J. Nucl. Mater. **206**, 266-286, 1993.

44. Edwards, D. J., E. P. Simonen, and S. M. Bruemmer, "Evolution of Fine-Scale Defects in Stainless Steels Neutron-Irradiated at 275°C," J. Nucl. Mater. **317**, 13-31, 2003.

45. Bruemmer, S. M., D. J. Edwards, B. W. Arey, and L. A. Charlot, "Microstructural, Microchemical and Hardening Evolution in LWR-Irradiated Austenitic Stainless Steels," Proc. Ninth Intl. Symp. on Environmental Degradation of Materials in Nuclear Power Systems - Water Reactor, Metallurgical Society, Warrendale, PA, pp. 1079-1087, 1999.

46. Bruemmer, S. M., "New Issues Concerning Radiation-Induced Material Changes and Irradiation-Assisted Stress Corrosion Cracking in Light-Water Reactors," Proc. Tenth Intl. Symp. on Environmental Degradation of Materials in Nuclear Power Systems - Water Reactor, Paper No. 0008V, NACE, Houston, TX, 2001.

47. Garner, F. A., "Evolution of Microstructures in Face-Centered Cubic Metals during Neutron Irradiation," J. Nucl. Mater. **205**, 98-111, 1993.

48. Edwards, D., E. Simonen, S. Bruemmer, and P. Efsing, "Microstructural Evolution in Neutron-Irradiated Stainless Steels: Comparison of LWR and Fast-Reactor Irradiations," Proc. 12th Intl. Conf. on Environmental Degradation of Materials in Nuclear Power System - Water Reactors, T. R. Allen, P. J. King, and L. Nelson, eds., Minerals, Metals, & Materials Society, pp. 419-428, 2005.

49. Tsukada, T., and T. Kondo, "Effects of Minor Elements on IASCC of Type 316 Model Stainless Steels," Proc. 8th Intl. Conf. on Environmental Degradation of Materials in Nuclear Power System - Water Reactors, Minerals, Metals, & Materials Society, pp. 795-802, 1997.

50. Fukuya, K., K. Fujii, M. Nakano, and N. Nakajima, "Stress Corrosion Cracking of Cold-Worked 316 Stainless Steel Irradiated to High Fluence," Proc. 10th Intl. Conf. on Environmental Degradation of Materials in Nuclear Power Systems - Water Reactors, NACE/ANS/TMS, Aug. 5-9, 2001, Lake Tahoe, NV.

51. Fujimoto, K., T. Yonezawa, E. Wachi, Y. Yamaguchi, M. Nakano, R. P. Shogan, J. P. Massoud, and T. R. Mager, "Effect of the Accelerated Irradiation and Hydrogen/Helium Gas on IASCC Characteristics for Highly Irradiated Austenitic Stainless Steels," Proc. 12th Intl. Conf. on Environmental Degradation of Materials in Nuclear Power System - Water Reactors, T. R. Allen, P. J. King, and L. Nelson, eds., Minerals, Metals, & Materials Society, pp. 299-310, 2005.

52. Edwards, D., E. Simonen, and S. Bruemmer, "Radiation-Induced Segregation Behavior in Austenitic Stainless Steels: Fast Reactor versus Light Water Reactor Irradiations," Proc. 13th Intl. Conf. on Environmental Degradation of Materials in Nuclear Power Systems - Water Reactors, T. R. Allen, P. J. King, and L. Nelson, eds., Canadian Nuclear Society, Toronto, Canada, Paper No. P0139, 2007.

53. Chung, H. M., and W. J. Shack, "Irradiation-Assisted Stress Corrosion Cracking Behavior of Austenitic Stainless Steels Applicable to LWR Core Internals," NUREG/CR-6892, ANL-04/10, 2006.

54. Lucas, G. E., "The Evolution of Mechanical Property Change in Irradiated Austenitic Stainless Steels," J. Nucl. Mater. **206**, 287-305, 1993.

55. Van Duysen, J. C., P. Todeschini, and G. Zacharie, "Effects of Neutron Irradiation at Temperatures below 500°C on the Properties of Cold-Worked 316 Stainless Steels: A Review," Effects of Radiation on Materials: 16th International Symposium, ASTM STP 1175, American Society for Testing and Materials, pp. 747-776, 1993.

56. Electric Power Research Institute, Materials Reliability, "Program Characterization of Decommissioned PWR Vessel Internals Material Samples - Material Certification, Fluence, and Temperature (MRP-128)," EPRI Report 1008202, Sept. 2004.

57. Electric Power Research Institute, Materials Reliability Program, "A Review of Radiation Embrittlement for Stainless Steels (MRP-79)," Rev. 1, EPRI Report 1008204, Sept. 2004.

58. Demma, A., R. Carter, A. Jenssen, T. Torimaru, and R. Gamble, "Fracture Toughness of Highly Irradiated Stainless Steels in Boiling Water Reactors," Proc. 13th Intl. Conf. on Environmental Degradation of Materials in Nuclear Power Systems - Water Reactors, T. R. Allen, P. J. King, and L. Nelson, eds., Canadian Nuclear Society, Toronto, Canada, Paper No. 114, 2007.

59. Ehrnsten, U., K. Wallin, P. Karjalainen-Roikonen, S. van Dyck, and P. Ould, "Fracture Toughness of Stainless Steels Irradiated to ≈9 dpa in Commercial BWRs," Proc. 6th Intl. Symp. on Contribution of Materials Investigations to Improve the Safety and Performance of LWRs, Vol. 1, Fontevraud 6, French Nuclear Energy Society, SFEN, Fontevraud Royal Abbey, France, pp. 661-670, Sept. 18-22, 2006.

60. Karlsen, T. M., M. Espeland, and A. Horvath, "Summary Report on the PWR Crack Growth Rate Investigation, IFA-657," HWR-773, OECD Halden Reactor Project, May 2005.

61. Conermann, J., R. Shogan, K. Fujimoto, T. Yonezawa, and T. Yamaguchi, "Irradiation Effects in a Highly Irradiated Cold Worked Stainless Steel Removed from a Commercial PWR," Proc. 12th Intl. Conf. on Environmental Degradation of Materials in Nuclear Power Systems - Water Reactors, T. R. Allen, P. J. King, and L. Nelson, eds., Minerals, Metals & Materials Society, Warrendale, PA, pp. 277-284, 2005.

62. Takakura, K., K. Nakata, M. Ando, K. Fujimoto, and E. Wachi, "Lifetime Evaluation for IASCC Initiation of Cold Worked 316 Stainless Steel's BFB in PWR Primary Water," Proc. 13th Intl. Conf. on Environmental Degradation of Materials in Nuclear Power Systems - Water Reactors, T. R. Allen, P. J. King, and L. Nelson, eds., Canadian Nuclear Society, Toronto, Canada, Paper No. P0009, 2007.

63. Electric Power Research Institute, Materials Reliability Program, "Development of Material Constitutive Model for Irradiated Austenitic Stainless Steels (MRP-135)," EPRI Report 1011127, Dec. 2004.

64. Odette, G. R., and G. E. Lucas, "The Effects of Intermediate Temperature Irradiation on the Mechanical Behavior of 300-Series Austenitic Stainless Steels," J. Nucl. Mater. **179-181**, 572-576, 1991.

65. Carter, R. G., and R. M. Gamble, "Assessment of the Fracture Toughness of Irradiated Stainless Steel for BWR Core Shrouds," Fontevraud 5 Intl. Symp., Contribution of Materials Investigation to the Resolution of Problems Encountered in Pressurized Water Reactors, Avignon, France, Sept. 25, 2002.

66. Hazelton, W. S., and W. H. Koo, "Technical Report on Material Selection and Processing Guidelines for BWR Coolant Pressure Boundary Piping, Final Report," NUREG-0313, Rev. 2, 1988.

67. Tribouilloy, L., F. Vaillant, J-M. Olive, M. Puiggali, L. Legras, T. Couvant, J.-M. Boursier, Y. Rouillon, and C. Amzallag, "Stress Corrosion Cracking of Cold-Worked Type Austenitic Stainless Steels in PWR Environment," Proc. 13th Intl. Conf. on Environmental Degradation of Materials in Nuclear Power Systems - Water Reactors, T. R. Allen, P. J. King, and L. Nelson, eds., Canadian Nuclear Society, Toronto, Canada, Paper No. P0074, 2007.

68. Andresen, P. L., P. W. Emigh, W. R. Catlin, L. M. Young, and R. M. Horn, "Effect of Yield Strength, Corrosion Potential, Stress Intensity Factor, Silicon, and Grain Boundary Character on the SCC of Stainless Steels," Proc. 11th Intl. Symp. on Environmental Degradation of Materials in Nuclear Power Systems - Water Reactor, pp. 816-830, 2003.

69. Shoji, T., "Progress in the Mechanistic Understanding of BWR SCC and Its Implications to the Prediction of SCC Growth Behavior in Plants," Proc. 11th Intl. Symp. on Environmental Degradation of Materials in Nuclear Power Systems - Water Reactor, pp. 888-897, 2003.

70. Castano Marin, M. L., M. S. Garcia Redondo, G. de Diego Velasco, and D. Gomez Briceno, "Crack Growth Rate of Hardened Austenitic Stainless Steels in BWR and PWR Environments," Proc. 11th Intl. Symp. on Environmental Degradation of Materials in Nuclear Power Systems - Water Reactor, pp. 845-854, 2003.

71. Shoji, T., G. Li, J. Kwon, S. Matsushima, and Z. Lu, "Quantification of Yield Strength Effects on IGSCC of Austenitic Stainless Steels in High Temperature Water," Proc. 11th Intl. Symp. on Environmental Degradation of Materials in Nuclear Power Systems - Water Reactor, pp. 834-843, 2003.

72. Ooki, S., Y. Tanaka, K. Takamori, S. Suzuki, S. Tanaka, Y. Saito, T. Nakamura, T. Kato, K. Chatani, and M. Kodama, "Study on SCC Growth Behavior of BWR Core Shroud," Proc. 12th Intl. Conf. on Environmental Degradation of Materials in Nuclear Power Systems - Water Reactors, T. R. Allen, P. J. King, and L. Nelson, eds., Minerals, Metals & Materials Society, Warrendale, PA, pp. 365-376, 2005.

73. Chatani, K., K. Takakura, M. Ando, K. Nakata, S. Tanaka, Y. Ishiyama, M. Hishida, and Y. Kaji, "IASCC Crack Growth Rates of Neutron Irradiated Low Carbon Austenitic Stainless Steels in Simulated BWR Condition," Proc. 13th Intl. Conf. on Environmental Degradation of Materials in Nuclear Power Systems - Water Reactors, T. R. Allen, P. J. King, and L. Nelson, eds., Canadian Nuclear Society, Toronto, Canada, Paper No. P0091, 2007.

74. Karlsen, T. M., and A. Horvath, "Final Report on the In-pile Crack Growth Behavior of Irradiated Compact Tension Specimens in IFA-639," HWR-770, OECD Halden Reactor Project, Dec. 2004.

75. Nakano, J., T. M. Karlsen, and M. Espeland, "Summary Report on the BWR Crack Growth Rate Experiment, IFA-658," HWR-862, OECD Halden Reactor Project, Feb. 2007.

76. Nakano, J., T. M. Karlsen, and M. Espeland, "Summary of Results from the PWR Crack Growth Rate Investigation, IFA-670," HWR-843, OECD Halden Reactor Project, Aug. 2008.

77. Karlsen, T. M., P. Bennett, and N. W. Hogberg, "In-core Crack Growth Rate Studies on Irradiated Austenitic Stainless Steels in BWR and PWR Conditions in the Halden Reactor," Proc. 12th Intl. Conf. on Environmental Degradation of Materials in Nuclear Power Systems - Water Reactors, T. R. Allen, P. J. King, and L. Nelson, eds., Minerals, Metals & Materials Society, Warrendale, PA, pp. 337-348, 2005.

78. Jenssen, A., K. Gott, P. Efsing, and P. O. Andersson, "Crack Growth Behavior of Irradiated Type 304L Stainless Steel in Simulated BWR Environment," Proc. 11th Intl. Symp. on Environmental Degradation of Materials in Nuclear Power Systems - Water Reactor, pp. 1015-1024, 2003.

79. Jenssen, A., J. Stjarnsater, and R. Pathania, "Crack Growth Rate Testing of Fast Reactor Irradiated Type 304L and 316 SS in BWR and PWR Environments," Proc. 14th Intl. Conf. on Environmental Degradation of Materials in Nuclear Power Systems - Water Reactors, American Nuclear Society, Lagrange Park, IL, 2009.

80. Nakamura, T., M. Koshiishi, T. Torimaru, Y. Kitsunai, K. Takakura, K. Nagata, M. Ando, Y. Ishiyama, and A. Jenssen, "Correlation between IASCC Growth Behavior and Plastic Zone Size of Crack Tip in 3.5 dpa Neutron Irradiated Type 304L SS CT Specimen," Proc. 13th Intl. Conf. on Environmental Degradation of Materials in Nuclear Power Systems - Water Reactors, T. R. Allen, P. J. King, and L. Nelson, eds., Canadian Nuclear Society, Toronto, Canada, Paper No. P0030, 2007.

81. Sumiya, R., S. Tanaka, K. Nakata, K, Takakura, M. Ando, T. Torimaru, and Y. Kitsunai, "K Validity Criterion of Neutron Irradiated Type 316L Stainless Steel CT Specimen for SCC Growth Test," Proc. 13th Intl. Conf. on Environmental Degradation of Materials in Nuclear Power Systems - Water Reactors, T. R. Allen, P. J. King, and L. Nelson, eds., Canadian Nuclear Society, Toronto, Canada, Paper No. P0072, 2007.

82. Andresen, P. L. and M. M. Morra, "Effects of Si on SCC of Irradiated and Unirradiated Stainless Steels and Nickel Alloys," Proc. 12th Intl. Conf. on Environmental Degradation of Materials in Nuclear Power System - Water Reactors, T. R. Allen, P. J. King, and L. Nelson, eds., Minerals, Metals, & Materials Society, pp. 87-106, 2005.

83. Shigenaka, N., T. Hashimoto, and M. Fuse, "Effects of Alloying Elements (Mo, Si) in an Austenitic Stainless Steel on Dislocation Loop Nucleation under Ion Irradiation," J. Nucl. Mater. **207**, 46-52, 1993.

84. Shack, W. J., and T. F. Kassner, "Review of Environmental Effects on Fatigue Crack Growth of Austenitic Stainless Steels," NUREG/CR-6176, ANL-94/1, 1994.

85. Tice, D., N. Platts, K. Rigby, and J. Stairmand, "Influence of Temperature and Flow Rate on Corrosion Fatigue Crack Growth of Austenitic Stainless Steel in a PWR Primary Coolant Environment," Proc. 13th Intl. Conf. on Environmental Degradation of Materials in Nuclear Power Systems - Water Reactors, T. R. Allen, P. J. King, and L. Nelson, eds., Canadian Nuclear Society, Toronto, Canada, Paper No. P0134, 2007.

86. Platts, N., D. Tice, K. Rigby, and J. Stairmand, "Influence of Load Ratio, Rise Time and Waveform on Corrosion Fatigue Crack Growth of Austenitic Stainless Steel in a PWR Primary Coolant Environment," Proc. ASME Pressure Vessels and Piping Division Conf., American Society of Mechanical Engineers, New York, PVP2007-26755, 2007.

87. Vaillant, F., J. M. Boursier, C. Amzallag, J. Champredonde, J. Daret, and C. Bosch, "Influence of a Cyclic Loading on Crack Growth Rates of Alloy 600 in Primary Environment: An Overview," Proc. 11th Intl. Symp. on Environmental Degradation of Materials in Nuclear Power Systems - Water Reactor, pp. 189-198, 2003.

88. Andresen, P. L. and M. M. Morra, "Effect of Rising and Falling K Profiles on SCC Growth Rates in High-Temperature Water," Trans. ASME **129**, 488-506, 2007.

89. Pathania, R., R. Carter, R. Horn, and P. Andresen, "Crack Growth Rates in Irradiated Stainless Steels in BWR Internals," Proc. 14th Intl. Conf. on Environmental Degradation of Materials in Nuclear Power Systems - Water Reactors, American Nuclear Society, Lagrange Park, IL, Paper No. 203178, 2009.

90. Davis, R. B., and P. Andresen, "Evaluation of Fundamental Linkage among SCC Phenomena," Cooperative IASCC Research (CIR) Final Report, EPRI 1007378, Oct. 2002.

91. James, L. A., and D. P. Jones, "Fatigue Crack Growth Correlation for Austenitic Stainless Steels in Air," Proc. Conf. on Predictive Capabilities in Environmentally-Assisted Cracking, PVP Vol. 99, R. Rungta, ed., American Society of Mechanical Engineers, New York, pp. 363-414, 1985.

92. Shahinian, P., H. E. Watson, and H. H. Smith, "Effect of Neutron Irradiation on Fatigue Crack Propagation in Types 304 and 316 Stainless Steels at High Temperature," NRL Report 7446, Naval Research Laboratory, Washington, DC, July 1972.

93. Shahinian, P., "Fatigue Crack Propagation in Fast Neutron Irradiated Stainless Steels and Welds," in Properties of Reactor Structural Alloys after Neutron or Particle Irradiation, ASTM STP 570, C. J. Baroch, ed., American Society for Testing and Materials, Philadelphia, PA, pp. 191-204, 1975.

94. James, L. A., and R. L. Knecht, "Fatigue-Crack Propagation in Fast-Neutron-Irradiated Types-304 and -316 Stainless Steels," Nucl. Technol. **19**, 148-155, 1973.

95. James, L. A., "The Effect of Fast Neutron Irradiation upon the Fatigue-Crack Propagation Behavior of Two Austenitic Stainless Steels," J. Nucl. Mater. **59**, 183-191, 1976.

96. Shahinian, P., H. E. Watson, and H. H. Smith, "Neutron Irradiation Effects on Fatigue Crack Growth in Types 304 and 316 Stainless Steels," in Irradiation Effects on Reactor Structural Materials, Quarterly Progress Report, 1 May - 31 July 1972, NRL Memorandum Report 2505, Naval Research Laboratory, Washington, DC, pp. 13-22, Aug. 1972.

97. Freyer, P. D., T. R. Mager, and M. A. Burke, "Hot Cell Crack Initiation Testing of Various Heats of Highly Irradiated 316 Stainless Steel Components Obtained from Three Commercial PWRs," Proc. 13th Intl. Conf. on Environmental Degradation of Materials in Nuclear Power Systems - Water Reactors, T. R. Allen, P. J. King, and L. Nelson, eds., Canadian Nuclear Society, Toronto, Canada, Paper No. P0034, 2007.

98. Nishioka, H., K. Fukuya, K. Fujii, and T. Torimaru, "IASCC Properties and Mechanical Behavior of Stainless Steels Irradiated up to 73 dpa," Proc. 13th Intl. Conf. on Environmental Degradation of Materials in Nuclear Power Systems - Water Reactors, T. R. Allen, P. J. King, and L. Nelson, eds., Canadian Nuclear Society, Toronto, ON, Canada, Paper No. P0040, 2007.

99. Fyfitch, S., H. Xu, P. Scott, L. Fournier, and A. Demma, "Criteria for Initiation of Irradiation-Assisted Stress Corrosion Cracking in Stainless Steels in PWR Systems," Proc. 14th Intl. Conf. on Environmental Degradation of Materials in Nuclear Power Systems - Water Reactors, American Nuclear Society, Lagrange Park, IL, 2009.

100. Shogan, R. P., and T. R. Mager, "Susceptibility of Type 316 Stainless Steel to Irradiation Assisted Stress Corrosion Cracking in a PWR Environment," Proc. 10th Intl. Conf. on Environmental Degradation of Materials in Nuclear Power Systems - Water Reactors, NACE/ANS/TMS, Lake Tahoe, NV, Paper No. 0030, Aug. 5-9, 2001.

101. Electric Power Research Institute, Materials Reliability Program, "PWR Internals Material Aging Degradation Mechanism Screening, and Threshold Values (MRP-175)," EPRI Report 1012081, Dec. 2005.

102. Gavenda, D. J., W. F. Michaud, T. M. Galvin, W. F. Burke, and O. K. Chopra, "Effects of Thermal Aging on Fracture Toughness and Charpy-Impact Strength of Stainless Steel Pipe Welds," NUREG/CR-6428, ANL-95/47, 1996.

103. Dufresne, J., B. Henry, and H. Larsson, "Fracture Toughness of Irradiated AISI 304 and 316L Stainless Steels," Effects of Radiation on Structural Materials, ASTM STP 683, J. A. Sprague and D. Kramer, eds., American Society for Testing and Materials, Philadelphia, PA, pp. 511-528, 1979.

104. Picker, C., A. L. Stott, and H. Cocks, "Effects of Low-Dose Fast Neutron Irradiation on the Fracture Toughness of Type 316 Stainless Steel and Weld Metal," Proc. Specialists Meeting on Mechanical Properties of Fast Reactor Structural Materials, Chester, UK, Paper IWGFR 49/440-4, 1983.

105. Huang, F. H., "The Fracture Characterization of Highly Irradiated Type 316 Stainless Steel," Int. J. Fracture **25**, 181-193, 1984.

106. Bernard, J., and G. Verzeletti, "Elasto-Plastic Fracture Mechanics Characterization of Type 316H Irradiated Stainless Steel up to 1 dpa," Effects of Radiation on Materials: 12th Intl. Symp., ASTM STP 870, F. A. Garner and J. S. Perrin, eds., American Society for Testing and Materials, Philadelphia, PA, pp. 619-641, 1985.

107. Mills, W. J., L. A. James, and L. D. Blackburn, "Results of Fracture Mechanics Tests on PNC SU 304 Plate," Westinghouse Hanford Report HEDL-7544, Hanford Engineering Development Laboratory, Richland, WA, 1985.

108. Mills, W. J., "Fracture Toughness of Irradiated Stainless Steel Alloys," Nucl. Technol. **82**, 290-303, 1988.

109. Michel, D. J., and R. A. Gray, "Effects of Irradiation on the Fracture Toughness of FBR Structural Materials," J. Nucl. Mater. **148**, 194-203, 1987.

110. Ould, P., P. Balladon, and Y. Meyzaud, Bull. Cercle Etud. Metaux **15**, 31.1-31.12, 1988.

111. Van Osch, E. V., M. G. Horsten, and M. I. De Vries, "Fracture Toughness of PWR Internals," ECN Contribution to CEC Contract on PWR Internals-Part 2 (ETNU/CT/94/0136-F), ECN-I-97-010 (71747/NUC/EvO/mh/006274), Netherlands Energy Research Foundation ECN, Petten, the Netherlands, 1997.

112. De Vries, M. I., "Fatigue Crack Growth and Fracture Toughness Properties of Low Fluence Neutron-Irradiated Type 316 and Type 304 Stainless Steels," Influence of Radiation on Mechanical Properties: 13th Symposium (Part II), ASTM STP 956, F. A. Garner et al., eds., American Society of Testing and Materials, Philadelphia, PA, pp. 174-190, 1987.

113. Alexander, D. J., J. E. Pawel, L. M. Grossbeck, A. F. Rowcliffe, and K. Shiba, "Fracture Toughness of Irradiated Candidate Materials for ITER First Wall/Blanket Structures," Effect of Radiation on Materials: 17th Intl. Symp., ASTM STP 1270, American Society of Testing and Materials, Philadelphia, PA, pp. 945-970, 1996.

114. Sindelar, R. L., G. R. Caskey, Jr., J. K. Thomas, J. R. Hawthorne, A. L. Hiser, R. A. Lott, J. A. Begley, and R. P. Shogan, "Mechanical Properties of 1950s Vintage Type 304 Stainless Steel Weldment Components after Low Temperature Neutron Irradiation," 16th Intl. Symp. on Effects of Radiation on Materials, ASTM STP 1175, American Society of Testing and Materials, Philadelphia, PA, pp. 714-746, 1993.

115. Hamilton, M. L., F. H. Huang, W. J. S. Yang, and F. A. Garner, "Mechanical Properties and Fracture Behavior of 20% Cold-Worked 316 Stainless Steel Irradiated to Very High Neutron Exposures," Influence of Radiation in Material, Properties: 13th Intl. Symp. (Part II), ASTM STP 956, American Society of Testing and Materials, Philadelphia, PA, pp. 245-270, 1987.

116. Little, E. A., "Dynamic J-Integral Toughness and Fractographic Studies of Fast Reactor Irradiated Type 321 Stainless Steel," Effects of Radiation on Material, Properties: 12th Intl. Symp., ASTM STP 870, American Society of Testing and Materials, Philadelphia, PA, pp. 563-579, 1985.

117. Haggag, F. J., W. L. Server, W. G. Reuter, and J. M. Beeston, "Effects of Irradiation Fluence and Creep on Fracture Toughness of Type 347/348 Stainless Steels," ASTM STP 870, American Society of Testing and Materials, Philadelphia, PA, pp. 548-562, 1985.

118. O'Donnell, I. J., H. Huthmann, and A. A. Tavassoli, "The Fracture Toughness Behaviour of Austenitic Steels and Weld Metal Including the Effects of Thermal Aging and Irradiation," Intl. J. Pressure Vessels and Piping **65** (3), 209-220, 1996.

119. Kim C., R. Lott, S. Byrne, M. Burke, and G. Gerzen, "Embrittlement of Cast Austenitic Stainless Steel Reactor Internals Components," Proc. 6th Intl. Symp. on Contribution of Materials Investigations to Improve the Safety and Performance of LWRs, Vol. 1, Fontevraud 6, French Nuclear Energy Society, SFEN, Fontevraud Royal Abbey, France, Sept. 18-22, 2006.

120. Balladon, P., J. Heritier, and P. Rabbe, "Influence of Microstructure on the Ductile Rupture Mechanisms of a 316L Steel at Room and Elevated Temperatures," Fracture Mechanics: 14th Symp., Vol. II: Testing and Applications, ASTM STP 791, American Society for Testing and Materials, Philadelphia, PA, pp. 496-516, 1983.

121. Fyfitch, S., H. Xu, A. Demma, R. Carter, R. Gamble, and P. Scott, "Fracture Toughness of Irradiated Stainless Steel in Nuclear Power Systems," Proc. 14th Intl. Conf. on Environmental Degradation of Materials in Nuclear Power Systems - Water Reactors, American Nuclear Society, Lagrange Park, IL, 2009.

122. Electric Power Research Institute, Materials Reliability Program, "Fracture Toughness Testing of Decommissioned PWR Core Internals Material Samples (MRP-160)," EPRI Report 1012079, Sept. 2005.

123. Fukuya, K., K. Fuji, H. Nishioka, and Y. Kitsunai, "Evolution of Microstructure and Microchemistry in Cold-Worked 316 Stainless Steel under PWR Irradiations," J. Nucl. Sci. Technol. **43 (2)**, 159-173, 2006.

124. Chopra, O. K., "Estimation of Fracture Toughness of Cast Stainless Steels during Thermal Aging in LWR Systems," NUREG/CR-4513, Rev. 1, ANL-93/22, Aug. 1994.

125. Chopra, O. K. and W. J. Shack, "Mechanical Properties of Thermally Aged Cast Stainless Steels from Shippingport Reactor Components," NUREG/CR-6275, ANL-94/37, April 1995.

126. Michaud, W. F., P. T. Toben, W. K. Soppet, and O. K. Chopra, "Tensile-Property Characterization of Thermally Aged Cast Stainless Steels," NUREG/CR-6142, ANL-93/35, Feb. 1994.

127. Bonnet, S., J. Bourgoin, J. Champredonde, D. Guttmann, and M. Guttmann, "Relationship between Evolution of Mechanical Properties of Various Cast Duplex Stainless Steels and Metallurgical and Aging Parameters: An Outline of Current EdF Programmes," Mater. Sci. Technol. **6**, 221-229, 1990.

128. Slama, G., P. Petrequin, and T. Mager, "Effect of Aging on Mechanical Properties of Austenitic Stainless Steel Castings and Welds," SMiRT Post-Conference Seminar 6, Assuring Structural Integrity of Steel Reactor Pressure Boundary Components, Aug. 29-30, 1983, Monterey, CA, 1983.

129. Chung, H. M., and O. K. Chopra, "Kinetics and Mechanism of Thermal Aging Embrittlement of Duplex Stainless Steels," Environmental Degradation of Materials in Nuclear Power Systems - Water Reactors, G. J. Theus and J. R. Weeks, eds., Metallurgical Society, Warrendale, PA, pp. 359-370, 1988.

130. Auger, P., F. Danoix, A. Menand, S. Bonnet, J. Bourgoin, and M. Guttmann, "Atom Probe and Transmission Electron Microscopy Study of Aging of Cast Duplex Stainless Steels," Mater. Sci. Technol. **6**, 301-313, 1990.

131. Brown, J. E., A. Cerezo, T. J. Godfrey, M. G. Hetherington, and G. D. W. Smith, "Quantitative Atom Probe Analysis of Spinodal Reaction in Ferrite Phase of Duplex Stainless Steel," Mater. Sci. Technol. **6**, 293-300, 1990.

132. Miller, M. K., and J. Bentley, "Characterization of Fine-Scale Microstructures in Aged Primary Coolant Pipe Steels," Environmental Degradation of Materials in Nuclear Power Systems - Water Reactors, G. J. Theus and J. R. Weeks, eds., Metallurgical Society, Warrendale, PA, pp. 341-349, 1988.

133. Hawthorne, J. R., and L. E. Steele, "Metallurgical Variables as Possible Factors Controlling Irradiation Response of Structural Steels," Effects of Radiation on Structural Metals, ASTM STP 426, American Society of Testing and Materials, Philadelphia, PA, pp. 534-572, 1967.

134. Grimes, C. I., U.S. Nuclear Regulatory Commission, License Renewal and Standardization Branch, letter to Douglas J. Walters, Nuclear Energy Institute, License Renewal Issue No. 98-0030, "Thermal Aging Embrittlement of Cast Stainless Steel Components," May 19, 2000.

135. Nickell, R. E., and M. A. Rinckel, "Evaluation of Thermal Aging Embrittlement for Cast Austenitic Stainless Steels Components in LWR Reactor Coolant Systems," EPRI TR-106092, Electric Power Research Institute, Palo Alto, CA, 1997.

136. Edmonds, E., W. Sloss, K. Q. Bagley, and W. Batey, "Mixed Oxide Fuel Performance," Intl. Conf. on Fast Breeder Reactor Fuel Performance, American Nuclear Society, Monterey, CA, pp. 54-63, 1979.

137. Garner, F. A., and H. R. Brager, "Swelling of Austenitic Fe-Cr-Ni Ternary Alloys during Fast Neutron Irradiation," Effects of Radiation on Materials: Twelfth Intl. Symp., ASTM STP 870, F. A. Garner and J. S. Perrin, eds., ASTM, Philadelphia, PA, pp. 185-201, 1985.

138. Garner, F. A., and M. A. Mitchell, "The Complex Role of Phosphorus in the Neutron-Induced Swelling of Titanium-Modified Austenitic Stainless Steel," J. Nucl. Mater. **187**, 223-229, 1992.

139. Sekimura, N., F. A. Garner, and J. W. Newkirk, "Silicon's Role in Determining Swelling in Neutron-Irradiated Fe-Cr-Ni-Si Alloys," J. Nucl. Mater. **191-194**, 1244-1247, 1992.

140. Porter, D. L., G. D. Hudman, and F. A. Garner, "Irradiation Creep and Swelling of Annealed Type 304L Stainless Steel at ~390°C and High Neutron Fluence," J. Nucl. Mater. **179-181**, 581-584, 1991.

141. Packan, N. H., K. Farrell, and J. O. Stiegler, "Correlation of Neutron and Heavy-Ion Damage," J. Nucl. Mater. **78**, 143-155, 1978.

142. Allen, T. R. J. I. Cole, C. L. Trybus, D. L. Porter, H. Tsai, F. Garner, E. A. Kenik, T. Yoshitake, and J. Ohta, "The Effect of Dose Rate on the Response of Austenitic Stainless Steel to Neutron Radiation," J. Nucl. Mater. **348**, 148-164, 2006.

143. Fujii, K., K. Fukuya, G. Furutani, T. Torimaru, A. Kohyama, and Y. Katoh, "Swelling in 316 Stainless Steel Irradiated to 53 dpa in a PWR," Proc. 10th Intl. Conf. on Environmental Degradation of Materials in Nuclear Power Systems - Water Reactors, NACE/ANS/TMS, Paper No. 0020, Aug. 5-9, 2001, Lake Tahoe, NV.

144. Foster, J. P., D. L. Porter, D. L. Harrod, T. R. Mager, and M. G. Burke, "316 Stainless Steel Cavity Swelling in a PWR," J. Nucl. Mater. **224**, 207-215, 1995.

145. Garner, F. A., L. R. Greenwood, and D. L. Harrod, "Potential High Fluence Response of Pressure Vessel Internals Constructed from Austenitic Stainless Steels," Proc. Sixth Intl. Symp. on Environmental Degradation of Materials in Nuclear Power Systems - Water Reactor, R. E. Gold and E. P. Simonen, eds., Minerals, Metals & Materials Society, Warrendale, PA, pp. 783-790, 1993.

146. Porter, D. L., and F. A. Garner, "Irradiation Creep and Embrittlement Behavior of AISI 316 Stainless Steel at very High Neutron Fluences," J. Nucl. Mater. **159**, 114-121, 1988.

147. Porollo, S. I., A. N. Vorobjev, Yu. V. Konobeev, A. M. Dvoriashin, V. M. Krigan, N. I. Budylkin, E. M. Mironova, and F. A. Garner, "Swelling and Void-Induced Embrittlement of Austenitic Stainless Steel Irradiated to 73-82 dpa at 335-365°C," J. Nucl. Mater. **258-263**, 1613-1617, 1998.

148. Huang, F. H., "Comparison of Fracture Behavior for Low-Swelling Ferritic and Austenitic Alloys Irradiated in the Fast Flux Test Facility (FFTF) to 180 DPA," Eng. Frac. Mech. **43**, 733-748, 1992.

This page is intentionally left blank.